MOISTURE AND INTERFACIAL ADHESION IN MICROELECTRONIC ASSEMBLIES

A Thesis
Presented to
The Academic Faculty

by

Timothy P. Ferguson

In Partial Fulfillment
of the Requirements for the Degree of
Doctor of Philosophy in Mechanical Engineering

Georgia Institute of Technology
Atlanta, Georgia

June 2004

MOISTURE AND INTERFACIAL ADHESION IN MICROELECTRONIC ASSEMBLIES

Approved:

Dr. Jianmin Qu, Chairman

Dr. S. Mostafa Ghiaasiaan

Dr. W. Steven Johnson

Dr. Suresh Sitaraman

Dr. C. P. Wong

Date Approved: June 11, 2004

This dissertation is dedicated to my parents, Patrick and Diana. Thank you for your love and support.

ACKOWLEDGEMENTS

I would like to take an opportunity to thank my wife and family. The completion of this study would not have been possible without their continued support, encouragement, and unconditional love. My thesis advisor, Dr. Jianmin Qu, is a tremendous mentor, and I am grateful to have had the opportunity work under his guidance and direction. I will always reflect on the numerous discussions we had in his office fondly, and I learned more from him than he will probably ever fully realize. I would also like to thank Dr. Steve Johnson, Dr. C.P. Wong, Dr. Suresh Sitaraman, and Dr. S. Mostafa Ghiaasiaan for their time, suggestions, comments, and support for serving as members of my thesis reading committee. Undoubtedly, this work has benefited from their input and discussion. To my good friends that were there for me during both the good and tough times, your encouragement, advice, and support will always be remembered. Know that I will always be available to come to your aid whenever called upon. Last, I would like to thank Dr. Brent Carter for his guidance and help with X-ray Photoelectron Spectroscopy, Dr. Marcus Weck for his discussions on oxidation-reduction chemistry and interfacial hydrophobicity, and Dr. Andrés Garcia for his support and input regarding contact angle measurements and hydrophobic interactions.

TABLE OF CONTENTS

LIST OF TABLES

LIST OF FIGURES

SUMMARY

Moisture poses a significant threat to the reliability of microelectronic assemblies and can be attributed as being one of the principal causes of many premature package failures. Since the vast majority of advanced underfills are epoxy based, they have the propensity to absorb moisture, which can lead to undesirable changes in stress and interfacial adhesion. To ensure the reliability and durability of the electronic packages, the effect of moisture must be understood. In addition to being a moisture sensitive property, the interfacial adhesion is also affected by the elastic mismatch, relative mode mixity, temperature, and the corresponding surface chemistry and topology of the adherends. Therefore, the study of the moisture effect on interfacial adhesion is inevitably a multidisciplinary effort.

In this research, a systematic and multi-disciplinary study was conducted to understand the fundamental science of moisture-induced degradation of interfacial adhesion. The research is comprised of both experimental and modeling components of analysis and consists of four primary components. First, the moisture transport behavior within underfill adhesives is experimentally characterized and incorporated into a finite element model to depict the moisture ingress and interfacial moisture concentration for each respective level of moisture preconditioning. Second, the effect of moisture on the variation of the underfill elastic modulus is demonstrated and the physical mechanisms for the change identified. Third, the aggregate effect of moisture on the interfacial

fracture toughness of underfill to both copper and FR-4 board substrates is determined. This includes the primary effect of moisture being physically present at the interface and the secondary effect of moisture changing the elastic modulus of the adhesive when absorbed. Last, the recovery of both the elastic modulus and interfacial fracture toughness from moisture preconditioning is assessed with reversible and irreversible components identified. Using adsorption theory in conjunction with fracture mechanics, an analytical model is developed that predicts the loss in interfacial fracture toughness as a function of moisture content. The model incorporates key parameters relevant to the problem of moisture in epoxy joints identified from the experimental portion of this research, including the interfacial hydrophobicity, active nanopore density, saturation concentration, and density of water.

This research results in a comprehensive understanding of the primary mechanisms responsible for the interfacial degradation due to the presence of moisture. The experimental results obtained through this research provide definitive data for the electronics industry to use in their product design, failure analysis, and reliability modeling. The predictive model developed in this research provides a useful tool for developing new adhesives, innovative surface treatment methods, and effective protection methodologies for enhancing interfacial adhesion.

CHAPTER I

INTRODUCTION

Moisture not only poses a significant threat to the reliability of microelectronic assemblies, but also to any component where maintaining the integrity of the adhesive joint is a critical consideration. Adhesively bonded structures in aerospace, structural, and electronic packaging applications can attribute moisture as being one of the principal causes of many premature joint failures. Although moisture is a primary factor when considering the reliability of these adhesive joints, the interfacial and material constitutive damage behavior from moisture exposure is not entirely understood.

The loss of adhesion due to moisture is governed by two fundamental mechanisms. The first is the rate at which moisture is delivered to the interface. The second is the response of the interfacial adhesion to varying levels of moisture concentration, which includes both the primary effect of moisture being present directly at the interface and the secondary effect of changes in the mechanical properties of the adhesive and adherend due to moisture uptake. Mass transport and in particular the diffusion of moisture in epoxy adhesives has been studied by several sources and is fairly well established; however, the response of interfacial adhesion to moisture is much less understood. Much of the current knowledge has resulted from joint strength measurements of epoxy / metal

interfaces. Limited work has been published regarding the extent that the loss in adhesion from moisture is recoverable; consequently, adhesion recovery from moisture is not well understood. Even less information is available regarding how moisture affects the interfacial fracture toughness of adhesively bonded structures. Since interfacial fracture mechanics characterizes the intrinsic adhesion of the interface, universal relationships can be established that are independent of specimen geometry. However, only a small handful of studies have addressed the issue of moisture, and much more experimental data is needed to establish the relationship of moisture to interfacial fracture toughness. Since there exists this lag in experimental data, even less effort has been spent on developing predictive models that account for the effect of moisture on interfacial adhesion.

In this research, a systematic and multi-disciplinary study is conducted to better understand the fundamental science of moisture-induced degradation of interfacial adhesion. The research is comprised of both experimental and modeling components of analysis and addresses some of the key issues needed to advance the understanding of the effect of moisture on interfacial adhesion:

1. Determines the role of moisture to observed changes in interfacial adhesion as a function of increasing interfacial moisture concentration. This includes both the primary effect of increasing moisture concentration levels directly at the interface and the secondary effect of changes in the mechanical properties of the adhesive and adherend due to moisture uptake.

2. Establishes the moisture absorption characteristics and mechanical response of no-flow underfill to increasing moisture concentration levels, outlining how the moisture present in the underfill can affect the interfacial adhesion. This includes identifying the contributions of moisture induced swelling stresses, moisture transport behavior, and changes in the elastic modulus from moisture uptake in the underfill to the interfacial adhesion.
3. Identifies both reversible and irreversible components of damage from moisture uptake in both the underfill and interface to aid in the development of new materials and adhesion mechanisms to increase the service life of components exposed to humid environments.
4. Investigates the role of interfacial hydrophobic interactions to the performance of interfacial fracture toughness in the presence of moisture.
5. Considers the possible existence of a critical concentration of water, which is a proposed threshold concentration of moisture below which there is no observed loss in interfacial adhesion irrespective of the length of time of exposure, and relates the debated phenomena to the interfaces and materials evaluated in this study.

The structure of this thesis is organized into eight chapters. Chapter II reviews the pertinent background material related to microelectronics, interfacial fracture mechanics, and important considerations regarding moisture effects on interfacial fracture. Chapter III details the experimental materials studied, specific testing

equipment used, and the motivation for performing particular tests for this research. Chapters IV - VII are devoted to discussing the results obtained from both experimental and modeling components of analysis. Chapters IV and V present the moisture absorption characteristics and the elastic modulus response of no-flow underfill to accelerated testing conditions respectively. Chapter VI details the interfacial fracture toughness results of the underfill / copper interface and the underfill / FR-4 board interfacial test specimens, demonstrating both the primary effect of increasing interfacial moisture concentration and the secondary effect of the change in the adhesive elastic modulus from moisture uptake on the interfacial fracture toughness of each interface. Chapter VI also discusses the effect of moisture on altering the interfacial fracture failure path, the hygro-swelling and thermal expansion mismatch strains at the interface, and the role of interfacial hydrophobicity on the behavior of moisture at the interface. A predictive model is presented at the end of Chapter VI that characterizes the loss in interfacial fracture toughness as a function of moisture content. Chapter VII presents the recovery behavior from moisture uptake of both the underfill elastic modulus and the interfacial fracture toughness of the underfill / copper interface after complete removal of moisture from drying, detailing both the reversible and irreversible damage components from exposure to moisture. Last, Chapter VIII discusses the major conclusions of this study as well as provides recommendations for future research.

CHAPTER II

BACKGROUND

2.1 Brief Overview of Electronic Packaging

Electronic packaging refers to the science and technology of providing a suitable environment for an electronic device to perform reliably over a given period of time. The functions of an electronic package are to protect, power, and cool the microelectronic chips or components and provide electrical and mechanical connection between the microelectronic part and the outside world (Tummala, 2001). At a rudimentary level, the insulation used to protect wires can be considered a very primitive electronic package.

Since electronic systems consist of several layers of packaging, with each level of packaging possessing its own devices for signal distribution, power distribution, heat removal, and environmental protection methods, packaging hierarchy can be divided into the following interconnection levels: zero-level packaging, first-level packaging, second-level packaging, third-level packaging, and fourth-level packaging. Zero-level packaging refers to all techniques and processes for gate-to-gate interconnections on a silicon chip. First-level packaging refers to the technology required to form the interconnections between silicon dies and chip packages. These interconnections are typically formed

using either wire bonding, flip chip bonding, or tape automated bonding (TAB) techniques. Second-level packaging refers to all the techniques and processes involved in forming the interconnections between an integrated circuit (IC) to printed wiring boards. Common techniques used in second-level packaging include pin through hole (PTH) and peripheral surface mount technology (SMT). Third-level packaging refers to the connections between second-level packages by assembling onto a mother board or backplane. Fourth-level packaging refers to an entire system with connections between several subassemblies such as boards, racks, and frames. It is important to keep in mind that with technology continuously evolving the distinction between the aforementioned levels of electronic packaging hierarchy can at times be blurred. A schematic of the various levels of electronic packaging hierarchy is shown in Figure 1.

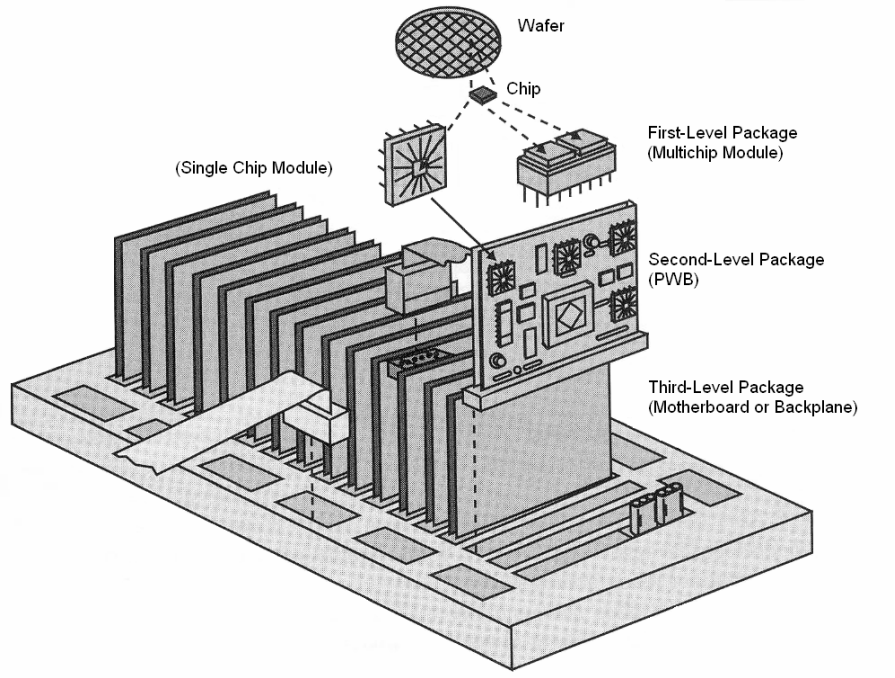

Figure 1. Schematic of electronic packaging hierarchy (Tummala, 2001)

Although the exact date attributed to the advent of electronic packaging is difficult to establish due to the diversity in opinion as to what exactly constitutes an electronic package, the beginning of modern electronic packaging can probably be dated around 1950, shortly after the invention of the transistor in 1949 by Brattain, Bardeen, and Shockley at Bell Labs (Brown, 1999). Early transistors were housed in plastic packages, which made them highly susceptible to environmental degradation. With a push for increased reliability from the military, these transistors were quickly replaced by the development of the metal transistor outline (TO) package, which hermetically sealed the transistor within an inert atmosphere using a metal lid. By the 1960s, the need to reduce manufacturing costs in conjunction with satisfying the large number of input/ouput (I/O) requirements for the integrated circuit (IC) led to the development of the ceramic flatpack, metal flatpack, and dual-in-line package (DIP) packages. In response to the need for a higher density printed wiring board (PWB), the 1970s and 1980s saw the development of the quad-flat package (QFP) and surface mount technology (SMT). Since packages used in SMT have leads that do no penetrate the PWB like those of pin-through-hole (PTH) packages, they can be mounted on both surfaces of the PWB. Driven by the need to make electronic products smaller, more powerful, and available at a lower cost, the ball grid array (BGA) package and chip scale package (CSP) were developed in the 1990s. These packages offered several advantages to the QFP package, including higher I/O density by utilizing the full area for I/O connections and shorter electrical paths yielding better electrical performance (Tummala, *et al.*, 1997). Both of these packages emerged from flip chip technology, which utilizes

the area underneath the chip for I/O connections rather than just the perimeter of the chip. A summary of the evolution of modern electronic packaging is given in Figure 2 and Table 1.

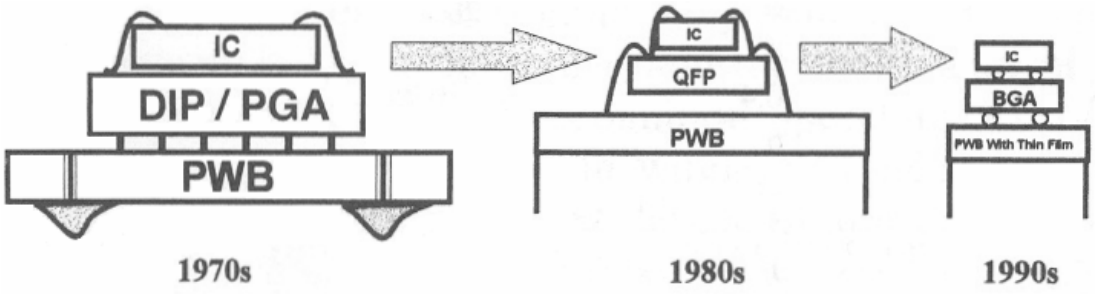

Figure 2. Modern electronic packaging evolution (Tummala, 1997)

Table 1. Modern electronic packaging evolution (Tummala, 1997)

	Past		Current		Future
	1970s	1980s	1990s	2000	2005
Chip connection	Wire bond	Wire bond	Wire bond	Flip chip	Low-cost flip chip
Package	DIP	PQFP	P/C-BGA		None
Package assembly	PTH	SMT	BGA-SMT		None
Passives	C-discretes	C-discretes	C-discretes	C-discretes	Intergrated
Board	Organic	Organic	Organic	DCA to board	SLIM
No. of levels	3	3	3	1	1
No. of types of components	5-10	5-10	5-10	5-10	1
Si efficiency (%)	2	7	10	25	>75

With the advent of SMT and flip-chip technology, several adaptations to modern module assembly techniques have been made to accommodate these new developments.

The four primary assembly processing techniques used in modern module SMT assembly today are Solder Paste Printing (Process 1), Discrete Fluxing Station (Process 2), Integrated Flux-Placement Process (Process 3), and Low Cost Next Generation Process (Process 4). Each process offers its own unique advantages and disadvantages, and an outline of each process is provided in Figure 3 and discussed below.

Figure 3. Four primary assembly processing techniques used in modern module SMT assembly (Baldwin, 2000)

Process 1, Process Using Solder Paste Printing, uses solder paste as the mechanism to join package interconnects to the footprints on the substrate. It is primarily used for SMT and some flip chip applications. The assembly steps for process 1 are shown in Figure 3. Solder paste is applied to the substrate by utilizing a squeegee action through a stencil into aperture holes. The stencil corresponds to the exact footprint of the package to be placed as well as the location of the footprint on the substrate. The solder paste literally rolls by the squeegee action, promoting filling of apertures in the stencil with the solder paste. Stencil printing can either be contact (stencil is touching the board) or noncontact (stencil is slightly raised from the board). Noncontact stencil printing offers the benefit of not having to be concerned with stencil release from the printed solder paste; however, this benefit comes at the expense of a decrease in printing accuracy. Primary advantages of Process 1 include standard sizes and footprints, high speed SMT compatible, low cost due to relatively shorter assembly time, and large infrastructure. Disadvantages include low interconnect density, reduction in yields for fine pitch SMT assembly, package handling, and large footprint requirements. As package interconnect density increased, solder paste technology became obsolete as a result of solder paste printing limitations. The increase in interconnect density required a more dense aperture spacing on the stencil, which introduced more adhesion between the solder paste and stencil, and thus made it more difficult to get a clean release using contact stencil printing. The increase in package interconnect density also was a barrier for noncontact stencil printing due to accuracy limitations. As a result, solder was

directly manufactured onto the flip chip site bumps, which lead to the development of Process 2.

Process 2, Discrete Fluxing Station, still utilized the placement of SMT components using solder paste technology, but had the added benefit of now being able to place higher density interconnect devices as well (see Figure 3). These devices did not utilize solder paste printing, but rather already incorporated solder into the bump sites. This has the added benefit of being able to place more dense components onto the substrate, but also has the disadvantage of requiring a flux application onto the board before chip placement, introducing longer assembly times if used in conjunction with packages requiring solder paste placement. This step is needed when solder paste is not used, which already contained the flux within the paste itself. Recognizing this increase in manufacturing time led to the development of Process 3.

Process 3, Integrated Flux-Placement Process, is very similar to Process 2, but has the added benefit of a decrease in manufacturing time (see Figure 3). This decrease occurs by having the flip chips dipped in flux during chip placement, rather than dispensing flux directly onto the board in a separate manufacturing step. This benefit increased profit by deceasing overall manufacturing time and made the overall process assembly more efficient. Recognizing that there was still room for improvement led to the development of Process 4.

Process 4, Low Cost Next Generation Process, addresses the issue of underfill application to reduce overall manufacturing assembly time. Underfill is a thermoset polymer that is applied between the chip and substrate to dramatically increase package

life. The underfill provides a medium that reduces localized stress concentrations on the solder interconnects and aids in the thermal expansion mismatch between the chip and board. The previous three assembly processes use a conventional underfill application. The conventional underfill process utilizes capillary action of the underfill polymer to evenly and fully distribute the underfill between the chip and board. The underfill is dispensed on either one edge or two edges of the chip, utilizing the capillary action to evenly distribute the underfill to the other side of the chip. The time required for the capillary action to completely distribute the underfill between the chip and board could take several seconds to a few minutes to fully develop. This capillary flow time requirement is complicated even further for larger chips with greater surface areas. In addition, some conventional underfills can take at least an hour to cure. Recent developments in underfill technology have introduced fast flow, snap cure underfills, which have significantly quicker capillary flow times (about 10 seconds) and underfill cure times (about 10 minutes). Yet even with this improvement in capillary flow and underfill cure time, conventional underfill processes still represent a bottleneck in packaging assembly. This disadvantage has been tolerated due to the tremendous added benefit of the significant increase in package reliability with the use of underfills (Suryanarayana, *et al.*, 1991). This led to the development of no-flow underfills and hence Process 4, the Low Cost Next Generation Process.

Process 4 represents a significant reduction in package assembly time (see Figure 3). Rather than utilizing capillary flow to evenly dispense the underfill between the chip and substrate as in a conventional underfill assembly process, a compression underfill

process is used and occurs when the chip is placed. By already having dispensed the no-flow underfill directly onto the package footprint on the board, the underfill is evenly distributed between the chip and board as the chip is placed onto the board. In addition, the underfill is simultaneously cured as the chip undergoes solder reflow, eliminating the need for a separate underfill cure process. The flux is incorporated into the no-flow underfill, thus eliminating the need for dispense or dip flux application. A comparison outlining the assembly steps for both conventional and no-flow underfill assembly is shown in Figure 4.

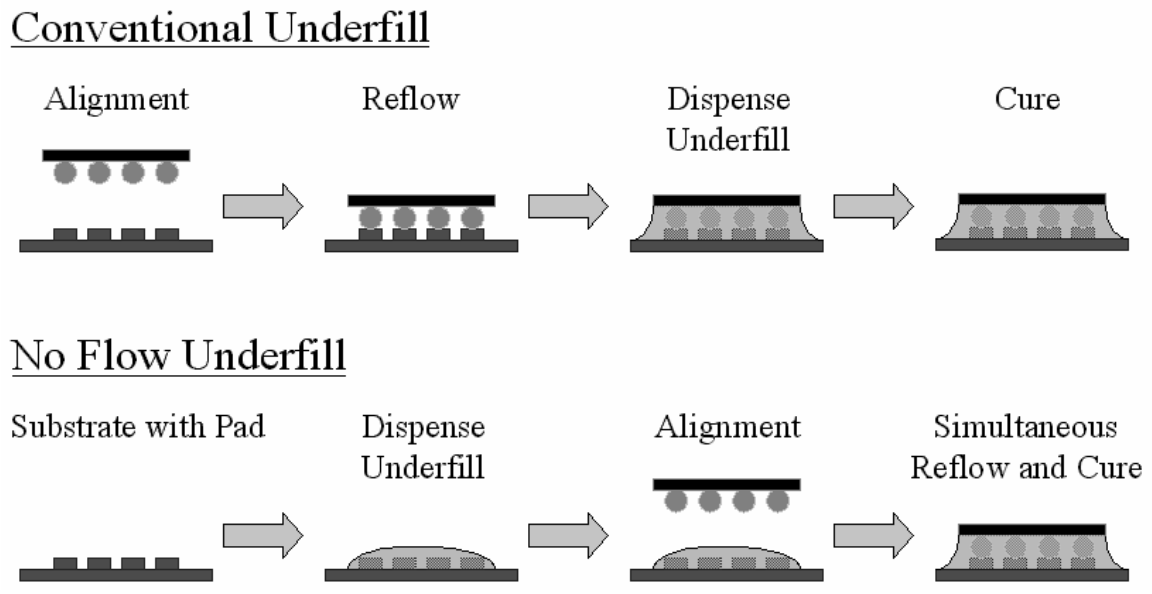

Figure 4. Conventional vs. no-flow underfill assembly process

The improvements introduced by Process 4 significantly reduce the manufacturing time and increase the factory floor space by removing the need for

separate underfill cure ovens. In addition, the chip is always protected by the underfill since it is simultaneously cured in solder reflow, rather than leaving the package interconnects unprotected during solder reflow. A disadvantage of no-flow underfills is the relative availability as a result of being a new product. In addition, no-flow underfills are more susceptible to moisture absorption than conventional underfills as a result of the lack of silicon filler present in the material. Moisture absorption is a significant concern in the packaging industry and can lead to several types of premature package failures such as corrosion, hygro-swelling, localized delamination, and polymer degradation. No-flow underfills were originally developed at Georgia Tech and are gradually being implemented by some industries. More research is needed to identify the limitations and reliability concerns when using no-flow underfills in package assembly.

2.2 Delamination in Microelectronics

Central to the long term reliability and life prediction of microelectronic assemblies is a rooted understanding in the interfacial failure mechanisms and associated debonding behavior of the interfaces within these assemblies. With the advent of flip-chip technology to accommodate the increasing demand in both cost and performance requirements of modern microelectronic packaging, the need for improved understanding in delamination of these assemblies has taken on added importance. This primarily arises due to the fact that one of the keys to the success of flip-chip technology lies in

development of underfill, which is an epoxy based encapsulant that mechanically couples the chip to the board. Underfill drastically enhances the reliability of microelectronic assembles when compared to unencapsulated devices (Suryanarayana, *et al.*, 1991), provided that the structural integrity of the adhesive bond between the underfill and the printed wiring board, solder mask, copper, silicon, chip passivation, and solder is maintained. Although delamination of the underfill in the microelectronic assembly tends to cause near immediate failure as soon as it reaches a solder joint, until recently the factors that affect the strength and durability of these interfaces have not been investigated and are the focal points of current studies in reliability research in microelectronic packaging (Fan, *et al*., 2002; Ferguson and Qu, 2002; and Dai, *et al*., 2000).

Another significant area of concern in microelectronic packaging occurs at the interface between the copper alloy lead frame and the epoxy mold compound. Due to its relatively low cost in conjunction with its high electrical and thermal conductivity, copper alloys are widely used as a lead frame material. However, the epoxy/copper interface has poor interfacial adhesion strength and relatively high residual stress, which predisposes it to delamination. The copper surface is also highly susceptible to oxidation, which is an additional consideration when evaluating the interfacial adhesion of interfaces involving copper (Chung, *et al*., 2002, and Kim, S., 1991). The delamination between the copper lead frame and the mold compound adversely affects the durability of these packages and is a common failure mode during the qualification process. In addition, the delamination can affect long term package reliability by yielding enchanced

transport of moisture along the epoxy/copper interface through moisture wicking. The moisture penetration can result in corrosion of the copper, as the corrosion process will be accelerated if the moisture is a carrier of ionic impurities from the surrounding external environment (Yoshioka, *et al.*, 1989). Consequently, the epoxy/copper interface is another significant area of concern in microelectronic packaging reliability, as several studies continue to investigate this topic to better understand the durability and failure mechanisms of this interface (Lee and Qu, 2003; Cho, K. and Cho, E., 2000; and Kim, J., *et al*., 2000).

2.3 Interfacial Fracture Mechanics

When applied to cracks at bimaterial interfaces, homogeneous fracture mechanics must be modified to account for the elastic mismatch across the interface. Consider a crack tip region for an interface crack formed between two linearly elastic, homogenous, isotropic materials as shown in Figure 5, where E_1, E_2 and ν_1, ν_2 are the respective Elastic moduli and Poisson's ratios of the bonded materials.

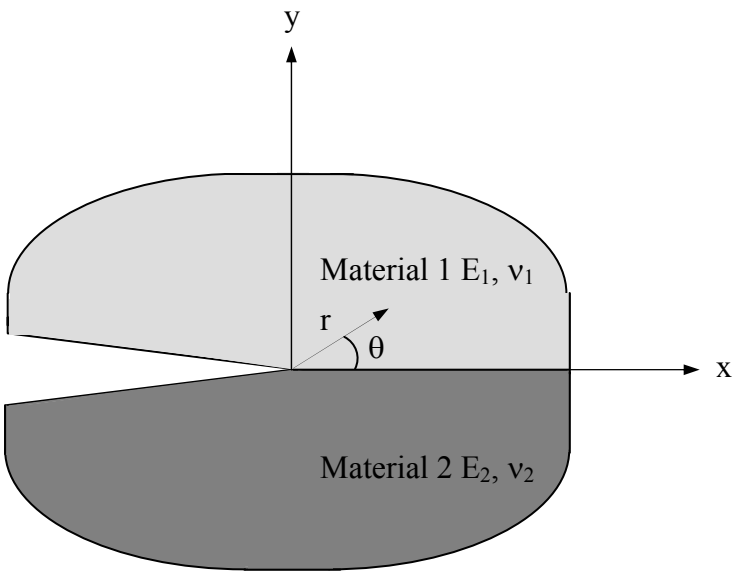

Figure 5. Bimaterial with an interface crack

Dundurs (1969) observed that the elastic dependence for the bimaterial system could be expressed by using the following two nondimensional parameters:

$$\alpha = \frac{\mu_1(\kappa_2 + 1) - \mu_2(\kappa_1 + 1)}{\mu_1(\kappa_2 + 1) + \mu_2(\kappa_1 + 1)} \tag{2.1}$$

$$\beta = \frac{\mu_1(\kappa_2 - 1) - \mu_2(\kappa_1 - 1)}{\mu_1(\kappa_2 + 1) + \mu_2(\kappa_1 + 1)} \tag{2.2}$$

where $\kappa_i = 3 - 4\nu_i$ for plane strain and $\kappa_i = (3 - \nu_i) / (1 + \nu_i)$ for plane stress. The parameter α is a measure of the mismatch in the plane tensile modulus across the interface, whereas the parameter β is a measure of the mismatch in the in-plane bulk

modulus. Note that α will approach (–1) if material 1 is extremely compliant to material 2 and approach (+1) if material 1 is extremely rigid. In addition, both α and β will naturally change sign if the two materials are exchanged, and they will vanish when there is no mismatch across the interface.

As a bimaterial interface fractures, the mechanical property mismatch between the two materials results in shear stresses being induced by tensile stresses, and vice versa. Therefore, a bimaterial interface under pure mode I loading, K_I, will yield both K_1 and K_2 locally at the crack tip (Charalambides, *et al.*, 1992). For a two-dimensional system the complex stress intensity factor, K, is given by:

$$K = K_1 + iK_2 \tag{2.3}$$

where $i = (-1)^{1/2}$ and K_1 and K_2 have the dimension of [stress][length]$^{1/2 - i\varepsilon}$. The parameter ε is a nondimensional quantity defined as:

$$\varepsilon = \frac{1}{2\pi} ln\left[\frac{1-\beta}{1+\beta}\right] \tag{2.4}$$

The tractions at the bimaterial interface at a distance r ahead of the crack tip take the form (Shih, 1991):

$$(\sigma_{yy} + i\sigma_{yx})_{\theta=0} = \frac{(K_1 + iK_2)r^{i\varepsilon}}{\sqrt{2\pi r}} \tag{2.5}$$

where $r^{i\varepsilon} = \cos(\varepsilon \ln r) + i\sin(\varepsilon \ln r)$. This represents an oscillatory stress singularity as the crack tip is approached ($r = 0$). Note that if $\varepsilon = 0$, both K_1 and K_2 play similar roles as the classical, homogenous stress intensity factors K_I and K_{II}, which measure the normal and shear stress singularity respectively.

Since K is a complex number with a material dependent dimension, it is more convenient to evaluate the state of stress at a fixed length, L, from the crack tip (Rice, 1988):

$$(K_1 + iK_2)L^{i\varepsilon} = \left|(K_1 + iK_2)\right|e^{i\psi} \tag{2.6}$$

with the mode mixity (or phase angle) being defined as:

$$\psi = \tan^{-1}\left(\frac{\mathrm{Im}(KL^{i\varepsilon})}{\mathrm{Re}(KL^{i\varepsilon})}\right) \tag{2.7}$$

The mode mixity for a test specimen requires the specification of some length quantity, L. The choice for L is arbitrary, but should be selected as a fixed length and reported with the calculated values for the mode mixity. This is necessary since the value

of the length quantity will affect the calculated value for ψ as shown in Equation 2.7 (recall $K = K_1 + iK_2$).

Interface toughness is defined as the critical value of the energy release rate, G_c, at which the bimaterial interface will begin to delaminate. It is not a single material parameter, but rather a function of the mode mixity, ψ, which measures the relative amount of "mode 2" to "mode 1" acting on the interface (Hutchinson and Suo, 1992). The stress intensity factor for a bimaterial interface is related to the energy release rate through the following relation (Malyshev and Salganik, 1965):

$$G = \frac{(1-\beta^2)}{E_*}(K_1^2 + K_2^2) \tag{2.8}$$

where

$$\frac{1}{E_*} = \frac{1}{2}\left(\frac{1}{\overline{E_1}} + \frac{1}{\overline{E_2}}\right) \tag{2.9}$$

$$\overline{E_i} \equiv \frac{E_i}{(1-\nu_i^2)} \quad \text{for plane strain} \tag{2.10}$$

$$\overline{E_i} \equiv E_i \qquad \text{for plane stress} \tag{2.11}$$

By measuring the critical load at which fracture occurs, P_c, the critical stress intensity factor, K_c, and corresponding critical value of the energy release rate, G_c, can be

determined for a given value of the mode mixity, ψ. A representative interfacial toughness curve as a function of mode mixity is shown in Figure 6.

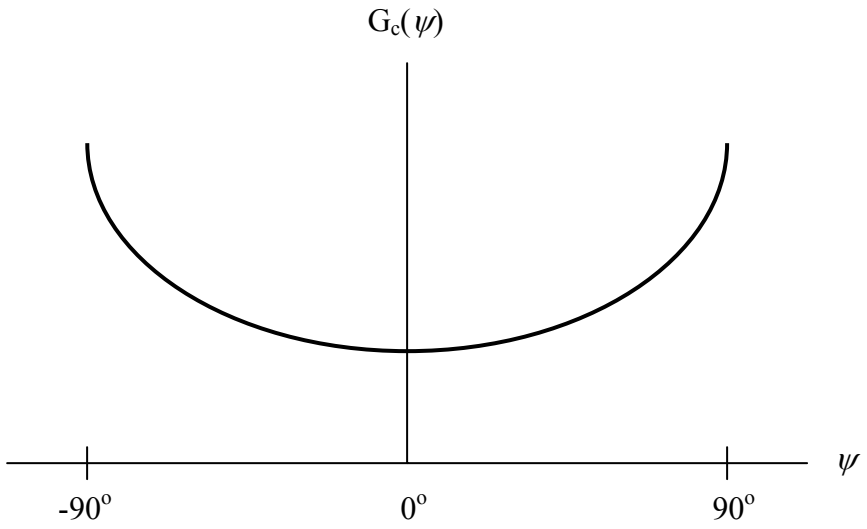

Figure 6. Representative interfacial toughness curve as a function of mode mixity

2.4 Interfacial Fracture Test Methods

A variety of test methods have been developed to determine the interfacial toughness of bimaterial specimens in recent years. All of these methods share the common principle of experimentally measuring the critical load at which fracture occurs, P_c, to calculate the corresponding critical value of the energy release rate, G_c, for a given value of mode mixity, ψ. Each method provides its own unique advantages and disadvantages for bimaterial toughness measurement, allowing the experimenter a variety

of options for interfacial toughness testing of samples for different specimen geometries and sample construction restrictions.

Charalambides, *et al.*, (1989), Hutchinson and Suo (1992), and Yan and Agarwal (1998) have developed interfacial test methods that utilize a bimaterial flexural beam specimen. A symmetric precrack is induced along the specimen interface as shown in Figure 7.

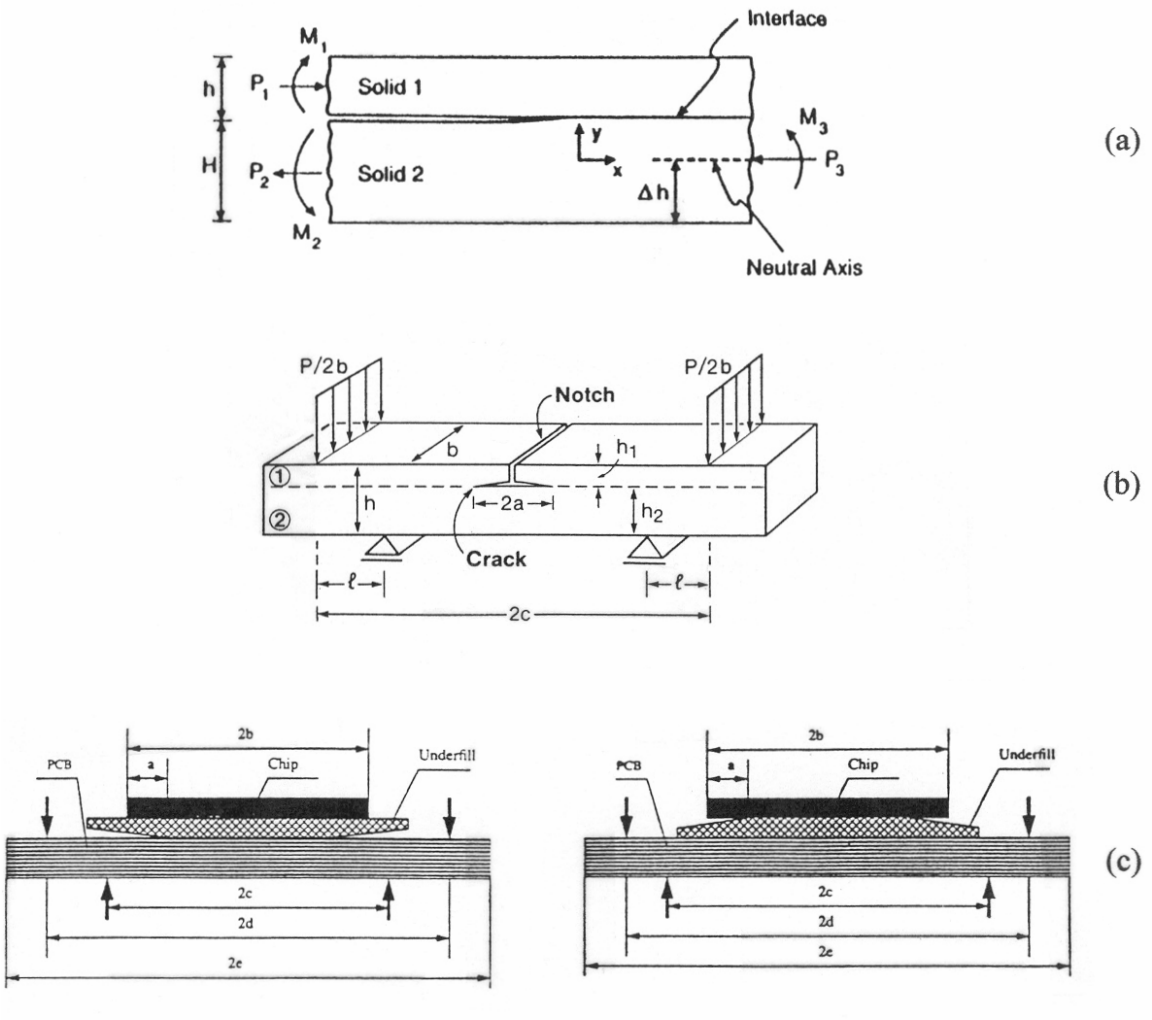

Figure 7. Schematics of four point bending interfacial test specimens with symmetrical interface cracks for (a) Hutchinson and Suo (1992), (b) Charalambides, *et al.*, (1989), and (c) Yan and Agarwal (1998)

Specimens are loaded in pure bending through the use of a four point bend fixture to measure the interfacial toughness. An analytical solution can be obtained for the interface cracks located between the inner loading points. Varying the specimen thickness ratio (h_1 / h_2) will alter the corresponding phase angle; however, most phase angle values will be of intermediate magnitude. Unfortunately this test method cannot provide interfacial toughness data over the entire range of phase angles, yet it is capable of generating consistent mixed mode interfacial fracture results, which are representative of practical delamination problems.

Another test method developed to measure interfacial toughness has been presented by Xiao, *et al.*, (1993). This test method utilizes an asymmetric double cantilever beam specimen (ADCB) as shown in Figure 8.

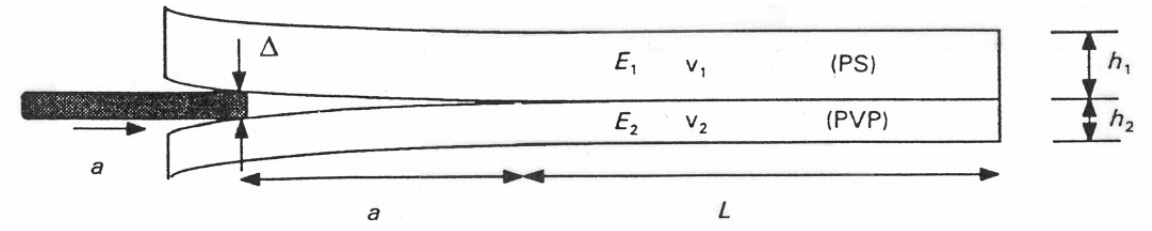

Figure 8. Schematic of an ADCB interfacial test specimen (Xiao, *et al*., 1993)

As with the previously mentioned test methods, interfacial toughness data cannot be obtained over the entire range of phase angles; however, a primary advantage of this test method is that numerous interfacial fracture tests can be performed from a single specimen to calculate a mean value of G_c, and hence increase the accuracy of the test.

Sundararaman and Davidson (1995) have proposed three test methods to generate interfacial toughness data over the entire range of phase angles for bimaterial interfaces. The three test methods consist of a unsymmetric double cantilever beam (UDCB), a single leg bending (SLB), and a unsymmetric end-notched flexure test (UENF) as shown in Figure 9.

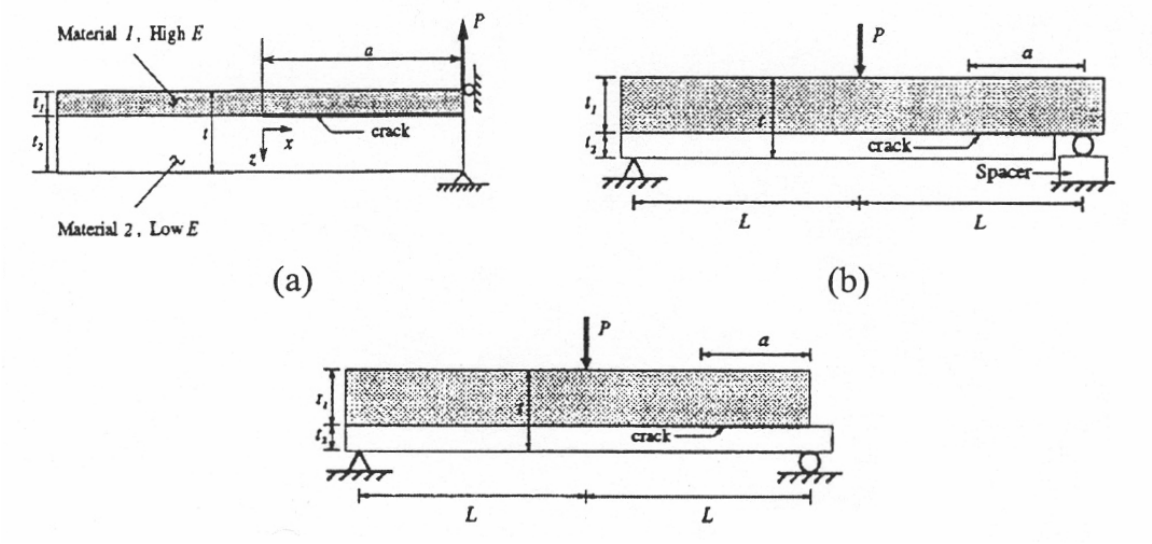

Figure 9. Schematics of (a) UDCB, (b) SLB, and (c) UENF interfacial test specimens (Sundararaman and Davidson, 1995)

Each test method focuses on a particular range of mode mixity values, with the UDCB producing small magnitude phase angle values, the SLB producing intermediate magnitude phase angle values, and the UENF producing large magnitude phase angle values. By varying the thickness ratio of each bimaterial specimen while keeping the overall specimen thickness constant, interfacial toughness values can be determined over the entire range of phase angles.

Other test methods include the Brazil-nut sandwich specimens (Suo and Hutchinson, 1989, and Kuhl, 1998), thin-layer sandwich specimens (Suo and Hutchinson, 1989; Thurston and Zehnder, 1993; and Pang and Seetoh, 1997), and brazilian disks (O'Dowd, *et al.*, 1992); however, all of these tests require a more difficult sample preparation, intricate loading fixtures, and specific sample geometry restrictions.

2.5 Variables Affecting Interfacial Fracture

There are several factors to be considered in interfacial adhesion. Such factors include the material and physical properties of the adhesives, the bulk and surface characteristics of adherends, and the nature of the forces involved in the bonding (Lee, 1979). Loss of adhesion resulting in delamination intensifies singular stress behavior, inducing higher stress concentrations between the adherend and adherate. This will result in more rapid crack growth than in comparison with undamaged devices (Vroonhoven, 1993).

Interfacial fracture toughness is defined as the critical value of the energy release rate, G_c, at which the bimaterial interface will begin to delaminate. It is not a single material parameter, but rather a function of the mode mixity, ψ, which measures the relative amount of "mode 2" to "mode 1" acting on the interface (Hutchinson and Suo, 1992). As a bimaterial interface fractures, the mechanical property mismatch between the two materials results in shear stresses being induced by tensile stresses, and vice

versa. Therefore, a bimaterial interface under pure mode I loading, K_I, will yield both K_1 and K_2 locally at the crack tip (Charalambides, *et al.*, 1992).

Surface processing of the adherend prior to bonding has been widely considered an important procedure in the preparation of reliable joints. Cui, *et al*., (1998) found that both surface roughening and chemical treatment of copper leadframe significantly increased the adhesion of epoxy compounds to the copper even after thermal simulation and temperature/humidity exposure. Kook, *et al*., (1998) showed that by increasing the surface roughness of the copper substrate prior to polymer bonding, interfacial fracture resistance values increased nearly three fold compared to the interfacial fracture resistance obtained using polished substrates.

Chemical bonding enhancement has also proven to successfully increase the adhesion of various underfill interfaces. Vincent, *et al*., (1998) demonstrated that the adhesion of the underfill to die and substrate surfaces could be improved by the addition of silane coupling agents to the underfill. Yao (2000) supports this result by concluding that the change of elastic modulus of the cured underfill induced by silane additives is not significant, yet he found interfacial adhesion values to increase by the addition of silane to the underfill, thus indirectly indicating that the chemical bonding across the interface enhanced by the silane coupling agent contributes to improve interfacial adhesion between the underfill/substrate interfaces. However, it should be noted that the degree of interfacial toughness enhancement depends on the type of silane additive and substrate used.

Last, environmental factors such as temperature and moisture can also have an adverse effect on adhesion. Ferguson and Qu (2002) showed that interfacial fracture toughness is significantly affected by the presence of moisture, with the interfacial adhesion of two different underfill/solder mask interfaces decreasing by approximately one half after 725 hours of exposure at 85^{o}C/85%RH. Gledhill and Kinloch (1974) tested joints consisting of a mild steel substrate and an epoxy adhesive at 20^{o}C/56%RH and submersion in water at 40^{o}C, 60^{o}C, and 90^{o}C for up to 2500 hours. They found that the 20^{o}C/56%RH specimens suffered no significant change in joint strength; however, all specimens submerged in water resulted in a significant loss in joint strength. They also noted that joints exposed to 20^{o}C, 40^{o}C, 60^{o}C, and 90^{o}C and 0%RH had no significant loss in joint strength even after prolonged exposure. Consequently, the testing temperatures themselves did not contribute to the loss of joint strength, and all the observed losses in joint strength were attributed to moisture. Similarly, Cotter (1977) showed that after 4 years of exposure of epoxy-polyamide/aluminium-alloy joints to a hot-wet tropical environment resulted in a significant loss in die shear strength, whereas the same amount of exposure to a hot-dry climate had little effect in die shear strength. As a result, the deleterious effect of moisture was much more damaging to the bond strength of the joints than temperature when comparing the two environments. Although the temperature had no effect in the two aforementioned studies, Kinloch (1979) warns that in general temperature will affect the durability of adhesive joints, with an increase in temperature generally yielding an increase in the rate of strength loss. However, a study by Ramani, *et al*., (2000) found that lap shear joints consisting of a low-modulus

thermoset adhesive bonded to fiber-reinforced plastics (FRP) and galvanized steel had a higher lap shear strength for joints exposed to 60^{o}C for 6 weeks when compared to controls kept at laboratory conditions (23 ^{o}C). Consequently, temperature actually increased the lap shear strength of the joints. Based on the results of the above studies, it is clear that both temperature and moisture can play a critical role in interfacial adhesion.

2.6 Moisture Effects on Interfacial Fracture

Since many contemporary electronic packages utilize epoxy based materials such as underfill and molding compounds, they are highly susceptible to moisture absorption, which can lead to undesirable changes in mechanical performance and interfacial adhesion. Consequently, moisture can be attributed as being one of the principal causes for many premature package failures. Central to understanding the effect of moisture to interfacial adhesion in microelectronic assemblies is to first identify the rate as which moisture is delivered to the interface, followed by understanding the response of the interfacial adhesion to increasing levels of moisture concentration. Moisture can affect the interfacial adhesion both directly by being physically present at the interface itself and indirectly by changing the mechanical properties of the adhesive and substrate due to moisture uptake. Moisture can also cause both reversible and irreversible damage to interfacial adhesion. Therefore a comprehensive study on the effect of moisture on interfacial adhesion in microelectronic assemblies will need to consider moisture

transport to the interface, moisture effects on epoxy adhesives, moisture effects at the interface, and recovery of adhesion and bulk properties from moisture uptake.

2.6.1 Mechanisms for Moisture Transport to the Interface

The loss of interfacial adhesion from moisture is driven by the rate at which moisture is delivered to the interface and the rate of degradation once the moisture reaches the interface. Thus, at the root of characterizing the effect of moisture on interfacial adhesion is first identifying the known mechanisms for moisture transport to the interface. There are three primary mechanisms that contribute to water penetration at the interface in epoxy adhesively bonded structures: bulk diffusion (Soles and Yee, 2000; Soles, *et al*., 2000; Vanlandingham, *et al.*, 1999), wicking along the interface (Bowditch, 1996; Zanni-Deffarges and Shanahan, 1995; Comyn, *et al*., 1994; and Drain, *et al*.,1984), and capillary action associated with micro-cracking (Bowditch, 1996) or channels formed by the addition of fillers (Lu, *et al*., 1998, and Uschitsky and Suhir, 1997) in polymer composites.

The first mechanism for moisture transport to the interface is through bulk diffusion. Diffusion is the result of the continual thermal motion of atoms, molecules, and particles from an area of high concentration to an area of low concentration. Diffusion occurs between environments of different concentration until equilibrium is established producing a homogenous, uniform composition in space. The three primary parameters that have the greatest effect on diffusion rates are the size of the diffusing particles, temperature, and viscosity of the environment. Lighter particles have a higher

velocity for the same kinetic energy as a heavier particle, thus lighter particles diffuse faster than heavier particles. Similarly, an increase in temperature will produce a higher kinetic energy yielding an increase in velocity, thus particles will diffuse more rapidly at elevated temperatures. Last, diffusion is more rapid in a gas than in a solid as a result of less atomic interactions, which retard the diffusion process.

Since the transfer of heat by conduction is also attributed to random molecular motions, it is clear that diffusion is analogous to heat conduction. Fick was the first to adopt Fourier's mathematical expression for heat conduction to quantify diffusion. Fick's First Law states that the rate of transfer of the diffusing particles per plane of unit area is proportional to the concentration gradient measured normal to the plane:

$$F_x = -D\frac{\partial C}{\partial x} \tag{2.12}$$

where F_x is the diffusion flux in the x direction, D is the diffusion coefficient, and $\partial C/\partial x$ is the concentration gradient. The negative sign in the above expression accounts for the fact that diffusion will occur in the opposite direction of increasing concentration. In addition, the expression is only valid for an isotropic medium.

Fick's second law of diffusion describes the nonsteady state diffusion of a substance and can be derived using Equation (2.12). Consider a box shaped element in

Cartesian coordinates with point *C(x,y,z)* being at the center of the element and sides of length 2 *dx*, 2 *dy*, and 2 *dz* as depicted in Figure 10.

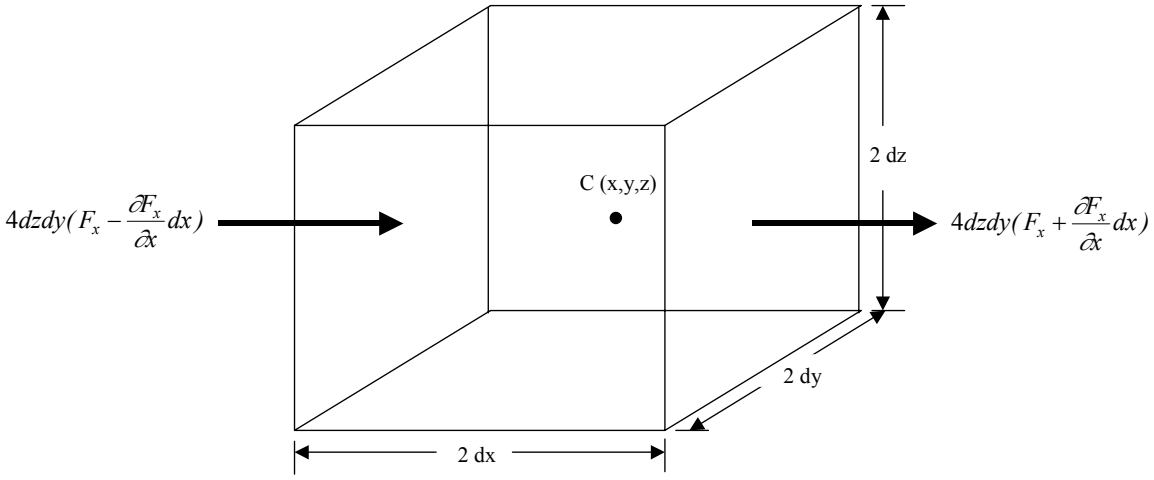

Figure 10. Volume element for derivation of Fick's Second Law of Diffusion

Using Figure 10 and Equation (2.12), Crank (1956) has shown that the following expression can be obtained assuming a constant diffusion coefficient:

$$\frac{\partial C}{\partial t} = D\left(\frac{\partial^2 C}{\partial x^2} + \frac{\partial^2 C}{\partial y^2} + \frac{\partial^2 C}{\partial z^2}\right) \tag{2.13}$$

where *C* is the concentration of the diffusing substance and *D* is the diffusion coefficient. For one-dimensional diffusion along the *x*-axis, the previous relation reduces to the following form:

$$\frac{\partial C}{\partial t} = D\left(\frac{\partial^2 C}{\partial x^2}\right) \tag{2.14}$$

where the above expression describes the concentration of the diffusing species as a function of both time and space, again assuming a constant diffusion coefficient. Note that the diffusion coefficient has the dimension of $[\text{length}]^2[\text{time}]^{-1}$. Provided that the diffusivity remains constant, strict mathematical solutions to Equation (2.14) exist, and the diffusion coefficient of a material can be experimentally determined by utilizing a test specimen that promotes primarily one-dimensional diffusion (Crank, 1956).

If on the other hand the diffusion coefficient, D, is a function of concentration, C, the one dimensional diffusion equation is written as:

$$\frac{\partial C}{\partial t} = \frac{\partial}{\partial x}\left(D\frac{\partial C}{\partial x}\right) \tag{2.15}$$

where D now depends on the concentration of the diffusant and therefore changes with respect to location. Consequently, if absorption behavior is characterized by a diffusion coefficient that is variable rather than constant, strict mathematical solutions no longer exist (Crank, 1956).

Epoxies are highly susceptible to moisture absorption and constitute a significant portion of microelectronic packaging products and assemblies. A typical epoxy formulation can absorb between 1 - 7 percent weight in moisture, which is due to both the

high polarity of the water molecule and the epoxy surface topology (Soles, *et al*., 1998). Although epoxies are extremely vulnerable to moisture penetration, they are widely used in electronic underfill applications. This is a result of epoxies possessing many attractive characteristics that make them very desirable for underfill applications. Such properties include excellent adhesion to many surfaces, superior thermal resistance, low dielectric constant, and ease of processing (Soles, *et al.*, 2000). In addition, the adhesion and mechanical properties of epoxies can be adapted to meet different requirements by using various additives such as silica fillers. Determining the bulk diffusion characteristic of moisture in epoxy is not only critical to predicting the mechanical response of the bulk adhesive, but also the interfacial adhesion for a given level of moisture preconditioning.

Diffusion of moisture into epoxy resins is affected by several factors; however, surface topology and resin polarity are the primary aspects that affect the equilibrium moisture uptake in epoxy resins. Soles and Yee (2000) have found that water traverses the epoxy network through the network of nanopores that are inherent in the epoxy structure. They have determined the average size of a nanopore diameter to vary from 5.0 to 6.1 Å and account for 3 - 7 % of the total volume of the epoxy material. Since the approximate diameter of a kinetic water molecule is just 3.0 Å, moisture can easily traverse into the epoxy via the nanopores. When attempting to correlate the volume fraction of nanopores to the diffusion coefficient of water, Soles, *et al*., (2000) found that that the volume fraction of nanopores does not affect the diffusion coefficient of water in any of the resins studied. They argued that polar groups coincident with the nanopores

are the rate-limiting factor in the diffusion process, which could explain why the diffusion coefficient is essentially independent of the nanopore content.

Although surface topology can influence moisture penetration into an epoxy, of primary importance is the resin polarity, with the high polarity of the water molecule being susceptible to specific epoxy-water interactions. Less polar resins such as non-amine resins have more enhanced moisture diffusion coefficients than amine-containing resins (Soles and Yee, 2000). Polar sites, such as amine functional groups, provide low energy wells for the water molecules to attach. Figure 11 demonstrates how polar hydroxyls and amines can regulate transport through the nanopores by either blocking or allowing moisture to traverse the epoxy resin depending on the orientation of the resin with respect to nanopore position.

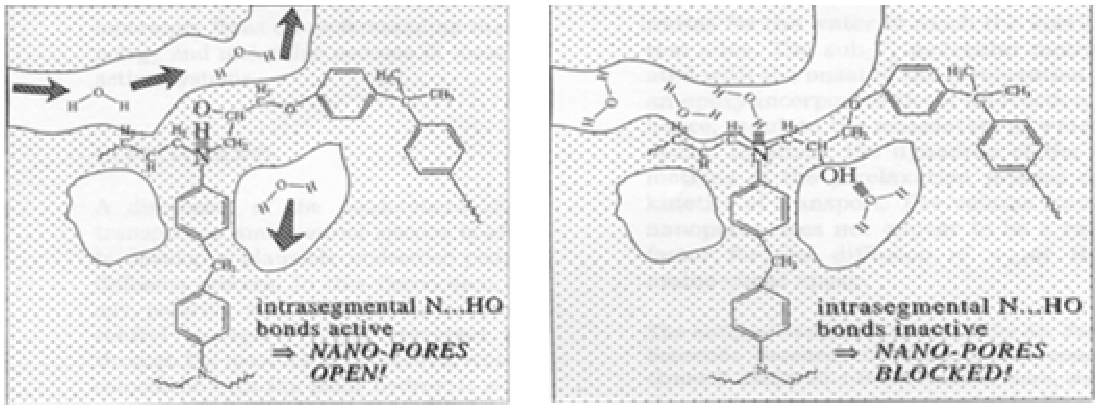

Figure 11. Moisture diffusion through the nanopores of an amine-containing epoxy resin (Soles and Yee, 2000)

Conversely, the absence of hydroxyls and amines in the non-amine resin leads to an enhanced moisture diffusion coefficient as shown in Figure 12.

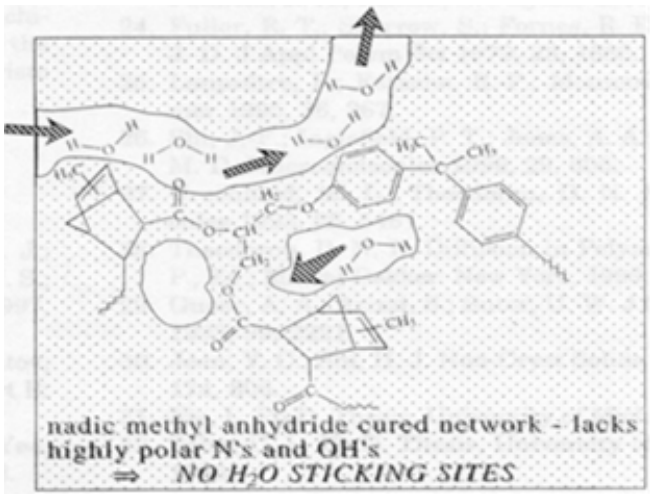

Figure 12. Moisture diffusion through the nanopores of a non-amine epoxy resin (Soles and Yee, 2000)

In addition, non-amine resins absorb very little water relative to more polar resins, such as amine resins. Soles and Yee (2000) have shown that by increasing the crosslink density, the intrinsic hole volume fraction is increased, which yields an increase in the equilibrium moisture content. Steric hindrances located at crosslink junctions open the epoxy matrix to facilitate interactions of water with polar groups, thus increasing the moisture uptake. Depending on the various chemical conformations of the epoxy resin in association with the inherent nanopores present in the epoxy structure, water molecules will behave differently in various epoxy resins.

In addition to Fickian bulk diffusion behavior, non-Fickian behavior can occur in some epoxy systems (Ferguson and Qu, 2001; Wong, *et al*., 1999; Wong and Broutman, 1985). Non-Fickian behavior may be a consequence of two effects. The diffusion may be coupled to a relaxation process or there may be an irreversible chemical reaction occurring between the polymer and moisture such as the formation of hydrogen bonds (Crank and Park, 1968). Jurf and Vinson (1985) have also added that some epoxies have exhibited non-Fickian moisture diffusion caused by microcracking during prolonged humidity exposures at temperatures above 70^{o}C. Uschitsky and Suhir (1997) found that moisture diffusion in epoxy compounds filled with silica and alumina nitride particles used in electronic packaging is non-Fickian, and that the moisture weight gain depends on the specimen's relative humidity and the concentration of fillers. Once the diffusion becomes non-Fickian, strict Fickian mathematical solutions no longer exist and other methods must be implemented to correctly model the moisture distribution within the epoxy. Examples of such methods include an integrated FEA-optimization technique (Wong, *et al*., 1999) and utilization of an effective diffusion coefficient (Ferguson and Qu, 2001).

The second mechanism for moisture transport to the interface is attributed to wicking along the interface. Comyn, *et al.*, (1994) found that the rate of weakening of glass-to-lead alloy joints bonded with an epoxide adhesive could not be accounted for by the rate at which water enters the epoxide adhesive by bulk diffusion alone. They concluded that the water must also enter the interface by "wicking" along debonded zones along the interface. Similarly, Zanni-Deffarges and Shanahan, (1995), observed

that a significantly higher value for the diffusion coefficient (almost an order of magnitude) was obtained when comparing torsional joint absorption data to bulk epoxy absorption data. They concluded that water was entering the joint by seepage close to the interface or in the interphase region by wicking, thus resulting in the over estimate of the diffusion coefficient.

The final mechanism for moisture transport to the interface is by capillary action associated with voids and cracks present in the epoxy or epoxy composite. Although the concept of capillary action is similar to wicking, the distinction lies in that wicking is used to describe enhanced moisture absorption due to voids or cracks at the interface, while capillary action is generally used to describe enhanced moisture absorption due to voids or cracks present inside the bulk adhesive itself. Lu, *et al*., (1998) found that the addition of filler to polymers resulted in faster sorption kinetics when compared to the bulk polymer alone. They concluded that water was not only absorbed by the epoxy, but also by the interfaces inside the epoxy introduced by the addition of filler. Uschitsky and Suhir (1997) arrived at a similar conclusion when evaluating the effect of silica and alumina nitride fillers in epoxy molding compounds used in electronic packaging.

2.6.2 Moisture Effects on Epoxy Adhesives

Throughout the literature, few investigations have taken place to identify the response of the mechanical properties of epoxy adhesives to moisture and more work is still needed to adequately characterize this response (Crocombe, 1997, and Harper, *et al*., 1997). From the work that has been published, it has been found that water absorption

can severely modify the mechanical properties of epoxy adhesives by decreasing the elastic modulus (Wylde and Spelt, 1998; Morgan, *et al*., 1980), shear modulus (Zanni-Deffarges and Shanahan, 1995), yield stress (Wahab, *et al*. 2002), and ultimate stress (Wahab, *et al*. 2002) while increasing the failure strain (Crocombe, 1997) as water concentration increases. A representative stress/strain diagram is shown in Figure 13 illustrating these effects.

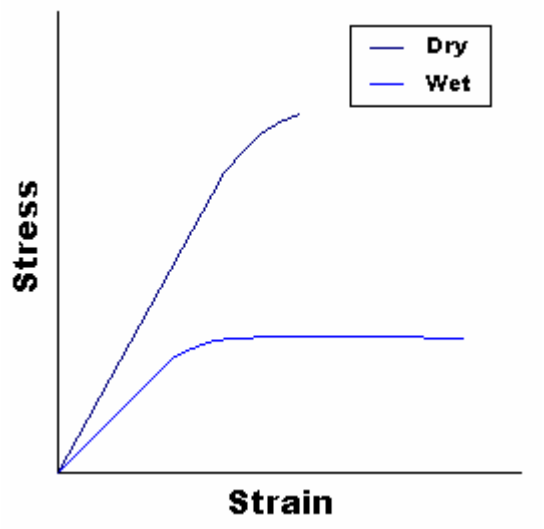

Figure 13. Representative stress/strain diagram depicting the effect of moisture on the mechanical properties of bulk epoxies adhesives

Studies by Crocombe, (1997); Wylde and Spelt, (1997); Zanni-Deffarges and Shanahan, (1995); Zanni-Deffarges and Shanahan, (1994); De Neve and Shanahan, (1992); Su, *et al.*, (1992); Brewis, *et al*., (1990); Sharon, *et al*., (1989), Jurf and Vinson, (1985) have all attributed the decrease in modulus due to the plasticizing action of the water on the adhesive. By acting as an external plasticizer to the polymer adhesive, the

water spreads the polymer molecules apart and reduces the polymer-polymer chain secondary bonding. This provides more room for the polymer molecules to untangle and move around, which results in a softer, more easily deformable mass (Rosen, 1993). Other studies attribute the decrease in epoxy modulus after moisture absorption predominately to crazing (Lu, *et al*., 2001; McMaster and Soane, 1989; Morgan, *et al*., 1980). The absorbed water can act as a crazing agent continuously decreasing the mechanical strength of epoxies with exposure time in water (Lu, *et al*. 2001). This is supported by scanning electron micrographs of epoxies, which have shown cavities and fractured fibrils which could only be explained by a moisture induced crazing mechanism (Morgan, *et al*. 1979). Consequently, the moisture induced swelling creates dimensional changes and internal stresses that can ultimately craze and/or crack the material. As a result, lightly cross-linked networks will be more susceptible to crazing than highly cross-linked networks (Morgan, *et al*., 1980). Last, studies have also attributed the decrease in modulus due to moisture causing hydrolysis leading to chain scission in the polymer network. The extent of hydrolysis depends on the material system and length of exposure. For short periods of exposure, chain scission from hydrolysis only results in the chemical addition of water that remains irreversibly in the epoxy network even after fully drying. For longer periods of exposure, the likelihood that chain scission from hydrolysis resulting in segments detaching from the polymer network is increased, and a net weight loss occurs in the epoxy network after fully drying (Xiao and Shanahan, 1997).

Studies by ZanniDeffarges and Shanahan (1994 and 1995) and DeNeve and Shanahan (1992) depict the decrease in elastic and shear modulus as a function of time exposure to moisture. Although this information is useful in evaluating the effect of exposure time to moisture on the modulus, it does not represent the inherent wet modulus values since a gradient of mechanical properties will exist in the adhesive until saturation is reached and water concentrations become steady and uniform. Other studies by Wylde and Spelt (1998), Su, *et al.*, (1992), and Brewis, *et al.*, (1990) evaluated the effect of moisture on epoxy adhesives after saturation had been established for a given level of moisture preconditioning; however, these studies only tested one level of moisture preconditioning to compare to fully dried test results. Consequently, information regarding the mechanical response of epoxy adhesives to different levels of moisture concentrations is incomplete, and fundamental insight into the response of the adhesives to increasing saturation concentrations of moisture cannot be ascertained.

Jurf and Vinson (1985) studied the change in shear modulus of epoxy adhesives as a function of temperature after three different levels of preconditioning: dry (control), 54^{o}C/63%RH, and 56-59^{o}C/95%RH. In both of the humid environments, specimens reached saturation before testing. The appearance of the three curves was nearly identical in shape, and it was clear that moisture had an adverse effect on adhesive stiffness as the 56-59^{o}C/95%RH specimens generally had the lowest modulus values over the entire range of temperatures. The results of their study show that there is a glassy region where the shear modulus is fairly temperature-independent, followed by a transition region

where the shear modulus decreases substantially. In addition, there was little variance between data at the two humidity levels in the glassy region.

2.6.3 Moisture Effects at the Interface

At present, there is limited information regarding the effect of moisture on the mechanical testing and behavior of adhesively bonded joints and a lack in empirical thermal and moisture data (Crocombe, 1997, and Jurf and Vinson, 1985). Of the few investigations that have explored this effect, water concentrations generally vary along the interface making it difficult to correlate a given strength to a particular level of moisture concentration. Consequently, developing physical relationships describing adhesion loss from moisture cannot be made due to this moisture concentration gradient existing at the interface during testing. In addition, since the body of experimental data is overwhelmingly based on joint strength studies, it does not represent a universal, intrinsic characteristic of the interfacial adhesion such as interfacial fracture toughness. Consequently, by making interfacial fracture toughness measurements, the intrinsic interfacial adhesion can be determined and used to develop predictive models to either supplement or replace accelerated testing techniques. Unfortunately, very few studies have attempted to address the issue of moisture preconditioning to interfacial fracture mechanics, with studies by Ferguson and Qu (2002), Lubke, *et al*., (2001), Johnson and Butkus (1998), Wylde and Spelt (1998), Ritter and Conley (1992), and Kinloch (1979) being the only known studies to date. Of those studies, only Ferguson and Qu (2002) and

Wylde and Spelt (1998) address the issue of moisture and interfacial fracture mechanics with respect to mode mixity.

The mechanisms by which strength reduction occurs in joints from moisture are not entirely understood, although the immediate causes of failure can be usually attributed to the breakdown of interfacial bonds and/or a decrease in the mechanical strength of the polymeric material constituting the adhesive itself (DeNeve and Shanahan, 1992). Adhesively bonded structures can fail in four different ways: cohesive failure within the adhesive itself, adhesive failure at the adhesive interface, mixed adhesive/cohesive failure where failure first occurs at the interface but then moves into the adhesive, and interphase failure where the failure is adhesive but occurs with small residual amounts of adhesive remaining on the substrate (Su, *et al*. 1992). As water enters the epoxy interface, the failure mode typically changes from cohesive/interphase failure to purely adhesive (or interfacial) failure (Comyn, *et al*., 1994; Zanni-Deffarges and Shanahan, 1994; DeNeve and Shanahan, 1992; Su, *et al*., 1992). However, it has been observed that the opposite can hold true, with failure modes changing from adhesive to cohesive after moisture preconditioning (Su, *et al*. 1992). Although it has been shown that this contradiction in failure mode change can occur after exposure to moisture for some joints, it is generally accepted that most adhesively bonded joints experience a change in failure mode from cohesive to adhesive after exposure to moisture. The reason for the change in failure modes due to moisture is presumed to occur as a result of local physical and/or chemical modifications caused by water at the interface, but the mechanisms for failure have yet to be completely identified and understood (DeNeve and

Shanahan, 1992). Consequently, it is essential to characterize the response of interfacial adhesion to moisture, especially when considering that interfacial failure is typically the dominant failure mode in moisture preconditioned adhesively bonded structures.

Moisture preconditioning will generally decrease joint strength (Bowditch, 1996; Zanni-Deffarges and Shanahan, 1994; Brewis, *et al*., 1990; Drain, *et al.*, 1984; Kinloch, 1979; Gledhill and Kinloch, 1974). Throughout the literature, there have been three primary mechanisms suggested that are responsible for moisture degradation of adhesive joints. The first is displacement of the adhesive by water reducing Van der Waals forces at the interfacial bond (Bowditch, 1996; Crocombe, 1997; and Comyn, *et al*., 1994). The second is plasticization of the bulk adhesive (Bowditch, 1996; and DeNeve and Shanahan, 1992), although some authors warn that low concentrations of water may actually have the net effect of strengthening some joints as discussed in further detail in the subsequent paragraph (Bowditch, 1996). The last mechanism is chemical degradation of the adhesive, substrate, and chemical bonds across the interface (Crocombe, 1997; Bowditch, 1996; Zanni-Deffarges and Shanahan, 1994). Generally this mechanism is not regarded as important due to the fact that adhesives are usually selected with essentially hydrolysis resistant chemistry.

Contrary to moisture preconditioning decreasing joint strength, it has been found that low concentrations of water can actually strengthen some joints (Bowditch, 1996). Other studies support this observation and have documented that small, initial amounts of moisture present at the epoxy resin interface may actually increase the adhesion for certain resin/substrate combinations (Wylde and Spelt, 1998; Armstrong, 1996; and Su, *et*

al., 1992). This is proposed to occur due to the relief of internal stresses within the joints due to the initial water plasticization of the adhesive resulting in stresses being distributed over a larger region (Wylde and Spelt, 1998, and Su, *et al*., 1992); however, there is no clear consensus on whether or not water plasticization will lead to an increase in joint strength (Su, *et al*., 1992).

Moisture can affect the interfacial adhesion not only directly at the interface itself, but also by changing the bulk adhesive mechanical properties. Brewis, *et al.*, (1990) suggested that the loss of joint strength from moisture may in part be attributed to the plasticization of the epoxy adhesive from the water uptake. However, as pointed out in the previous paragraph, Wylde and Spelt (1998) claim that the contribution from plasticization of the epoxy adhesive from water uptake may actually cause the adhesive strength to be increased. Although both of these studies have argued that the plasticization of the adhesive will produce two completely different results on interfacial adhesion, it can be agreed that the rate at which moisture will affect both the bulk adhesive and interface will occur neither instantaneously nor simultaneously (Crocombe, 1997). Consequently, the contribution from each effect will vary differently with time.

One of the more interesting discoveries in regards to moisture effects on interfacial adhesion is the proposition of the critical concentration of water concept. It has been observed that a critical concentration of water may exist where there may be a concentration and associated humidity level below which the interface is not weakened by moisture (Kinloch, 1979). Kinloch (1979) found that epoxy/mild-steel joints suffered no loss in adhesion from environmental attack at 50%RH, even though the adhesive still

absorbed water up to an equilibrium concentration. As a direct consequence of this observation, Kinloch proposed that a minimum, critical concentration of water must b e a requirement for the loss of adhesion due to the presence of moisture. Gledhill, *et al*., (1980) supports this concept and documents that joints consisting of epoxy adhesives bonded to steel substrates kept at 20°C/55%RH prior to testing did not appear to suffer from attack by moisture even when conditioned for long times. There was no significant decrease in joint strength even though the adhesive had absorbed water up to an equilibrium value. Conversely, similar joints exposed to water baths of 20°C, 40°C, 60°C, and 90°C experienced a loss in adhesive strength. Comyn, *et al*., (1994) also supports the critical concentration of water concept, and states that there may indeed exist a critical concentration of water corresponding to a relative humidity level below which the interface is not weakened. The conclusion was reached after observing no loss in joint strength for adhesive joints consisting of glass bonded to lead alloy with an epoxide adhesive after exposure to 50°C/50%RH for 3 months. Brewis, *et al*., (1990) identified a critical relative humidity of 65% exists for exposure of aluminum/epoxide joints of 10080 hours. This critical relative humidity corresponds to a critical concentration of water of 1.45%. However, Wylde and Spelt (1998) consistently showed a loss in adhesion for the aluminum/epoxy adhesive specimens evaluated in their study even when exposed to a relative humidity as low as 30%RH at 65°C. As a result, a limiting concentration below which no degradation will take place was not observed. Overall, the critical concentration of water concept is not widely known and appears in only a handful of studies. The concept is not well understood, and no publication can be found that

adequately characterizes its behavior or attempts to resolve the aforementioned observed discrepancy between experiments.

2.6.4 Recovery of Adhesion and Adhesives from Moisture

Investigations on the recovery of either adhesion or adhesives from moisture are extremely scarce. Consequently, knowledge regarding the reversible and irreversible effects of moisture is severely lacking and those processes are presently not well understood. Most of the studies that were found on the recovery of adhesion from moisture resulted from joint strength tests. Lubke, *et al*., (2001) and Butkus (1997) were the only studies found that used interfacial fracture mechanics to address recovery from moisture preconditioning.

Butkus (1997) examined the permanent change in Mode I fracture toughness of Aluminum/FM73M/Aluminum and Aluminum/FM73M/Boron-Epoxy joints after 5,000 hours at 71^{o}C and > 90%RH followed by 5,000 hours of desiccation at 22^{o}C/10%RH prior to testing. Both the Al/FM73M/Al joints and the Al/FM73M/Boron-Epoxy joints recovered very little of their fracture toughness on subsequent drying, demonstrating large, permanent losses in toughness after exposure to moisture. Similarly, Orman and Kerr (1971) studied the extent that epoxy-bonded aluminum joints could recover strength from exposure to 90^{o}C/5%RH and 90^{o}C/100%RH. After exposure to the aforementioned moisture preconditioning levels for up to 30 days, they dried the specimens in a vacuum at 90^{o}C for 24 hours. In both cases, some of the strength lost from moisture preconditioning was recovered; however, not all of the strength was recovered suggesting

an irreversible disruption at the interface as a result of attack by water. Conversely, Shaw, *et al*., (1992) found that nearly all of the strength lost after immersing steel/epoxy lap shear joints in distilled water for three weeks was recovered after drying. They attributed the loss in strength after moisture preconditioning to plasticization of the epoxy adhesive, which is generally regarded as a reversible process. Dodiuk, *et al*., (1984) evaluated the effect of moisture on the lap shear strength of four commercial epoxy adhesives to aluminum. It was found that exposure to moisture caused a reduction in lap shear strength; however, if the moisture concentration was below 0.3%, the strength was fully recoverable after drying indicating a completely reversible process. The authors gave no explanation to this observed behavior other than to state that moisture concentrations exceeding 0.3% would result in an irreversible process.

Netravali, *et al*., (1986) examined the interaction of water and an epoxy during water absorption and desorption using thermogravimetric analysis (TGA). Two sets of cured samples were soaked in distilled water at 25^{o}C and 70^{o}C for 750 and 675 hours respectively. The 25^{o}C moisture preconditioned specimens were then dried for 150 hours at 30^{o}C, and the 70^{o}C moisture preconditioned specimens were dried for 95 hours at 70^{o}C. The dynamic weight loss of both sets of specimens after accounting for the water loss after drying was less than their respective moisture preconditioned samples. It was proposed that this was the result of two primary factors. First, insufficient time was given for the water to completely diffuse out of the specimens. Second, some water either reacts or is strongly bonded to the epoxy. In addition, the 70^{o}C moisture preconditioned samples exhibited a lower net weight loss than the 25^{o}C moisture

preconditioned samples after drying. The authors suggest that this may represent a higher extent of reaction between the water and epoxy in the 70°C moisture preconditioned samples.

Buehler and Seferis (2000) evaluated the flexural strength and modulus of various laminates made from epoxy prepegs of various fiber reinforcement and solver content after 1200 hours of immersion in a 71°C water bath and 450 hours of desorption in a convection oven at 50°C. Both the flexural modulus and strength of all samples decreased significantly after moisture preconditioning, which was attributed primarily to matrix plasticization. The modulus and strength were not fully recovered after the water desorption, and no explanation was given by the authors for this observed behavior other than reporting the results. It should be noted that none of the samples evaluated in this study were fully dry after the 450 hours of desorption, with 3% weight concentrations of moisture still existing in the specimens. More time was needed to completely dry the specimens.

CHAPTER III

MATERIALS AND INSTRUMENTATION

Since the study of moisture and interfacial adhesion requires an interdisciplinary analysis, it is important to outline the motivation for performing particular tests as well as detail the specific testing equipment used for this research. In addition, it is also equally important to specify the material properties and characteristics of the components that constitute the materials and interfaces being tested. This will aid future research to extend the results and conclusions obtained from this study to advance the understanding of moisture and its role in affecting interfacial adhesion.

3.1 Description of Materials

The following section gives an overview of the requirements and functionality for substrates and underfill adhesives used in electronic packaging as well as detail the specific materials evaluated in this study. Material properties and characteristics for all materials tested are also provided in tables at the conclusion of each respective subsection.

3.1.1 Substrates

The substrate provides mechanical support for electronic packages, utilizing multiple layers of conductors to interconnect them. At a fundamental level, the primary purpose of the substrate is to provide a conductor matrix for the interconnection of various microelectronic devices. Typical requirements for an effective substrate include the following: low CTE, high modulus, low density, low moisture absorption, and good planarity. Individual mechanical properties obtained are dependent on the type of base material used.

A variety of base materials are available to the electronic industry for substrate fabrication. Examples include glass epoxy (FR-4), Copper, Aluminum Nitride, polymide, Alumina, Bismaleimide Triazine, silicon wafer, and Kapton film. These materials offer a variety of benefits and range from very stiff (i.e. FR-4) to very flexible (i.e. Kapton film). Material selection is dependent on the specific type of application that the package assembly will be used relative to desired mechanical properties, reliability, thermal performance, and manufacturing cost. With package size decreasing and interconnect density increasing, there are numerous challenges that lie ahead in substrate development in order to not represent a bottleneck in technological advancement.

The following two substrates were evaluated in this study: alloy 101, oxygen-free electronic grade copper and FR-4 board. The oxygen-free electronic grade copper was obtained from a commercial vendor and contains virtually no oxygen with a 99.99% chemical composition of copper. The FR-4 board was supplied by a commercial manufacturer and consisted of a double-sided, epoxy-coated board with full copper

plating present on both sides underneath the solder mask. The mechanical properties for the two substrates are given in Table 2.

Table 2. Mechanical properties of substrates

	Copper, Alloy 101	FR-4 Board
Elastic Modulus, E (GPa)	115	23
Poisson's Ratio, *v*	0.31	0.21
Coefficient of Thermal Expansion α (ppm / ^{o}C)	17 (20 - 100 ^{o}C) 17.5 (20 - 300 ^{o}C)	14 - X (20 - 180^{o}C) 15 - Y (20 - 180^{o}C) 50 - Z (20 - 180^{o}C)

3.1.2 Underfill Adhesives

Underfills have two primary purposes in electronic packaging. First, the underfill encapsulant provides a medium that reduces localized shear stress concentrations on the solder interconnects that occurs due to the coefficient of thermal expansion mismatch between the silicon semiconductor devices (CTE ≈ 3 ppm / ^{o}C) and the substrate (CTE of FR4 ≈ 18 ppm / ^{o}C). Second, the underfill provides environmental protection from moisture, ionic contaminants, radiation, and hostile operating conditions to the package assembly (Wong, 2000). The addition of underfill to package assemblies has significantly improved the reliability of the assemblies in both thermal cycle and thermal shock performance (Suryanarayana, *et al.*, 1991).

There are several material requirements that characterize a successful underfill. These requirements include excellent resistance to moisture absorption, elongation at break that is greater than 1%, comparable coefficient of thermal expansion to that of solder joints, glass transition temperature that guarantees dimensional stability during reliability testing, elastic modulus that will not play a significant role in stresses development during thermal cycling, strong adhesion, high purity, good flow characteristics such as good wetting to the surfaces to be encapsulated, and relative ease of application in production. Since epoxy alone does not contain all of the above mentioned characteristics, silicon filler is added to produce an underfill that satisfies the above requirements. Other packaging materials to be selected for encapsulation include cyanate ester, silicone, and urethane. An overview of flip chip underfill requirements is given in Table 3.

Table 3. Flip chip underfill requirements (Wong, 2000)

Properties	Desirable Values	Comments
Flow	> 0.5 mm/s	Fast flow with no air bubble entrapment
Adhesion	> 50 MPa shear force	Key to device protection
CTE	18 - 30 ppm/^{o}C	Matches CTE of solder (26 ppm/^{o}C)
Elongation	> 1%	Resists CTE mismatch stress
Modulus	5 - 8 GPa	Provides mechanical coupling
Tg	> 130 ^{o}C	Maintains dimensional stability
Stress after cure	< 10 Mpa	Minimizes internal stress caused by shrinkage of polymer
Water absorption	< 1%	Reduces moisture-induced failures
Ionic impurities	< 10 ppm	Prevents corrosion and metal electromigration
Thermal stability, 1% weight loss	> 250 ^{o}C	Prevents underfill decomposition during solder reflow
Curing time @ 160 deg C	< 0.5 hr	Maintains good product output
Volatility during cure	< 1% weight loss	Maintains correct stoichiometry
Pot life @ RT, 20% increase in viscosity	> 8 hr	Provides long, useable underfill life

A new development in underfill technology is the introduction of no-flow underfills. Primary advantages of no-flow underfills include a reduction in floor space by removing underfill dispensers and cure ovens, improvement of overall production efficiency, and elimination of narrow limitations on package size and underfill viscosity. Rather than utilizing capillary action from a single or double edge dispense to distribute the underfill between the chip and substrate as with a conventional capillary underfill, a

no-flow underfill is directly applied to the substrate before chip placement. The no-flow underfill is also simultaneously cured during solder reflow, saving manufacturing time and reducing cost. In addition, no-flow underfills contain flux, eliminating the need for flux dispensing and cleaning steps. No-flow underfills represent a higher assembling efficiency and lower manufacturing cost over conventional capillary flow underfills (Shi and Wong, 1999).

Two no-flow underfills were evaluated in this study. No-flow underfills were selected as test materials since they represent the state of the art in underfill technology, do not contain any filler particles, and contain flux. The addition of filler adds a degree of complexity to the moisture absorption kinetics by forming voids in the epoxy matrix of the underfill. The filler also increases the complexity of the chemical interactions of the adhesive at the bonding interface. In addition, the flux in the no-flow underfill will help insure that bonding of the adhesive to the substrate occurred at an unoxidized state. This is important to help determine the role of oxidation to any observed changes in interfacial adhesion results after environmentally preconditioning. The material properties of the underfill adhesives are listed in Table 4.

Table 4. Material properties of underfill resins A and B (Shi, 2000)

	Underfill Resin A	Underfill Resin B
Elastic Modulus, E (GPa) [ASTM D638M; *ASTM D790]	3.0	2.6*
Storage Modulus, E' @ 30°C (GPa) [Measured by DMA]	3.1	3.0
Tg (°C) [Measured by TMA]	128	125
CTE (50 - 100°C) (ppm/°C)	65	75
Die Shear Strength, σ_{DS} (MPa)	62	59
Material Bulk Strength, σ_M (MPa)	68.9	72.4
K_{IC} (MPa*$m^{1/2}$) [ASTM E-24]	5.25	9.21

Underfill resin A (UR-A) was developed at the Georgia Institute of Technology. Underfill resin B (UR-B) was supplied by a commercial manufacturer. In order to select an underfill that would be an ideal candidate for interfacial fracture test specimen design, both underfills were experimentally tested to determine their moisture absorption behavior. Based on the results of the moisture absorption analysis, an adhesive was selected that was best suited for evaluating how moisture affects interfacial adhesion.

3.2 Experimental Test Equipment

The following section discusses the details regarding the experimental test equipment used in this research. It also briefly describes the motivation for using each piece of equipment. Specific experimental procedures and test specimen fabrication techniques used in each individual stage of this research are described in corresponding, subsequent chapters.

3.2.1 Load Frame

A computer controlled load frame shown in Figure 14 and manufactured by the United Calibration Company, model SSTM-500, was used for both flexural bend testing and interfacial fracture toughness testing. Flexural bend testing was performed using a three-point bend fixture to determine the elastic modulus of test materials. Tests were performed at a crosshead rate of 1.2 mm/min on a support span of 38.1 mm. Load displacement graphs were generated for each individual test specimen to determine the slope of the tangent of the initial straight-line portion of the load-deflection curve, which was used to calculate the elastic modulus of the material according to the test standard ASTM D790 (1999). Interfacial fracture toughness testing was performed using a four-point bend fixture to characterize the interfacial adhesion of the bimaterial interface. The top span of the fixture was set to 49.2 mm between loading pin centers, and the bottom span of the fixture was set to 31.7 mm between loading pin centers. The computer inputs for all interfacial fracture testing were as follows: 0.1 N preload, 1.5 mm/min preloading

rate, 0.5 mm/min testing rate, and 0.75 mm/min return rate for return to the original span vertical position. Load displacement curves were generated for each individual interfacial fracture test specimen to determine the critical load at fracture, P_c, which was used to calculate the interfacial fracture toughness on the bimaterial interface being tested.

Figure 14. Computer controlled load frame used for flexural bend testing and interfacial fracture toughness testing

3.2.2 Humidity Chambers

Figure 15 shows the humidity chambers used to moisture precondition test specimens. The chamber pictured on the left was manufactured by Thermotron, model

5M-8C, while the chamber pictured on the right was manufactured by Tenney Environmental, model THJR. The chambers were set at 85^{o}C/50%RH, 85^{o}C/65%RH, 85^{o}C/85%RH, and 85^{o}C/95%RH to study the effect of different levels of preconditioning on moisture absorption behavior, elastic modulus variation, and interfacial adhesion. All test specimens were maintained in the chambers for a duration of 168 hours for each respective level of environmental preconditioning being evaluated. The tolerance of both humidity chambers were observed to be within ±1 ^{o}C and ±1 %RH, and the conditions were monitored daily using digital outputs of both the relative humidity and temperature inside the chamber. Redundant instrumentation was periodically placed inside the chambers to verify that the digital output readings of both temperature and humidity by the chambers were correct. Good agreement was obtained between the chambers and redundant instrumentation readings, indicating conditions inside the chambers were accurate for each desired level of moisture preconditioning.

Figure 15. Humidity chambers used for moisture preconditioning test specimens

3.2.3 Convection Ovens

The convection ovens shown in Figure 16 were used to cure the underfill resins and thermally age test specimens. The oven on the left was manufactured by Blue M, model DC-256C, and had a maximum operating temperature of 343^{o}C, while the oven on the right was manufactured by Precision Scientific and had a maximum operating temperature of 210^{o}C. Since all moisture preconditioned test groups were exposed to the same temperature component of 85^{o}C as well as the same duration of 168 hours, thermal aging for 168 hours at 85^{o}C only with no moisture component was necessary to isolate the contribution of thermal aging on any observed changes from test results after moisture preconditioning. This allowed the contributions of moisture and thermal aging from moisture preconditioning to both the elastic modulus and interfacial adhesion to be identified separately. The ovens were also used to dry moisture preconditioned test

samples at 95^{o}C during recovery experiments to evaluate the permanent effect of moisture uptake on both the elastic modulus and interfacial adhesion.

Figure 16. Convection ovens used for curing underfill resins and thermal aging test specimens

3.2.4 Differential Scanning Calorimeter (DSC)

In view of the fact that cure rates depend on both the efficiency of the heat source and the mass of the material to be heated, it is critical to insure that any observed changes to the underfill performance after moisture preconditioning was indeed due to the preconditioning itself and not influenced from incomplete curing due to the size and geometry of the test specimens. The degree of cure of the underfill can be determined by using the heat of cure measured during a DSC test. Figure 17 shows the Differential Scanning Calorimeter used to establish the degree of cure of the underfill for the test

specimen sizes, geometry, and curing conditions used in this research. The DSC was performed using a modulated differential scanning calorimeter manufactured by TA instruments, model 2920, and implemented a heat flux cell during testing. During a DSC evaluation, a 10 mg test sample was removed from a representative test specimen and placed in a hermetic DSC Aluminum sample pan at room temperature. The pan was placed inside the differential scanning calorimeter and heated to 300^{o}C at a rate of 5^{o}C/min with a nitrogen purge rate of 40 ml/min to obtain a DSC thermo-diagram of the underfill. The DSC thermo-diagram result was compared to an uncured underfill sample to ascertain the degree of cure for the underfill for the curing conditions of 190^{o}C for 40 minutes used in this study.

Figure 17. Differential Scanning Calorimeter used to determine the degree of cure of underfill

3.2.5 Optical Microscope with Precision Controlled Platform

As moisture is absorbed in a material, the material will swell to accommodate the uptake in moisture. Depending on the relative swelling in the two materials that constitute the bimaterial interface, the moisture induced swelling can affect the intrinsic interfacial adhesion between the two materials. To ascertain this effect, a Nikon optical microscope was used in conjunction with a precision controlled platform to determine the moisture swelling coefficient, β, of the materials evaluated in this study. The experimental equipment used is shown in Figure 18. The precision platform was manufactured by RSF Electronics, model MSA 6709, and provided x, y, and z movement by three Vexta, 2-Phase stepping motors, model PK266-02B. A digital display showed the x, y, and z position of the platform to the nearest ± 0.0001 mm. By focusing on the edge of a test sample under a magnification of 20X and then moving the platform to the opposite edge, the length of the test sample could be precisely determined. Note that the sample was placed on the platform in such a manner that only one dimension changed as the platform moved to the opposite edge. By comparing the fully dry length to the moisture saturated length in the test sample, the moisture swelling coefficient of the material could be determined for a particular moisture saturation level.

Figure 18. Optical microscope and precision controlled platform used to measure the moisture swelling coefficient of test materials

3.2.6 Surface Profilometer

Since surface roughness can affect interfacial adhesion, it is important to document the degree of roughness of the substrate before bonding with the adhesive. A profilometer manufactured by Hommelwerke, model T8000, and shown in Figure 19 was used to measure the surface roughness of the substrates used in this study. Data acquisition software, Turbo Roughness (version 2.17a), was used to analyze the results and calculate the surface roughness. Test samples were tested at a speed of 0.05 mm/sec, measuring range of 80 microns, and an assessment length of 0.48 mm at room temperature. Several tests were performed in different locations of a test sample and

averaged for each surface roughness value reported. In addition, a precision test grading with a known surface roughness was used to determine the accuracy of the profilometer before testing the surface roughness of the actual test specimen. The measured roughness and actual roughness of the test grading was always within the recommended manufacturer tolerance limits before determining the roughness of the test sample, indicating that accurate results were obtained from experimental test results.

Figure 19. Profilometer used to measure surface roughness

3.2.7 Goniometer

The goniometer shown in Figure 20 and manufactured by Rame-Hart, Inc., model 100-07-00, was used to measure the contact angle of water with the adhesives and substrates used in this study. By measuring the contact angle of water with the substrate

and adhesives, insight is gained regarding the behavior of moisture once it arrives at the interface and how surface hydrophobicity can affect observed changes to interfacial adhesion in the presence of moisture. To measure the contact angle, a 2 – 3 μL drop of water was dispensed from a micro-syringe on the surface of each substrate and adhesive and allowed to reach equilibrium. A digital image of the drop was taken and the steady-state contact angle determined using a Microsoft Excel macro in conjunction with the software, Image Pro Plus (version 4.5.1). Since theoretically the same contact angle should be formed from each side of the two-dimensional drop profile, two contact angle measurements were obtained from each drop. In all, five drops for a total of ten contact angle measurements were performed for each test material and the average reported.

Figure 20. Goniometer used to measure the contact angle of water

3.2.8 Scanning Electron Microscope (SEM)

A Hitachi S800 FEG Scanning Electron Microscope (SEM) shown in Figure 21 was used to examine the interfacial fracture failure surface of test specimens after fracture testing. Characterizing the path of fracture is important to examine if moisture preconditioning changed the fracture failure path. For the copper/underfill failure surface, the copper surface was intentionally not sputter coated with gold, which is typically done to enhance the SEM image of insulators by coating them with a thin conductive layer. By not sputter coating the copper surface, any underfill adhesive that may possibly remain on the copper surface after fracture testing will charge and become easily visible upon SEM inspection. Images were taken of the fracture surfaces at magnifications ranging from 50 - 5000X for each level of moisture preconditioning.

Figure 21. Scanning Electron Microscope used to examine fracture surfaces

3.2.9 X-ray Photoelectron Spectroscope (XPS)

Figure 22 shows the X-ray Photoelectron Spectroscope manufactured by Surface Science, model SSX 100, used to determine the type of copper oxide present on the copper substrate after moisture preconditioning at 85°C/50%RH, 85°C/65%RH, and 85°C/85%RH for one week, as well as thermal aging at 85°C only for one week. Since copper substrates were cleaned prior to bonding and the presence of flux in the no-flow underfill will remove additional oxides that form during curing, it is important to identify if the development of oxides at the interface after moisture preconditioning can affect interfacial adhesion results. Two different types of copper oxide, cuprous oxide and cupric oxide, can develop on the copper surface at the copper/underfill interface after bonding the underfill adhesive to the copper substrate and environmentally preconditioning for 168 hours. The first type of oxide that will develop is cuprous oxide, which is followed by the formation of a second layer of cupric oxide. By using XPS to determine the type of oxide present on the copper surface for a particular level of moisture preconditioning, the extent and type of oxide growth can be identified to ascertain if the oxide growth contributed to the observed changes in the interfacial adhesion after moisture preconditioning. It is important to note that since the underfill will effectively shield and reduce the degree of oxidation on the copper substrate in the interfacial fracture test specimens when compared to bare copper substrates, bare copper substrates could not simply be moisture preconditioned for a similar duration as actual interfacial fracture test specimens and expect similar levels of oxidation to exist on both surfaces. Consequently, when performing an XPS evaluation, unique test specimens

were made and moisture preconditioned for the purpose of XPS testing only. These specimens were immediately taken for XPS evaluation upon removal from the humidity chamber for a particular level of moisture preconditioning. In addition, test specimens were placed in a hermetically sealed bag to minimize the effect of atmospheric conditions contributing to the oxidation level at the copper/underfill interface during transport from the humidity chamber to the X-ray Photoelectron Spectrometer. During the XPS evaluation, an 800 micron spot size was used, and vacuum conditions were maintained inside the chamber to less than 3 x 10^{-8} Torr. When needed, a low energy electron flood gun was utilized to minimize the effect of sample charging.

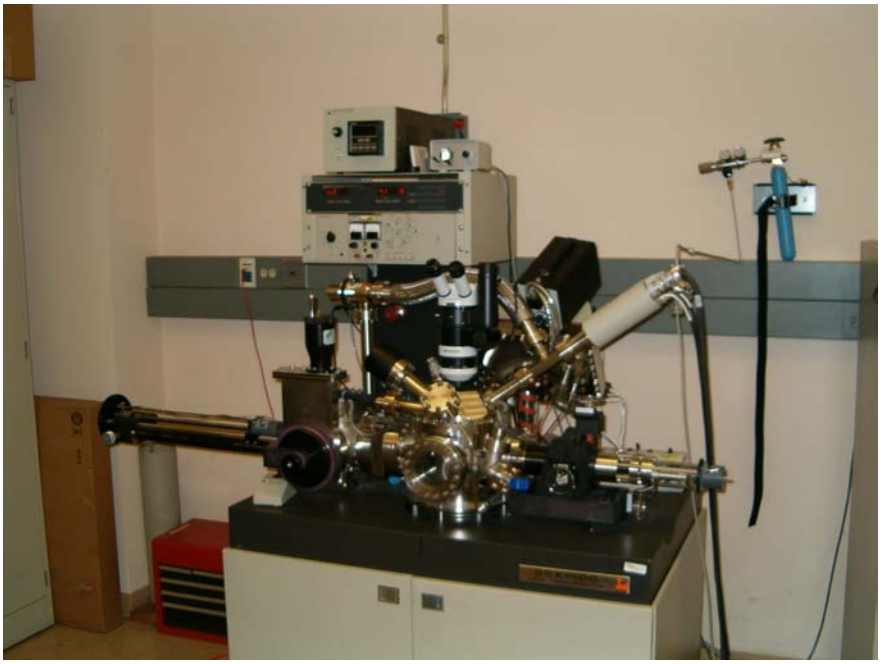

Figure 22. X-Ray Photoelectron Spectroscope used to determine the chemical composition of fracture surfaces

CHAPTER IV

MOISTURE ABSORPTION KINETICS

Central to understanding the effect of moisture on interfacial adhesion is to first identify the rate as which moisture is delivered to the interface. This involves a detailed study of the moisture absorption kinetics of the materials that constitute a bimaterial interface. Since the substrate used in this study is metallic and impermeable to moisture uptake, the moisture transport to the interface will be governed by the diffusion rate in the epoxy based underfill adhesive. Based on the results from the moisture absorption analysis, both the diffusivity and moisture saturation concentrations in the underfill for each respective moisture preconditioning environment will be known. This information is used in a finite element analysis to model the transient moisture ingress in interfacial fracture test specimens, as well as provide insight on how varying degrees of moisture uptake can affect bulk material and adhesion performance.

4.1 Introduction

A significant problem in the microelectronic packaging industry is the presence of moisture induced failure mechanisms. Moisture is a multi-dimensional concern in packaging, having an adverse effect on package reliability by introducing corrosion, development of hygro-stresses, popcorn failure, and degradation of polymers present in the package. Moisture can also accelerate delamination by deteriorating the polymer interfaces within the package. As the interfacial adhesion between the chip, underfill, and substrate decreases, the likelihood of delamination at each encapsulant interface increases. Once the package delaminates, the solder joints in the delaminated area are exposed to high stress concentrations, resulting in a reduction of overall package life.

Central to developing more robust packages to moisture absorption is understanding the kinetics and behavior of the moisture absorption process within the package. Since the vast majority of contemporary underfills used are epoxy based, these underfills are highly susceptible to moisture absorption. A standard epoxy formulation can absorb between 1 and 7 wt% moisture (Soles and Yee, 2000). The diffusion of moisture into epoxies can be affected by a variety of phenomena. Generally speaking, the three primary parameters that predominantly have the greatest effect on diffusion rates are the size of the diffusing particles, temperature, and viscosity of the environment. Lighter particles have a higher velocity for the same kinetic energy as a heavier particle, thus lighter particles diffuse faster than heavier particles. Similarly, an increase in temperature will produce a higher kinetic energy yielding an increase in velocity, thus

particles will diffuse more rapidly at elevated temperatures. Last, diffusion is more rapid in a gas than in a solid as a result of less atomic interactions, which retard the diffusion process.

Additional considerations that apply specifically to moisture diffusion in epoxies include the epoxy surface topology and resin polarity. Soles, *et al.*, (2000) have found that water initially enters the epoxy network through the nanopores that are inherent in the epoxy surface topology. They have determined the average size of a nanopore diameter to vary from 5.0 to 6.1 *Å* and account for 3 - 7 % of the total volume of the epoxy material. Since the approximate diameter of a kinetic water molecule is just 3.0 Å, moisture can easily traverse into the epoxy via the nanopores. When attempting to correlate the volume fraction of nanopores to the diffusion coefficient of water, Soles, *et al*., (2000) found that that the volume fraction of nanopores does not affect the diffusion coefficient of water in any of the resins studied. They argued that polar groups coincident with the nanopores are possibly the rate-limiting factor in the diffusion process, which could explain why the diffusion coefficient is essentially independent of the nanopore content.

Although surface topology can influence moisture penetration into an epoxy, of primary importance is the resin polarity, with the high polarity of the water molecule being susceptible to specific epoxy-water interactions. Less polar resins such as non-amine resins have more enhanced moisture diffusion coefficients than amine-containing resins. Soles and Yee (2000) have shown that polar sites, such as amine functional groups, provide low energy wells for the water molecules to attach.

Consequently, polar hydroxyls and amines can regulate transport through the nanopores by either blocking or allowing moisture to traverse the epoxy resin depending on the orientation of the resin with respect to nanopore position. Conversely, Soles and Yee (2000) have also shown that the absence of hydroxyls and amines in the non-amine resin leads to an enhanced moisture diffusion coefficient. In addition, non-amine resins absorb very little water relative to more polar resins, such as amine resins. Soles and Yee (2000) have shown that by increasing the crosslink density, the intrinsic hole volume fraction is increased, which yields an increase in the equilibrium moisture content. Steric hindrances located at crosslink junctions open the epoxy matrix to facilitate interactions of water with polar groups, thus increasing the moisture uptake. Depending on the various chemical conformations of the epoxy resin in association with the inherent nanopores present in the epoxy structure, water molecules will behave differently in various epoxy resins.

Two no-flow underfill encapsulants were evaluated in this study. To further investigate the mechanisms for the change in interfacial toughness from moisture, a diffusion analysis based on Fick's second law of diffusion was implemented to determine the diffusion coefficient and basic absorption behavior of each underfill. A finite element analysis was performed to model the associated moisture distribution within the underfill of the interfacial fracture test specimens for small times of exposure at 85^{o}C/85%RH. Based on the results of the moisture absorption analysis and model, an ideal underfill was selected for a comprehensive study into the effect of moisture on interfacial adhesion. Since several different moisture preconditioning environments will need to be evaluated

to identify the intrinsic change in interfacial adhesion as a function of moisture concentration, the moisture absorption characteristics of this underfill were evaluated for 85^{o}C/50%RH and 85^{o}C/65%RH environments, in addition to the previously studied response at 85^{o}C/85%RH .

4.2 Experimental Procedure

4.2.1 Materials

Two no-flow underfills were evaluated to determine their absorption behavior to select an ideal candidate for a fundamental study in the effect of moisture on interfacial adhesion. Underfill resin A (UR-A) was developed at the Georgia Institute of Technology. Underfill resin B (UR-B) was supplied by a commercial manufacturer. It should be noted that since both underfills were formulated for no-flow assembly, neither contained any filler content.

4.2.2 Diffusion Coefficient Test Specimen

Diffusion coefficient test specimens were constructed to experimentally determine the moisture diffusivity for both underfill resins A and B. Five grams of underfill resin was dispensed into a 60 *mm* diameter aluminum dish. Each resin was cured as prescribed by their respective manufacturer. The cured underfill was removed from the aluminum dish and polished using 600 grit sandpaper to ensure a uniform thickness. Next, the

samples were cleaned to remove excess residue from polishing and baked at 115^{o}C for at least 12 hours to remove moisture before exposure to the humidity chamber at 85^{o}C/85%RH. During test specimen construction, latex gloves were worn at all times to prevent oils and other contaminants on the skin from interacting with the sample surfaces. Completed diffusion coefficient test samples were approximately 60 *mm* in diameter and 2 *mm* thick, hence promoting predominately one-dimensional diffusion through the thickness of the sample.

4.2.3 Moisture Absorption Analysis

Test specimens were placed into a humidity chamber for moisture preconditioning. During moisture preconditioning, tests specimens were periodically removed from the chamber and weighed on an electronic balance to the nearest 0.1 *mg*. The percentage weight gain was determined to monitor the level of moisture absorption with respect to time.

4.3 Discussion of Results

4.3.1 Moisture Absorption Characteristics

Being epoxy based, underfill resins are highly susceptible to moisture ingress. The diffusivity of moisture through the thickness of the underfill resin is needed for each material to apply an analytical, Fickian solution for modeling the moisture diffusion into

the interfacial fracture test specimens. The diffusion coefficient, *D*, can be experimentally determined using a test specimen that promotes predominantly one-dimensional diffusion into the test specimen. Although the interfacial fracture test specimens promoted predominantly one-dimensional diffusion into the test specimens, they also introduced small components of diffusion into the *y* and *z*-planes in addition to the intended one-dimensional *x*-plane of the specimen. Consequently, diffusion coefficient test specimens were made to experimentally obtain the value of the diffusivity of moisture into each underfill resin at 85^{o}C/85%RH. Based on the results from the diffusion coefficient test specimens, it can be concluded whether the resins exhibit true Fickian behavior without additional factors compromising the results. This information will give insight into the fundamental behavior of each underfill resin at 85^{o}C/85%RH and subsequently aid in the development of modeling the moisture distribution within the interfacial test specimens.

Since both resins were homogenous in composition, the diffusion coefficient will be uniform throughout the sample, assuming no concentration dependence of the diffusivity. Three diffusion coefficient test specimens were constructed from each underfill resin to evaluate the repeatability of the experiment. After the samples were baked at 115^{o}C for at least 12 hours to remove moisture, they were placed into the humidity chamber in an atmosphere maintained at a constant temperature (85 ± 1 ^{o}C), humidity (85 ± 1 %RH), and pressure (P_{atm}). In addition, the samples were placed on a special rack that held the samples perpendicular to the shelf in the humidity chamber. This was done to promote primarily one-dimensional diffusion on both sides of the

samples, eliminating the possibility that the shelf in the humidity chamber would obstruct some of the moisture penetration. Again, this method assumes that the diffusion process is controlled by a constant diffusion coefficient and that samples were initially dry before exposure to the moisture.

Samples were periodically removed from the chamber and weighed to the nearest 0.1 mg to monitor the moisture uptake. The moisture uptake profiles for the three diffusion coefficient samples constructed from each underfill resin are shown in Figures 23 and 24.

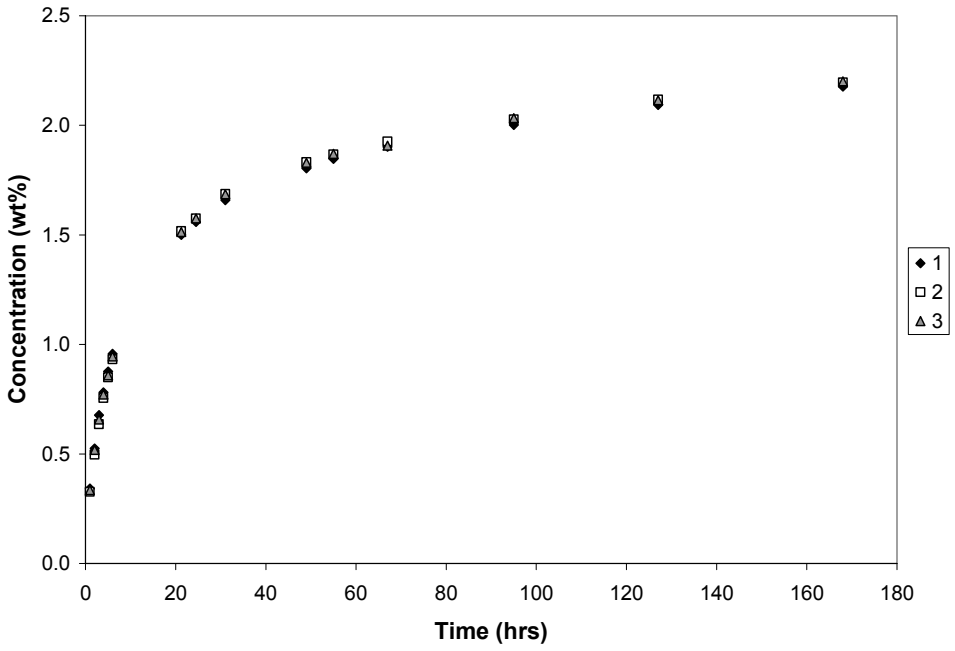

Figure 23. Moisture uptake profile for UR-A test specimens at 85°C/85%RH

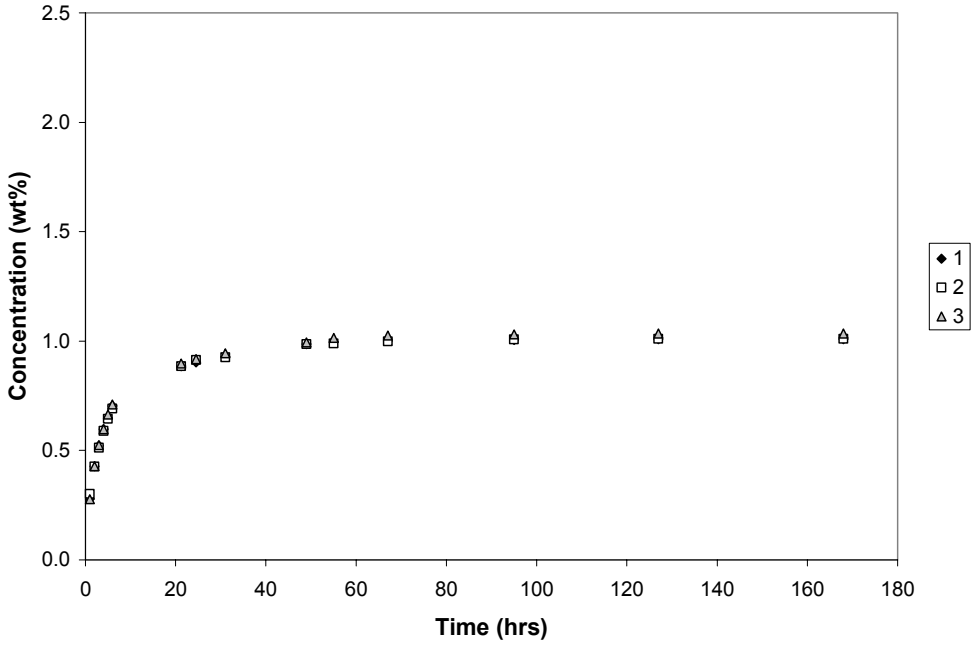

Figure 24. Moisture uptake profiles for UR-B test specimens at 85°C/85%RH

It is evident from Figures 23 and 24 that UR-A had not reached saturation after 168 hours of exposure, whereas UR-B had approached a saturated state within that same timeframe. In fact, diffusion coefficient test specimens constructed from UR-A did not reach saturation even after 725 hours of exposure. This absorption behavior is not uncommon, with Vanlandingham, *et al*., (1999) noting that some of the epoxies evaluated in their study had not reached saturation even after 3000 - 4000 hours of exposure at 50°C/85%RH. Similarly, Ardebili, *et al*., (2003) found some of their epoxies to exhibit a gradual increase in moisture content with time, attributing this increase to void growth in the epoxy network caused by swelling. Due to this observed behavior in UR-A, the saturation limit, M_∞, for all UR-A moisture preconditioned samples was taken to be at 168 hours as a result of that being the JEDEC duration level for 85°C/85%RH

preconditioning. The rationale for this is discussed in further detail in subsequent paragraphs.

By recording the moisture uptake as a function of time, the diffusion coefficient for each underfill resin can be experimentally determined using analytical solutions in conjunction with mass uptake data, provided that the diffusivity remains constant. The analytical solution of Equation (2.14) for the concentration of a diffusing substance in an isotropic plane sheet of finite thickness as a function of time and space is given by (Crank, 1956):

$$\frac{C(x,t)}{C_1} = 1 - \frac{4}{\pi}\sum_{n=0}^{\infty}\frac{(-1)^n}{2n+1}exp\left\{\frac{-D(2n+1)^2\pi^2 t}{4\ell^2}\right\}cos\frac{(2n+1)\pi x}{2\ell} \qquad (5.1)$$

where D is the diffusion coefficient, ℓ is the half-thickness of the sheet ($-\ell < x < \ell$), C is the concentration of the diffusing substance absorbed by the sample at position x and time t, and C_1 is the saturation concentration of the absorbed substance. The application of Equation (5.1) assumes that immediately after the sheet is placed in the vapor that both surfaces obtain a concentration that is equivalent to the equilibrium uptake, remaining constant. In addition, the equation assumes that D remains constant throughout the diffusion process, and that the initial concentration of the diffusing substance in the specimen is zero.

The corresponding expression given on a mass basis for a plane sheet with the same prescribed boundary conditions has been shown by Crank (1956) to be the following:

$$\frac{M_t}{M_\infty} = 1 - \frac{8}{\pi^2}\sum_{m=0}^{\infty}\frac{1}{(2m+1)^2}exp\left\{\frac{-D(2m+1)^2\pi^2 t}{h^2}\right\} \tag{5.2}$$

where D is the diffusion coefficient, h is the total sheet thickness, M_t is total mass of the diffusing substance absorbed by the sample at time t, and M_∞ is the equilibrium mass of the absorbed substance. In the initial stages of absorption where $M_t / M_\infty < ½$ and assuming a constant diffusion coefficient, D, Equation (5.2) can be shown to be approximated by the following (Crank, 1956):

$$\frac{M_t}{M_\infty} = \frac{4}{h}\sqrt{\frac{Dt}{\pi}} \tag{5.3}$$

If absorption data is plotted with M_t / M_∞ as a function of $(t/h^2)^{½}$ and exhibits linear behavior for $M_t / M_\infty < ½$, the diffusion coefficient can be determined by rearranging Equation (5.3) to the following form:

$$D = \frac{\pi}{16}\left(\frac{M_t / M_\infty}{\sqrt{t}/h}\right)^2 \tag{5.4}$$

The diffusivity, *D*, can now be experimentally determined using absorption data with Equation (5.4). Again, Equations (5.1), (5.2), (5.3), and (5.4) all assume that the one-dimensional absorption occurs on both sides of the plane sheet with a concentration-independent, constant diffusivity. If absorption results in a diffusion coefficient that is variable rather than constant, explicit analytical solutions are no longer available (Crank, 1956).

The diffusion coefficients were experimentally determined using Equation (5.4) and averaged from the three independent samples of both underfill resins A (UR-A) and B (UR-B). The results are shown in Table 5.

Table 5. Experimentally determined diffusion coefficients for UR-A and UR-B at 85°C/85%RH

Test Specimen	Material	Environment	Diffusion Coefficient, D (m^2/s)
1	UR-A	85C/85%RH	5.86E-12
2	UR-A	85C/85%RH	5.35E-12
3	UR-A	85C/85%RH	5.89E-12
		AVERAGE:	**5.70E-12**
		STANDARD DEVIATION:	2.48E-13

Test Specimen	Material	Environment	Diffusion Coefficient, D (m^2/s)
1	UR-B	85C/85%RH	1.49E-11
2	UR-B	85C/85%RH	1.51E-11
3	UR-B	85C/85%RH	1.42E-11
		AVERAGE:	**1.47E-11**
		STANDARD DEVIATION:	3.86E-13

From the results shown in Table 5, it is clear that the average diffusion coefficient for UR-B was greater than UR-A. Since the diffusion coefficient is a measure of how quickly a material will respond to mass concentration changes in its environment, the larger value of diffusivity for UR-B indicates it will respond more quickly to those changes. Conversely, the smaller value of diffusivity for UR-A indicates it will respond more slowly to changes in its environment, taking longer to reach a condition of mass concentration equilibrium with its environment. As a result, UR-B test specimens will approach saturation more rapidly than UR-A test specimens, which quantitatively supports what was already qualitatively observed in Figures 23 and 24.

After the diffusion coefficient for each resin was determined, a Fickian curve was generated for each data set to examine the extent that the moisture uptake of the specimens demonstrated Fickian behavior at conditions of 85°C/85%RH. Rather than utilizing Equation (5.2) for the Fickian profile, the following relation developed by Shen and Springer (1976) was implemented since it simplifies the infinite series of Equation (5.2):

$$\frac{M_t}{M_\infty} = 1 - exp\left[-7.3\left(\frac{Dt}{h^2}\right)^{0.75}\right] \tag{5.5}$$

The resulting Fickian curve for each data set at 85°C/85%RH is shown in Figures 25 – 27 for UR-A and Figures 28 – 30 for UR-B.

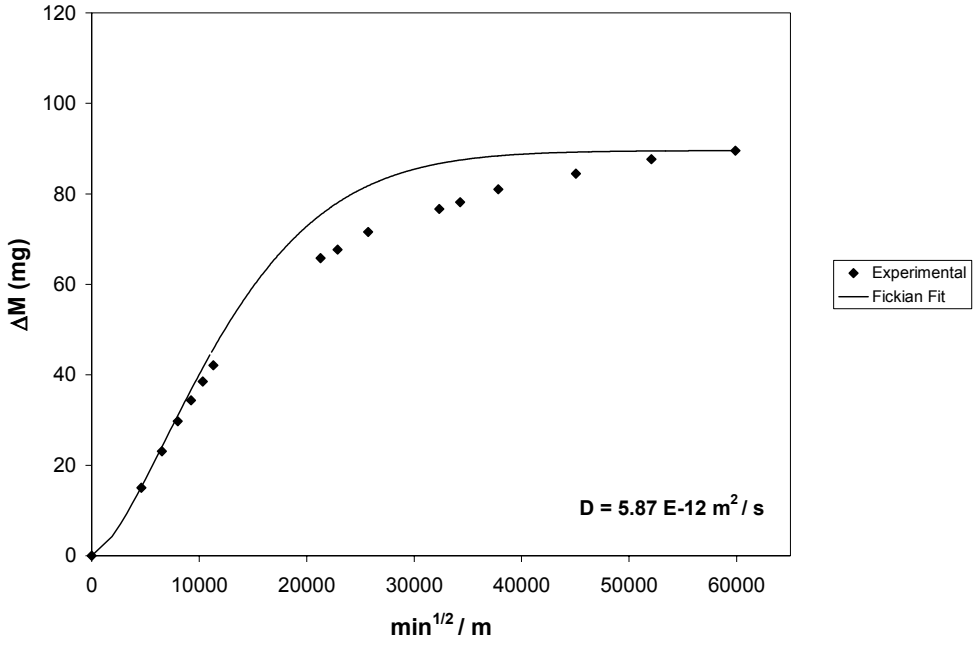

Figure 25. Diffusion coefficient determination and Fickian curve fit at 85°C/85%RH for UR-A (1)

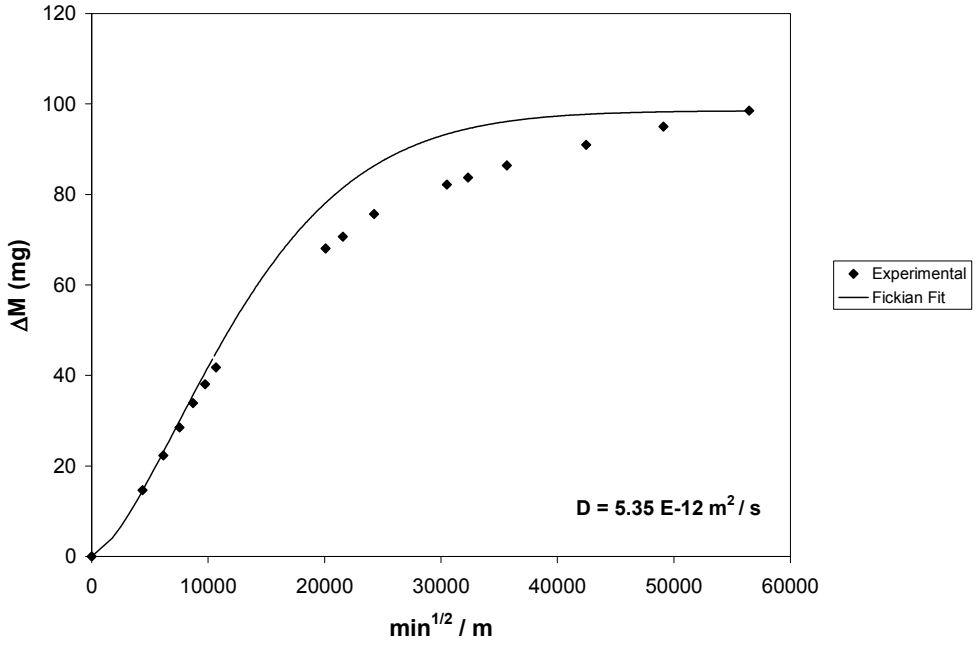

Figure 26. Diffusion coefficient determination and Fickian curve fit at 85°C/85%RH for UR-A (2)

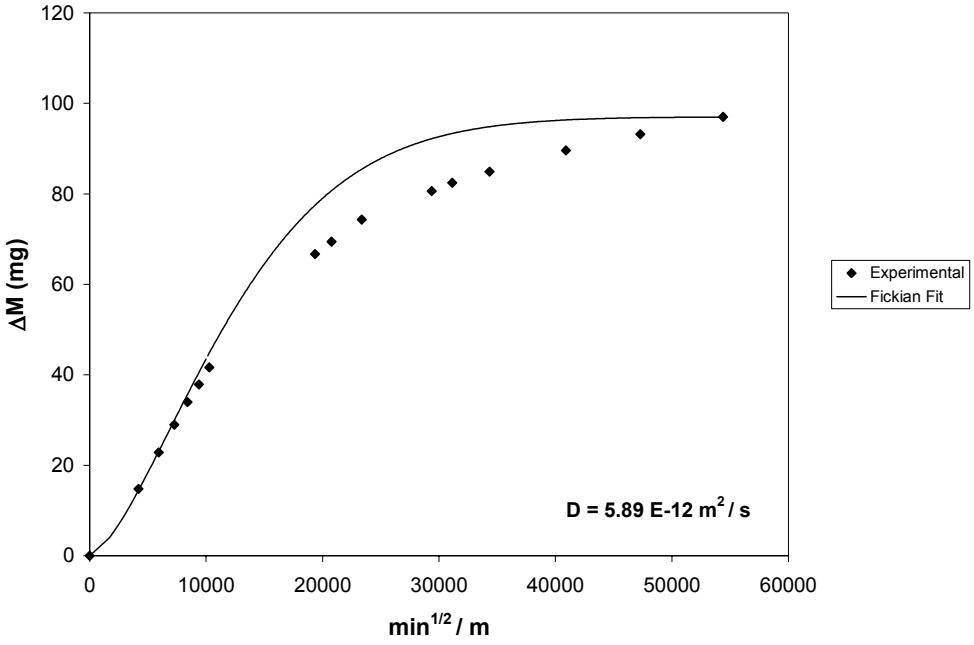

Figure 27. Diffusion coefficient determination and Fickian curve fit at 85°C/85%RH for UR-A (3)

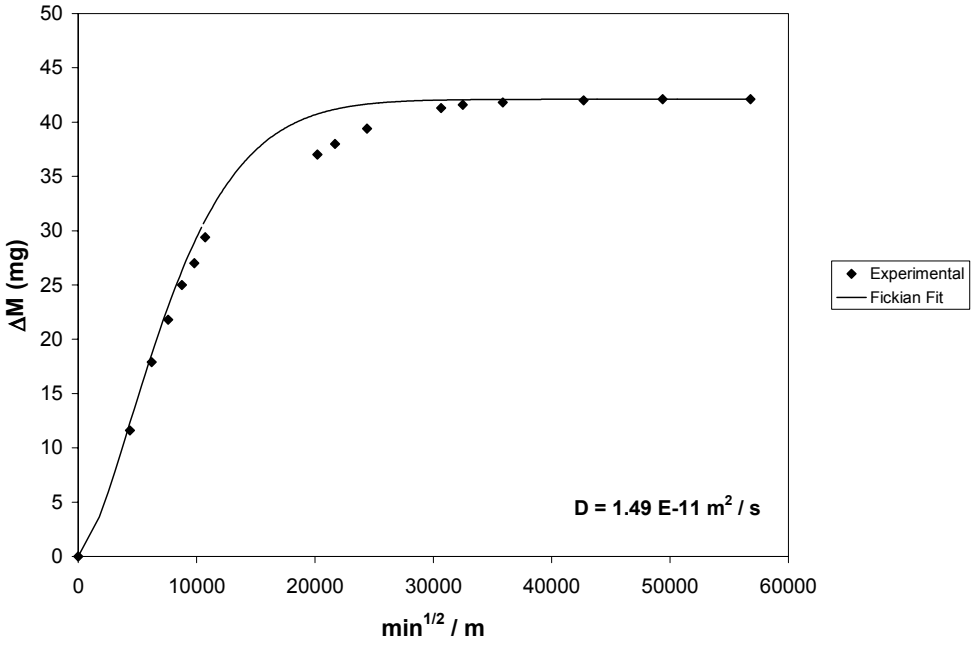

Figure 28. Diffusion coefficient determination and Fickian curve fit at 85°C/85%RH for UR-B (1)

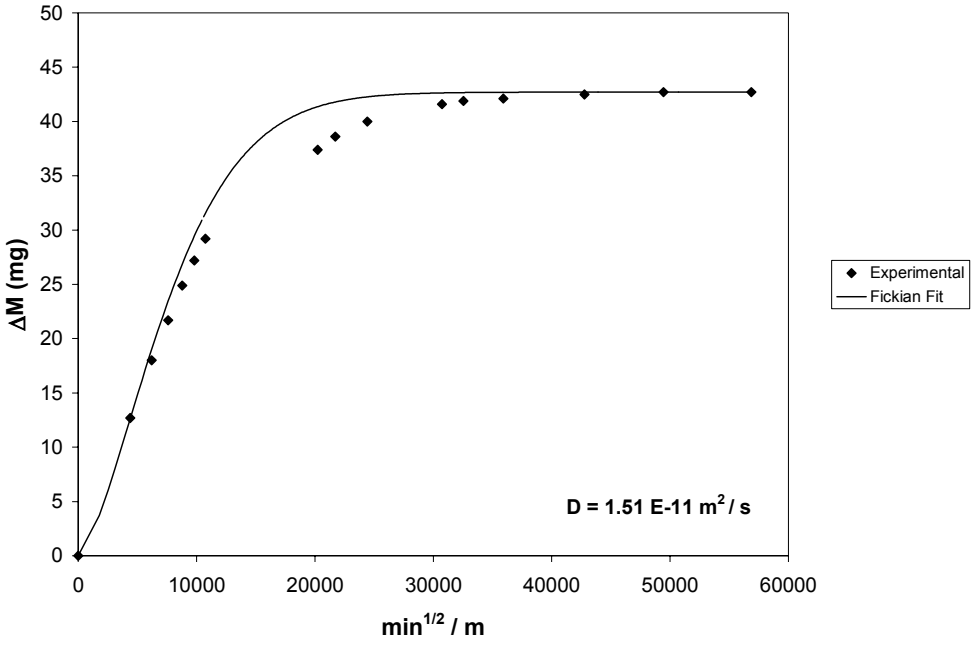

Figure 29. Diffusion coefficient determination and Fickian curve fit at 85°C/85%RH for UR-B (2)

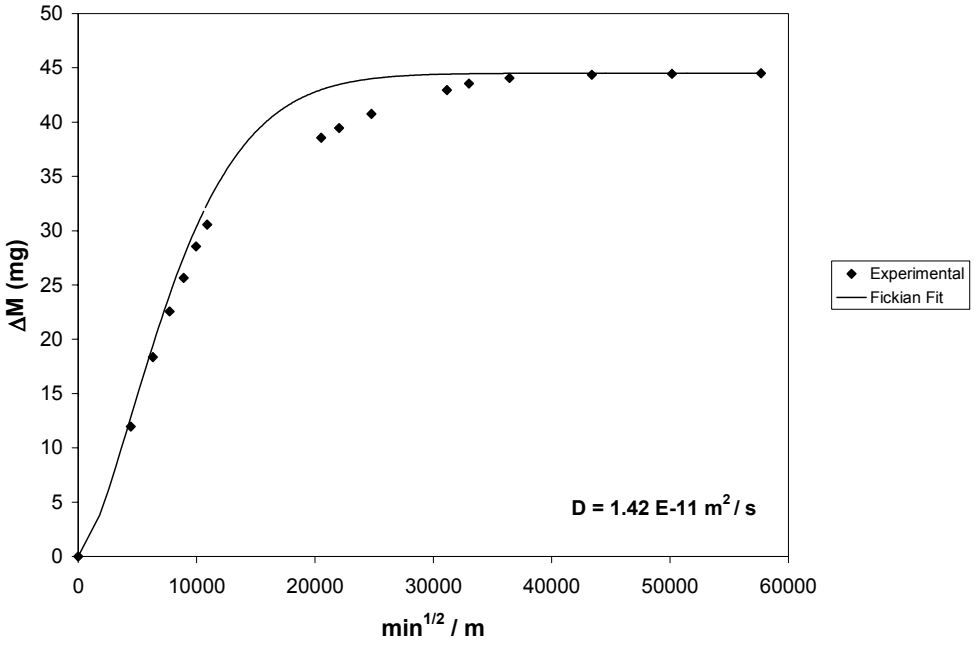

Figure 30. Diffusion coefficient determination and Fickian curve fit at 85°C/85%RH for UR-B (3)

It is clear from Figures 25 - 30 that neither UR-A nor UR-B exhibited true Fickian behavior at 85°C/85%RH, although UR-B appeared to obtain a better curve fit than UR-A. Since the test specimens promoted predominately one-dimensional diffusion and exhibited non-Fickian absorption behavior, it can be concluded that the diffusion coefficients of both UR-A and UR-B were dependent on the concentration rather than being constant throughout the entire diffusion process at 85°C/85%RH.

Wong, *et al.*, (1999) found varied diffusion behavior in the epoxy resins they evaluated at 85°C/85%RH, with some resins exhibiting Fickian diffusion while others did not. They postulated that diffusivity is constant and moisture diffusion exhibits Fickian behavior for epoxy resins at lower temperature and humidity levels such as 30°C/60%RH. Test specimens in this study were evaluated at higher temperatures and humidity levels to drive as much moisture into the interface of the interfacial fracture test specimens as quickly as possible. Increasing the humidity level results in a corresponding amplification of the saturation level, while increasing the temperature level produces more prominent non-Fickian behavior (Vanlandingham, *et al.*, 1999). Although test specimens will absorb more moisture in less time at higher temperature and relative humidity levels, the trade-off is that the specimens will also exhibit an increased likelihood of non-Fickian diffusion behavior. Wong, *et al*., (1999) recommended that if the standard experimental procedure for the determination of the diffusion coefficient assuming constant diffusivity is used for non-Fickian behavior, the moisture properties should be determined at a duration similar to the JEDEC moisture sensitivity level for the respective experimental moisture preconditioning used. This study concurs with that

recommendation, with the accuracy of the Fickian curve fit improving as the saturation limit, M_∞, was decreased for UR-A. Therefore, the saturation limit for the diffusion coefficient test specimens was taken to be at 168 hours as a result of that being the JEDEC duration level for the moisture preconditioning environment of 85°C/85%RH.

4.3.2 Moisture Absorption Modeling

Having concluded that both underfill resins evaluated in this study exhibited non-Fickian behavior at 85°C/85%RH, the focus of this study now centered on to what extent an analytical diffusion analysis could be implemented to model the moisture distribution in the interfacial fracture test specimens. Vanlandingham, *et al.*, (1999) observed that several of the epoxy resins tested in their study at 20°C/75%RH, 20°C/85%RH, and 50°C/85%RH exhibited Fickian behavior only during the initial stages of diffusion. Similarly, it is clear from Figures 25 – 30 that the underfill resins examined in this study exhibited more pronounced Fickian behavior during the initial stages of absorption as well; consequently, the associated error introduced from utilizing a Fickian solution to model the moisture absorption behavior will be minimal for small times of exposure at 85°C/85%RH. As a result, the experimentally determined diffusion coefficients for each underfill resin will provide a reasonable approximation for modeling the moisture distribution in the interfacial fracture test specimens for preliminary exposure to the humid environment.

To illustrate the moisture distribution graphically in the interfacial fracture test specimens, a transient, finite element analysis utilizing four-noded quad elements was

implemented to model the associated moisture concentration distribution in test specimens for small times of exposure. (The details of the interfacial fracture test specimen construction are given in Section 6.2.3, Interfacial Fracture Test, of Chapter 6, Effect of Moisture on Interfacial Fracture Toughness). Since the substrates were metallic and impermeable to moisture, it should be noted that only the moisture distribution in the each underfill was modeled in the interfacial fracture test specimens. In addition, the mesh convergence was determined to be over 99%, which is well above the 90% mesh convergence design guideline for modeling. Although such a fine mesh was not necessary, the simple geometry and homogenous material model resulted in a solution that was not very demanding on computational resources. Results of the finite element model illustrating the transient moisture distribution in the underfill resins are shown in Figures 31 and 32. Both figures refer to the interfacial fracture test specimens as unmodified, which means that this is the moisture absorption behavior exhibited by the test specimens if placed in 85^{o}C/85%RH conditions immediately after manufacture without consideration to how the moisture uptake could influence fracture results.

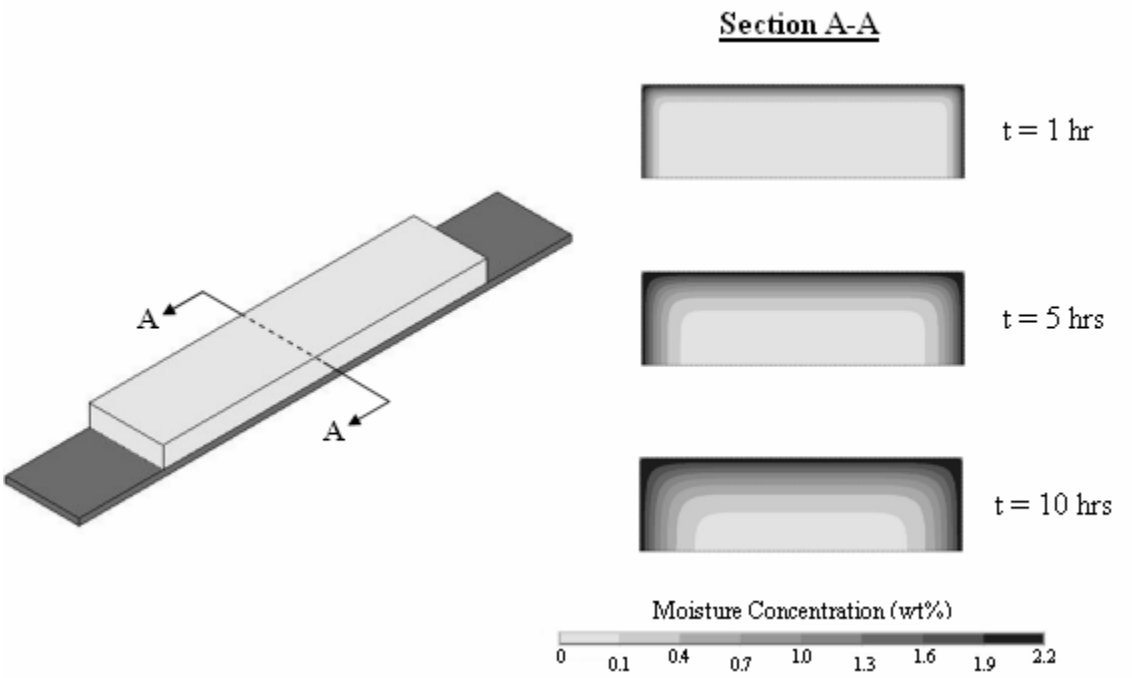

Figure 31. Moisture concentration distribution for unmodified UR-A interfacial fracture test specimen at 85°C/85%RH after 1, 5, and 10 hours of exposure

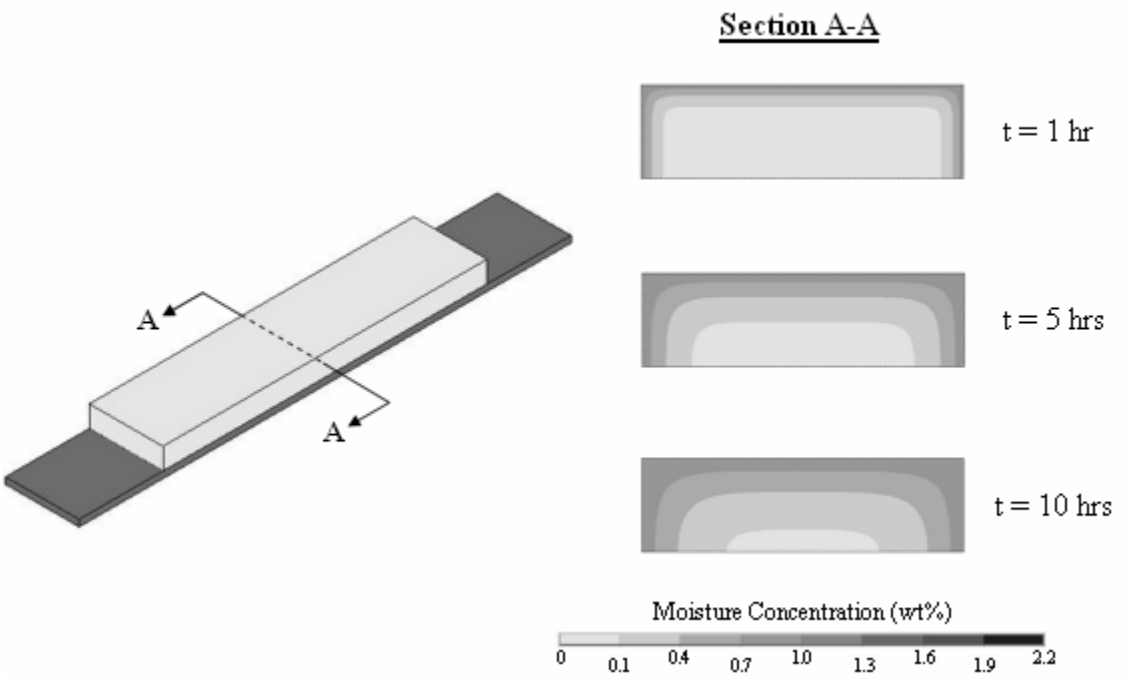

Figure 32. Moisture concentration distribution for unmodified UR-B interfacial fracture test specimen at 85°C/85%RH after 1, 5, and 10 hours of exposure

It is apparent from the model of the transient moisture ingress in the interfacial fracture test specimens that edge effects are significant. This can be clearly seen by examining the interface of the test specimens (bottom of each cross section A-A) in Figures 31 and 32, where it is evident a gradient of moisture will exist at the interface until saturation is reached in the test specimens. This is undesirable since the non-uniform moisture gradient at the interface will not allow a fracture toughness measurement to be identified with a particular level of interfacial moisture concentration unless saturation is reached in the test specimen. Furthermore, it is also possible the non-uniform moisture gradient at the interface could influence interfacial fracture toughness results even if saturation is reached in a test specimen. This is due to different areas of the interface being exposed to varying degrees of moisture for different periods of time, which could possibly have an effect on fracture toughness results even if test specimens are in a saturated state. Last, wicking along the interface could also introduce moisture concentration levels that remain unidentified through modeling of the absorption process alone, which would make it difficult to attribute a particular fracture toughness measurement with an associated interfacial moisture concentration level. In view of these observations, the interfacial fracture test specimen design and model was revised with a water-proof perimeter applied to test specimens before moisture preconditioning to force 1-D moisture uptake through the top surface of the test specimens and prevent wicking along the interface. Not only will this yield uniform concentrations spatially at the interface, but it will also aid in the identification of an interfacial moisture concentration level by utilizing the inherent moisture absorption characteristics of the

adhesive. Figures 33 and 34 depict the moisture concentration distribution in the modified interfacial test specimens.

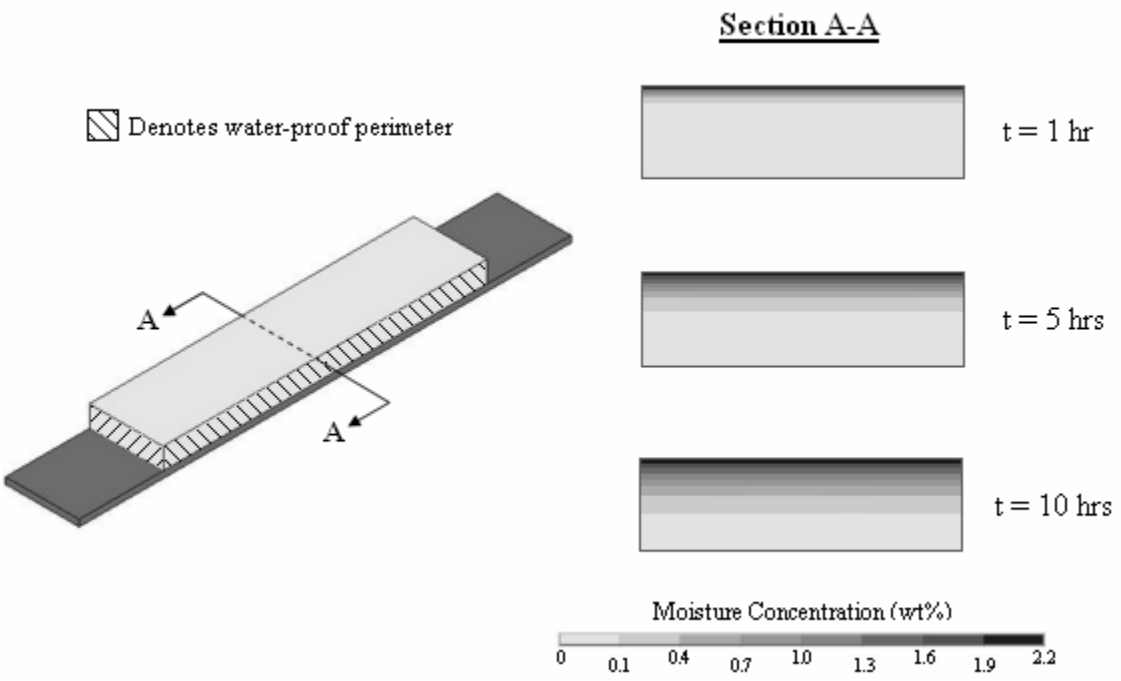

Figure 33. Moisture concentration distribution for modified UR-A interfacial fracture test specimen at 85°C/85%RH after 1, 5, and 10 hours of exposure

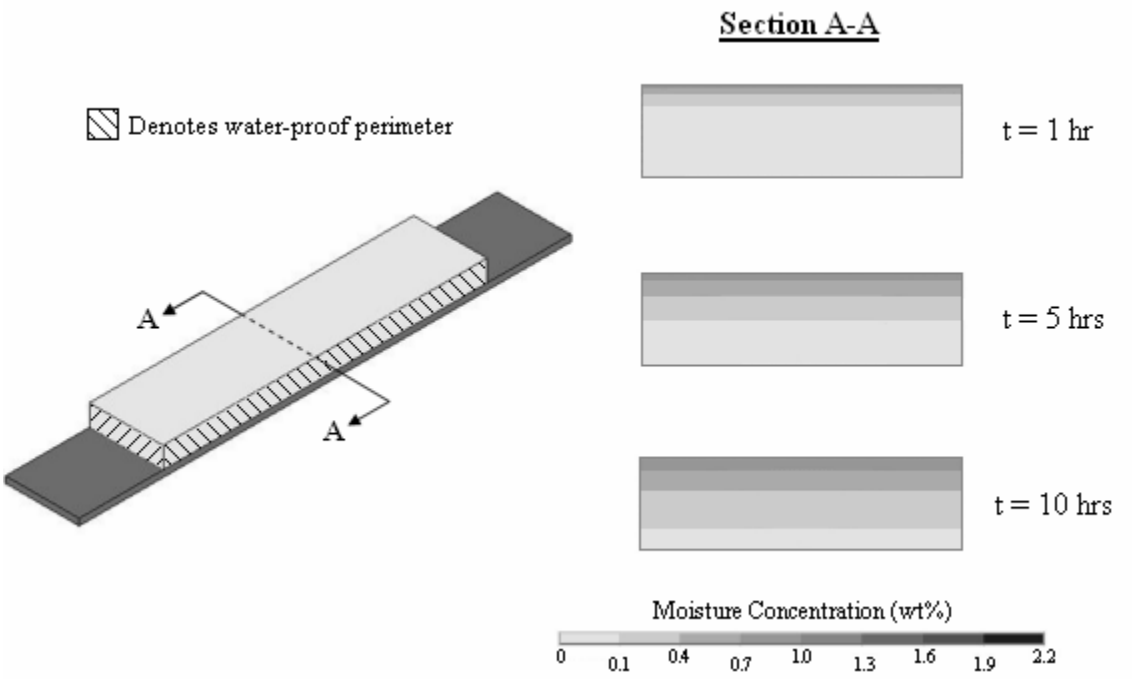

Figure 34. Moisture concentration distribution for modified UR-B interfacial fracture test specimen at 85°C/85%RH after 1, 5, and 10 hours of exposure

Although percent weight is dependent on both the specimen volume and density, a comparison between the moisture concentration distributions can be made as a result of both underfills having similar densities (UR-A, ρ = 1.14E-03 g/mm^3 and UR-B, ρ = 1.16E-03 g/mm^3) and volumes. Figures 33 and 34 illustrate that although UR-A interfacial fracture test specimens contain a significantly higher concentration of moisture near the underfill surface, the moisture will actually penetrate the interface first for comparably sized UR-B interfacial fracture test specimens. It is clear from the progression of the constant-concentration lines depicted in Figures 33 and 34 that the moisture traversed much more easily through the UR-B interfacial test specimens. An explanation for this behavior lies in the particular chemistry of each underfill epoxy with

respect to the polarity of water molecules. As previously noted, amine functional groups regulate transport through the nanopore channels of the epoxy by either blocking or allowing moisture to traverse the channels depending on the orientation of the resin with respect to nanopore position (Soles and Yee, 2000). On further investigation, it was found that amine functional groups were present in UR-A, whereas UR-B was a non-amine containing underfill. Consequently, it would be anticipated that UR-B would have an enhanced diffusion coefficient than UR-A, which was found to be true based on the results from the diffusion coefficient test specimens. As demonstrated in Figures 33 and 34, the amine functional groups present in UR-A contributed to retard moisture penetration into the amine containing epoxy resin, UR-A, whereas the moisture diffused more easily through the non-amine epoxy resin, UR-B. Therefore, degradation of interfacial adhesion over the entire interface due to the presence of moisture will begin to occur in UR-B interfacial fracture test specimens before comparably sized UR-A interfacial fracture test specimens.

4.3.3 Moisture Absorption Behavior at Different Environments

In order to evaluate the effect of moisture on interfacial adhesion, several different moisture preconditioning environments will need to be employed to determine the intrinsic change in the interfacial fracture toughness as function of increasing moisture concentration. Two epoxy-based, no-flow underfills, UR-A and UR-B, were evaluated as possible candidates for a detailed study on the effect of moisture on interfacial adhesion. The optimum adhesive selected will need to exhibit moisture

absorption behavior that will allow the identification of the interfacial moisture concentration within the test specimen for a particular, measured value of interfacial fracture toughness.

Based on the moisture absorption characteristics of both materials (Section 4.3.1), UR-B represents an ideal candidate for a detailed study on the effect of moisture on interfacial adhesion. As seen in Figure 24, UR-B reached saturation well within 168 hours of exposure at 85^{o}C/85%RH, whereas UR-A had not approached saturation within that same period of time as demonstrated in Figure 23. Longer exposure times could be employed in an attempt to reach saturation; however, UR-A had not reached saturation even after 725 hours of exposure at 85^{o}C/85%RH. In addition, longer durations could also introduce more significant thermal aging effects on interfacial adhesion performance, making it more difficult to ascertain the effect of moisture. Last, the 168 hour duration for moisture preconditioning is desired since it represents a common JEDEC industry standard for moisture preconditioning. Since a significant gradient of moisture concentration will exist in interfacial fracture test specimens composed of UR-A upon removal from the humidity chamber after 168 hours of preconditioning, it does not represent an ideal candidate for a fundamental study in the effect of moisture on interfacial adhesion. This is attributed to two primary reasons. First, the moisture concentration gradient will affect the accuracy of the interfacial fracture toughness values by requiring the use of an aggregate value for the elastic modulus for the entire adhesive. This is due to the moisture concentration gradient decreasing the elastic modulus to varying degrees, effectively making the adhesive a composite in regards to mechanical

performance. Second, the gradient will also make it difficult to ascertain the interfacial moisture concentration level at the time of fracture testing. This is a result of both the non-Fickian absorption behavior and lack of an attainable saturation level within a reasonable exposure timeframe. Consequently, fracture toughness results could not be accurately attributed with a particular level of moisture concentration, which would introduce error when identifying the intrinsic change in toughness as a function of moisture concentration. Conversely, since UR-B reaches a saturated state within the 168 hour exposure timeframe, it represents an adhesive that is much better suited for evaluating the effect of moisture on interfacial adhesion. By reaching a saturated state, UR-B allows the identification of a particular moisture concentration level to correspond with a measured interfacial fracture toughness result.

To identify the intrinsic change in interfacial adhesion as a function of moisture concentration, the response of UR-B to several different moisture preconditioning environments will need to be evaluated. The environments selected include fully dry (used as a control), 85^{o}C/50%RH, 85^{o}C/65%RH, and 85^{o}C/85%RH. The increasing humidity component in each moisture preconditioning environment will result in a gradual amplification of the saturation concentration of moisture in test specimens, allowing the identification of the change in interfacial fracture toughness as a function of increasing moisture content. The 85^{o}C temperature component in each moisture preconditioning environment will enhance diffusion rates and drive more moisture into test specimens over a smaller timeframe when compared to lower temperature moisture preconditioning environments. In addition, the 85^{o}C temperature component was used in

all moisture preconditioning environments to maintain a directly comparable meaning for the relative humidity between each environment. Relative humidity, ϕ, is defined as the following:

$$\phi = \frac{m_v}{m_g} \tag{5.6}$$

where m_v is the amount of moisture the air holds and m_g is the maximum amount of moisture the air can hold at the same temperature. Since m_g is dependent on temperature, the relative humidity of air is also dependent on temperature. As temperature increases, the moisture capacity of air increases, and the relative humidity will decrease for the same amount of moisture content, m_g, in the air when comparing the relative humidity at lower temperatures to higher temperatures. For additional information on psychometrics, refer to *Thermodynamics: An Engineering Approach* by Cengel and Boles (1994).

The moisture absorption characteristics of UR-B to 85°C/85%RH moisture preconditioning was previously identified in Section 4.3.1; however, the response of UR-B to the remaining moisture preconditioning environments of 85°C/50%RH and 85°C/65%RH still needed to be characterized. Consequently, diffusion coefficient test specimens were made to identify the moisture absorption behavior of UR-B at both 85°C/50%RH and 85°C/65%RH environments. The diffusivity was experimentally determined for each moisture preconditioning environment using Equation (5.4) and

averaged from the three independent samples. The results for 85°C/50%RH and 85°C/65%RH are shown in Tables 6 and 7 respectively.

Table 6. Experimentally determined diffusion coefficients for UR-B at 85°C/50%RH

Test Specimen	Material	Environment	Diffusion Coefficient, D (m^2/s)
1	UR-B	85C/50%RH	2.03E-11
2	UR-B	85C/50%RH	2.01E-11
3	UR-B	85C/50%RH	1.87E-11
		AVERAGE:	**1.97E-11**
		STANDARD DEVIATION:	7.12E-13

Table 7. Experimentally determined diffusion coefficients for UR-B at 85°C/65%RH

Test Specimen	Material	Environment	Diffusion Coefficient, D (m^2/s)
1	UR-B	85C/65%RH	1.86E-11
2	UR-B	85C/65%RH	1.77E-11
3	UR-B	85C/65%RH	1.71E-11
		AVERAGE:	**1.78E-11**
		STANDARD DEVIATION:	5.97E-13

Table 8 provides a summary of both the saturation concentration and diffusivity of UR-B for moisture preconditioning environments of 85°C/50%RH, 85°C/65%RH, and 85°C/85%RH.

Table 8. Summary of diffusion coefficients and saturation concentrations of UR-B for various levels of moisture preconditioning

Environment	Material	Csat (wt%)	Diffusion Coefficient, D (m^2/s)
85C / 50%RH	UR-B	0.65	1.97E-11
85C / 65%RH	UR-B	0.77	1.78E-11
85C / 85%RH	UR-B	1.02	1.47E-11

As shown in Table 8, the saturation concentration increases as the relative humidity increases. This is expected since all environments were at the same temperature, thus an increase in the relative humidity would increase the amount of moisture content in the air relative to the other environments. Naturally this increase in moisture content in the air would result in a higher saturation concentration in the underfill for each environment. Also, there appears to be a trend indicating that the diffusivity of the underfill slightly decreases as the relative humidity increases for a given temperature; however, it is difficult to state this conclusion unequivocally for two primary reasons. First, the absorption process was actually non-Fickian in behavior, which is discussed in further detail in subsequent paragraphs. This is important since the experimental determination of diffusivity utilizing absorption data with Equation (5.4) is obtained assuming Fickian absorption behavior. As a result, error will be introduced when determining diffusion coefficients experimentally for non-Fickian behavior. Second, the diffusivity values were all within an order of magnitude of one another with only slight variation for each environment. This fact relative to the aforementioned error makes it difficult to conclude that the diffusivity of the underfill decreases as the relative

humidity increases for a given temperature. However, it should be noted that a previous study has shown that moisture diffusivity does indeed decrease as the relative humidity increases for a given temperature (Bhattacharyya, *et al*., 1988), which would support the trend observed in Table 8. An explanation for this behavior could be attributed at least in part to how each particular epoxy system responds to moisture induced swelling relative to their moisture absorption characteristics. If a material swelled in such a manner that it produced voids inside the epoxy matrix, the diffusing moisture would collect in pools of water at these voids. Since the diffusivity of water vapor is at least an order higher than that of liquid water, these collection pools could potentially yield a measurable decrease in the aggregate diffusivity of the material as the water vapor condensed from vapor to liquid form. As the relative humidity increases for a given temperature, the moisture concentration increases inside the material, which will cause additional swelling in the material when compared to less humid environments. This additional swelling could form larger voids that could ultimately yield additional condensation, possibly explaining at least in part how the diffusivity of a material could decrease as the relative humidity increases for a given temperature.

After the diffusion coefficient of UR-B for each environment was determined, a Fickian curve was generated for each data set to examine the extent that the moisture uptake of the specimens demonstrated Fickian behavior. Since Figures 28 – 30 already depict the absorption behavior of UR-B for conditions of 85^{o}C/85%RH, only the results for conditions of 85^{o}C/50%RH and 85^{o}C/65%RH are shown below. Rather than utilizing Equation (5.2) for the Fickian profile, the simplification relation developed by Shen and

Springer (1976) given by Equation (5.5) was used. The resulting Fickian curve for each data set for UR-B at 85°C/50%RH and 85°C/65%RH is shown in Figures 35 – 40**.**

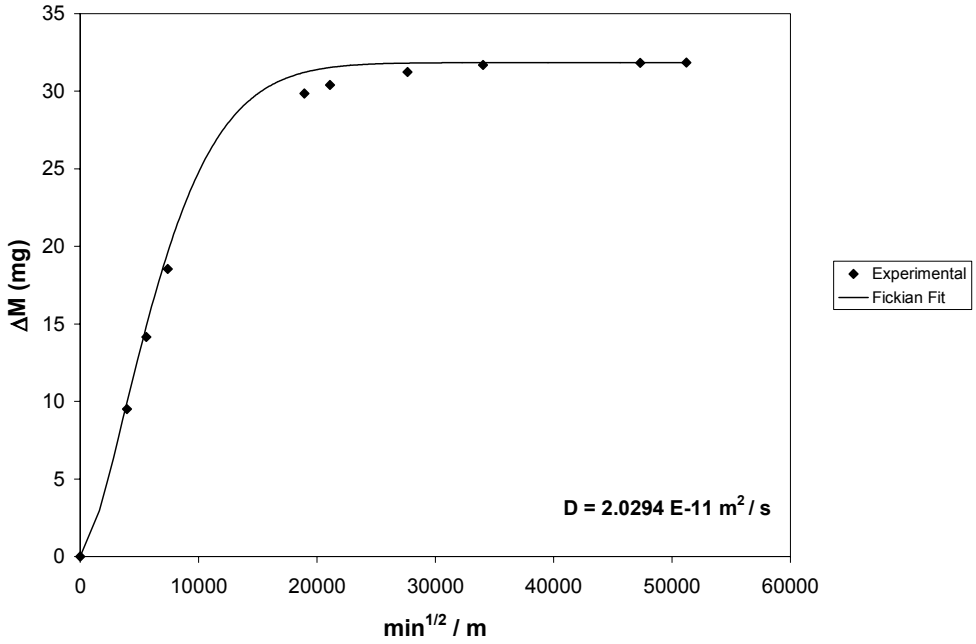

Figure 35. Diffusion coefficient determination and Fickian curve fit at 85°C/50%RH for UR-B (1)

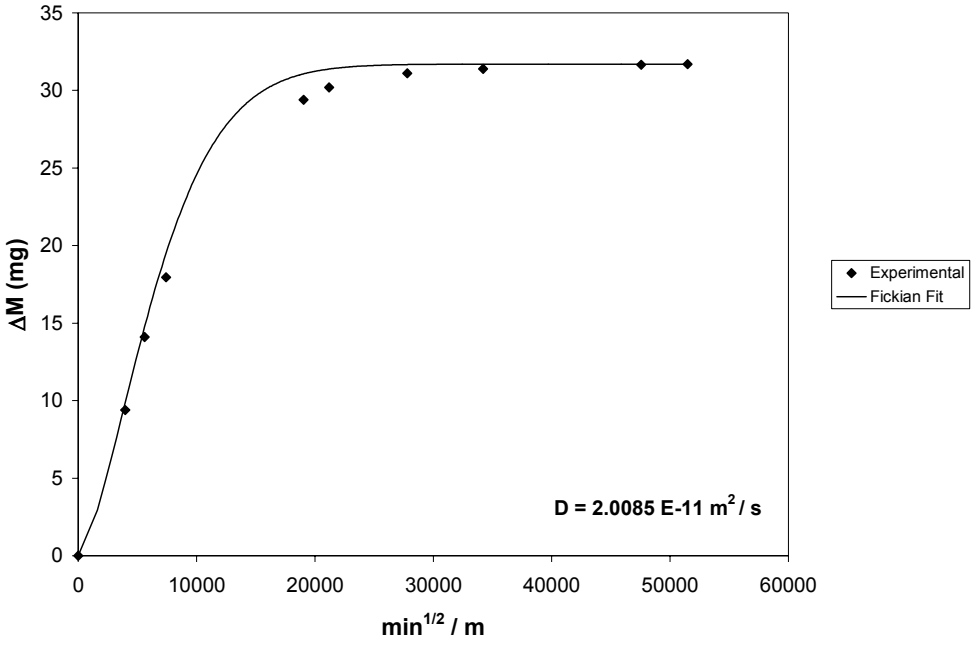

Figure 36. Diffusion coefficient determination and Fickian curve fit at 85°C/50%RH for UR-B (2)

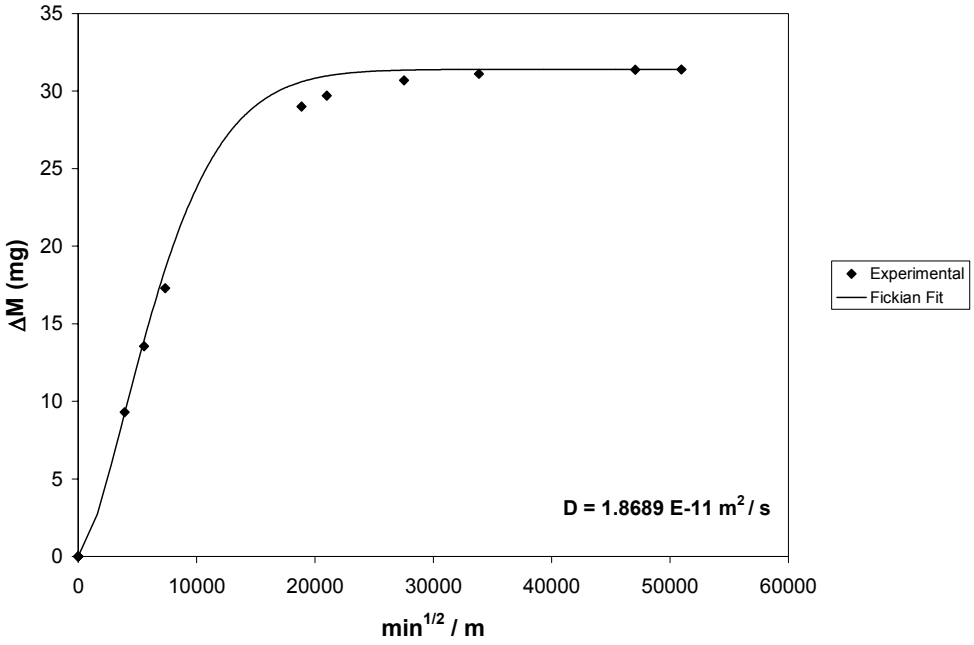

Figure 37. Diffusion coefficient determination and Fickian curve fit at 85°C/50%RH for UR-B (3)

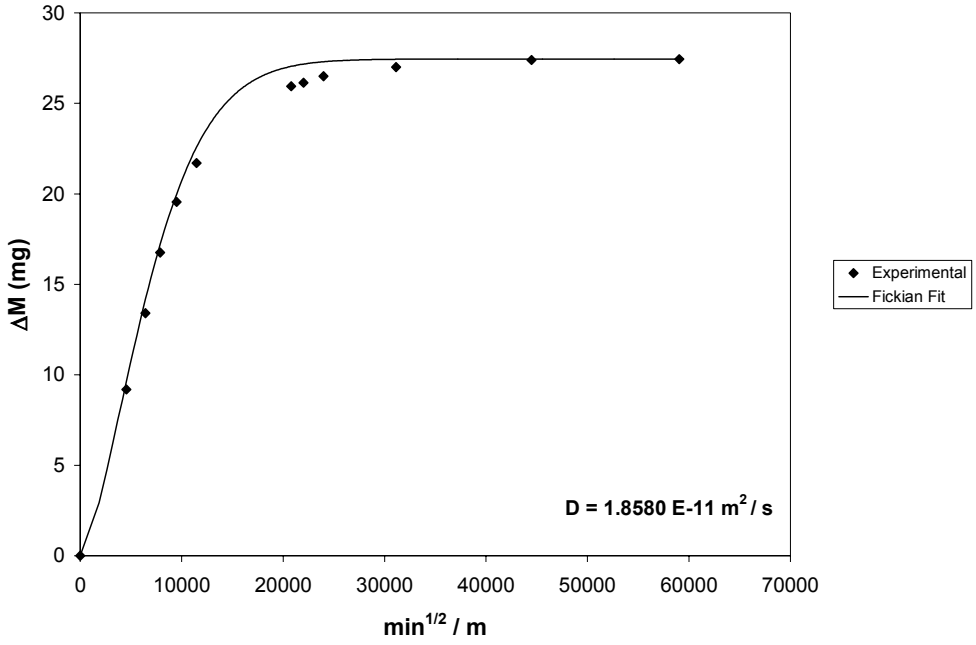

Figure 38. Diffusion coefficient determination and Fickian curve fit at 85°C/65%RH for UR-B (1)

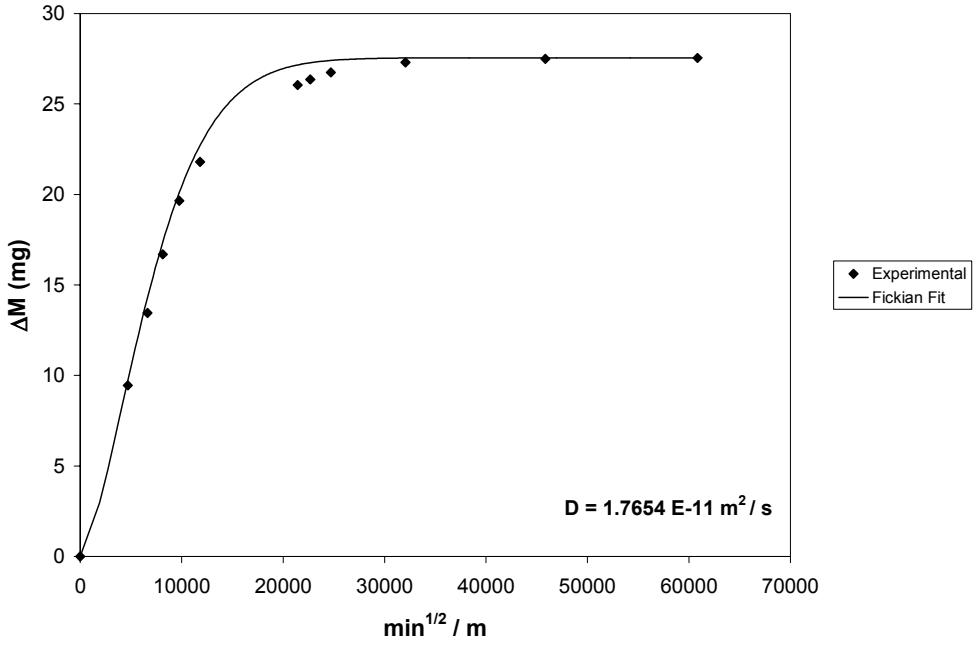

Figure 39. Diffusion coefficient determination and Fickian curve fit at 85°C/65%RH for UR-B (2)

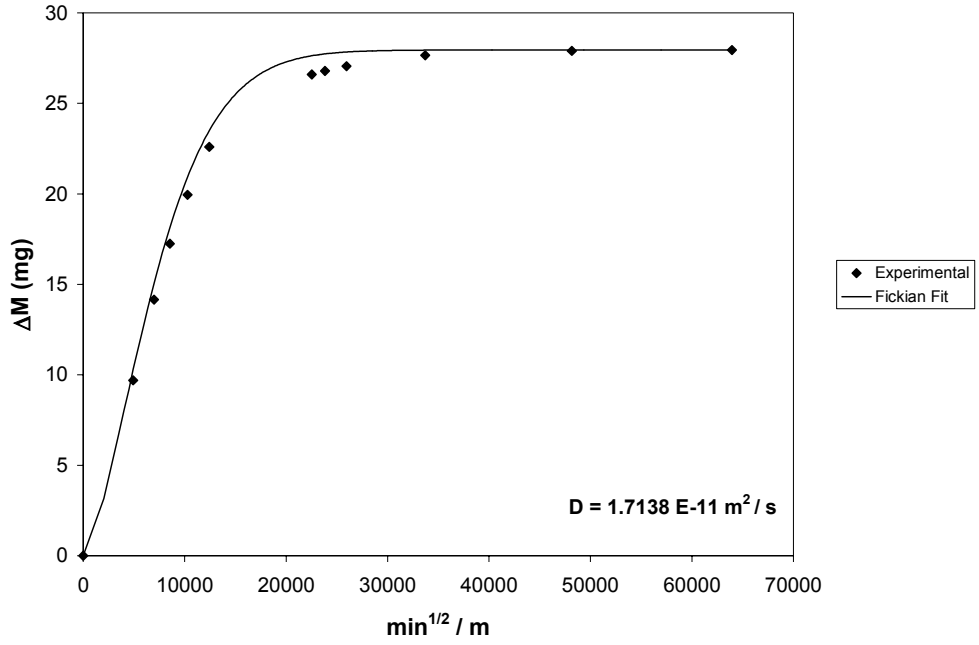

Figure 40. Diffusion coefficient determination and Fickian curve fit at 85°C/65%RH for UR-B (3)

Using Equation (5.5) with moisture absorption data, it is clear from Figures 35 - 40 that UR-B exhibited non-Fickian absorption behavior for both 85°C/50%RH and 85°C/65%RH environments. Similar non-Fickian absorption behavior occurred when moisture preconditioning at 85°C/85%RH, as indicated by Figures 28 – 30. Since the test specimens promoted predominately one-dimensional diffusion and exhibited non-Fickian absorption behavior, it can be concluded that the diffusion coefficients for UR-B were dependent on the concentration rather than being constant throughout the entire diffusion process for 85°C/50%RH, 85°C/65%RH, and 85°C/85%RH moisture preconditioning environments. Although UR-B does exhibit non-Fickian moisture absorption behavior for those environments, it represents a good candidate for evaluating the effect of moisture on interfacial adhesion. This is due to the fact that saturation was obtained in

each environment within the 168 hour exposure time, which will yield a uniform distribution of moisture throughout the test specimen and known concentration of moisture at the time of testing.

4.4 Conclusions

To ascertain the fundamental moisture absorption behavior and identify the rate of moisture transport to the interface within the interfacial fracture toughness test specimens, a moisture absorption analysis was performed on each underfill resin at 85^{o}C/85%RH. The analysis was based on traditional, analytical solutions of Fick's second law of diffusion. From this analysis, it was determined that the diffusion coefficient for both underfill resins was concentration dependent and not constant, as indicated by the disparity between the Fickian solution and the moisture absorption data from the diffusion coefficient test samples. Since both underfill resins exhibited more pronounced Fickian behavior initially, the associated error between the Fickian solution and the actual absorption behavior was minimal for small times of exposure at 85^{o}C/85%RH. Consequently, the experimentally determined diffusion coefficients for each underfill resin provided a reasonable approximation for modeling the moisture distribution in the interfacial fracture test specimens for preliminary exposure to the humid environment.

A finite element analysis was implemented to model the associated moisture concentration distribution in the interfacial fracture toughness test specimens for small times of exposure. Two primary conclusions were obtained from this model. First, the model demonstrated that unmodified interfacial fracture toughness test specimens would need to be revised for a comprehensive evaluation of the effect of moisture on interfacial adhesion. The term unmodified in relation to the interfacial fracture toughness test specimens indicates test specimens placed in a moisture preconditioned environment immediately after manufacture without consideration to how the moisture uptake could influence interfacial fracture results. Based on the results of the model, edge effects from moisture uptake in unmodified interfacial fracture toughness test specimens are significant, yielding a moisture concentration gradient at the interface. This is undesirable since the interface will experience different levels of moisture spatially relative to the exposure time, which will not allow a fracture toughness measurement to be identified with a particular level of interfacial moisture concentration until saturation is reached. Furthermore, it is also possible the non-uniform moisture gradient at the interface could influence interfacial fracture toughness results even if saturation is reached in a test specimen. This is due to different areas of the interface being exposed to varying degrees of moisture for different periods of time, which could possibly have an effect on fracture toughness results even if test specimens are in a saturated state. Last, wicking along the interface could also introduce moisture concentration levels that remain unidentified through modeling of the absorption process inside the adhesive alone. In view of these observations, the interfacial fracture test specimen design and

model was revised with a water-proof perimeter applied to test specimens before moisture preconditioning. This forced 1-D moisture uptake through the top surface of the test specimens, yielding uniform concentrations of moisture spatially across the entire interface for the full duration of exposure to the moist environment. Also, the application of the water-proof perimeter removed the possibility that moisture could wick along the interface. This will aid in the identification of an interfacial moisture concentration level by utilizing the inherent moisture absorption characteristics of the adhesive, which can be used with interfacial fracture toughness results to identify the intrinsic behavior of interfacial fracture toughness as a function of moisture content. Second, the model demonstrated that although UR-A specimens contained a significantly higher concentration of moisture at the surface compared to UR-B specimens, the moisture actually penetrated the interface of the UR-B specimens before similar sized UR-A specimens. This moisture absorption behavior can be attributed to the presence or absence of amine functional groups in each underfill resin. Amine functional groups in UR-A contributed to retard moisture penetration through the underfill, whereas the moisture diffused more easily through the non-amine epoxy resin, UR-B. Consequently, moisture will initially penetrate the interface and begin to decrease the interfacial adhesion at the interface for UR-B interfacial fracture test specimens before comparably sized UR-A interfacial fracture test specimens.

Based on the moisture absorption analysis and modeling of the two underfills, UR-B was identified as an ideal candidate for use in a fundamental study to identify the effect of moisture on interfacial adhesion. UR-B had achieved a saturated state at the

conclusion of the moisture preconditioning duration of 168 hours, whereas UR-A never reached a saturated state, even after 725 hours of exposure. This will result in a concentration gradient of moisture within interfacial fracture test specimens composed of UR-A upon removal from the humidity chamber, which results in two primary drawbacks when attempting to identify the intrinsic effect of moisture on interfacial adhesion. First, the moisture concentration gradient will yield a gradient of mechanical properties within the adhesive at the time of fracture testing. Since interfacial fracture toughness is a function of the elastic modulus of both the adhesive and substrate, an aggregate value for the elastic modulus of the adhesive will need to be used, which will introduce some error in the interfacial fracture toughness evaluation. Second, the moisture concentration gradient will also make it difficult to ascertain the interfacial moisture concentration of test specimens at the time of testing. This is a result of both the non-Fickian absorption behavior and lack of an attainable saturation level within a reasonable exposure timeframe. Consequently, the accuracy of attributing a particular interfacial moisture concentration level to a measured fracture toughness value will be compromised, inhibiting the identification of the intrinsic change in fracture toughness as a function of interfacial moisture concentration. Conversely, since UR-B does achieve a saturated state within the 168 hour exposure timeframe, it represents an adhesive that is better suited for evaluating the effect of moisture on interfacial adhesion. By reaching a saturated state, UR-B allows the identification of a particular moisture concentration level to correspond with a measured interfacial fracture toughness result.

To determine the intrinsic change in interfacial fracture toughness as a function of moisture concentration, several different moisture preconditioning environments will need to be evaluated. As a result, the moisture absorption characteristics of UR-B were identified for conditions of 85°C/50%RH, 85°C/65%RH, and 85°C/85%RH. It is important to note that since all environments shared the same temperature component of 85°C, the relative humidity maintained a directly comparable meaning between each environment. Based on the results of the moisture absorption analysis, UR-B exhibited non-Fickian behavior in each environment. The results also demonstrated that UR-B achieved a saturated state for each condition at the conclusion of the 168 hour exposure time, which allows the identification of a moisture concentration level when interfacial fracture testing. As anticipated, the saturation concentration increased as the relative humidity increased for each respective environment. Conversely, the diffusivity appeared to slightly decrease as the relative humidity increased for a given temperature. Due to the small variation in the measured values of diffusivity for each environment relative to the non-Fickian absorption behavior, it is difficult to state this conclusion unequivocally; however, it is plausible that the observed trend in diffusivity occurred due to the moisture expansion characteristics of the material. As the moisture caused the material to swell, small voids can form within the material, yielding localized pools of moisture. Since the diffusivity of water vapor is at least an order higher than that of liquid water, the localized diffusion rate of the material will decrease as moisture fills these pools, which if significant enough could yield a slight decrease in the aggregate diffusivity of the material as moisture concentration increases.

Having identified the moisture absorption transport characteristics of the interfacial fracture toughness test specimens in each environment, the next phase of this research focuses on understanding the response of the interfacial adhesion to increasing levels of moisture concentration. This includes identifying the primary effect of moisture being physically present at the interface, and the secondary effect of the moisture changing the elastic modulus of the adhesive, which is discussed in the following chapter.

CHAPTER V

ELASTIC MODULUS VARIATION DUE TO MOISTURE ABSORPTION

The deleterious effect of moisture not only damages interfacial adhesion by being physically present at the interface, but also through the degradation of the elastic modulus of the adhesive and substrate due to moisture uptake. The change in the elastic modulus after moisture uptake can be substantial, which can significantly affect material performance and interfacial fracture toughness results. Consequently, the variation in the elastic modulus of the adhesive and substrate as a function of moisture concentration should be determined to completely characterize the loss in interfacial adhesion due to moisture absorption. Since the substrates in this study are metallic and impermeable to moisture, it is only necessary to characterize the change in the elastic modulus as a function of moisture concentration for the underfill adhesive, which is epoxy based and highly susceptible to moisture uptake.

5.1 Introduction

Epoxy adhesives are found in many microelectronic packaging applications and widely used throughout the industry. One of the more substantial developments within the last ten years is underfill, which is an epoxy based encapsulant that mechanically couples the chip to the board. Underfill drastically enhances the fatigue life of microelectronic assemblies when compared to unencapsulated devices (Suryanarayana, *et al*., 1991); however, since underfills are epoxy based, they are also particularly vulnerable to moisture ingress (Uschitsky and Suhir, 1997; Wong, *et al*., 1999; and Ferguson and Qu, 2003). Although the absorbed moisture can significantly alter its mechanical performance and the overall microelectronic assembly reliability, very few studies in the electronic packaging literature have addressed the issue of moisture on the mechanical properties of epoxies, and no known papers found to address the effect of moisture on the elastic modulus. Consequently, it is a necessary requirement to step outside of the electronic packaging community in order to gain a better understanding of the state of the art of the effect of moisture on the mechanical properties of bulk epoxies.

Throughout the literature, the availability of information regarding the effect of moisture on the mechanical properties of epoxy adhesives is in general limited and more work is needed to adequately characterize this response (Crocombe, 1997, and Harper and Kenner, 1997). From the work that has been published, it has been found that water absorption can severely modify the mechanical properties of epoxy adhesives by decreasing the elastic modulus (Morgan, *et al*., 1980, and Zanni-Deffarges and Shanahan,

1995), shear modulus (Jurf and Vinson, 1985, and Zanni-Deffarges and Shanahan, 1994), yield stress (Wahab, *et al.*, 2002), and ultimate stress (Wahab, *et al.*, 2002) while increasing the failure strain (Crocombe, 1997, and Wahab, *et al.*, 2002) as water concentration increases.

Moisture primarily affects the mechanical properties of adhesives through three mechanisms: plasticization, crazing, and hydrolysis. The first is considered reversible upon drying, while the latter two are irreversible. Several studies attribute the decrease in modulus due to the plasticizing action of the water on the adhesive (Jurf and Vinson, 1985; Brewis, *et al*., 1990; DeNeve and Shanahan, 1992; Su, *et al*., 1992; Zanni-Deffarges and Shanahan, 1994; Zanni-Deffarges and Shanahan, 1995; Crocombe, 1997; and Wahab, *et al.*, 2002). By acting as an external plasticizer to the polymer adhesive, the water spreads the polymer molecules apart and reduces the polymer-polymer chain secondary bonding. This provides more room for the polymer molecules to untangle and move, which results in a softer, more easily deformable mass (Rosen, 1993). Other studies show the decrease in epoxy modulus after moisture absorption resulting from crazing (Morgan, *et al*., 1979; Morgan, *et al*., 1980; and Lu, *et al*., 2001), where the absorbed water can act as a crazing agent continuously decreasing the mechanical strength of epoxies with exposure time in water (Lu, *et al*., 2001). This is supported by scanning electron micrographs of epoxies, which show cavities and fractured fibrils that could only be explained by a moisture induced crazing mechanism (Morgan, *et al*., 1979). Consequently, the moisture induced swelling creates dimensional changes and internal stresses that can ultimately craze and/or crack the material. As a result, lightly

cross-linked networks will be more susceptible to crazing than highly cross-linked networks (Morgan, *et al*., 1980). Last, moisture can also affect the mechanical properties of adhesives by causing hydrolysis leading to chain scission. Short term exposure to moisture results in chain scission with a chemical addition of water that remains permanently in the epoxy system even after subsequent drying, while long term exposure to moisture can result in an increased probability of chain scission detaching segments from the polymer network, yielding a permanent loss in weight after subsequent drying (Xiao and Shanahan, 1997).

Studies by Zanni-Deffarges and Shanahan (1994 and 1995) and DeNeve and Shanahan (1992) depict the decrease in elastic and shear modulus of an epoxy as a function of time exposure to moisture. Although this information is useful in evaluating the effect of exposure time to moisture on the modulus, it does not depict how the inherent wet modulus values change as a function of concentration since a gradient of mechanical properties will exist in the adhesive until saturation is reached and water concentrations become steady and uniform. Other studies have evaluated the effect of moisture on epoxy adhesives after saturation is established for a given level of moisture preconditioning. These studies have shown a decrease in the elastic modulus of epoxy adhesives of 24% (Zanni-Deffarges and Shanahan, 1994), 29% (Su, *et al*., 1992), and 86% (Su, *et al*., 1992) for saturation concentrations of 4 wt%, 0.9 wt%, and 3.1 wt% respectively; however, they only tested one level of moisture preconditioning to compare to fully dried test results. Consequently, information regarding the mechanical response of epoxy adhesives to different levels of moisture concentrations is incomplete and

fundamental insight into the intrinsic response of the adhesives to increasing saturation concentrations of moisture cannot be ascertained.

In this study, a comprehensive evaluation of the effect of moisture on the elastic modulus of an epoxy based no-flow underfill is experimentally determined. Flexural bend test specimens are used to determine the elastic modulus, and different test groups of moisture preconditioning at 85^{o}C and varying levels of relative humidity for 168 hours are evaluated to ascertain the effect of increasing moisture content on the elastic modulus. Since saturation is reached in all test groups after moisture preconditioning at 168 hours, the inherent wet modulus of the underfill is identified as a function of increasing moisture content. In addition, a thermal aging test at 85^{o}C only for 168 hours is performed to isolate the effect of the 85^{o}C temperature component from the moisture preconditioning results.

5.2 Experimental Procedure

5.2.1 Materials

Since the substrates evaluated in this study are metallic and impermeable to moisture, only the underfill was considered for the effect of moisture uptake on the elastic modulus variation. The particular underfill evaluated was UR-B, which was determined to be ideal for studying the fundamental effect of moisture on interfacial adhesion due to its moisture diffusion kinetics and saturation behavior established from

the moisture absorption portion of this research. It should be noted this underfill was formulated for no-flow assembly, thus it does not contain any filler content.

5.2.2 Flexural Bend Test

Flexural bend test specimens were tested in a three-point bend test according to ASTM D790 (1999) to determine the effect of moisture on the elastic modulus. Test specimens were made by placing two 76.2 x 12.7 x 4.0 mm Teflon coated steel bars on either side of a 76.2 x 12.7 x 2.0 mm Teflon coated steel bar. Two 12.7 x 12.7 x 2.0 mm Teflon coated steel pieces were placed on top of the exposed ends of the 76.2 x 12.7 x 2.0 mm bar and in between the two 76.2 x 12.7 x 4.0 mm bars. The completed structure formed a mold with a 50.8 x 12.7 x 2.0 mm open reservoir. Teflon tape was wrapped around the assembly to hold the structure together without interfering with the reservoir opening. Underfill was dispensed from a syringe into the reservoir and cured at 190^{o}C for 40 minutes in a natural convection oven. After curing, the completed underfill flexural bend test specimens were removed from the mold. The final test specimen dimensions were 50.8 x 12.7 x 2.0 mm.

Tests were performed on a United Load Frame (Model SSTM 500) at a crosshead rate of 1.2 mm/min on a support span of 38.1 mm. The modulus of elasticity was calculated by drawing a tangent to the steepest initial straight-line portion of the load-deflection curve and using the following equation:

$$E = \frac{L^3 m}{4bd^3} \tag{5.1}$$

where E is the modulus of elasticity, L is the length of the support span, b is the width of the beam tested, d is the depth of the beam tested, and m is the slope of the tangent of the initial straight-line portion of the load-deflection curve. For each reported value of elastic modulus, a minimum of at least five and a maximum of twenty specimens were tested and the results averaged. Error measurements represent the standard deviation in the test results.

5.2.3 Differential Scanning Calorimetry (DSC)

To insure the accuracy in all reported values for the elastic modulus and correctly attribute any observed changes to moisture preconditioning rather than incomplete curing of the underfill, Differential Scanning Calorimetry (DSC) was used to establish the degree of cure of the no-flow underfill flexural bend test specimens for the curing conditions of 190^{o}C for 40 minutes. The degree of cure (or percent cure) of the no-flow underfill material can be determined by using the heat of cure measured during a DSC test. All thermosetting systems share the commonality of the heat accompanying cure (Prime, 1997):

$$reactants \xrightarrow{-\Delta H_{Rxn}} products \tag{5.2}$$

where ΔH_{Rxn} is the exothermic heat of reaction that occurs during the cure expressed per mass of material (*J/g*). The heat of reaction is a characteristic quantity specific to each thermoset material. The fundamental assumption for the application of DSC to a thermoset cure is that the measured heat flow, *dH/dt*, is proportional to the reaction rate, $d\alpha/dt$. This is valid for materials with a single curing reaction with no other enthalpic events and in practice has been proven to be a good assumption (Prime, 1997):

$$\frac{d\alpha}{dt} = \frac{dH/dt}{\Delta H_{Rxn}} \tag{5.3}$$

which after integration yields:

$$\alpha = \frac{\Delta H_t}{\Delta H_{Rxn}} = \frac{\Delta H_{Rxn} - \Delta H_r}{\Delta H_{Rxn}} \tag{5.4}$$

where α is the conversion or degree of cure of the reaction, ΔH_t is the heat generated up to time, *t*, ΔH_{Rxn} is the total heat of reaction obtained from an uncured sample, and ΔH_r is the residual heat of reaction, which is the heat evolved from a test sample during completion of cross linking as a result of residual cure in the test sample. The numeric values of ΔH_{Rxn} and ΔH_r can be determined from the area under the exothermic peak of a DSC thermo-diagram of an uncured and cured sample respectively, where the baseline is usually determined by drawing a straight line between the onset and the end of the

exotherm in such a way that the baseline is tangent to the DSC curve at those two points (Prime, 1997).

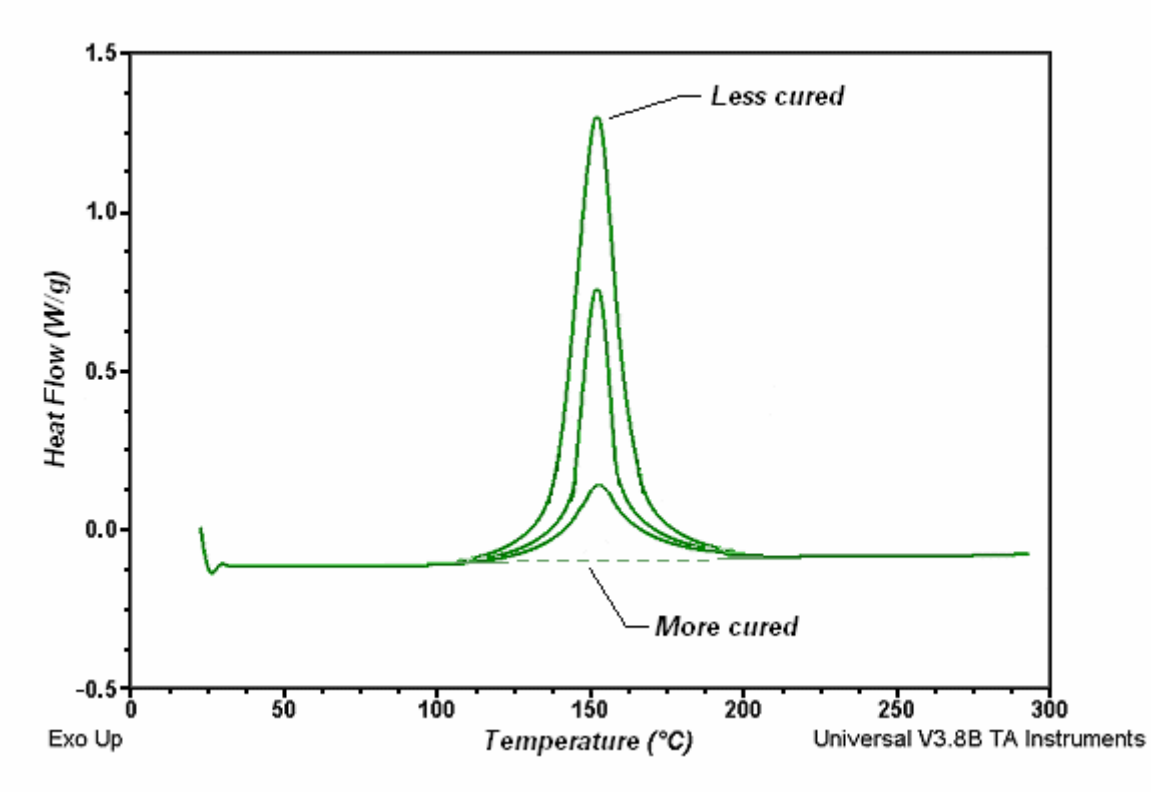

Figure 41. DSC thermo-diagram illustrating the degree of cure increases as the exothermic peak decreases.

As shown in Figure 41, at low levels of cure a more pronounced exothermic peak can be observed, and ΔH_r will result in a larger value yielding a lower degree of cure, α. Conversely, at high levels of cure the exothermic peak can no longer be detected and ΔH_r will equal zero, which indicates that the sample is completely cured.

By observing the occurrence of a residual curing exothermic peak during a DSC test, DSC can be used to establish the degree of cure achieved by an epoxy resin. If no peak is observed, this is indicative of a resin system that is nearly completely cured and fully crosslinked. DSC can also be used to examine the glass transition temperature, T_g, of an epoxy as shown in Figure 42, as well as determine the curing onset temperature, the curing peak temperature, and the curing ending temperature as shown in Figure 43. Further information on the fundamentals and use of differential scanning calorimetry may be found in the works of Prime (1997) and Pasztor (1997).

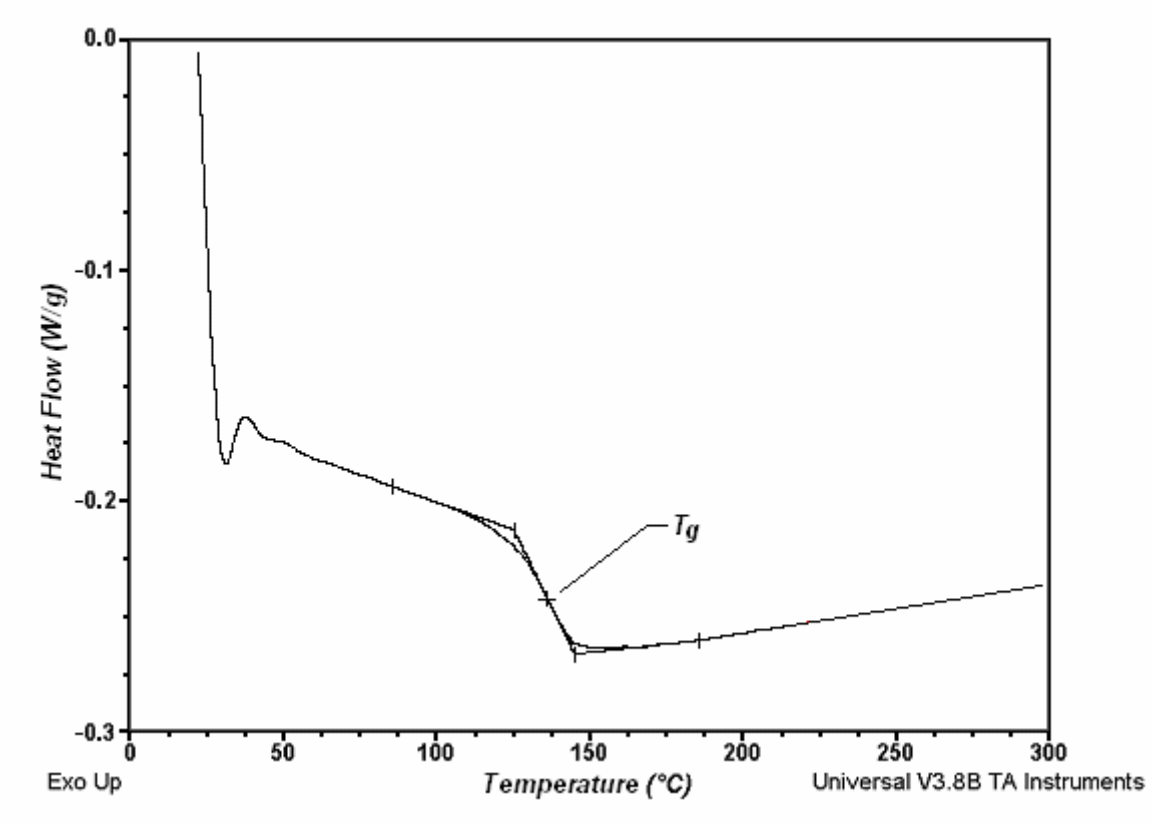

Figure 42. Representative thermo-diagram of glass transition temperature measurement with DSC.

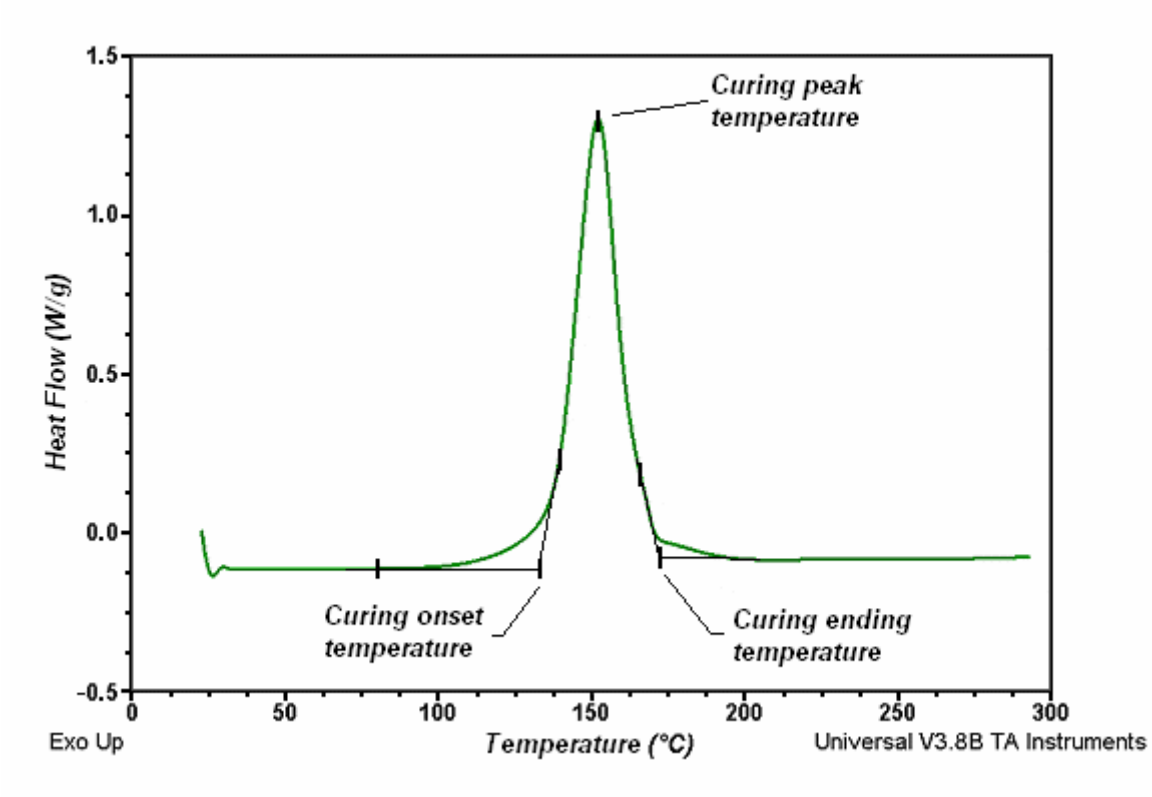

Figure 43. Representative thermo-diagram of curing onset, peak, and ending temperature measurement with DSC.

The DSC was performed using a modulated differential scanning calorimeter manufactured by TA instruments, model 2920. In addition, a heat flux cell was implemented during testing. During the DSC evaluation, a test sample weighing approximately 10 *mg* was removed from a representative flexural bend test specimen and placed in a hermetic DSC Aluminum sample pan at room temperature. The sample pan was placed inside the differential scanning calorimeter and heated to 300^{o}C at a rate of 5^{o}C / min to obtain a DSC thermo-diagram of the no-flow underfill. A nitrogen purge rate of 40 ml / min was implemented during all DSC evaluations. The DSC thermo-

diagram result was compared to an uncured no-flow underfill sample to ascertain the degree of cure for the underfill for the curing conditions used in this study.

5.2.4 Moisture Preconditioning

Test specimens were divided into six test groups and subjected to five different levels of moisture preconditioning to ascertain the effect of moisture on the elastic modulus of the underfill. The test groups included fully dry, 85°C only, 85°C/50%RH, 85°C/65%RH, 85°C/85%RH, and 85°C/95%RH, with the latter five test groups being environmentally preconditioned for 168 hours. A summary of the experimental test matrix is shown in Table 9.

Table 9. Elastic modulus experimental test matrix

Test Group	Environment (168 hours of exposure)
1	N/A
2	85C
3	85C / 50%RH
4	85C / 65%RH
5	85C / 85%RH
6	85C / 95%RH

The motivation for the 85°C temperature condition in all accelerated testing environments was two fold: (1) To increase the diffusivity of moisture in the underfill for each respective humidity level to insure that saturation was reached in all specimens

before the conclusion of the 168 hour exposure time and (2) to use a value that was common to several JEDEC industry standards for moisture preconditioning prior to reliability testing. All test specimens were baked at 115^{o}C for at least 12 hours to remove any moisture that may have been introduced during sample preparation prior to environmental aging, which was performed in a humidity chamber in an atmosphere maintained at a constant temperature (±1^{o}C), humidity (±1^{o}C), and pressure (P_{atm}).

Test group 1 was the control test group and used for comparison against environmentally preconditioned test groups. Test group 2 was used to identify the contribution of thermal aging at 85^{o}C for 168 hours on elastic modulus results. Test groups 3, 4, 5, and 6 were used to identify the effect of increasing moisture concentration on the elastic modulus. All moisture preconditioned test specimens were periodically removed from the humidity chamber and weighed on an electronic balance to the nearest 0.1 mg to monitor the percentage weight gain in the specimens from moisture uptake. It is important to note that all specimens in test groups 3, 4, 5, and 6 had reached fully saturated moisture conditions at the conclusion of the 168 hour exposure time. Consequently, a gradient of moisture concentration did not exist in specimens during testing, allowing the identification of the intrinsic wet modulus for a particular level of moisture content inside the specimens. In addition, all flexural bend tests were performed with both the surrounding environment and test specimens being at room temperature after environmental preconditioning. No measurable loss in moisture uptake occurred in the test specimens from the time they were removed from the environmental chamber, allowed to cool to room temperature, and experimentally tested. This was

supported by mass uptake data, where specimens were weighed to the nearest 0.1 mg upon immediate removal from the humidity chamber and then weighed again at the conclusion of testing.

5.3 Discussion of Results

The results of this study are comprised of two sections. First, the degree of cure of the underfill is evaluated to insure incomplete curing did not influence any observed changes to the elastic modulus after moisture preconditioning for the flexural bend test specimen size and geometry used in this study. Second, the effect of moisture preconditioning itself is shown with both thermal aging and moisture absorption effects identified separately.

5.3.1 Underfill Degree of Cure

Since cure rates depend on the mass of the material to be heated and the efficiency of the heat source, Differential Scanning Calorimetry (DSC) was used to verify that the no-flow underfill was fully cured for the flexural bend test specimen size and geometry used in this study. The curing conditions given by the no-flow underfill manufacturer was only a suggestion for our particular specimen configuration, and it was recommended to verify the degree of cure of the underfill in the test specimens for those conditions. This is critical to insure that any observed changes in the modulus from

moisture preconditioning were indeed due to the preconditioning itself and not influenced from incomplete curing of the no-flow underfill in the flexural bend test specimens.

To examine the degree of cure of the no-flow underfill, a 50 mm x 10 mm x 3 mm sample was constructed and cured as prescribed by the commercial manufacturer (190^{o}C for 40 minutes). The sample geometry was similar in size to experimental test samples used in this study to accurately ascertain the level of cure for those specimens. After curing the sample, two DSC test specimens, one specimen from the edge of the sample and one specimen from the center of the sample, were removed for DSC analysis as shown in Figure 44.

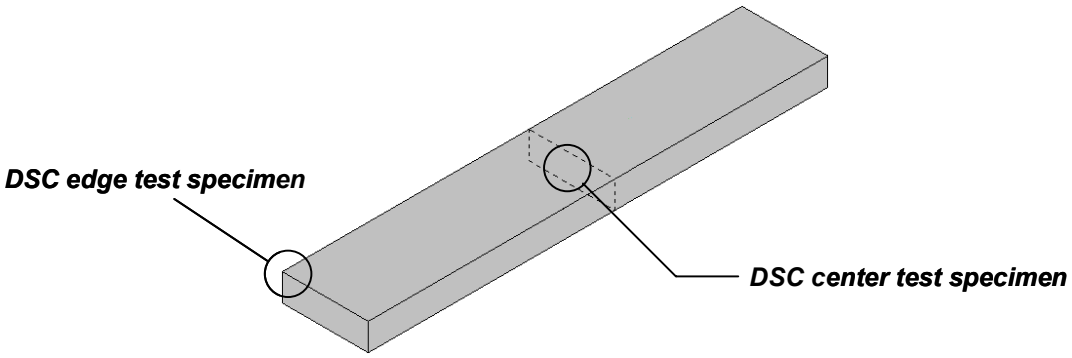

Figure 44. Location of DSC test specimens obtained from cured underfill sample

The DSC test specimens were removed from both the edge and center of the sample for means of comparison between results and to adequately document the degree of cure of the entire sample. Each DSC test specimen weighed approximately 10 *mg* and was tested independently. Since the center test specimen will be the last location to reach

steady state heating conditions, it represents a lower bound for the degree of cure for the sample. Conversely, since the edge test specimen will be the first section to receive steady state heating conditions, it represents an upper bound for the degree of cure for the sample. DSC test results for both the center and edge test specimens are shown in figures 45 and 46 respectively.

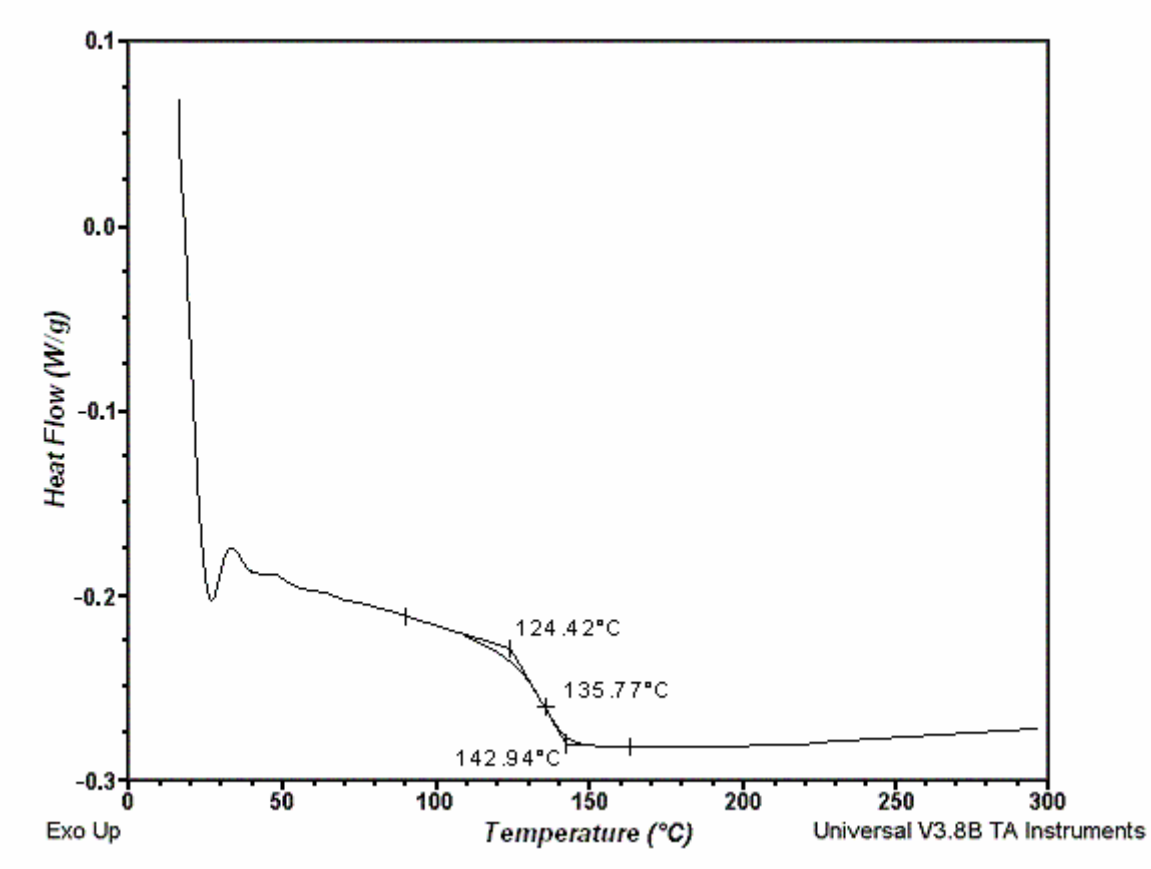

Figure 45. DSC results for the cured underfill center test specimen

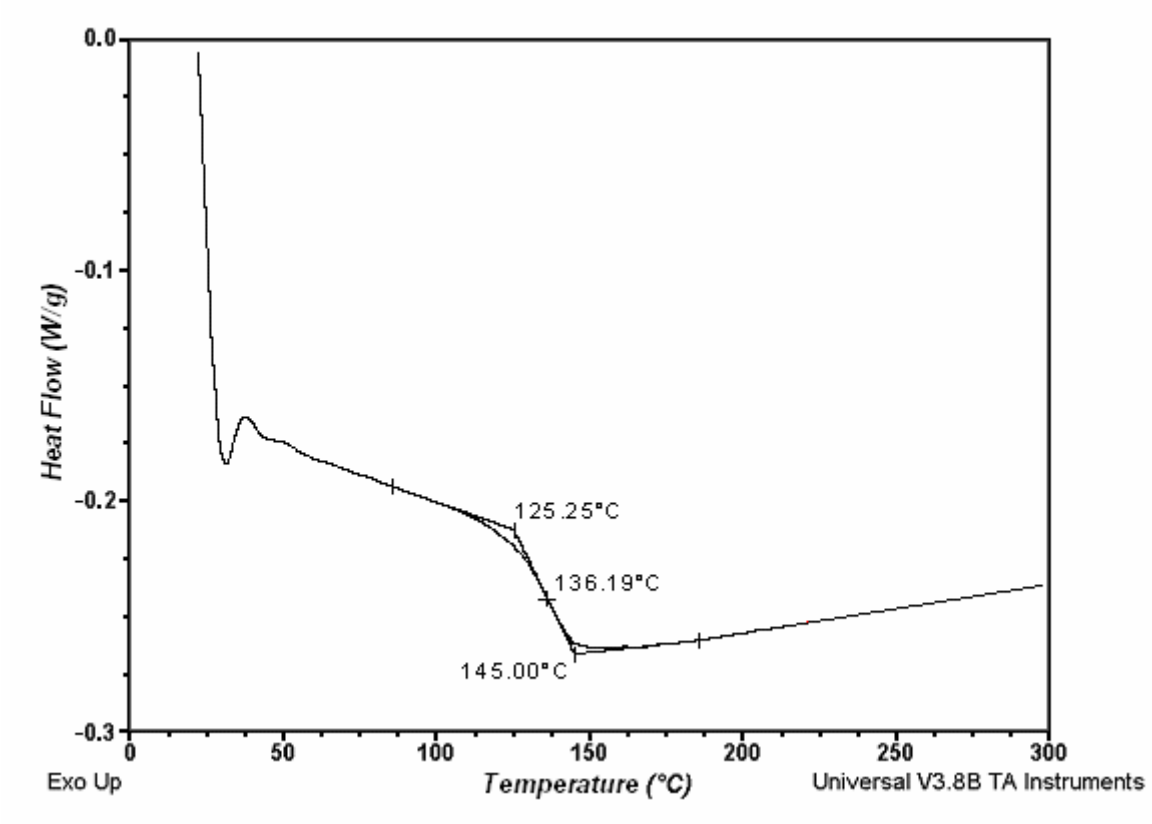

Figure 46. DSC results for the cured underfill edge test specimen

As shown in figures 45 and 46, good agreement both graphically and in the measurement of the glass transition temperature, *Tg*, were obtained when comparing the DSC test results of both the edge (*Tg* = 136.19^{o}C) and center samples (*Tg* = 135.77 ^{o}C), indicating that the flexural bend test specimen experienced a similar degree of cure throughout its bulk geometry. To ascertain the degree of cure of the underfill in the flexural bend test specimen, the DSC result from an uncured no-flow underfill sample was compared to the cured DSC test result from the center test sample as shown in Figure 47.

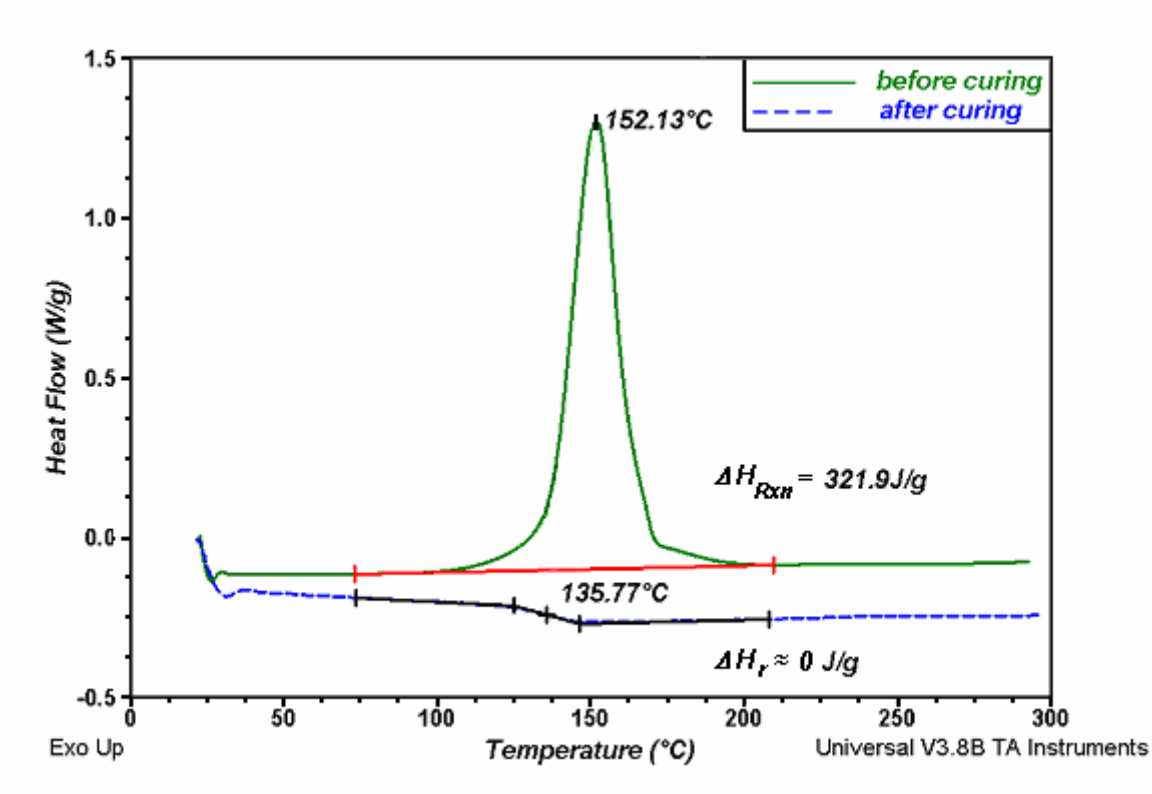

Figure 47. DSC results comparing both uncured and cured samples to illustrate the degree of cure of the underfill in the flexural bend test specimens

From Figure 47, it is clear that the uncured underfill sample exhibited an exothermic peak at a temperature of 152.13°C and a total heat of reaction, ΔH_{Rxn}, of 321.9 J/g. It is also evident by the absence of an exothermic peak in the cured underfill test results that there was no residual heat of reaction, ΔH_r. As a result, the degree of cure, α, for the underfill as given in equation (5.4) was measured to be approximately 100%, indicating that the underfill was fully cured in the flexural bend test specimens for the curing conditions used in this study. Consequently, any observed changes in the mechanical properties of the underfill from moisture preconditioning can be attributed to

the effects of moisture and thermal aging alone and not influenced from incomplete curing of the underfill in the flexural bend test specimens.

5.3.2 Effect of Moisture Preconditioning

Elastic modulus data for fully dried test results and moisture preconditioned test results are shown in Tables 10 - 15. It is important to note that all moisture preconditioned test specimens were fully saturated with moisture at the conclusion of the 168 hour exposure time, hence a gradient of increasing moisture concentration did not exist within the specimens and the inherent wet modulus was identified. This is supported by there being no change in the mass of the specimens from moisture uptake after approximately five days of exposure, indicating fully saturated, steady state conditions existed within the specimens prior to removal from the humidity chamber for testing.

Table 10. Elastic modulus data for control underfill test specimens

Flexural Test Specimen	Preconditioning	Csat (wt%)	E (GPa)
1	None	0.00	2.47
2	None	0.00	2.62
3	None	0.00	2.55
4	None	0.00	2.45
5	None	0.00	2.60
6	None	0.00	2.63
7	None	0.00	2.51
8	None	0.00	2.47
9	None	0.00	2.63
10	None	0.00	2.46
11	None	0.00	2.49
12	None	0.00	2.48
13	None	0.00	2.57
14	None	0.00	2.51
15	None	0.00	2.63
16	None	0.00	2.47
17	None	0.00	2.54
18	None	0.00	2.47
19	None	0.00	2.49
20	None	0.00	2.56
		AVERAGE:	**2.53**
		STANDARD DEVIATION:	**0.06**

Table 11. Elastic modulus data for underfill test specimens after 85°C thermal aging for 168 hours

Flexural Test Specimen	Preconditioning	Csat (wt%)	E (GPa)
21	85C	0.00	2.59
22	85C	0.00	2.44
23	85C	0.00	2.58
24	85C	0.00	2.46
25	85C	0.00	2.46
		AVERAGE:	**2.51**
		STANDARD DEVIATION:	**0.07**

Table 12. Elastic modulus data for underfill test specimens after moisture preconditioning at 85°C/50%RH for 168 hours

Flexural Test Specimen	Preconditioning	Csat (wt%)	E (GPa)
26	85C / 50%RH	0.65	2.45
27	85C / 50%RH	0.65	2.49
28	85C / 50%RH	0.65	2.50
29	85C / 50%RH	0.65	2.45
30	85C / 50%RH	0.65	2.56
		AVERAGE:	**2.49**
		STANDARD DEVIATION:	**0.05**

Table 13. Elastic modulus data for underfill test specimens after moisture preconditioning at 85°C/65%RH for 168 hours

Flexural Test Specimen	Preconditioning	Csat (wt%)	E (GPa)
31	85C / 65%RH	0.77	2.46
32	85C / 65%RH	0.77	2.45
33	85C / 65%RH	0.77	2.40
34	85C / 65%RH	0.77	2.45
35	85C / 65%RH	0.77	2.51
		AVERAGE:	**2.45**
		STANDARD DEVIATION:	**0.04**

Table 14. Elastic modulus data for underfill test specimens after moisture preconditioning at 85°C/85%RH for 168 hours

Flexural Test Specimen	Preconditioning	Csat (wt%)	E (GPa)
36	85C / 85%RH	1.02	2.37
37	85C / 85%RH	1.02	2.33
38	85C / 85%RH	1.02	2.31
39	85C / 85%RH	1.02	2.29
40	85C / 85%RH	1.02	2.27
		AVERAGE:	**2.31**
		STANDARD DEVIATION:	**0.04**

Table 15. Elastic modulus data for underfill test specimens after moisture preconditioning at 85°C/95%RH for 168 hours

Flexural Test Specimen	Preconditioning	Csat (wt%)	E (GPa)
41	85C / 95%RH	1.19	2.15
42	85C / 95%RH	1.19	2.01
43	85C / 95%RH	1.19	2.10
44	85C / 95%RH	1.19	2.02
45	85C / 95%RH	1.19	2.17
		AVERAGE:	**2.09**
		STANDARD DEVIATION:	**0.07**

Figure 48 provides a graphical depiction of the effect of environmental preconditioning on the underfill elastic modulus.

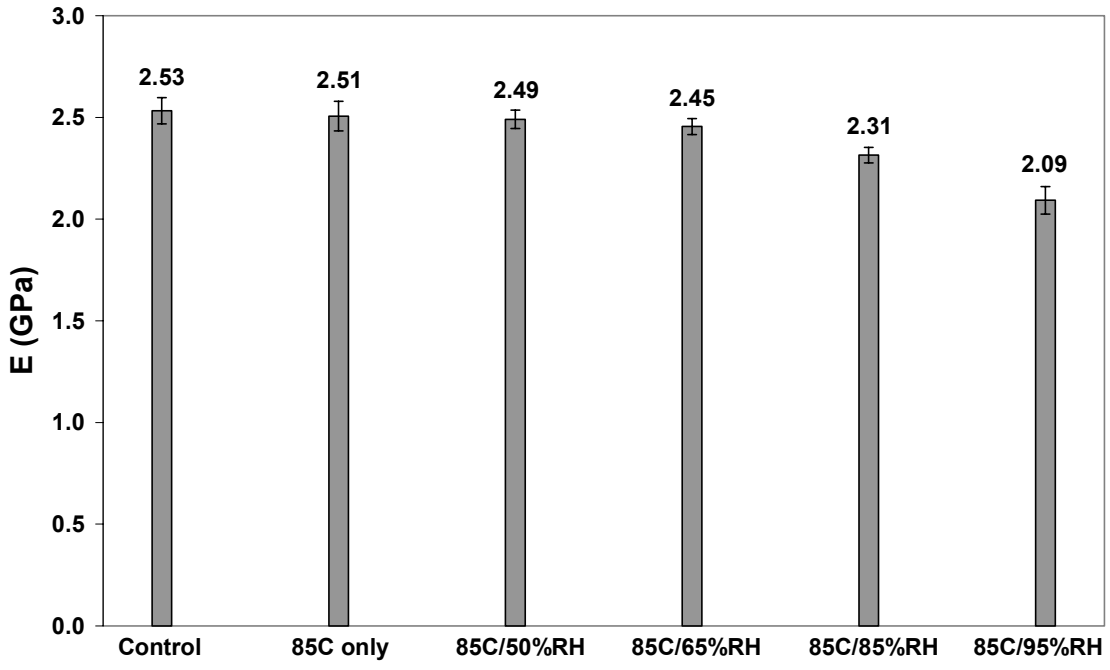

Figure 48. Effect of moisture preconditioning on underfill elastic modulus

When compared to unaged, control test specimen values, moisture preconditioning at 85°C/50%RH and 85°C/65%RH was found to have little to no effect on the elastic modulus of the underfill. A more noticeable effect occurs at 85°C/85%RH, while conditions of 85°C/95%RH yielded a significant decrease in modulus. To isolate the possible effect of thermal aging at 85°C from moisture preconditioning contributing to the observed changes in the elastic modulus of the underfill, flexural bend test specimens were exposed to conditions of 85°C only for 168 hours and compared to unaged, control test specimen values. As shown in Figure 48, thermal aging at 85°C for 168 hours was found to have no effect on the elastic modulus with similar values obtained when compared to the control test group results. Again, it is important to note that all tests were performed at room temperature, hence only the effects of thermal aging were evaluated rather than the effect of testing at higher temperatures on elastic modulus. Since all environmental preconditioned test groups in this study were exposed to the same temperature component of 85°C as well as the same duration of 168 hours, the observed changes in modulus from moisture preconditioning given in Figure 48 can be attributed to the effect from moisture and moisture alone. In addition, since the 85°C temperature represents an upper bound for the temperature component for environmental preconditioning given by JEDEC industry standards, the results can be extended to any JEDEC based accelerated environmental testing model with confidence that thermal aging has no effect on the elastic modulus of the no-flow underfill evaluated in this study for the standard aging of 168 hours. A summary of the effect of moisture preconditioning on the elastic modulus of the underfill is given in Table 16, where Csat represents the

saturation concentration of moisture in the test specimens for each respective level of moisture preconditioning and given as both a percent weight change (wt%) and mg H_2O / mm^3.

Table 16. Change in underfill elastic modulus from moisture uptake

T (C)	RH (%)	Csat (wt%)	Csat (mg H_2O/ mm^3)	E (GPa)	Modulus Change (%)
Control	--	0	0.0000	2.53 ± 0.06	--
85	50	0.65	0.0075	2.49 ± 0.05	1.6
85	65	0.77	0.0089	2.45 ± 0.04	3.2
85	85	1.02	0.0118	2.31 ± 0.04	8.7
85	95	1.19	0.0138	2.09 ± 0.07	17.4

Since saturation had been reached in all moisture preconditioned test specimens prior to removal from the humidity chamber and thermal aging from the 85°C temperature component of moisture preconditioning was found to have no effect on the elastic modulus, the inherent wet modulus was identified and all observed changes in the modulus occurred solely from the influence of moisture. This allows the characterization of the change in modulus of the underfill from moisture uptake as a function of moisture concentration as shown in Figures 49 and 50.

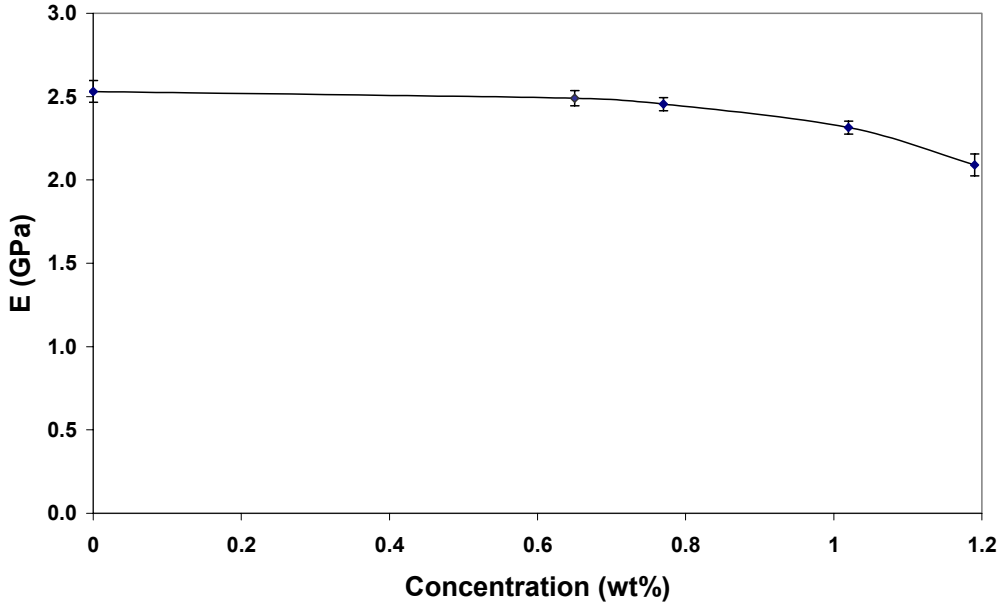

Figure 49. Underfill elastic modulus variation as a function of moisture concentration (wt%)

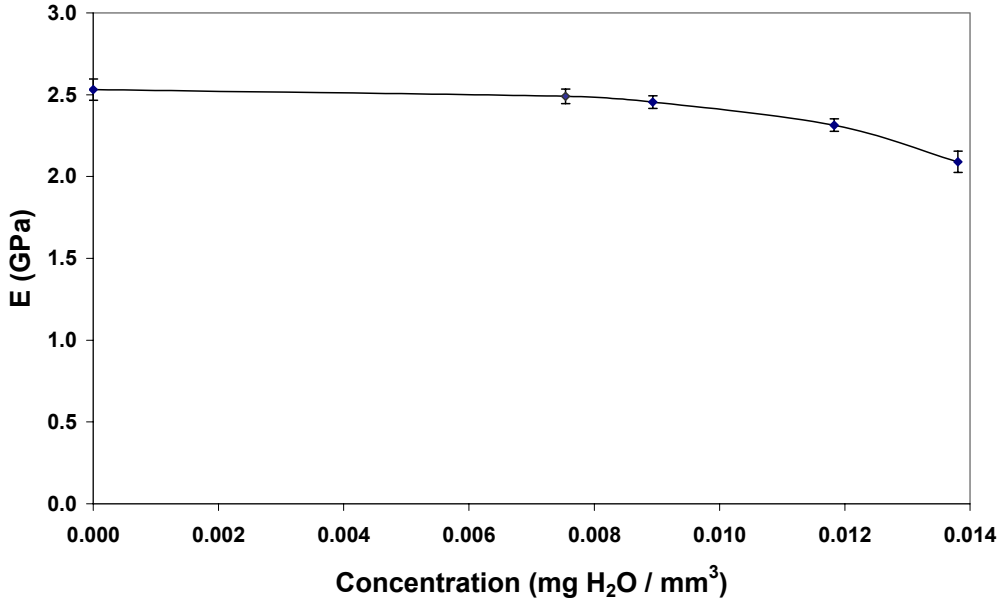

Figure 50. Underfill elastic modulus variation as a function of moisture concentration (mg H_2O / mm^3)

To the author's knowledge, Figures 49 and 50 are the first figures depicting the inherent change in elastic modulus of an epoxy based adhesive as a function of moisture concentration. Time dependent variation in the elastic modulus after saturation is assumed to be negligible, although it could be a consideration for longer durations of exposure at higher concentrations of moisture as a result of hydrolysis (Xiao and Shanahan, 1997). Previous studies on epoxy adhesives have shown the variation in modulus as a function of the square root of time corrected for specimen thickness (Zanni-Deffarges and Shanahan, 1995); however, this information depicts the change in modulus resulting from a transient, gradient of moisture concentration rather than demonstrating how the inherent wet modulus changes with increasing moisture content. Other studies have identified the inherent wet modulus for a single saturation level and compared to fully dry results (Brewis, *et al.*, 1990; Su, *et al*., 1992; and Zanni-Deffarges and Shanahan, 1995) however, these studies do not show the inherent wet modulus of the same adhesive for several different saturation levels and thus do not show the characteristic response of the adhesive as a function of increasing moisture concentration as given in Figures 49 and 50. Such information is extremely useful in predictive modeling efforts, where the intrinsic response of the elastic modulus as a function of increasing moisture concentration can be used in a coupled mechanical-diffusion analysis (Wahab, *et al*., 2002) to incorporate the transient effect of the continual variation of elastic modulus as moisture diffuses into the adhesive. This data is not only significant when modeling the effect of moisture on the bulk material behavior, but also on

interfacial adhesion, where changes in the mechanical properties of the adhesive due to moisture uptake can play a significant role in the onset of package delamination.

5.4 Conclusions

A comprehensive evaluation of the effect of moisture on the elastic modulus of a no-flow underfill was performed. Flexural bend test specimens were constructed and tested in a three-point bend to measure the elastic modulus. DSC test results show that the underfill was fully cured in the flexural bend test specimens for the curing conditions and test specimen size and geometry used in this study. Therefore, incomplete curing of the underfill in the flexural bend test specimens did not influence any observed changes to the elastic modulus of the underfill. Test specimens were moisture preconditioned at 85^{o}C and several different humidity levels for 168 hours to characterize the effect of absorbed moisture on the elastic modulus. Fully saturated, steady state conditions existed in the moisture preconditioned test specimens at the conclusion of the 168 hour exposure time as supported by mass uptake data, which remained at a constant value prior to removal from the humidity chamber for testing. As a result, the inherent wet modulus of the underfill was identified for each respective level of moisture preconditioning. When compared to unaged test specimen results, moisture preconditioning had a noticeable effect on the elastic modulus, yielding as much as a 17% decrease in modulus. Thermal aging from the 85^{o}C temperature component of moisture preconditioning was found to

have no effect on the elastic modulus; consequently, all observed changes to the elastic modulus from moisture preconditioning resulted from the effect of moisture alone. Results depict the inherent change in elastic modulus of the underfill as a function of increasing moisture concentration, which can be used to model the transient change in the underfill elastic modulus as moisture is absorbed.

The characterization of the effect of moisture on the elastic modulus of the underfill is the first step in evaluating the influence of environmental conditions on overall package reliability. The response of underfill to increasing moisture content is not only recommended when evaluating the effect of moisture on the bulk material behavior, but also on interfacial adhesion, where changes in the mechanical properties of the adhesive and adherend due to moisture uptake can play a significant role in the onset of package delamination. The results presented in this study provide fundamental insight into the behavior of moisture in an epoxy based underfill and could be used in predictive modeling efforts, where the intrinsic response of the elastic modulus as a function of increasing moisture concentration can be used in a coupled mechanical-diffusion analysis.

CHAPTER VI

EFFECT OF MOISTURE ON INTERFACIAL FRACTURE TOUGHNESS

The effect of moisture on interfacial adhesion is governed by two fundamental mechanisms. The first is the rate at which moisture is delivered to the interface, and the second is the change in adhesion performance as a consequence of moisture being present in the adhesive structure. This includes not only the primary effect of moisture being directly present at the interface itself, but also the secondary effect of moisture altering the mechanical performance of the two materials that constitute the bimaterial interface. Having previously quantified both the rate at which moisture is delivered to the interface and the degrading effect of moisture on the elastic modulus of the materials that constitute the bimaterial interface, a model depicting the intrinsic change in interfacial adhesion as a function of moisture concentration is developed. Interfacial fracture mechanics is used to characterize this change to develop relationships that are independent of test specimen geometry.

6.1 Introduction

Microelectronic packaging is a very transient, rapidly progressing technology. With interconnect density increasing and package size decreasing, several adaptations to microelectronic assemblies have been developed to accommodate the increasing demand in both cost and performance requirements. In particular, epoxy based encapsulants have been extensively used in microelectronic devices to enhance package reliability, provide environmental protection, and improve manufacturing yields provided the structural integrity of the adhesive bond is maintained. Consequently, characterizing the primary adhesion mechanisms and identifying the factors that affect the strength and durability of these encapsulants are the focal points of several contemporary studies in reliability and adhesion research.

Traditional encapsulation processes such as transfer molding, cavity filling, and glob-topping are commonly employed throughout the industry to protect the IC device from environmental pollutants and provide mechanical protection. In these devices, copper alloys are widely used as a lead frame material due to their relatively low cost in conjunction with their high electrical and thermal conductivity. However, the interfacial adhesion at the epoxy/copper interface is poor and several studies have examined the durability and failure mechanisms at this interface (Lee and Qu, 2003; Chung, *et al*., 2002; Cho and Cho, 2000; and Kim, *et al*., 2000). In addition, the copper surface is highly susceptible to oxidation, which is an additional consideration when evaluating the interfacial adhesion of interfaces involving copper.

A more recent encapsulant developed within the last ten years is underfill, which is an epoxy based encapsulant that mechanically couples the chip to the board. Underfill drastically enhances the fatigue life of microelectronic assembles when compared to unencapsulated devices (Suryanarayana, *et al*., 1991), provided that the structural integrity of the adhesive bond between the underfill and the printed wiring board, solder mask, copper, silicon, passivation, and solder is maintained. Characterizing the adhesion of underfill to these substrates has been the focus of several studies in adhesion and reliability research (Fan, *et al.*, 2002; Dai, *et al*., 2000; and Yeung, *et al*., 2000).

Although epoxy encapsulants have many benefits, one of the primary drawbacks is their susceptibility to moisture uptake. A typical epoxy formulation can absorb between 1 and 7 wt% moisture (Soles, *et al*., 2000), which can have a detrimental affect on interfacial adhesion and drastically reduce the reliability of encapsulated devices. While it has been shown that moisture can significantly alter adhesive performance in microelectronic packaging (Ferguson and Qu, 2002; and Luo and Wong, 2001), the interfacial and material constitutive damage behavior from moisture exposure is not well understood. This largely arises due to the difficulty of the problem, which is governed by two fundamental mechanisms. The first is the rate at which moisture is delivered to the interface. The second is the response of the interfacial adhesion to varying levels of moisture concentration, where the deleterious effect of moisture not only affects interfacial adhesion by being physically present at the interface, but also through the degradation of the mechanical properties of the epoxy adhesive due to moisture uptake (Lu, *et al*., 2001; and Morgan, *et al*., 1980). Mass transport and in particular the diffusion

of moisture in epoxy adhesives has been studied by several sources and is fairly well established (Uschitsky and Suhir, 2001; Soles and Yee, 2000; Soles, *et al*., 2000; Vanlandingham, *et al*., 1999; and Wong, *et al*., 1999); however, the response of interfacial adhesion to moisture is much less understood. Although several studies have addressed the issue of moisture, much more work needs to be completed and there currently exists a lag in fundamental empirical data depicting the loss in interfacial adhesion as a function of interfacial moisture concentration. Since there exists this lag in experimental data, even less effort has been spent on developing predictive models that account for the effect of moisture on interfacial adhesion.

In this study, the effect of moisture on the interfacial adhesion of an epoxy based underfill adhesive with both copper alloy and solder mask coated FR-4 substrates are experimentally characterized. Both the change in underfill elastic modulus and the critical load of fracture are quantified to ascertain the interfacial fracture toughness for a particular level of moisture preconditioning. Interfacial fracture toughness results are determined for conditions of fully dry, 85^{o}C only, 85^{o}C/50%RH, 85^{o}C/65%RH, and 85^{o}C/85%RH, with the latter four test conditions being preconditioned for a duration of 168 hours. Results are presented for the various levels of moisture preconditioning and their respective saturation moisture concentrations. Optical microscopy was used to determine the hygro-swelling coefficient to ascertain the effect of moisture induced swelling relative to the thermal expansion mismatch at the interface. Scanning Electron Microscopy was used to characterize the failure locus of the interface crack before and after moisture preconditioning. X-ray Photoelectron Spectroscopy (XPS) was used to

determine the type of copper oxide present at the interface. Water contact angle measurements were used to identify the role and effect of interfacial hydrophobicity on fracture toughness results. Based on the interfacial fracture toughness results in conjunction with the aforementioned tests, an analytical model was developed to depict the inherent change in interfacial fracture toughness as a function of key parameters identified from the interaction of moisture.

6.2 Experimental Procedure

6.2.1 Materials

The adhesive used in this study was an epoxy based underfill developed for no-flow assembly, designated as UR-B in this research. This particular underfill was determined to be ideal for studying the fundamental effect of moisture on interfacial adhesion due to its moisture diffusion kinetics and saturation behavior established from the moisture absorption portion of this research. Since the underfill adhesive was designed for no-flow assembly, it should be noted that it did not contain any filler content. The substrates used in this study were oxygen-free electronic grade copper, alloy 101, and solder mask coated FR-4 printed wiring board.

6.2.2 Profilometry

Profilometry was used to quantify the surface roughness of all substrates before adhesive bonding. There were three primary parameters determined when reporting the surface roughness for each substrate. The first is roughness average, R_a, which is the area between the roughness profile and its mean line as shown in Equation (6.1)

$$R_a = \frac{1}{L}\int_0^L |r(x)|dx \tag{6.1}$$

where L is the assessment length and $r(x)$ is the roughness profile height at position x. The roughness average is the arithmetical mean deviation of the profile. The second parameter is the root mean square roughness (RMS), R_q, which is determined from another integral of the roughness profile:

$$R_q = \sqrt{\frac{1}{L}\int_0^L r^2(x)dx} \tag{6.2}$$

where again L is the assessment length and $r(x)$ is the roughness profile height at position x. As the name implies, the root mean square roughness is the root mean square deviation of the profile. The final parameter used to characterize the surface roughness of the substrates is the total waviness height, W_t, which is the height from the lowest valley to the highest peak of the waviness profile. Six tests were performed for each substrate and the results of each parameter averaged.

6.2.3 Interfacial Fracture Test

Interfacial fracture test specimens were tested in a four-point bend to determine the effect of moisture on interfacial fracture toughness. This proved to be the most optimum method for interfacial fracture testing for three primary reasons. First, the flexural beam test yields intermediate values for mode mixity, which is representative of the values experienced by electronic devices during actual application. Second, it provides a means for successful interfacial fracture test specimen construction utilizing the substrates and adhesives evaluated in this study. Last, the flexural beam test configuration yields an open-faced test specimen design, which allows moisture saturated, steady state conditions to be reached in the test specimens in a relatively short amount of time. This is due to the large surface area for moisture uptake relative to the short diffusion path to the interface.

Interfacial fracture test specimens were constructed in the following manner. First, the substrates were sectioned into the appropriate sizes. Due to the difference in sizes of the bulk material received by each manufacturer, the copper substrates were sectioned into 50.8 x 9.7 x 1.5 mm strips using a mill while the FR-4 substrates were sectioned into 50.8 x 7.5 x 0.67 mm strips using a shear machine. The edges of all substrates were polished using 1200 grit sand paper to ensure they were smooth after sectioning. To minimize the effects of mechanical interlocking on adhesion, the bonding surface for all copper substrates was polished to a mirror finish. Since polishing the bonding surface of the FR-4 substrates would have damaged the solder mask of the composite structure, the surface roughness of those substrates remained as received from

the manufacturer. Next, each substrate was cleaned. The copper substrates were cleaned using the following routine procedures outlined by Shi and Wong (1998): 5 minutes rinse / immersion in acetone, then 5 minutes in methanol, then 50/50 HCl solution for ~ 20 seconds, followed by a DI water rinse and clean air-jet drying. The FR-4 board substrates were cleaned by lightly wiping with Isopropanol to remove contaminants from the surface. It should be noted that latex gloves were worn at all times to prevent oils and other contaminants on the skin from interacting with all test specimens. After cleaning, a molding compound release agent was applied to the ends of the substrate followed by two Teflon coated steel bars being placed on either side of the substrate. For the copper substrates, each bar had dimensions of 76.2 x 9.7 x 3.75 mm, while for the FR-4 board substrates each bar had dimensions of 76.2 x 9.7 x 2.47 mm. Two Teflon coated steel end pieces were placed on top of the ends of each substrate and in between the two side bars. For the copper substrates, each piece had dimensions of 9 x 9.7 x 2.25 mm while for the FR-4 board substrates each piece had dimensions of 9 x 7.5 x 1.8 mm. The completed structure formed a mold with a 32.8 x 9.7 x 2.25 mm open reservoir using the copper substrates and a 32.8 x 7.5 x 1.8 mm open reservoir using the FR-4 board substrates. In addition, a portion of the molding compound release agent was still visible on the substrate surface after the application of the steel end pieces, which would form two symmetric interface cracks once the adhesive was applied. Teflon tape was wrapped around the assembly to hold the structure together without interfering with the reservoir opening. Underfill was dispensed from a syringe into the open reservoir and continually applied until the meniscus was visible on the plane formed from the top surfaces of the

steel bars. In addition, the underfill was slowly dispensed to prevent air bubbles from being introduced into the resin medium. After dispensing the underfill, test specimens were cured at 190^{o}C for 40 minutes in a natural convection oven. Once curing was complete, test specimens were removed from the mold. The non-uniformity of the adhesive thickness in all test specimens was controlled to be less than 0.025 mm. The geometry of the interfacial fracture test specimens was designed such that plain strain conditions existed as well as satisfying beam bending theory. A completed representative interfacial fracture toughness test specimen is shown in Figure 51.

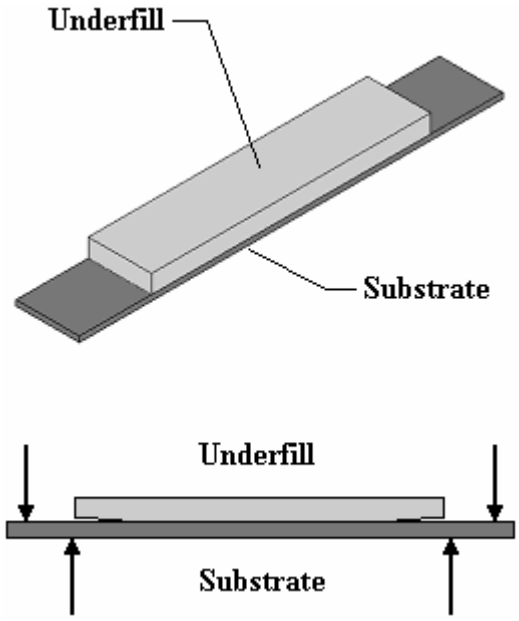

Figure 51. Interfacial fracture toughness test specimen

Interfacial fracture tests were performed on a United Load Frame (Model SSTM 500) at a crosshead rate of 0.5 mm/min. The top span of the four point bend fixture was

set to 49.2 mm between loading pin centers, and the bottom span of the fixture was set to 31.7 mm. Load displacement plots were generated for each individual test specimen to determine the critical load of fracture, P_c. A typical load displacement plot is shown in Figure 52.

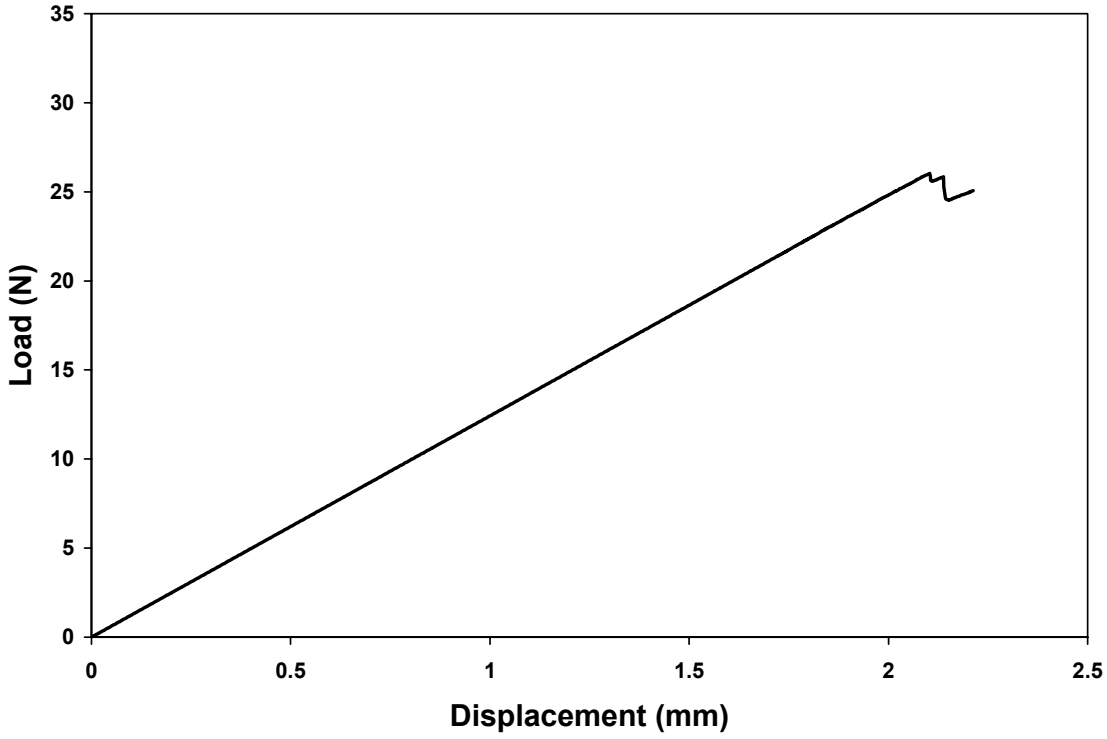

Figure 52. Representative load displacement curve

Once the value for the critical load was known, the interfacial fracture toughness can be determined. Interface toughness is defined as the critical value of the energy release rate, G_c, at which a bimaterial interface will begin to delaminate. For a bimaterial interface loaded in four point bending under plane strain conditions, it can be shown that

the critical value of the energy release rate, G_c, can be determined using the following equation (Hutchinson and Suo, 1992):

$$G = \frac{1}{2\overline{E_1}}\left(\frac{12M^2}{h^3}\right) - \frac{1}{2\overline{E_2}}\left(\frac{M^2}{Ih^3}\right) \tag{6.3}$$

where

$$\overline{E_i} \equiv \frac{E_i}{(1-\nu_i^2)} \tag{6.4}$$

M is the moment, ν is poisson's ratio, E is the elastic modulus, subscript 1 refers to material 1, subscript 2 refers to material 2, h is the height of material 1, and I is the dimensionless moment of inertia.

Since the interfacial fracture toughness only specifies the magnitude of the crack tip singularity, the mode mixity, ψ, must be determined from the complex stress intensity factor K. For a two-dimensional system, the complex stress intensity factor, K, is given by:

$$K = K_1 + iK_2 \tag{6.5}$$

For four-point loading conditions it can be shown (Hutchinson and Suo, 1992):

$$K = h^{-i\varepsilon}\sqrt{\frac{1-\alpha}{1-\beta^2}}\left(\frac{P}{\sqrt{2hU}} - ie^{i\gamma}\frac{M}{\sqrt{2h^3V}}\right)e^{i\omega} \tag{6.6}$$

with the mode mixity given by:

$$\left(K_1 + iK_2\right)L^{i\varepsilon} = \left|\left(K_1 + iK_2\right)\right|e^{i\psi} \tag{6.7}$$

$$\psi = \tan^{-1}\left(\frac{\mathrm{Im}(KL^{i\varepsilon})}{\mathrm{Re}(KL^{i\varepsilon})}\right) \tag{6.8}$$

where L is the characteristic length and ε is a dimensionless quantity given by Hutchinson and Suo (1992). As shown in Equation (6.8), the mode mixity for a test specimen requires the specification of some length quantity, L. The choice for L is arbitrary, but it should be selected as a fixed length and reported with the calculated values for the mode mixity. In this study, the substrate height was used to define the characteristic length. In addition, for each reported value of the interfacial fracture toughness, a minimum of at least ten and a maxmimum of fifteen specimens were tested and the results averaged. Error measurements represent the standard deviation in the test results.

6.2.5 Moisture Preconditioning

Test specimens were divided into five test groups and subjected to four different levels of moisture preconditioning to ascertain the effect of moisture interfacial fracture

toughness. The test groups included fully dry, 85°C only, 85°C/50%RH, 85°C/65%RH, and 85°C/85%RH, with the latter four test groups being environmentally preconditioned for 168 hours. A summary of the experimental test matrix is shown in Table 17.

Table 17. Interfacial fracture toughness experimental test matrix

Test Group	Environment (168 hours of exposure)
1	N/A
2	85C
3	85C / 50%RH
4	85C / 65%RH
5	85C / 85%RH

The motivation for the 85°C temperature condition in all accelerated testing environments was two fold: (1) To increase the diffusivity of moisture in the underfill for each respective humidity level to insure that saturation was reached in all specimens before the conclusion of the 168 hour exposure time and (2) to use a value that was common to several JEDEC industry standards for moisture preconditioning prior to reliability testing. All test specimens were baked at 115°C for at least 12 hours to remove any moisture that may have been introduced during sample preparation prior to environmental aging, which was performed in a humidity chamber in an atmosphere maintained at a constant temperature (±1°C), humidity (±1°C), and pressure (P_{atm}).

Test group 1 was the control test group and used for comparison against environmentally preconditioned test groups. Test group 2 was used to identify the contribution of thermal aging at 85^{o}C for 168 hours on elastic modulus results. Test groups 3, 4, 5, and 6 were used to identify the effect of increasing moisture concentration on the elastic modulus. All moisture preconditioned test specimens were periodically removed from the humidity chamber and weighed on an electronic balance to the nearest 0.1 mg to monitor the percentage weight gain in the specimens from moisture uptake. It is important to note that all specimens in test groups 3, 4, 5, and 6 had reached fully saturated moisture conditions at the conclusion of the 168 hour exposure time. Consequently, a gradient of moisture concentration did not exist in specimens during testing, allowing the identification of the intrinsic wet modulus for a particular level of moisture content inside the specimens. In addition, all interfacial fracture tests were performed with both the surrounding environment and test specimens being at room temperature after environmental preconditioning. No measurable loss in moisture uptake occurred in the test specimens from the time they were removed from the environmental chamber, allowed to cool to room temperature, and experimentally tested. This was supported by mass uptake data, where specimens were weighed to the nearest 0.1 mg upon immediate removal from the humidity chamber and then weighed again at the conclusion of testing.

6.2.5 Optical Microscopy

To determine the extent of swelling in a particular material for a particular moisture saturation level, the moisture swelling coefficient (or hygro-swelling coefficient), β, can be experimentally measured. The swelling coefficient is analogous to the coefficient of thermal expansion for a material, and can be determined by using an optical microscope to measure the change in length of a test specimen after moisture uptake. Since the substrates evaluated in this study are impermeable to moisture, the swelling coefficient was determined for the underfill only. The moisture swelling coefficient is defined as

$$\beta = \frac{\Delta \ell / \ell_o}{C_{sat}} \tag{6.9}$$

where $\Delta\ell$ is the change in length of the specimen due to moisture absorption, ℓ_o is the initial dry length of the specimen, and C_{sat} is the saturation moisture concentration.

Moisture swelling coefficient test samples were made using the procedure outlined in section 5.2.2, Flexural Bend Test. The final dimensions of the test samples were 50.8 x 12.7 x 2.0 mm. By focusing on the edge of a test sample under a magnification of 20X and then moving the platform to the opposite edge, the length of the test sample could be precisely determined. Note that the sample was placed on the platform in such a manner that only one dimension changed as the platform moved to the opposite edge. By comparing the fully dry length to the moisture saturated length in the

test sample, the moisture swelling coefficient of the material was identified for a particular moisture saturation level. The largest dimension was used to record the change in length to increase the accuracy and minimize measurement error from visual inspection by the operator. Five tests were performed for each moisture preconditioning environment and the results averaged. Error measurements represent the standard deviation in the test results.

6.2.6 Scanning Electron Microscopy

Scanning Electron Microscopy was used to characterize the nature of the failure surface after fracture testing for different levels of moisture preconditioning. Interfacial fracture test specimens were taken immediately to the Scanning Electron Microscope after testing for inspection. Latex gloves were worn at all times to prevent oils and other contaminants from interacting with the fracture surface. Only the metallic substrate of the failed interfacial fracture test specimen was examined. Since the substrate was electrically conductive, the fracture surface was intentionally not sputter coated with gold to prevent electrostatic charging when examining the surface with the SEM. Consequently, any portions of the polymer adhesive present on the surface after fracture will charge and be readily visible as sites of flaring. In addition, a 15kV electron beam was used for the scanning to accentuate the charging effects and distinguish any noticeable change in the failure locus after moisture preconditioning.

6.2.7 X-ray Photoelectron Spectroscopy

X-ray Photoelectron Spectroscopy (XPS) was used to examine the chemical composition of the surface of the copper substrates after fracture testing. Since oxides were removed from the copper surface before adhesive bonding and the flux present in the no-flow underfill would have removed any oxides that developed during adhesive curing, it is possible that oxidation growth from environmental preconditioning would have an effect on the interfacial fracture toughness results. An X-ray Photoelectron Spectroscope manufactured by Surface Science, model SSX 100, was used to determine the type and intensity of copper oxide present after moisture preconditioning at 85^{o}C/50%RH, and 85^{o}C/85%RH for 168 hours, as well as thermal aging at 85^{o}C for 168 hours. The XPS results were compared to interfacial fracture toughness results to ascertain the effect of oxidation growth on adhesion.

6.2.8 Goniometry

To gain further insight into the moisture interaction at the bimaterial interface, goniometry was used to measure the static contact angle of water with both the adhesive and substrate surfaces. The contact angle, θ, represents a balance between the adhesive forces between the liquid and solid and cohesive forces in the liquid. The adhesive forces cause the liquid drop to spread, while the cohesive forces cause the liquid drop to retain the shape of a sphere. The contact angle is a direct measure of wettability and provides an effective means to evaluate many surfaces properties such as surface contamination, surface hydrophobicity, surface energetics, and surface heterogeneity. When $\theta > 0$, the

liquid is nonspreading and reaches an equilibrium position between the liquid-fluid and solid-liquid interfaces. When $\theta = 0$ the liquid wets without limit and spontaneously spreads freely over the surface. By utilizing water as the probe liquid, the interfacial hydrophobicity of the interface can be ascertained by measuring the water contact angle of both the adhesive and substrate. Surfaces that repel water are considered hydrophobic and produce high contact angles, while surfaces that attract water are considered hydrophylic and produce low contact angles.

The sessile drop method was used to measure the contact angle. A 4 μL drop of water was placed on a flat, planar test sample and the image profile enlarged using a microscope. The contact angle was determined by drawing a tangent to the profile at the point of three-phase contact between the liquid drop, solid surface, and surrounding gaseous environment. Image analysis software was used to measure the contact angle to remove some of the operator bias inherent in direct measurements of contact angles. Contact angles were measured for fully dry conditions, 85^{o}C thermal aging, 85^{o}C/50%RH, 85^{o}C/65%RH, and 85^{o}C/85%RH moisture preconditioning. The later four test groups were aged for 168 hours, which was identical to the duration experienced by the interfacial fracture test specimens. The results were averaged for each preconditioning environment. Error measurements represent the standard deviation in the test results.

6.3 Discussion of Results

The results of this study are comprised of seven sections. First, profilometry is used to characterize the roughness of the substrate surface prior to adhesive bonding. Second, the effect of environmental preconditioning on the interfacial fracture toughness of the underfill / copper and underfill / FR-4 board test specimens is shown, with moisture and thermal aging effects identified separately. Third, optical microscopy is used to measure the hygro-swelling coefficient to characterize the hygro-swelling and thermal contraction mismatch effects between the adhesive and substrate on interfacial fracture toughness results. Fourth, Scanning Electron Microscopy is utilized to determine if moisture preconditioning altered the fracture failure locus. Fifth, X-ray Photoelectron Spectroscopy is used to characterize the effect of oxidation growth on interfacial fracture test results. Sixth, goniometry is performed to ascertain if moisture preconditioning changed the interfacial hydrophobicity of the interfaces. Last, an analytical model is developed to predict the intrinsic loss in interfacial fracture toughness as a function of moisture concentration. This model is based on the key parameters relevant to moisture identified from experimental results.

6.3.1. Surface Roughness

The surface roughness for both the copper and FR-4 substrates were experimentally measured prior to bonding with the underfill adhesive. This is important since surface roughness will increase the interfacial adhesion due to mechanical

interlocking (Yao, 2000). All surface roughness measurements were performed using an assessment length of 0.48 mm and a test speed of 0.05 mm/s.

Two surface roughness measurements were made on the copper. The first measurement identified the surface roughness characteristics of the copper as received from the manufacturer and unpolished. The second measurement identified the effect of polishing the copper substrates to a mirror finish on the surface characteristics of the copper. The motivation for polishing the copper substrates was to minimize the effect of mechanical interlocking on ascertaining the effect of moisture on interfacial adhesion. For this reason, it should be noted that all interfacial fracture tests were performed using polished copper substrates. A representative test result for the surface roughness measurement of the unpolished copper is shown in Figure 53.

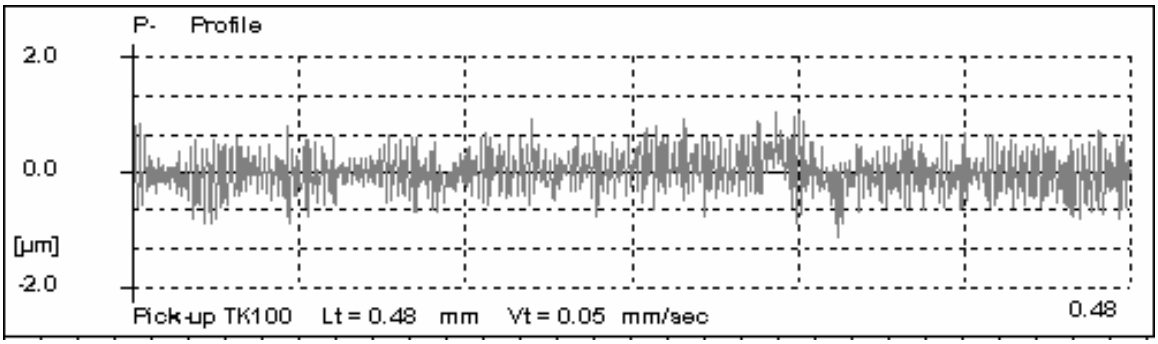

Figure 53. Surface roughness measurement for unpolished copper

Table 18 provides a summary of the surface roughness test results for the unpolished copper.

Table 18. Unpolished copper surface roughness

Test	Assessment Length (mm)	Roughness Average Ra (μm)	Root Mean Square Roughness, Rq (μm)	Waviness Height Wt (μm)
1	0.48	0.24	0.30	0.20
2	0.48	0.24	0.30	0.25
3	0.48	0.24	0.29	0.23
4	0.48	0.24	0.29	0.23
5	0.48	0.25	0.30	0.25
6	0.48	0.24	0.29	0.24
AVERAGE:		**0.24**	**0.30**	**0.23**
STANDARD DEV:		0.004	0.005	0.017

The unpolished copper yielded an average root mean square roughness of 0.30 μm, roughness average of 0.24 μm, and waviness height of 0.23 μm. A representative test result for the surface roughness measurement of the polished copper is shown in Figure 54.

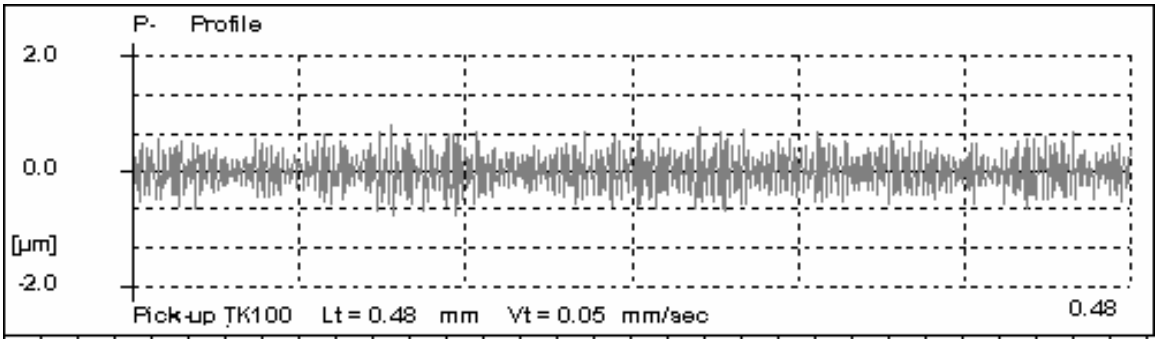

Figure 54. Surface roughness measurement for polished copper

Table 19 provides a summary of the surface roughness test results for the polished copper.

Table 19. Polished copper surface roughness

Test	Assessment Length (mm)	Roughness Average Ra (μm)	Root Mean Square Roughness, Rq (μm)	Waviness Height Wt (μm)
1	0.48	0.24	0.29	0.03
2	0.48	0.24	0.29	0.02
3	0.48	0.23	0.28	0.02
4	0.48	0.24	0.29	0.02
5	0.48	0.23	0.28	0.02
6	0.48	0.23	0.29	0.03
AVERAGE:		**0.24**	**0.29**	**0.02**
STANDARD DEV:		0.005	0.005	0.005

The polished copper yielded an average root mean square roughness of 0.29 μm, roughness average of 0.24 μm, and waviness height of 0.02 μm. When compared to the unpolished copper surface roughness results, it would appear on first inspection that polishing the copper to a mirror finish did not have a significant affect on changing the surface roughness of the copper; however, on further inspection, it is clear that the polishing did have a significant affect. First, although the roughness average and root mean square roughness between the polished and unpolished copper were similar, the waviness height was significantly different. The waviness height for the unpolished copper was 0.23 μm, while the waviness height of the polished copper was 0.02 μm. This indicates that the polished copper had a considerably more consistent roughness throughout the entire surface roughness assessment length, which is important when minimizing the variation in interfacial fracture toughness results as a result of surface roughness contributions. Second, it is important to note that the surface roughness measurement for the unpolished copper was performed on areas of the unpolished copper

that was void of noticeable pitting and scratching. Consequently, the measured value for the surface roughness over the 0.48 mm assessment length does not yield a true depiction of the roughness of the entire area of copper available for bonding with the adhesive. Polishing the copper removed the numerous scratches and visible pits present in the copper when received from the manufacturer, yielding a smooth, consistent surface for bonding and interfacial fracture testing.

After measuring the surface roughness of the copper, the surface roughness of the FR-4 board was determined. Unlike the copper, the FR-4 board was not polished as it would have damaged the structure and removed the solder mask coating applied by the commercial manufacturer from the surface of the board. A representative test result for the surface roughness measurement of the FR-4 board is shown in Figure 55.

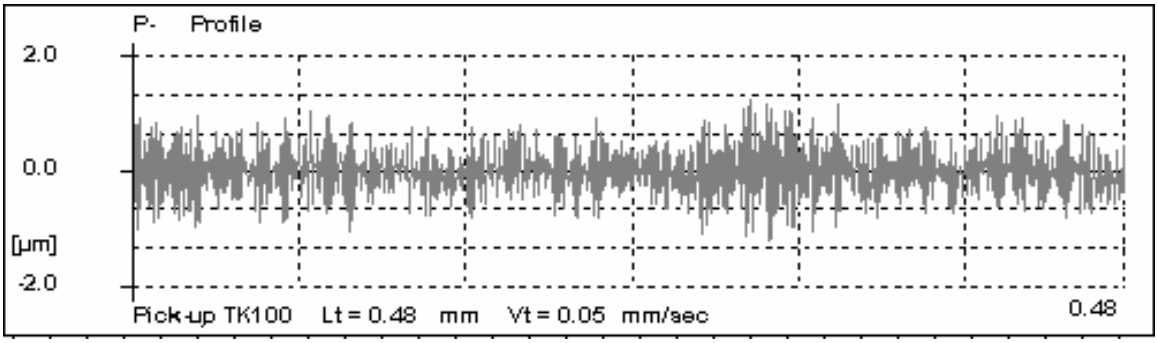

Figure 55. Surface roughness measurement for FR-4 board

Table 20 provides a summary of the surface roughness test results for the FR-4 board.

Table 20. FR-4 board surface roughness

Test	Assessment Length (mm)	Roughness Average Ra (μm)	Root Mean Square Roughness, Rq (μm)	Waviness Height Wt (μm)
1	0.48	0.30	0.38	0.10
2	0.48	0.31	0.39	0.11
3	0.48	0.31	0.39	0.11
4	0.48	0.30	0.39	0.11
5	0.48	0.30	0.38	0.10
6	0.48	0.31	0.39	0.10
AVERAGE:		**0.31**	**0.39**	**0.11**
STANDARD DEV:		0.005	0.005	0.005

The FR-4 board yielded an average root mean square roughness of 0.39 μm, roughness average of 0.31 μm, and waviness height of 0.11 μm.

6.3.2 Effect of Moisture Preconditioning

With the change in the underfill elastic modulus known for each level of moisture preconditioning, interfacial fracture toughness test specimens were constructed to measure the critical load of fracture for underill / copper test specimens and underfill / FR-4 board test specimens for each environment. The interfacial fracture toughness specimens had an open configuration, which allowed easy moisture ingress through the bulk adhesive to the interface. Since the substrates used were metallic, bulk diffusion to the interface only occurred through the underfill. (The FR-4 board contained full copper plating on both sides, which effectively acted as a barrier to moisture transport through the board to the interface). Based on moisture absorption analysis portion of this research, the external sides of the interfacial fracture toughness test specimens were

protected by a water-proof sealant. The application of the sealant served two purposes. First, it prevented wicking of moisture along the interface. Second, the sealant prevented three-dimensional moisture uptake in the underfill and forced one-dimensional moisture diffusion through the top surface of the underfill. The sealant was removed from the specimens before fracture testing. By eliminating the effects of moisture wicking along the interface and three-dimensional moisture uptake in the underfill, uniform concentrations of moisture existed spatially across the entire interface for the full duration of exposure to each moisture preconditioning environment.

6.3.2.1 Underfill / Copper Test Specimens

Using both the critical load of fracture and underfill elastic modulus value for each level of moisture preconditioning, the interfacial fracture toughness of the underfill / copper interface was determined using Equation 6.3 for each respective environment. The results for the interfacial fracture toughness and saturation moisture concentrations for each environment are shown in Tables 21 – 25.

Table 21. Interfacial fracture toughness data for control underfill / copper test specimens

Underfill Adhesive:
E = 2.53E+9 Pa
v = 0.37
G = 9.23E+8 Pa

Copper Substrate:
E = 1.15E+11 Pa
v = 0.31
G = 4.39E+10 Pa

Interfacial Parameters:
α = 0.955
β = 0.196
$\bar{E}_1$ = 1.27E+11 Pa
$\bar{E}_2$ = 2.93E+9 Pa
Ψ = -37.41°
L = 1.5 mm

Interfacial Test Specimen	Preconditioning	Csat (wt%)	G_c (J/m^2)
1	None	0.00	9.43
2	None	0.00	7.46
3	None	0.00	8.96
4	None	0.00	8.60
5	None	0.00	10.10
6	None	0.00	10.95
7	None	0.00	8.44
8	None	0.00	8.94
9	None	0.00	9.68
10	None	0.00	8.26
11	None	0.00	9.76
12	None	0.00	8.98
13	None	0.00	7.94
14	None	0.00	7.75
15	None	0.00	9.25
		AVERAGE:	**8.97**
		STANDARD DEVIATION:	**0.91**

Table 22. Interfacial fracture toughness data for underfill / copper test specimens after 85°C thermal aging for 168 hours

Underfill Adhesive:
E = 2.51E+9 Pa
v = 0.37
G = 9.16E+8 Pa

Copper Substrate:
E = 1.15E+11 Pa
v = 0.31
G = 4.39E+10 Pa

Interfacial Parameters:
α = 0.955
β = 0.196
$\bar{E}_1$ = 1.27E+11 Pa
$\bar{E}_2$ = 2.91E+9 Pa
Ψ = -37.43°
L = 1.5 mm

Interfacial Test Specimen	Preconditioning	Csat (wt%)	G_c (J/m^2)
16	85C	0.00	8.01
17	85C	0.00	7.83
18	85C	0.00	9.46
19	85C	0.00	7.05
20	85C	0.00	9.77
21	85C	0.00	8.71
22	85C	0.00	7.09
23	85C	0.00	9.02
24	85C	0.00	8.50
25	85C	0.00	7.63
26	85C	0.00	9.43
27	85C	0.00	8.94
28	85C	0.00	8.74
29	85C	0.00	9.34
30	85C	0.00	7.62
		AVERAGE:	**8.48**
		STANDARD DEVIATION:	**0.86**

Table 23. Interfacial fracture toughness data for underfill / copper test specimens after 85°C/50%RH moisture preconditioning for 168 hours

Underfill Adhesive:
E = 2.49E+9 Pa
v = 0.37
G = 9.09E+8 Pa

Copper Substrate:
E = 1.15E+11 Pa
v = 0.31
G = 4.39E+10 Pa

Interfacial Parameters:
α = 0.956
β = 0.196
$\bar{E}_1$ = 1.27E+11 Pa
$\bar{E}_2$ = 2.88E+9 Pa
Ψ = -37.45°
L = 1.5 mm

Interfacial Test Specimen	Preconditioning	Csat (wt%)	G_c (J/m^2)
31	85C / 50%RH	0.65	5.73
32	85C / 50%RH	0.65	4.98
33	85C / 50%RH	0.65	4.60
34	85C / 50%RH	0.65	6.04
35	85C / 50%RH	0.65	5.04
36	85C / 50%RH	0.65	5.08
37	85C / 50%RH	0.65	5.87
38	85C / 50%RH	0.65	5.38
39	85C / 50%RH	0.65	5.24
40	85C / 50%RH	0.65	4.62
		AVERAGE:	**5.26**
		STANDARD DEVIATION:	**0.47**

Table 24. Interfacial fracture toughness data for underfill / copper test specimens after 85°C/65%RH moisture preconditioning for 168 hours

Underfill Adhesive:
E = 2.45E+9 Pa
v = 0.37
G = 8.94E+8 Pa

Copper Substrate:
E = 1.15E+11 Pa
v = 0.31
G = 4.39E+10 Pa

Interfacial Parameters:
α = 0.956
β = 0.196
$\bar{E}_1$ = 1.27E+11 Pa
$\bar{E}_2$ = 2.83E+9 Pa
Ψ = -37.49°
L = 1.5 mm

Interfacial Test Specimen	Preconditioning	Csat (wt%)	G_c (J/m^2)
41	85C / 65%RH	0.77	4.76
42	85C / 65%RH	0.77	3.98
43	85C / 65%RH	0.77	5.31
44	85C / 65%RH	0.77	4.62
45	85C / 65%RH	0.77	3.70
46	85C / 65%RH	0.77	4.24
47	85C / 65%RH	0.77	4.56
48	85C / 65%RH	0.77	5.59
49	85C / 65%RH	0.77	3.97
50	85C / 65%RH	0.77	4.98
		AVERAGE:	**4.57**
		STANDARD DEVIATION:	**0.58**

Table 25. Interfacial fracture toughness data for underfill / copper test specimens after 85°C/85%RH moisture preconditioning for 168 hours

Underfill Adhesive:
E = 2.31E+9 Pa
v = 0.37
G = 8.43E+8 Pa

Copper Substrate:
E = 1.15E+11 Pa
v = 0.31
G = 4.39E+10 Pa

Interfacial Parameters:
α = 0.959
β = 0.196
$\bar{E}_1$ = 1.27E+11 Pa
$\bar{E}_2$ = 2.68E+9 Pa
Ψ = -37.64°
L = 1.5 mm

Interfacial Test Specimen	Preconditioning	Csat (wt%)	G_c (J/m^2)
51	85C / 85%RH	1.02	3.97
52	85C / 85%RH	1.02	3.75
53	85C / 85%RH	1.02	3.48
54	85C / 85%RH	1.02	3.59
55	85C / 85%RH	1.02	3.69
56	85C / 85%RH	1.02	4.04
57	85C / 85%RH	1.02	3.96
58	85C / 85%RH	1.02	4.33
59	85C / 85%RH	1.02	3.00
60	85C / 85%RH	1.02	3.88
		AVERAGE:	**3.76**
		STANDARD DEVIATION:	**0.36**

The entire range of mode mixity for all interfacial test specimens fell between -37.41^{o} to -37.64^{o}. Since the variation in mode mixity was negligible, the effect of this variation affecting interfacial fracture toughness results between different test groups is insignificant. Consequently, interfacial fracture toughness results for different moisture preconditioned test groups can be compared to one another to ascertain the effect of increasing moisture content on toughness values. It is also important to note that saturation was reached in each moisture preconditioning environment prior to fracture testing. As a result, a gradient of moisture concentration did not exist in the interfacial fracture toughness test specimens during testing. Figure 56 provides a graphical depiction of the effect of environmental preconditioning on the underfill / copper interfacial fracture toughness.

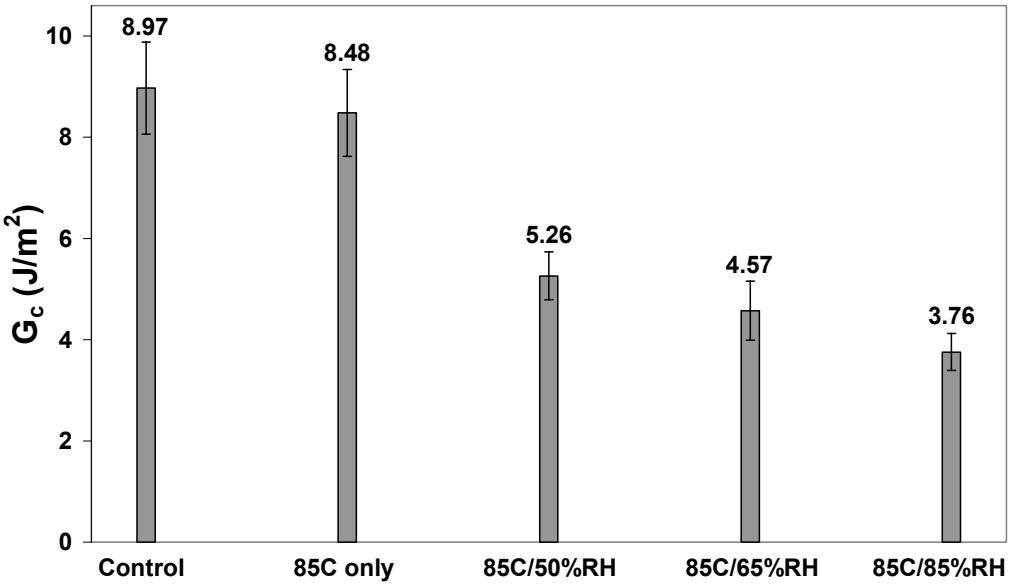

Figure 56. Effect of environmental preconditioning on the interfacial fracture toughness of the underfill / copper interface

As shown in Figure 56, it is clear that the contribution of thermal aging at 85°C did not significantly affect the interfacial fracture toughness of the underfill / copper interface. It is important to remember that all tests were performed at room temperature, hence only the effects of thermal aging were evaluated rather than the effect of testing at higher temperatures. Since all environmental preconditioned test groups were exposed to the same temperature component of 85°C and duration of 168 hours, any observed changes in the fracture toughness after moisture preconditioning can be attributed to the contribution of moisture. Moisture preconditioning at 85°C/50%RH, 85°C/65%RH, and 85°C/85%RH had a substantial effect on the interfacial fracture toughness and yielded decreases of 41.4%, 49.1%, and 58.1% respectively. A summary of the effect of moisture preconditioning on the interfacial fracture toughness is provided in Table 26, where Csat represents the saturation concentration of moisture for each respective level of moisture precondtioining and given as a percent weight change (wt%).

Table 26. Change in underfill / copper test specimen interfacial fracture toughness from moisture uptake

T (C)	RH (%)	Csat (wt%)	Csat (mg H_2O/ mm^3)	G_c (J/m^2)	Toughness Change (%)
Control	--	0	0.0000	8.97 ± 0.91	--
85	50	0.65	0.0075	5.26 ± 0.47	41.4
85	65	0.77	0.0089	4.57 ± 0.58	49.1
85	85	1.02	0.0118	3.76 ± 0.36	58.1

Since saturation was reached in all moisture preconditioned test specimens prior to fracture testing and thermal aging at 85^{o}C was found to have little to no effect on fracture toughness results, the change in the interfacial fracture toughness due to increasing amounts of moisture was characterized. Figures 57 and 58 depict the inherent change in the underfill / copper interfacial fracture toughness as a function of moisture concentration.

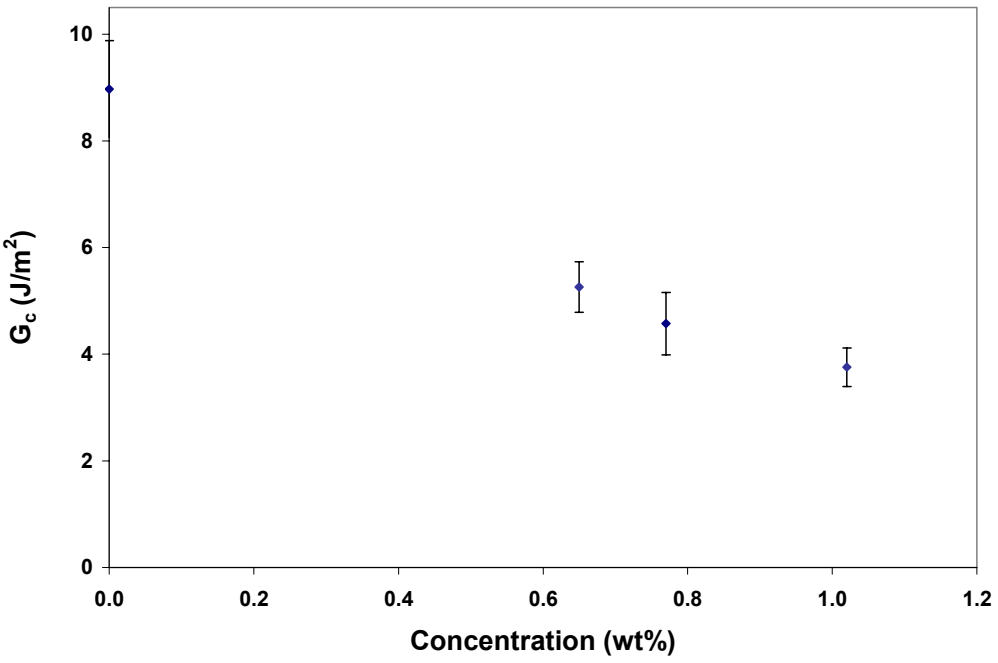

Figure 57. Underfill / copper interfacial fracture toughness variation as a function of moisture concentration (wt%)

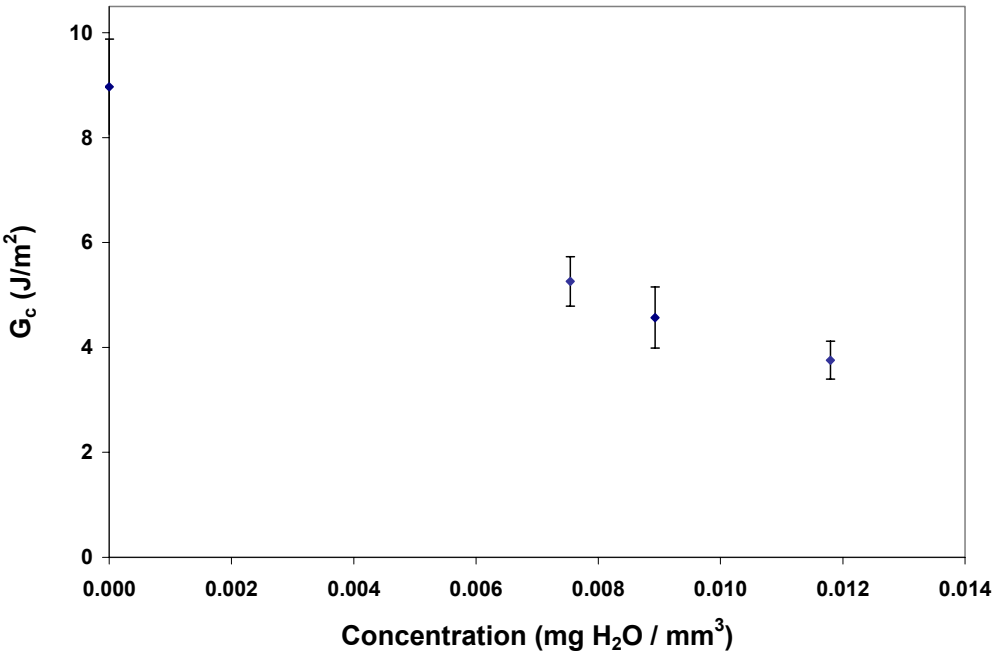

Figure 58. Underfill / copper interfacial fracture toughness variation as a function of moisture concentration (mg H_2O / mm^3)

Based on Figures 57 and 58, it is clear that the change in the interfacial fracture toughness is sensitive to small amounts of moisture. A significant reduction in interfacial adhesion was observed for concentrations as low as 0.65 wt%. Since the moisture did not significantly change the elastic modulus of the underfill adhesive for the moisture conditions evaluated for the interfacial fracture toughness, plasticization of the underfill from moisture contributed little to the change in the interfacial fracture toughness. As a result, the reduction in the toughness is primarily attributed to the weakening of the underfill / copper interface due to the direct presence of moisture at the interface. The moisture at the interface could decrease the adhesion through displacement of the underfill reducing Van der Waals forces as well as possible chemical

degradation of adhesive bonds. Further investigations into the exact failure mechanism from moisture at the interface are provided in detail in subsequent sections of this chapter.

6.3.2.1 Underfill / FR-4 Board Test Specimens

Having established the intrinsic response of interfacial fracture toughness to the underfill / copper test specimens, a new interface was characterized to examine any changes in the toughness response from moisture. This bimaterial interface consisted of the same underfill for the adhesive, but used FR-4 board rather than copper for the substrate. It is important to note that the FR-4 board was a composite structure, consisting of copper with a very thin coating of solder mask on the surface; consequently, the underfill adhesive bond and precrack in the interfacial fracture test specimens occurred at the underfill / solder mask interface. Figure 59 provides a graphical depiction of the underfill / FR-4 interfacial fracture test specimens.

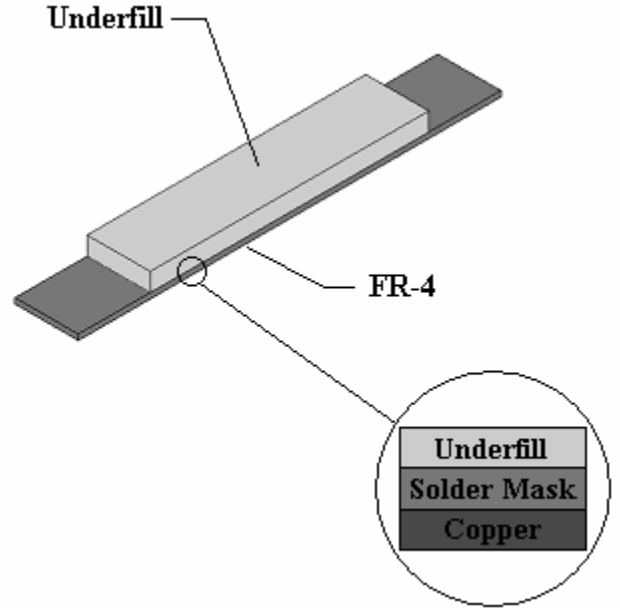

Figure 59. Underfill / FR-4 interfacial fracture test specimens

Using both the critical load of fracture and underfill elastic modulus value for each level of moisture preconditioning, the interfacial fracture toughness of the underfill / FR-4 test specimens was determined using Equation 6.3 for each respective environment. The results for the interfacial fracture toughness and saturation moisture concentrations for each environment are shown in Tables 27 – 31.

Table 27. Interfacial fracture toughness data for control underfill / FR-4 board test specimens

Underfill Adhesive:
E = 2.53E+9 Pa
v = 0.37
G = 9.23E+8 Pa

FR-4 Substrate:
E = 2.31E+10 Pa
v = 0.21
G = 9.52E+9 Pa

Interfacial Parameters:
α = 0.783
β = 0.144
$\bar{E}_1$ = 2.41E+10 Pa
$\bar{E}_2$ = 2.93E+9 Pa
Ψ = -38.81°
L = 0.67 mm

Interfacial Test Specimen	Preconditioning	Csat (wt%)	G_c (J/m^2)
91	None	0.00	189.84
92	None	0.00	174.05
93	None	0.00	178.80
94	None	0.00	190.48
95	None	0.00	171.35
96	None	0.00	168.67
97	None	0.00	182.25
98	None	0.00	185.90
99	None	0.00	193.94
100	None	0.00	175.07
		AVERAGE:	**181.03**
		STANDARD DEVIATION:	**8.33**

Table 28. Interfacial fracture toughness data for underfill / FR-4 board test specimens after 85°C thermal aging for 168 hours

Underfill Adhesive:
E = 2.51E+9 Pa
v = 0.37
G = 9.16E+8 Pa

FR-4 Substrate:
E = 2.31E+10 Pa
v = 0.21
G = 9.52E+9 Pa

Interfacial Parameters:
α = 0.785
β = 0.145
$\bar{E}_1$ = 2.41E+10 Pa
$\bar{E}_2$ = 2.91E+9 Pa
Ψ = -38.24°
L = 0.67 mm

Interfacial Test Specimen	Preconditioning	Csat (wt%)	G_c (J/m^2)
101	85C	0.00	183.29
102	85C	0.00	183.06
103	85C	0.00	183.53
104	85C	0.00	156.66
105	85C	0.00	168.88
106	85C	0.00	171.20
107	85C	0.00	194.58
108	85C	0.00	189.71
109	85C	0.00	194.36
110	85C	0.00	178.32
		AVERAGE:	**180.36**
		STANDARD DEVIATION:	**11.37**

Table 29. Interfacial fracture toughness data for underfill / FR-4 board test specimens after 85°C/50%RH moisture preconditioning for 168 hours

Underfill Adhesive:
E = 2.45E+9 Pa
v = 0.37
G = 8.94E+8 Pa

FR-4 Substrate:
E = 2.31E+10 Pa
v = 0.21
G = 9.52E+9 Pa

Interfacial Parameters:
α = 0.786
β = 0.145
$\bar{E}_1$ = 2.41E+10 Pa
$\bar{E}_2$ = 2.88E+9 Pa
Ψ = -38.11°
L = 0.67 mm

Interfacial Test Specimen	Preconditioning	Csat (wt%)	G_c (J/m^2)
111	85C / 50%RH	0.65	116.49
112	85C / 50%RH	0.65	100.43
113	85C / 50%RH	0.65	111.50
114	85C / 50%RH	0.65	99.52
115	85C / 50%RH	0.65	113.45
116	85C / 50%RH	0.65	91.27
117	85C / 50%RH	0.65	104.99
118	85C / 50%RH	0.65	85.57
119	85C / 50%RH	0.65	88.12
120	85C / 50%RH	0.65	103.28
		AVERAGE:	**101.46**
		STANDARD DEVIATION:	**10.13**

Table 30. Interfacial fracture toughness data for underfill / FR-4 board test specimens after 85°C/65%RH moisture preconditioning for 168 hours

Underfill Adhesive:
E = 2.45E+9 Pa
v = 0.37
G = 8.94E+8 Pa

FR-4 Substrate:
E = 2.31E+10 Pa
v = 0.21
G = 9.52E+9 Pa

Interfacial Parameters:
α = 0.789
β = 0.146
$\bar{E}_1$ = 2.41E+10 Pa
$\bar{E}_2$ = 2.84E+9 Pa
Ψ = -37.97°
L = 0.67 mm

Interfacial Test Specimen	Preconditioning	Csat (wt%)	G_c (J/m^2)
121	85C / 65%RH	0.77	87.15
122	85C / 65%RH	0.77	107.12
123	85C / 65%RH	0.77	96.88
124	85C / 65%RH	0.77	94.65
125	85C / 65%RH	0.77	79.15
126	85C / 65%RH	0.77	81.38
127	85C / 65%RH	0.77	85.07
128	85C / 65%RH	0.77	83.77
129	85C / 65%RH	0.77	96.59
130	85C / 65%RH	0.77	89.28
		AVERAGE:	**90.11**
		STANDARD DEVIATION:	**8.18**

Table 31. Interfacial fracture toughness data for underfill / FR-4 board test specimens after 85°C/85%RH moisture preconditioning for 168 hours

Underfill Adhesive:
E = 2.31E+9 Pa
v = 0.37
G = 8.43E+8 Pa

FR-4 Substrate:
E = 2.31E+10 Pa
v = 0.21
G = 9.52E+9 Pa

Interfacial Parameters:
α = 0.800
β = 0.149
$\bar{E}_1$ = 2.41E+10 Pa
$\bar{E}_2$ = 2.68E+9 Pa
Ψ = -37.22°
L = 0.67 mm

Interfacial Test Specimen	Preconditioning	Csat (wt%)	G_c (J/m^2)
131	85C / 85%RH	1.02	64.02
132	85C / 85%RH	1.02	66.78
133	85C / 85%RH	1.02	67.05
134	85C / 85%RH	1.02	71.42
135	85C / 85%RH	1.02	71.60
136	85C / 85%RH	1.02	65.29
137	85C / 85%RH	1.02	68.86
138	85C / 85%RH	1.02	80.48
139	85C / 85%RH	1.02	69.06
140	85C / 85%RH	1.02	70.08
		AVERAGE:	**69.46**
		STANDARD DEVIATION:	**4.37**

Although symmetric precracks were introduced at the underfill / solder mask interface before interfacial fracture testing, only 4% of the interfacial failures occurred at that interface. The vast majority of the failures (96%) occurred at the solder mask / copper interface. This was surprising considering a precrack was placed between the underfill / solder mask interface before interfacial fracture testing. In addition, there seemed to be no distinct pattern regarding if the failure mode changed before or after moisture preconditioning, as the 4% of failures that did occur at the underfill / solder mask interface were randomly distributed between dry and moisture preconditioned environments. If failure initially occurred at the solder mask / copper interface, the test specimen was unloaded, and a second interfacial fracture test was performed with the crack now existing at the solder mask / copper interface. This is to insure that the fracture toughness was obtained from the critical load of fracture of the solder mask / copper interface rather than cohesive failure in the solder mask. Although this does not represent an ideal interfacial fracture test since there is neither distinct control over how the initial interfacial crack was formed nor a known orientation of the crack at the time of testing, the crack propagation remained interfacial at the solder mask / copper interface when tested to complete failure. The entire range of mode mixity for all interfacial test specimens fell between -38.81^{o} to -37.22^{o}. Since the variation in mode mixity was negligible, the effect of this variation affecting interfacial fracture toughness results between different test groups is insignificant. Consequently, interfacial fracture toughness results for different moisture preconditioned test groups can be compared to one another to ascertain the effect of increasing moisture content on toughness values. It

is also important to note that saturation was reached in each moisture preconditioning environment prior to fracture testing. As a result, a gradient of moisture concentration did not exist in the interfacial fracture toughness test specimens during testing. Figure 60 provides a graphical depiction of the change in fracture toughness of the underfill / FR-4 board specimens, while Table 32 gives a summary of the effect of moisture preconditioning on the interfacial fracture toughness.

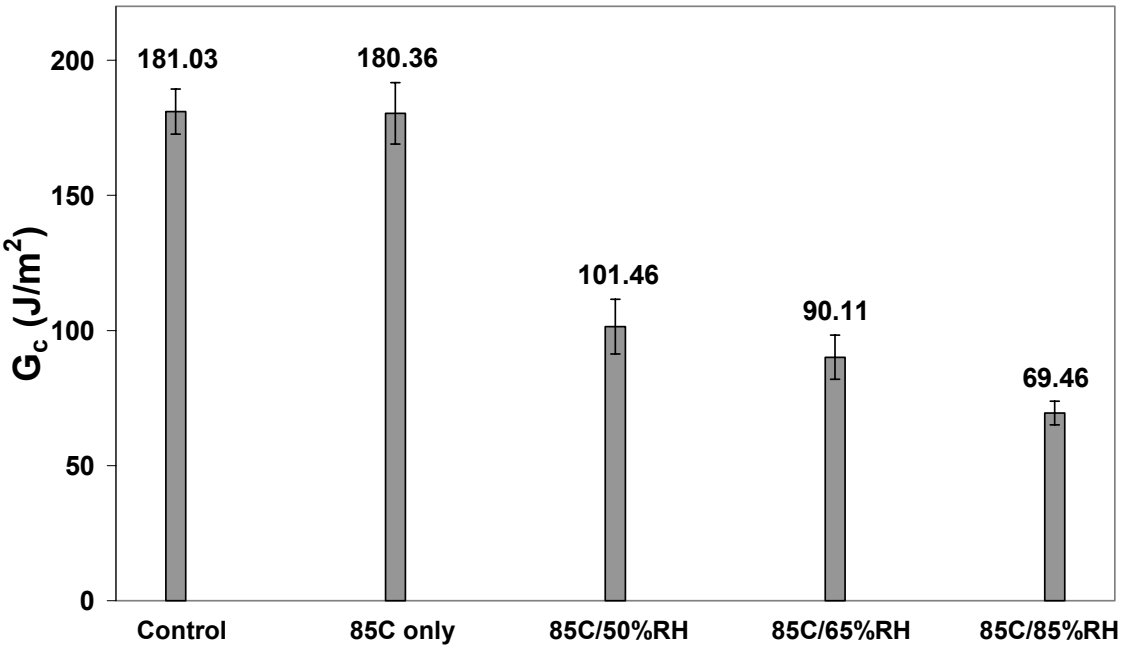

Figure 60. Effect of environmental preconditioning on underfill / FR-4 interfacial fracture toughness test specimens

Table 32. Change in underfill / FR-4 board test specimen interfacial fracture toughness from moisture uptake

T (C)	RH (%)	Csat (wt%)	Csat (mg H_2O/ mm^3)	G_c (J/m^2)	Toughness Change (%)
Control	--	0	0.0000	181.03 ± 8.33	--
85	50	0.65	0.0075	101.46 ± 10.13	44.0
85	65	0.77	0.0089	90.11 ± 8.18	50.2
85	85	1.02	0.0118	69.46 ± 4.37	61.6

As shown in Figure 60, it is clear that the contribution of thermal aging at 85°C did not significantly affect the interfacial fracture toughness of the solder mask / copper interface. It is important to recall that all tests were performed at room temperature, hence only the effects of thermal aging were evaluated rather than the effect of testing at higher temperatures. Since all environmental preconditioned test groups were exposed to the same temperature component of 85°C and duration of 168 hours, any observed changes in the fracture toughness after moisture preconditioning can be attributed to the contribution of moisture. Moisture preconditioning at 85°C/50%RH, 85°C/65%RH, and 85°C/85%RH had a substantial effect on the interfacial fracture toughness and yielded decreases of 44.0%, 50.2%, and 61.6% respectively given by Table 32. Figures 61 and 62 illustrate the change in interfacial fracture toughness as a function of moisture concentration.

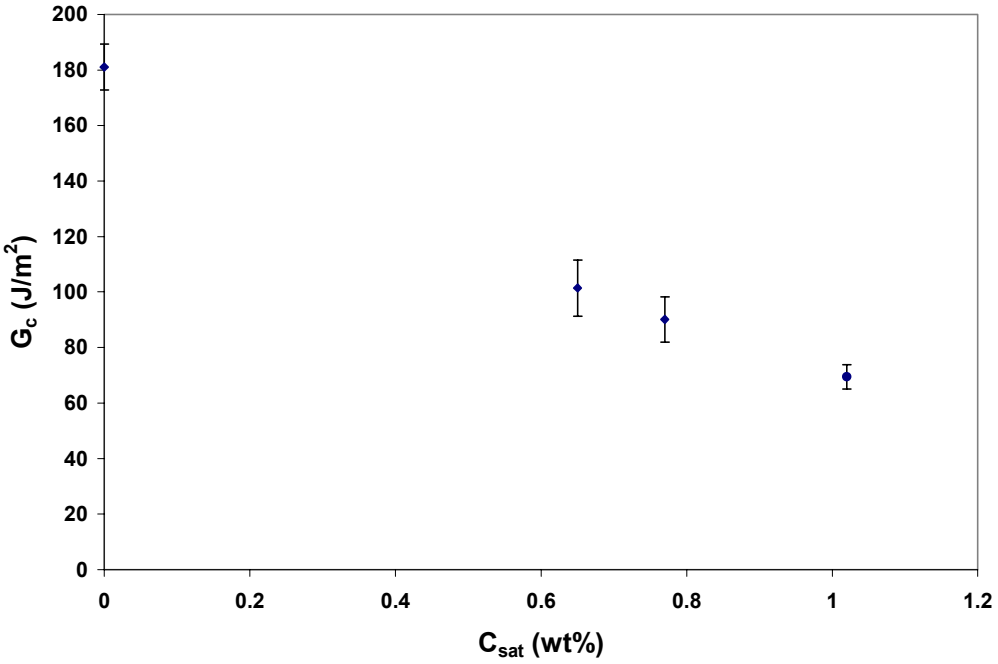

Figure 61. Solder mask / copper interfacial fracture toughness variation as a function of moisture concentration (wt%)

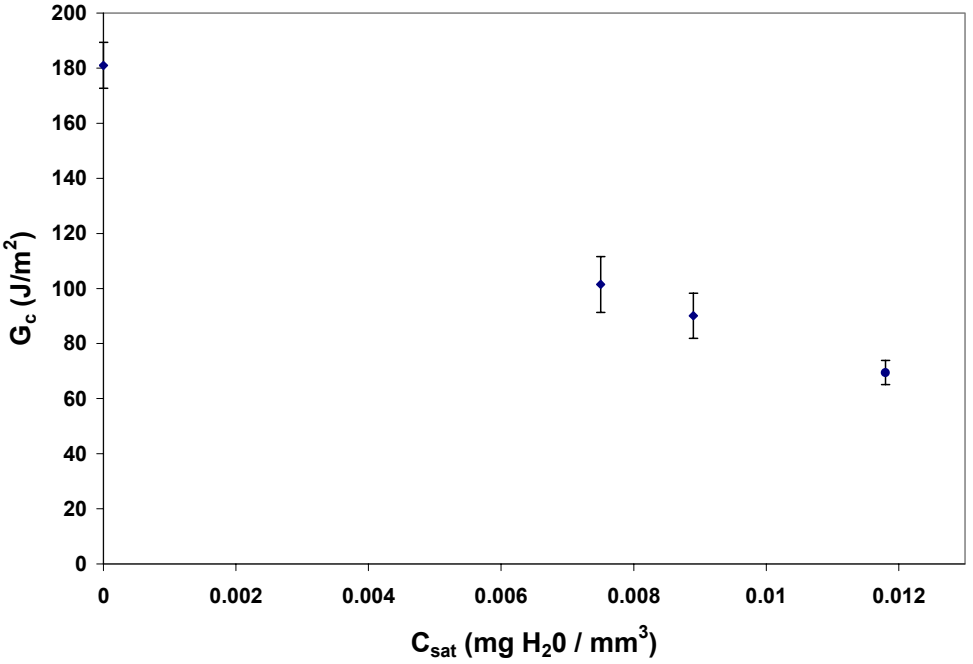

Figure 62. Solder mask / copper interfacial fracture toughness variation as a function of moisture concentration (mg H_2O / mm^3)

Similar to the underfill / copper interfacial fracture test results, the solder mask / copper interface was very sensitive to small concentrations of moisture. A significant reduction in interfacial adhesion was observed for concentrations as low as 0.65 wt%. Since the moisture did not significantly change the elastic modulus of the underfill adhesive for the moisture conditions evaluated for the interfacial fracture toughness, plasticization of the underfill from moisture contributed little to the change in the interfacial fracture toughness. As a result, the reduction in the toughness is primarily attributed to the weakening of the solder mask / copper interface due to the direct presence of moisture at the interface.

6.3.3 Moisture Induced Swelling

In addition to the mechanical load applied to test specimens during interfacial fracture testing, the interface is also subjected to hygro-swelling and thermal contraction mismatch effects between the adhesive and substrate. These two effects have opposite outcomes on the interface, as the contribution from the hygro-swelling mismatch will cause the underfill to be in compression, while the contribution from the thermal contraction mismatch will cause the underfill to be in tension. This is attributed to the different stress free environments for each case. For the case of the hygro-swelling mismatch, fully dry conditions represent a stress-free state for the interface. As moisture is absorbed in the underfill, it will cause the underfill to expand, while the moisture impermeable substrates will retain their original dimensions. Since the moisture expansion in the underfill will be constrained by the substrate, the expansion in the

underfill will yield compressive stresses within the underfill. For the case of the thermal contraction mismatch, the curing temperature of the underfill represents a stress-free state for the interface. As the underfill is curing in the oven, the thermoset polymer undergoes a transition from a liquid state to a solid state, thus representing a stress-free state at the interface for the curing temperature of 190^{o}C. Once test specimens are removed from the oven and allowed to cool to room temperature, the thermal mismatch between the copper and the underfill as well as the FR-4 board and the underfill will cause the underfill to be in tension due to it wanting to shrink more than the two substrates (CTE of experimental materials: underfill = 75 ppm / ^{o}C, copper = 17 ppm / ^{o}C, and FR-4 = 15 ppm / ^{o}C). Whether the interface is dominated by the hygro-swelling mismatch, thermal contraction mismatch, or possibly neither due to the effects of one another canceling each other out for a particular moisture saturation level will depend on the characteristics of the materials that constitute each bimaterial interface relative to their moisture preconditioning environment.

To investigate the effect of hygro-swelling on interfacial fracture test results, the moisture swelling coefficient, β, of the underfill was experimentally determined for each moisture preconditioning environment. It is important to note that moisture swelling test specimens were moisture preconditioned for 168 hours, and fully moisture saturated conditions existed within the test specimens at the conclusion of the exposure time. Consequently, a gradient of moisture concentration did not exist in the test specimens and the moisture swelling coefficient was properly identified for each environment. This is supported by there being no change in the mass of the specimens from moisture uptake

after approximately five days of exposure, indicating fully saturated, steady state conditions existed within the specimens prior to removal from the humidity chamber for measurement. The results are shown in Tables 33 – 35.

Table 33. Moisture expansion coefficient data for underfill after moisture Preconditioning at 85°C/50%RH for 168 hours

Test Specimen	Preconditioning	C_{sat} (wt%)	β (ppm / wt%)
1	85C / 50%RH	0.65	2075
2	85C / 50%RH	0.65	1692
3	85C / 50%RH	0.65	2044
4	85C / 50%RH	0.65	2058
5	85C / 50%RH	0.65	2067
		AVERAGE:	**1987**
		STANDARD DEVIATION:	**148**

Table 34. Moisture expansion coefficient data for underfill after moisture Preconditioning at 85°C/65%RH for 168 hours

Test Specimen	Preconditioning	Csat (wt%)	β (ppm / wt%)
6	85C / 65%RH	0.77	1700
7	85C / 65%RH	0.77	1962
8	85C / 65%RH	0.77	1913
9	85C / 65%RH	0.77	2030
10	85C / 65%RH	0.77	1929
		AVERAGE:	**1907**
		STANDARD DEVIATION:	**111**

Table 35. Moisture expansion coefficient data for underfill after moisture Preconditioning at 85°C/85%RH for 168 hours

Test Specimen	Preconditioning	Csat (wt%)	β (ppm / wt%)
11	85C / 85%RH	1.02	1708
12	85C / 85%RH	1.02	1802
13	85C / 85%RH	1.02	1777
14	85C / 85%RH	1.02	1949
15	85C / 85%RH	1.02	1803
		AVERAGE:	**1808**
		STANDARD DEVIATION:	**79**

Having identified the moisture swelling coefficient for each moisture preconditioning environment, a comparison can be made between the hygro-swelling and thermal mismatch strains for both the underfill / copper and underfill / FR-4 board interfaces. The hygro-swelling mismatch strain, ε_h, and thermal mismatch strain, ε_t, are defined as follows:

$$\varepsilon_h = \beta_1 C_{sat,1} - \beta_2 C_{sat,2} \tag{6.10}$$

$$\varepsilon_t = (\alpha_1 - \alpha_2)(T_f - T_i) \tag{6.11}$$

where β is the moisture swelling coefficient, C_{sat} is the equilibrium moisture saturation concentration, α is the coefficient of thermal expansion, T is the temperature, and subscripts 1 and 2 refer to the two materials that constitute the bimaterial interface. The hygro-swelling mismatch strain and thermal expansion mismatch strain were calculated

using Eqs. (6.10) and (6.11) respectively for both the underfill / copper and underfill / FR-4 test specimens for each moisture preconditioning environment. Since the cooling of the interfacial fracture test specimens from the cure temperature to room temperature will result in a thermal contraction, while the uptake of moisture will result in an expansion from swelling, it should be noted that the hygro-swelling and thermal expansion mismatch strains act in opposite directions. In addition, since both substrates were impermeable to moisture, one of the terms in Equation (6.10) will drop out. The results are given in Tables 36 and 37.

Table 36. Comparison of hygro-swelling and thermal mismatch strains for underfill / copper interfacial fracture test specimens

Environment	β (ppm/wt%)	C_{sat} (wt%)	ε_h	α_{uf} (ppm/C)	α_{Cu} (ppm/C)	T_i (C)	T_f (C)	ε_t
85C/50%RH	1987	0.65	**0.0013**	75	17	190	25	**0.0096**
85C/65%RH	1907	0.77	**0.0015**	75	17	190	25	**0.0096**
85C/85%RH	1808	1.02	**0.0018**	75	17	190	25	**0.0096**

Table 37. Comparison of hygro-swelling and thermal mismatch strains for underfill / FR-4 board interfacial fracture test specimens

Environment	β (ppm/wt%)	C_{sat} (wt%)	ε_h	α_{uf} (ppm/C)	α_{FR-4} (ppm/C)	T_i (C)	T_f (C)	ε_t
85C/50%RH	1987	0.65	**0.0013**	75	15	190	25	**0.0099**
85C/65%RH	1907	0.77	**0.0015**	75	15	190	25	**0.0099**
85C/85%RH	1808	1.02	**0.0018**	75	15	190	25	**0.0099**

As shown in Tables 36 and 37, the thermal mismatch strains were significantly greater than the hygro-swelling mismatch strains for both interfaces and for all moisture preconditioning environments by roughly an order of magnitude. It is clear that the thermal mismatch strain dominated the interaction at the interface and was only slightly offset by a small contribution from the hygro-swelling mismatch strain. As a result, the underfill will be in tension during interfacial fracture testing, effectively preloading the interface and requiring a lower critical load of fracture, P_c, from mechanical testing to advance the interface crack. Consequently, interfacial fracture toughness values will represent a conservative estimate of the interfacial fracture toughness of the interface. In addition, it is clear that increasing the saturation concentration did not significantly increase the hygro-swelling mismatch strain. All interfaces for all environments experienced similar hygro-swelling mismatch strains for the materials and moisture preconditioning environments tested in this study. Consequently, the trends exhibited in the interfacial fracture toughness as moisture concentration increases are essentially independent of the hygro-swelling mismatch relative to one another, and the observed changes between the different moisture preconditioning environments can be predominately attributed to more moisture being present at the interface resulting in a greater loss of adhesion.

6.3.4 Fracture Failure Locus

Once water enters the epoxy interface, previous studies have reported a change in the fracture failure locus from cohesive/interphase failure to purely interfacial after lap

shear testing (Comyn, *et al*. 1994; Zanni-Deffarges and Shanahan, 1994; DeNeve and Shanahan, 1992; and Su, *et al*., 1992). Unlike lap shear test specimens where failure can either be cohesive within the adhesive or interfacial at the interface, the pre-crack that exists in interfacial fracture test specimens will cause interfacial failure to dominate in most cases. From visual inspection of the interfacial fracture test specimens used in this study, it appeared that interfacial failure occurred between the adhesive and substrate; however, it is possible interphase failure occurred that was not observable to the naked eye. Although there was no observable change in the failure locus of the test specimens from visual inspection, Scanning Electron Microscopy was used to further investigate if the failure locus may have been altered after moisture preconditioning.

Interfacial failures of the underfill / copper and underfill / FR-4 board interfacial fracture test specimens both occurred at the adhesive / copper interface. Based on the significantly higher values for interfacial fracture toughness of the copper in the FR-4 board compared to the copper substrates, it is clear that surface modifications of the copper used in the FR-4 board were introduced to improve the adhesion between the solder mask and copper. Since the FR-4 board was received from a commercial vendor, the processing and surface preparation of the copper present in the FR-4 board during manufacture is proprietary and unknown. The improvement in the copper adhesion could have resulted from the addition of coatings applied to the copper surface and/or by roughening the copper surface before the application of the solder mask. Therefore, it makes it difficult to accurately study a possible change in failure locus due to moisture preconditioning and attribute any observed changes to solely the effect of moisture on the

copper surface. Conversely, the processing, roughness, and surface preparation of the copper substrate used in the underfill / copper interfacial fracture test specimens is completely known. As a result, the copper failure surface of the underfill / copper interfacial fracture test specimen represents an ideal candidate for observing a potential change in failure locus after moisture preconditioning.

A variety of magnifications were used to explore if any changes in the failure locus had occurred after moisture preconditioning; however, a magnification of 50X proved to yield the best perspective to obtain the most accurate visual depiction of the failure surface and locus. Figures 63 – 66 show the copper failure surface at 50X for fully dry, 85^{o}C/50%RH , 85^{o}C/65%RH , and 85^{o}C/85%RH moisture preconditioning for 168 hours.

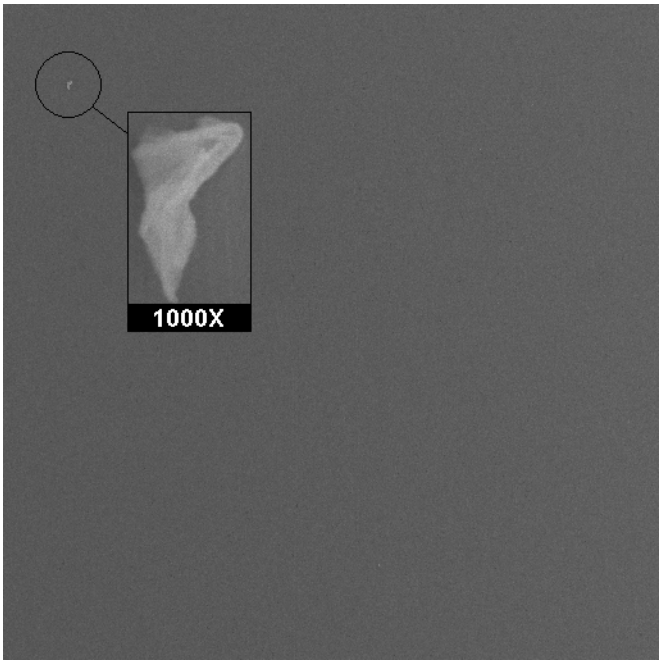

Figure 63. Copper failure surface at 50X after interfacial fracture testing for fully dry conditions

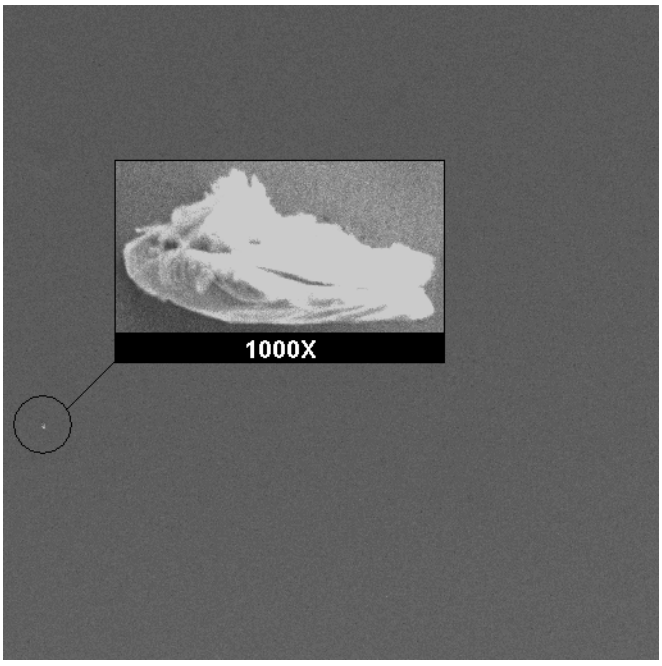

Figure 64. Copper failure surface at 50X after interfacial fracture testing for 85^{o}C/50%RH moisture preconditioning

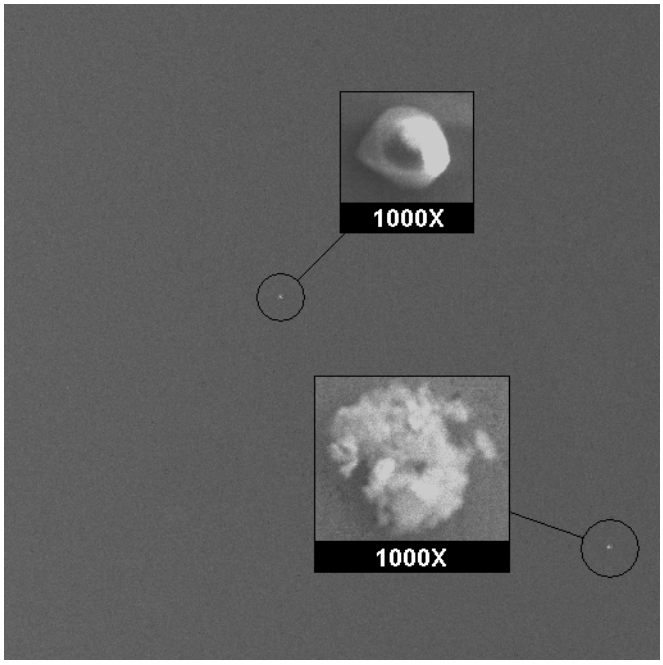

Figure 65. Copper failure surface at 50X after interfacial fracture testing for 85°C/65%RH moisture preconditioning

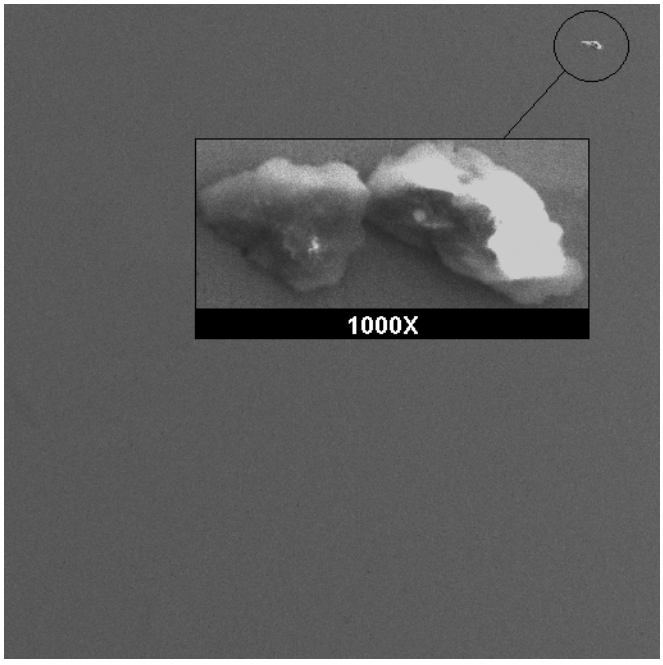

Figure 66. Copper failure surface at 50X after interfacial fracture testing for 85°C/85%RH moisture preconditioning

As shown in Figures 63 – 66, the failure mode was virtually purely interfacial, with only very slight evidence of occasional interphase failure as evident by the occasional presence of adhesive on the substrate failure surface shown in the 1000x magnification windows. It should be noted that several failure surfaces were examined for each moisture preconditioning environment, which also included an inspection of the entire area rather than the small section shown in Figures 63 – 66. These figures are accurate representations of what was commonly observed when examining these failure surfaces. In addition, higher magnifications of up to 5,000X were used to examine if localized areas of adhesive remained on the substrate that were not detectable at a magnification of 50X. No additional areas were found at the higher magnifications. It is also clear from Figures 63 – 66 that there was no observable change in the failure locus after moisture preconditioning. The very slight distribution of localized interphase failure on the substrate failure surfaces was common to all moisture preconditioning environments, with no observable change in the amount of adhesive distribution on the failure surface before and after moisture preconditioning. Consequently, moisture preconditioning did not appear to change the failure locus for the test specimens evaluated in this study.

6.3.5 Oxidation Growth

Copper has a strong affinity to oxygen, and the development of an oxidation layer between the substrate and adhesive over time is inevitable. Initially, cuprous oxide, Cu_2O, will form followed by the formation of a layer of cupric oxide, CuO (Cho and

Cho, 2000). X-ray Photoelectron Spectroscopy was used to identify the type of copper oxide present on the surface of the copper substrate for each environmentally preconditioned test group after fracture testing. A wide scan identified the presence of oxygen on the surface, indicating oxides had formed after adhesive bonding for each environmentally preconditioned test group. A narrow scan was conducted to identify the particular type of copper oxide that had formed on the copper substrate surface after thermal aging at 85°C for 168 hours, moisture preconditioning at 85°C/50%RH for 168 hours, and moisture preconditioning at 85°C/85%RH for 168 hours. The results are shown in Figures 67 - 69.

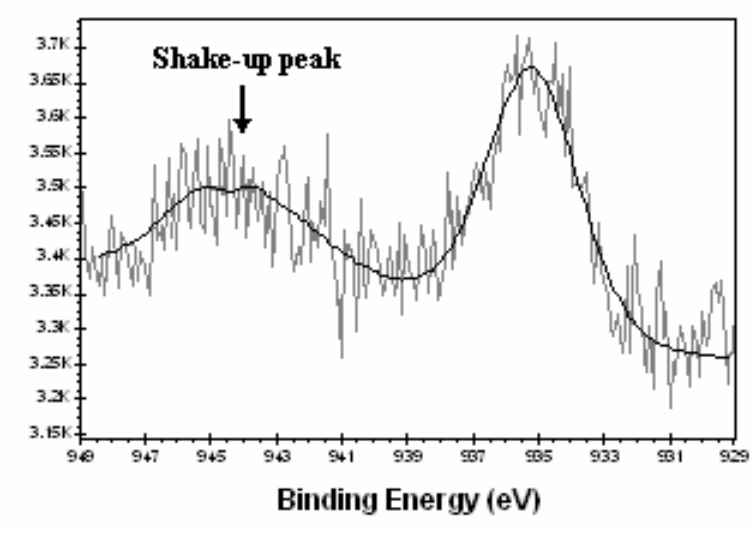

Figure 67. XPS spectra of copper surface after fracture for 85°C thermal aging

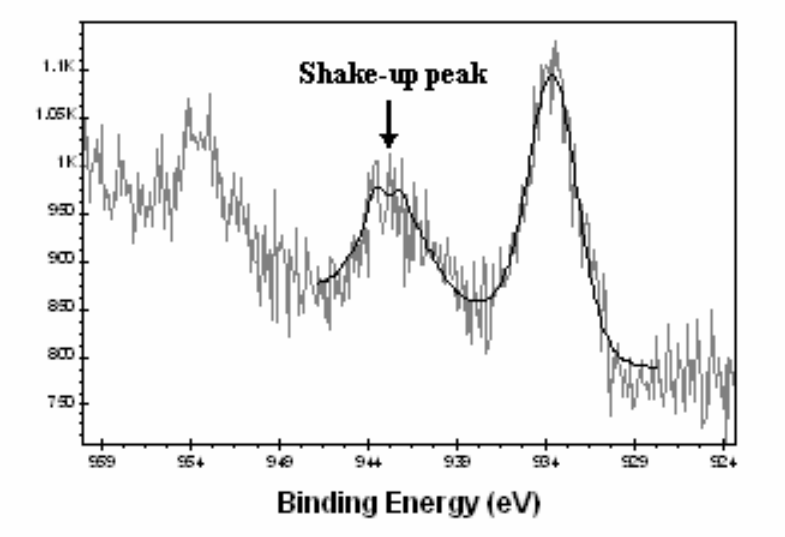

Figure 68. XPS spectra of copper surface after fracture for 85°C/50%RH moisture preconditioning

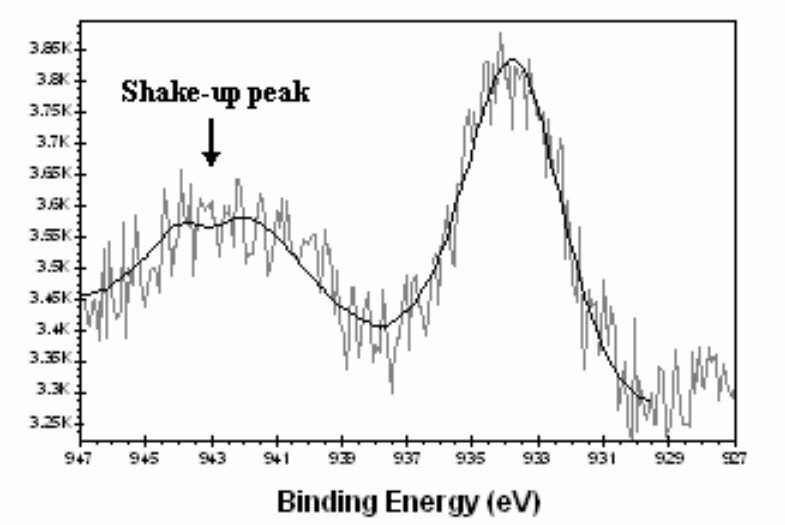

Figure 69. XPS spectra of copper surface after fracture for 85°C/85%RH moisture preconditioning

The appearance of a distinct shake-up satellite that developed to the left of the primary Cu 2p3/2 peak indicates the presence of CuO on the copper surface. As seen in Figures 67 – 69, this shake-up satellite was found on all copper substrate surfaces for conditions of 85°C thermal aging, 85°C/50%RH moisture preconditioning, and 85°C/85%RH moisture preconditioning after 168 hours exposure. Since the shake-up satellite was found for both the upper and lower bounds of 85°C/85%RH and 85°C/50%RH moisture preconditioning, it is anticipated that the cupric oxide would also be present after 85°C/65%RH moisture preconditioning as well. This is supported from visual inspection, where a black tint could be seen on the copper substrate surface after fracture testing for all moisture preconditioned environments. This black tint is indicative of the formation of cupric oxide, also known as black oxide, whereas cuprous oxide forms a red tint. Therefore, it can be concluded that cupric oxide was present on the copper substrate during interfacial fracture testing for all preconditioning environments tested in this study.

Since the copper substrate were cleaned to remove oxides before adhesive bonding, it is possible the formation of the oxides on the copper substrates during adhesive curing and subsequent environmental preconditioning may have affected interfacial fracture test results. When evaluating the effect of oxidation on interfacial adhesion, there are two primary aspects to consider. The first consideration is the variation in the chemistry at the interface from oxidation. Due to the polarity of the water molecule, a chemical variation at the interface from different moisture preconditioning environments could affect the behavior of the moisture at the interface and subsequent

interfacial fracture test results. Based on the XPS results, it is clear that all preconditioning environments produced cupric oxide on the copper substrate surface, eliminating the possibility that some environments yielded only cuprous oxide, while others developed cupric oxide. Consequently, all environmentally preconditioned interfacial fracture test specimens experienced identical chemical formations at the interface, which will yield similar interactions of moisture at the interface. The second consideration is the degree of oxidation at the interface. As the oxidation thickness on the substrate increases, it could displace the adhesive from the substrate and reduce the Van der Waals adhesive forces at the interface, yielding a reduction in interfacial adhesion. The relative intensity of the CuO development can be ascertained by comparing the atomic percentage of the CuO shake-up satellite to the Cu_2O peak. The atomic percentages for each environmentally preconditioned test specimens are shown in Table 38.

Table 38. Atomic percentage of CuO to Cu_2O

Preconditioning	Cu_2O (%)	CuO (%)
85C Thermal Aging	68	32
85C / 50%RH	69	31
85C / 85%RH	68	32

Based on the atomic percentages shown in Table 38, a similar development of oxidation existed on the copper substrate surface for all environmentally preconditioned test specimens. The similar atomic percentages obtained when comparing thermal aging

at 85°C to the moisture preconditioning environments of 85°C/50%RH and 85°C/85%RH indicates that the moisture component had a minimal contribution to oxidation growth rates compared to the available oxygen in the air common to all environmental preconditioned environments. Consequently, a similar level of oxidation thickness existed on all environmentally preconditioned test specimens. It should be noted that supporting results discussed in Section 6.3.6, Interfacial Hydrophobicity, demonstrate similar water contact angle measurements were obtained for all environmental preconditioned copper substrates, which also indicates a similar degree of oxidation for all environmentally preconditioned test groups. The effect of this oxide growth on interfacial fracture toughness can be ascertained by comparing the 85°C thermal aging test results to the control test results. As shown in Figure 56, thermal aging at 85°C appeared to possibly decrease the interfacial adhesion of the copper / underfill interface, although considering the overlap in the uncertainty in test results it is difficult to make such a conclusion unequivocally. Any loss in adhesion due to thermal aging could in part be attributed to the growth of oxides on the copper substrate displacing the underfill at the adhesive bond. Both Mino, *et al*., 1998 and Chong, *et al*., 1995 have shown that the development of the copper oxide layer thickness is significantly slower and minimal for temperatures below 100°C and 120°C. Consequently, since the test specimens in this study had a temperature component of only 85°C, it is anticipated that the oxide layer thickness that developed on test specimens was very small, which would explain in part why the interfacial fracture toughness results were not significantly affected by the oxidation growth. This would indicate that the observed losses in interfacial adhesion

from moisture preconditioning can be attributed to the presence of moisture rather than the growth of oxides at the interface.

6.3.6 Interfacial Hydrophobicity

The polarity of the water molecule will affect its behavior at the interface, which can influence the extent of environmental degradation of an adhesive joint due to the presence of moisture (Luo, 2003). The polar behavior of water arises from its structure, which is composed of a single oxygen atom bonded to two hydrogen atoms. The hydrogen atoms are covalently bonded to the oxygen atom through shared electrons. Two pairs of electrons surrounding the oxygen atom are involved in covalent bonds with hydrogen; however, there are also two unshared pairs of electrons (lone-pair) on the other side of the oxygen atom, which shift the electron cloud of the water molecule over to the oxygen atom as shown in Figure 70.

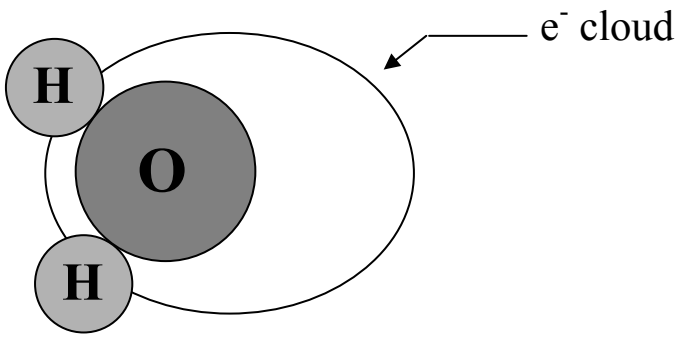

Figure 70. Electron cloud distribution on a water molecule

This uneven distribution of electron density in the water molecule yields a partial negative charge (δ^-) on the oxygen atom and a partial positive charge (δ^+) on the hydrogen atoms, giving rise to the polarity of the water molecule. Polarity allows water molecules to bond with each other, and hydrogen bonds will form between two oppositely charged ends of a water molecule as shown in Figure 71.

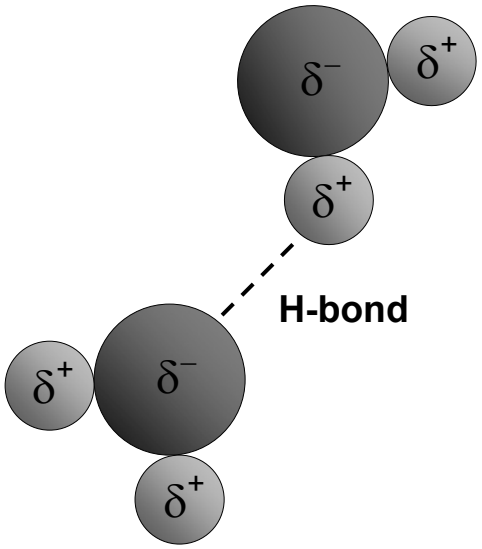

Figure 71. Hydrogen bonding between water molecules

The hydrogen bonds have about a tenth of the strength of an average covalent bond, and are being constantly broken and reformed in liquid water. The polarity will also allow water to molecules to bond with other polar molecules, which will affect how the water will wet on different surfaces. Surfaces that contain polar molecules are hydrophilic. They interact with the water molecules to enhance wetting and produce low contact angles. If a surface contains alcohols, S, O, or N, it will probably be hydrophilic.

Conversely, surfaces that contain nonpolar substances are hydrophobic. They cannot interact with the water molecules and produce high contact angles. In general, if a surface contains C, H, or F, it will probably be hydrophobic.

Most materials will not be purely hydrophobic or hydrophilic, but will have varying degrees to which they are considered one or the other. This is addressed in Hydrophobicity, which is the study of the wetting characteristics of water on surfaces. One method used to test the hydrophobicity of a surface is through measurement of the contact angle, θ, using water as the probe liquid. Very hydrophobic surfaces will cause the water to form a bubble on the surface, whereas very hydrophilic surfaces will cause the water to wet the surface and smear flat. This arises due to the fact that for a hydrophobic surface, water will want to minimize its contact with the surface and organize itself into a sphere. Conversely, for a hydrophilic surface, water will want to maximize its contact with the surface and spread itself as much as possible. Figure 72 illustrates the contact angle behavior of water on both hydrophobic and hydrophilic surfaces.

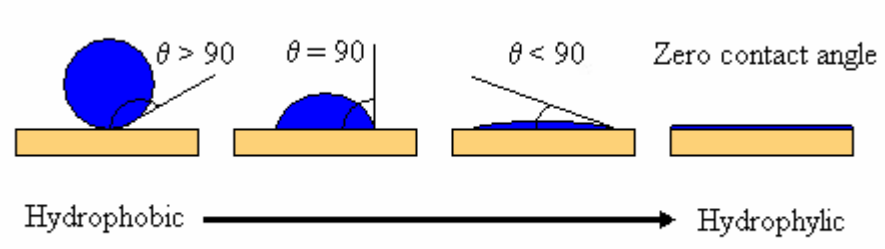

Figure 72. Hydrophobic and hydrophilic water contact angle behavior

To determine the hydrophobicity of interfacial fracture test specimens, contact angle measurements were made for the adhesive and substrates evaluated in this study. Representative water droplet images for each surface are shown in Figures 73 – 75, while the contact angle results are given in Tables 39 – 41.

Figure 73. Representative water droplet image on copper

Figure 74. Representative water droplet image on solder mask

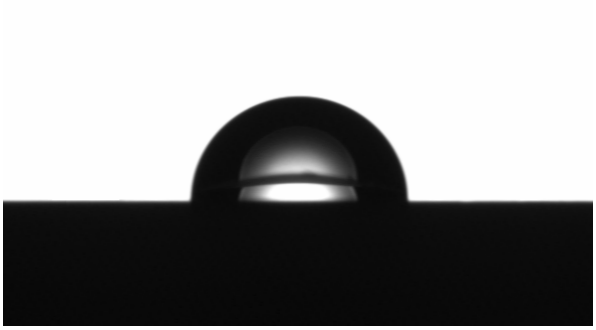

Figure 75. Representative water droplet image on underfill

Table 39. Contact angles of water on copper

Test	Preconditioning	Probe Liquid	Surface	θ (degrees)
1	None	Water	Copper	73.61
2	None	Water	Copper	74.14
3	None	Water	Copper	74.05
4	None	Water	Copper	73.81
5	None	Water	Copper	74.70
			AVERAGE:	**74.06**
			STANDARD DEVIATION:	**0.37**

Table 40. Contact angles of water on solder mask

Test	Preconditioning	Probe Liquid	Surface	θ (degrees)
1	None	Water	Solder Mask	23.70
2	None	Water	Solder Mask	24.14
3	None	Water	Solder Mask	27.58
4	None	Water	Solder Mask	24.17
5	None	Water	Solder Mask	25.61
			AVERAGE:	**25.04**
			STANDARD DEVIATION:	**1.42**

Table 41. Contact angles of water on underfill

Test	Preconditioning	Probe Liquid	Surface	θ (degrees)
1	None	Water	Underfill	83.31
2	None	Water	Underfill	82.17
3	None	Water	Underfill	82.61
4	None	Water	Underfill	84.96
5	None	Water	Underfill	83.03
			AVERAGE:	**83.22**
			STANDARD DEVIATION:	**0.95**

Both the clean copper substrate and underfill adhesive exhibited fairly hydrophobic behavior with contact angles of 74.06^{o} and 83.22^{o} respectively, while the solder mask was considerably hydrophilic with an average contact angle of only 25.04^{o}. This is attributed in part to the surface preparation of the FR-4, where the solder mask surface was cleaned by lightly wiping with isopropanol to remove contaminants from the surface prior to adhesive bonding. Any residual presence of isopropoanol on the solder mask surface would have contributed to the measured water contact angle results. In addition, it is possible that since the FR-4 board was received from a commercial manufacturer, both the surface preparation by the manufacturer and the particular formulation of solder mask used would have contributed to a lower contact angle.

Having established the hydrophobicity of the substrates and adhesive, the interfacial hydrophobicity of the underfill / copper and underfill / FR-4 board interfacial fracture test specimens can be evaluated. When addressing the relative hydrophobicity of the substrate and adhesive to moisture behavior at the interface, the interaction can become complex. The surface with the most dominant degree of hydrophobicity will govern the shape and response of the water at the interface. For example, if a hydrophobic substrate is bonded with a hydrophilic adhesive, then the water at the interface will want to minimize contact with the substrate and maximize contact with the adhesive. Depending on imperfections in the bonding, surface roughness, and the relative degree of hydrophobicity of the substrate to the adhesive, water at the interface will more or less form a somewhat hemi-spherical shape at the interface, with the spherical end minimizing contact on the substrate and the open end maximizing contact

on the adhesive. Naturally, the shape of the water at the interface can have various permutations of the aforementioned shape, depending on the degree of hydrophobic behavior of the substrate relative to the hydrophilic behavior of the adhesive, but the general idea remains the same. For other systems with varying degrees of hydrophobicity, the shape of the water at the interface relative to the hydrophobicity of the substrate and adhesive can be extremely difficult to characterize; however, qualitative conclusions can be made. For the case of the underfill / copper interfacial fracture test specimens, the relative hydrophobicity of the adhesive to substrate was similar; consequently, the wetting behavior of the moisture at the interface would not be significantly dominated by either the adhesive or substrate. For the case of the underfill / FR-4 board interfacial fracture test specimens, the solder mask was very hydrophilic compared to the moderately hydrophobic underfill; consequently, interfacial wetting characteristics would be dominated by the solder mask. Assuming the copper used in the FR-4 board was not coated with any substance and exhibited similar wetting behavior of typical copper, the interfacial hydrophobicity of both the solder mask / copper interface and the underfill / solder mask interface would be similar for this particular FR-4 board. Consequently, similar wetting characteristics of moisture would occur at both interfaces resulting in similar interfacial concentrations of moisture. However, the vast majority of failures occurred at the solder mask / copper interface rather than the solder mask / underfill interface. This can be attributed to the weaker bonding mechanism of the Van der Waals bonds between the solder mask / copper interface compared to the strong covalent bonds of the solder mask / underfill interface.

An additional consideration unique to environmental preconditioning is the growth of oxides affecting the interfacial hydrophobicity. Both the underfill adhesive and solder mask on the FR-4 board will not significantly oxidize; however, the oxidation of the copper substrates can be significant, and previous studies have shown that the water contact angle on copper is affected by oxidation (Cho and Cho, 2000; Yi, *et al*., 1999; Hong, *et al*., 1994; and Kim, 1991). Due to oxidation growth on the copper substrates, contact angle measurements were made for each preconditioning environment to monitor any change in the hydrophobicity of the copper surface. Since the copper bonding surface of the interfacial fracture test specimen will be shielded by the underfill adhesive, the oxidation growth rate will be different than for bare copper environmentally aged for a similar duration of time. Consequently, the water contact angles for each environmental test group were measured using special test specimens that mimicked the exposure of the copper bonding surface to similar amounts of oxygen and moisture as the interfacial fracture test specimens. These specimens used the same geometry as the interfacial fracture test specimens, but the underfill adhesive was cured separately in an individual mold. After curing the adhesive, the underfill was placed on top of the copper substrate and held in place by c-clamps. Similar to the interfacial fracture test specimens, a water-proof sealant was applied around the perimeter of the test specimen to eliminate wicking of moisture at the interface and force 1-D diffusion through the underfill. After moisture preconditioning, the water-proof perimeter and c-clamps were removed from the test specimen followed by the underfill from the copper bonding surface for contact

angle measurement. Water contact angle results for the various preconditioning environments are given in Tables 42 – 45.

Table 42. Contact angles of water on copper after 85°C thermal aging for 168 hours

Test	Preconditioning	Probe Liquid	Surface	θ (degrees)
1	85C	Water	Copper	77.41
2	85C	Water	Copper	75.62
3	85C	Water	Copper	75.54
4	85C	Water	Copper	76.08
5	85C	Water	Copper	75.38
			AVERAGE:	**76.01**
			STANDARD DEVIATION:	**0.74**

Table 43. Contact angles of water on copper after 85°C/50%RH moisture preconditioning for 168 hours

Test	Preconditioning	Probe Liquid	Surface	θ (degrees)
1	85C/50%RH	Water	Copper	75.13
2	85C/50%RH	Water	Copper	77.02
3	85C/50%RH	Water	Copper	76.91
4	85C/50%RH	Water	Copper	75.27
5	85C/50%RH	Water	Copper	76.64
			AVERAGE:	**76.19**
			STANDARD DEVIATION:	**0.82**

Table 44. Contact angles of water on copper after 85°C/65%RH moisture preconditioning for 168 hours

Test	Preconditioning	Probe Liquid	Surface	θ (degrees)
1	85C/65%RH	Water	Copper	75.80
2	85C/65%RH	Water	Copper	77.47
3	85C/65%RH	Water	Copper	76.46
4	85C/65%RH	Water	Copper	77.61
5	85C/65%RH	Water	Copper	75.76
			AVERAGE:	**76.62**
			STANDARD DEVIATION:	**0.79**

Table 45. Contact angles of water on copper after 85°C/85%RH moisture preconditioning for 168 hours

Test	Preconditioning	Probe Liquid	Surface	θ (degrees)
1	85C/85%RH	Water	Copper	76.96
2	85C/85%RH	Water	Copper	79.29
3	85C/85%RH	Water	Copper	76.98
4	85C/85%RH	Water	Copper	77.40
5	85C/85%RH	Water	Copper	76.03
			AVERAGE:	**77.33**
			STANDARD DEVIATION:	**1.08**

As shown in Tables 42 – 45, all levels of environmental preconditioning did not significantly alter the water contact angle and associated hydrophobicity of the interface. Consequently, similar interfacial wetting characteristics of moisture at the interface will occur for all preconditioning environments. Although the contact angle did not significantly change, there did appear to be a slight increase in the water contact angle with moisture preconditioning. Previous studies have shown both an increase (Yi, *et al*., 1999; Kim, 1991) and decrease (Cho and Cho, 2000; Hong, *et al*., 1994) in the water contact angle of copper with oxidation. The oxidation – reduction chemistry occurring at

the interface relative to environmental preconditioning is complex, and the differences in trends could be attributed to the degree of oxidation altering the surface chemistry (Cho and Cho, 2000), change in surface roughness of the substrate from oxidation growth (Hong, *et al*., 1994), and contamination of the surface by hydrocarbons from the environment (Luo, 2003). In addition, Yi, *et al*., (1999) has provided data correlating the oxide layer thickness on copper leadframes to water contact angles. This data shows a slow, gradual increase in oxide thickness from water contact angles ranging from 72^{o} – 78^{o}, but depicts a sharp increase in oxide layer thickness for contact angles exceeding 80^{o}. Based on the results shown in Tables 42 - 45, all measurements yielded average contact angles less than 78^{o} with vary little variation, which would suggest that a comparable oxidation layer thickness existed in all environmentally preconditioned test groups. This supports X-ray Photoelectron Spectroscopy results discussed in Section 6.3.5, Oxidation Growth, where a similar conclusion was reached.

6.3.7. Interfacial Fracture Toughness Moisture Degradation Model

Having implemented an extensive experimental program to ascertain the role of moisture in adhesion degradation and the physical mechanisms responsible for the change in interfacial adhesion, the focus of this study now shifted to developing a model depicting the intrinsic loss in interfacial fracture toughness as a function of the critical parameters relevant to moisture. At the root of this model is characterizing the dominant mechanism for adhesion between the adhesive and substrate. There are four primary mechanisms for adhesion which have been proposed. They include mechanical

interlocking, diffusion theory, electronic theory, and adsorption theory (Kinloch, 1987). For the underfill / copper interface, the contributions of interfacial diffusion and electrostatic forces between the adhesive and substrate causing adhesion is far lower than the effects of mechanical interlocking and adsorption. Since the copper substrates in this study were polished to a mirror finish, the effects from mechanical interlocking of the adhesive into irregularities present on the substrate surface will be small compared to the effects from intermolecular secondary forces (i.e. Van der Waals) between the atoms and molecules in the surfaces of the adhesive and substrate. Consequently, adsorption theory will dominate the adhesive bonding at the underfill / copper interface.

Provided adsorption theory governs adhesion and only secondary forces are acting across an interface, the stability of an adhesive / substrate interface in the presence of moisture can be ascertained from thermodynamic arguments. The thermodynamic work of adhesion, W_A, in an inert medium is given by (Kinloch, 1987):

$$W_A = \gamma_a + \gamma_s - \gamma_{as} \tag{6.12}$$

where γ_a is the surface free energy of the adhesive, γ_s is the surface free energy of the substrate, and γ_{as} is the interfacial free energy. In the presence of a liquid, the thermodynamic work of adhesion, W_{Al}, is given by:

$$W_{Al} = \gamma_{al} + \gamma_{sl} - \gamma_{as} \tag{6.13}$$

where γ_{al} and γ_{sl} are the interfacial free energies between the adhesive / liquid and substrate / liquid interfaces, respectively. Typically the thermodynamic work of adhesion of an adhesive / substrate interface in an inert medium, W_A, is positive, which indicates the amount of energy required to separate a unit area of the interface. However, the thermodynamic work of adhesion in the presence of a liquid, W_{Al}, can be negative, which indicates the interface is unstable and will separate when it comes in contact with the liquid. Thus, the calculation of W_A and W_{Al} can indicate the environmental stability of the adhesive / substrate interface. Kinloch (1987) has shown that W_A and W_{Al} may be calculated from the following expressions:

$$W_A = 2\sqrt{\gamma_a^D \gamma_s^D} + 2\sqrt{\gamma_a^P \gamma_s^P} \tag{6.14}$$

$$W_{Al} = 2(\gamma_{lv} - \sqrt{\gamma_a^D \gamma_{lv}^D} - \sqrt{\gamma_a^P \gamma_{lv}^P} - \sqrt{\gamma_s^D \gamma_{lv}^D} - \sqrt{\gamma_s^P \gamma_{lv}^P} + \sqrt{\gamma_a^D \gamma_s^D} + \sqrt{\gamma_a^P \gamma_s^P}) \tag{6.15}$$

where γ^D is the dispersion component of surface free energy, γ^P is the polar component of surface free energy, and γ_{lv} is the surface free energy of the liquid. Table 46 gives the polar and dispersion surface free energies of epoxy, copper, and water:

Table 46. Polar and dispersion surface free energies of epoxy, copper, and water (Kinloch, 1987)

Substance	γ (mJ/m^2)	γ^D (mJ/m^2)	γ^P (mJ/m^2)
Epoxy	46.2	41.2	5.0
Copper	1360	60	1300
Water	72.2	22.0	50.2

Using the values given in Table 46 and substituting into Equation (6.14), the thermodynamic work of adhesion of the epoxy / copper interface is 260.7 mJ/m^2. If water is present at the epoxy / copper interface, the thermodynamic work of adhesion given by Equation (6.15) is -270.4 mJ/m^2. Therefore, since the work of adhesion is positive before exposure to moisture and negative after exposure, all adhesion of the epoxy / copper interface is lost if water comes in contact with the interface.

Using adsorption theory as the physical basis for the loss in adhesion from moisture, expressions are now developed depicting the amount of moisture delivered to the underfill / copper interface. Since the interfacial fracture test specimens were designed to prevent wicking of moisture at the interface and the copper substrate provides a barrier for moisture transport, the moisture transport to the interface is governed by the epoxy network of the underfill. Soles and Yee (2000) have shown that water traverses within the epoxy through the network of nanopores inherent in the epoxy structure, with typical nanopores ranging from 5.0 to 6.1 $\AA$ in diameter. Figure 76 illustrates the transport of moisture through the bulk epoxy of a fracture test specimen.

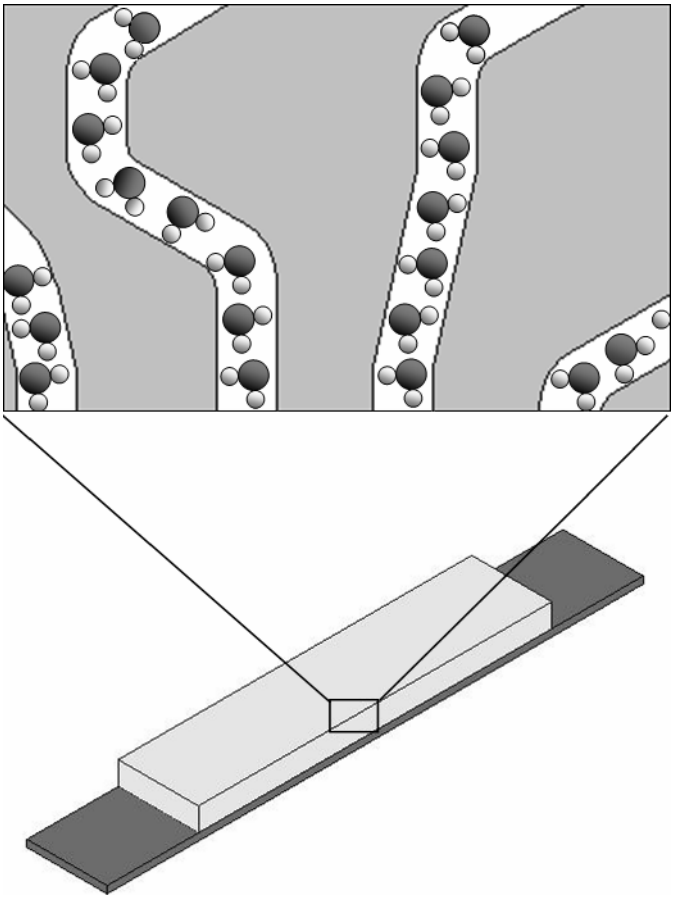

Figure 76. Moisture transport through the bulk epoxy of a fracture test specimen

Assuming that the nanopore channels are the only mechanism by which moisture can be delivered to the interface, the saturation concentration in the epoxy expressed in mg H_2O / mm^3 is given by:

$$C_{sat} = \frac{\rho_{H_2O}(N_N V_N)}{V_{tot}} \tag{6.16}$$

where ρ_{H2O} is the density of water, N_N is the number of nanopores actively participating within the epoxy network, V_N is the volume occupied by a single nanopore in the epoxy network, and V_{tot} is the total volume of the epoxy. After rearrangement of Equation (6.16), the number of nanopores actively participating within an epoxy system for a given saturation concentration is as follows:

$$N_N = \frac{4A_{tot}C_{sat}}{\pi\rho_{H_2O}D_N^2} \tag{6.17}$$

where A_{tot} is the total area of the interface and D_N is the nanopore diameter. Assuming adsorption theory holds, the adhesive bond area, A_{bond}, that remains intact after exposure to moisture will depend on the area occupied by the moisture at the interface, A_{H2O}:

$$A_{bond} = A_{tot} - A_{H_2O} \tag{6.18}$$

Relating this adhesive bond area to the number of nanopores actively participating in transport yields:

$$A_{bond} = A_{tot} - \pi N_N r_{debond}^2 \tag{6.19}$$

where r_{debond} represents the debond radius of moisture at the interface that occurs at each nanopore. The debond radius must be greater or equal to the nanopore radius and is

governed by the interfacial hydrophobicity of the adhesive / substrate interface. Figure 77 provides a graphical depiction of the parameter, r_{debond}, at the interface.

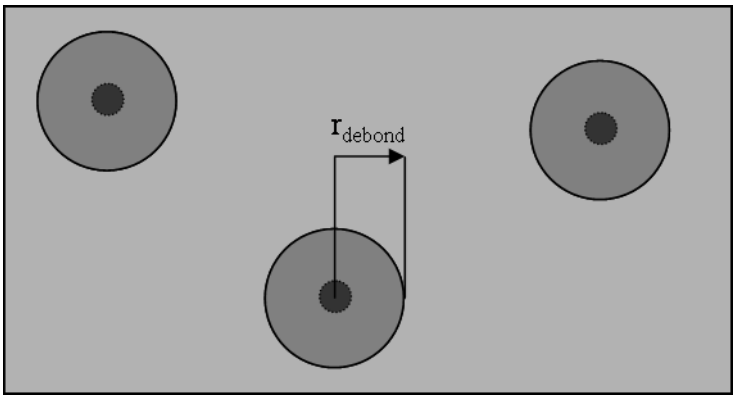

Figure 77. Graphical illustration of the parameter, r_{debond}, at the interface

Substituting Equation (6.17) into (6.19) provides an expression for the adhesive bond area that remains intact after exposure to a particular moisture saturation concentration:

$$A_{bond} = A_{tot} - \frac{4A_{tot}C_{sat}r_{debond}^2}{\rho_{H_2O}D_N^2} \tag{6.20}$$

We now want to employ a fracture mechanics development to relate the change in bond area due to the presence of moisture at the interface. Recall from fracture mechanics the general form of the stress intensity factor:

$$K = So\sqrt{\pi a} \tag{6.21}$$

where S is a dimensionless constant that depends on the geometry and mode of loading, σ is the remotely applied stress, an a is the crack length. The stress intensity factor is related to the fracture toughness, G_c, by the following expression:

$$G_c = Z\sigma^2 \tag{6.22}$$

where

$$Z = \frac{\pi a S^2 (1-\upsilon^2)}{E}$$

Based on thermodynamic work of adhesion for the epoxy / copper interface, the interface will become unstable and debond in the presence of moisture; however, since interfacial fracture toughness is a material property that characterizes the adhesion of the interface, the toughness must be the same in all areas that remain bonded after exposure to moisture. Using mode I loading and making the following three assumptions: 1.) Adsorption theory dominates the interfacial bonding; 2.) The change in the mechanical properties of both the adhesive and substrate from moisture is small relative to the change in bond area from moisture, and 3.) The relative change in fracture toughness from moisture remains constant irrespective to the means of measuring the toughness for a given moisture saturation concentration; An expression is obtained relating the change in bond area due to the presence of moisture to the change in the critical load of fracture:

$$\frac{P_{wet}}{A_{tot} - \pi N_N r_{debond}^2} = \frac{P_{dry}}{A_{tot}} \tag{6.23}$$

Rearranging Equation (6.23) to obtain an expression for P_{wet} and substituting that value into Equation (6.22) for the wet, saturated case yields the following expresson:

$$G_{c,wet} = \left(1 - \frac{\pi N_N r_{debond}^2}{A_{tot}}\right)^2 G_{c,dry} \tag{6.24}$$

As the saturation moisture concentration increases, so will the number of active nanopores participating. The incremental change in fracture toughness due to the participation of a single additional nanopore, $N_N + 1$, is given by:

$$G_{c,wet} = \left(1 - \frac{\pi (N_N + 1) r_{debond}^2}{A_{tot}}\right)^2 G_{c,dry} \tag{6.25}$$

For convenience, define f such that for N_N nanopores participating:

$$f_{N_N} = \frac{\pi N_N r_{debond}^2}{A_{tot}} \tag{6.26}$$

For N_N+1 nanopores participating:

$$f_{N_N+1} = \frac{\pi r_{debond}^2}{A_{tot}}(N_N + 1) \tag{6.27}$$

Restating Equations (6.24) and (6.25) in terms of f:

$$G_{c,wet}(f_{N_N}) = \left(1 - \frac{\pi N_N r_{debond}^2}{A_{tot}}\right)^2 G_{c,dry} \tag{6.28}$$

$$G_{c,wet}(f_{N_N+1}) = \left(1 - \frac{\pi r_{debond}^2}{A_{tot}}\right)^2 G_{c,wet}(f_{N_N}) \tag{6.29}$$

Subtracting (6.28) from (6.29) and dividing by $f_{N+1} - f_N$ gives:

$$\frac{G_{c,wet}(f_{N_N+1}) - G_{c,wet}(f_{N_N})}{f_{N_N+1} - f_{N_N}} = \frac{\left[1 - \frac{\pi r_{debond}^2}{A_{tot}}\right]^2 G_{c,wet}(f_{N_N}) - G_{c,wet}(f_{N_N})}{f_{N_N+1} - f_{N_N}} \tag{6.30}$$

Utilizing a Taylor series expansion of f_N with first order accuracy and substituting Equations (6.26) and (6.27) into (6.30) yields:

$$\frac{dG_{c,wet}(f_{N_N})}{df_{N_N}} = \frac{\left[1 - \frac{\pi r_{debond}^2}{A_{tot}}\right]^2 G_{c,wet}(f_{N_N}) - G_{c,wet}(f_{N_N})}{\frac{\pi r_{debond}^2}{A_{tot}}} \tag{6.31}$$

Simplification and elimination of higher order terms gives the following differential equation characterizing the loss in interfacial fracture toughness due to moisture:

$$\frac{dG_{c,wet}(f_{N_N})}{df_{N_N}} = -2G_{c,wet}(f_{N_N}) \tag{6.32}$$

subject to the boundary condition:

$$G_{c,wet}(f_{N_N} = 0) = G_{c,dry} \tag{6.33}$$

Solution of Equation (6.32) and substitution of Equation (6.26) gives:

$$G_{c,wet} = G_{c,dry} \exp\left[\frac{-8C_{sat}r_{debond}^2}{\rho_{H_2O}D_N^2}\right] \tag{6.34}$$

Equation (6.34) characterizes the loss in interfacial fracture toughness from moisture in terms of key parameters relevant to moisture. Using the value for the density of water at room temperature (0.99823 mg / mm^3), an average nanopore diameter of 5.5 *Å*, and the moisture saturation concentration determined from the experimental portion of this study in conjunction with Equations (6.17) and (6.34), the number of active nanopores participating, N_N, and value of r_{debond} can be determined by the intrinsic

response of each material system to each level of moisture preconditioning. The results are shown in Table 47.

Table 47. Key parameters relevant to moisture for the underfill / copper and solder mask / copper interfaces

Environment	Substrate	Adhesive	Csat (mg H_2O / mm^3)	N_N	r_{debond} (mm)
85C/50%RH	Copper	Underfill	0.0075	1.006E+13	1.640E-06
85C/65%RH	Copper	Underfill	0.0089	1.194E+13	1.692E-06
85C/85%RH	Copper	Underfill	0.0118	1.583E+13	1.669E-06

Environment	Substrate	Adhesive	Csat (mg H_2O / mm^3)	N_N	r_{debond} (mm)
85C/50%RH	Copper	Solder Mask	0.0075	7.779E+12	1.707E-06
85C/65%RH	Copper	Solder Mask	0.0089	9.232E+12	1.720E-06
85C/85%RH	Copper	Solder Mask	0.0118	1.224E+13	1.750E-06

As shown in Table 47, the number of nanopores participating increases with saturation concentration. This is expected since an increase in saturation concentration would increase the available moisture for transport through the nanopores. In addition, the values for r_{debond} were similar for each moisture preconditioning environment for both respective interfaces, which is also expected since X-ray Photoelectron Spectroscopy and water contact angle results did not indicate a change in the interfacial hydrophobicity of the copper surface from moisture preconditioning. The slight variation in the values for r_{debond} could in part be attributed to experimental scatter. Since the results were similar, they were averaged to obtain a representative value for r_{debond} in the presence of moisture

for each interface. Note that since the FR-4 board was received from a commercial manufacturer and surface processing of the copper in the board is proprietary, it is assumed that the behavior of the solder mask / copper interfacial hydrophobicity would not change significantly from moisture preconditioning.

Using the moisture parameters identified for each interfacial material system, Equation (6.34) was used to predict the interfacial fracture toughness of both the underfill / copper and solder mask / copper interfaces as a function of increasing saturation concentration. The results are shown in Figures 78 and 79.

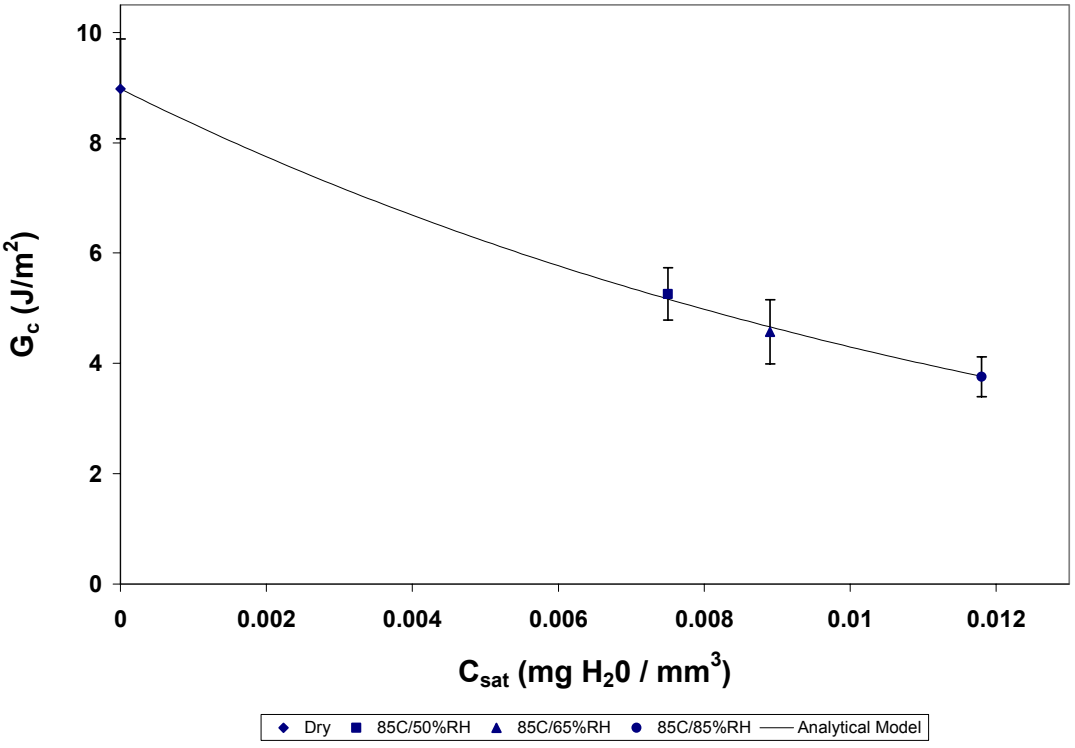

Figure 78. Analytical prediction of the loss in interfacial fracture toughness from moisture for the underfill / copper interface

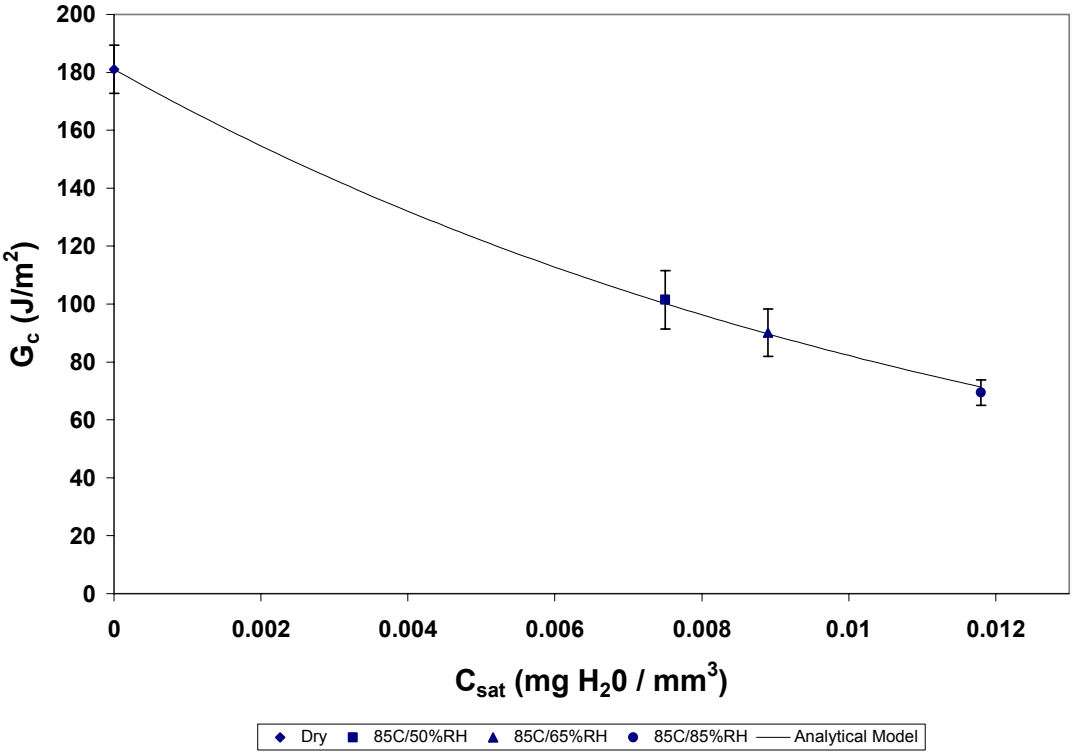

Figure 79. Analytical prediction of the loss in interfacial fracture toughness from moisture for the solder mask / copper interface

As shown in Figures 78 and 79, Equation (6.34) accurately predicted the loss in interfacial fracture toughness as a function of increasing moisture concentration. Since Equation (6.34) was based on the physics of adsorption theory, it will yield a loss in interfacial fracture toughness provided there is moisture at the interface, no matter how small the concentration. This contradicts the results of previous studies, who have reported a critical concentration of water may exist below which there is no measurable loss in adhesion (Comyn, *et al*., 1994; Gledhill, *et al*., 1980; and Kinloch, 1979). Based on the results of adsorption theory, it does not appear possible that a critical concentration

of water could exist in theory. It is possible in those studies that other mechanisms for adhesion in addition to adsorption theory governed the adhesion at the interface, which could explain why a critical concentration of water was observed. An additional consideration is the method to testing to obtain adhesion results. The aforementioned studies used lap shear test specimens to determine the interfacial strength after moisture preconditioning. Due to lacking a precrack at the interface and the applied load being distributed over the entire bonding area, these test specimens are not as sensitive to interfacial failure; consequently, possibly also explaining in part why a critical concentration of water appeared to exist for low concentrations of moisture. Conversely, interfacial fracture toughness test specimens are designed for interfacial failure through the use of a precrack at the interface, making them more sensitive to environmental attacks at the interface. The work of Wylde and Spelt (1998) supports this observation. Using interfacial fracture toughness test specimens with a similar material system previously reported to exhibit a critical concentration of water from lap shear results, they found a decrease in the interfacial toughness from moisture for all concentrations of moisture, including those lower than the previously reported critical concentration of water. Consequently, provided adsorption theory dominates the adhesive bonding at the adhesive / substrate interface and the assumptions in the development of the model as satisfied, Equation (6.34) should accurately predict the loss in interfacial fracture toughness for a given moisture concentration.

6.4 Conclusions

Interfacial fracture mechanics was used to characterize the intrinsic effect of moisture on adhesion. Both underfill / copper and underfill / FR-4 board bilayer test specimens with prefabricated interface cracks were used in a four-point bend test at room temperature to measure the critical load of fracture for the interface as a function of increasing moisture concentration. All interfacial fracture tests were quasi-static and viscoelastic effects were assumed negligible. Test specimens were divided into five test groups and subjected to four different levels of moisture preconditioning. The test groups included fully dry, 85^{o}C only, 85^{o}C/50%RH, 85^{o}C/65%RH, and 85C^{o}/85%RH, with the latter four test groups being exposed for a duration of 168 hours. The fully dry test group was used as a control to establish the baseline interfacial fracture toughness of the test specimens. The 85^{o}C only test group established the effect of thermal aging from the 85^{o}C temperature component of the moisture preconditioning environments on interfacial fracture toughness, while the moisture preconditioned test groups establish the effect of increasing moisture content on the interfacial fracture toughness.

Based on the results from the moisture absorption analysis, a water-proof perimeter was applied to the interfacial fracture test specimens during moisture preconditioning and removed before fracture testing. This perimeter served two purposes. First, the application of the perimeter forced 1-D diffusion through the top, open surface of the underfill, yielding uniform concentrations of moisture spatially across the entire interface for the full duration of exposure to the humid preconditioning

environment. Second, the water-proof perimeter prevented moisture wicking at the interface, which allowed identification of the test specimen moisture concentration by utilizing the inherent moisture absorption characteristics of the adhesive.

Using the experimentally measured value for the critical load of fracture in conjunction with previously identified elastic modulus results, the interfacial fracture toughness of the underfill / copper and underfill / FR-4 board test specimens was determined for a particular level of moisture preconditioning. Although the underfill / copper test specimens experienced interfacial failure at the location of the interfacial precrack, the underfill / FR-4 board test specimens did not. Symmetric precracks were introduced into the underfill / FR-4 test specimens at the underfill / solder mask interface; however, the vast majority of interfacial failures occurred at the solder mask / copper interface. This is attributed to the strong covalent bonding present at the underfill / solder mask interface compared to the weaker secondary bonding of the solder mask / copper interface. It is clear from the order of magnitude difference in the interfacial toughness of the underfill / copper interface to the solder mask / copper interface that the copper surface in the FR-4 was modified to enhance adhesion; however, since the FR-4 board was received from a commercial manufacturer, the surface preparation of the copper prior to the application of the solder mask is proprietary and unknown. Although this preparation is unknown, both the underfill / copper and solder mask / copper interfaces are similar in that they represent failures at a polymer / metal interface. Thermal aging at 85^{o}C did not significantly affect the interfacial fracture toughness of either interface, while moisture preconditioning at 85^{o}C/50%RH, 85^{o}C/65%RH, and 85^{o}C/85%RH had a

substantial effect on the interfacial fracture toughness and yielded decreases of 41.4%, 49.1%, and 58.1% for the underfill / copper interface and 44.0%, 50.2%, and 61.6% for the solder mask / copper interface. Since all moisture preconditioned test groups were exposed to the same temperature component of 85^{o}C and duration of 168 hours, any observed changes in the fracture toughness after moisture preconditioning can be attributed to the contribution of moisture.

The interfacial fracture toughness results were correlated with the test specimen moisture concentration level at the time of testing to depict the intrinsic change in toughness as a function of moisture content. Results show that the underfill / copper and solder mask / copper interfaces were very sensitive to relatively small concentrations of moisture. A significant reduction in interfacial adhesion was observed for concentrations as low as 0.65 wt%. Since the moisture did not significantly change the elastic modulus of the underfill adhesive for the moisture conditions evaluated for the interfacial fracture toughness, plasticization of the underfill from moisture contributed little to the change in the interfacial fracture toughness. As a result, the reduction in the toughness is primarily attributed to the weakening of the underfill / copper and solder mask / copper interfaces due to the direct presence of moisture at the interface.

To investigate the effect of hygro-swelling on interfacial fracture test results, the moisture swelling coefficient, β, of the underfill was experimentally determined for each moisture preconditioning environment. The measured value of the moisture swelling coefficient was used in conjunction with values of the coefficient of thermal expansion to determine the hygro-swelling and thermal mismatch strains at the interface for each

environmental preconditioned test group. Results show that the thermal mismatch strains were significantly greater than the hygro-swelling mismatch strains for both interfaces and for all moisture preconditioning environments by roughly an order of magnitude. It is clear that the thermal mismatch strain dominated the interaction at the interface and was only slightly offset by a small contribution from the hygro-swelling mismatch strain. As a result, the underfill will be in tension during interfacial fracture testing, effectively preloading the interface and requiring a lower critical load of fracture, P_c, from mechanical testing to advance the interface crack. Consequently, interfacial fracture toughness values will represent a conservative estimate of the interfacial fracture toughness of the interface. In addition, it is clear that increasing the saturation concentration did not significantly increase the hygro-swelling mismatch strain. Therefore, all interfaces for all environments experienced similar hygro-swelling mismatch strains for the materials and moisture preconditioning environments tested in this study. Consequently, the trends exhibited in the interfacial fracture toughness as moisture concentration increases are essentially independent of the hygro-swelling mismatch relative to one another, and the observed changes between the different moisture preconditioning environments can be predominately attributed to more moisture being present at the interface resulting in a greater loss of adhesion.

Scanning Electron Microscopy was used to examine if a change in the fracture failure locus occurred after moisture preconditioning. There was no observable change in the failure locus after moisture preconditioning. The failure mode remained virtually purely interfacial for all environments, with only very slight evidence of occasional

interphase failure as evident by the occasional presence of adhesive on the substrate failure surface. The very slight distribution of localized interphase failure on the substrate failure surfaces was common to all moisture preconditioning environments, with no observable change in the amount of adhesive distribution on the failure surface before and after moisture preconditioning. Consequently, moisture preconditioning did not appear to change the failure locus for the test specimens evaluated in this study.

X-ray Photoelectron Spectroscopy (XPS) and water contact angle measurements were used to examine the effect of the growth of oxides on the copper surface after adhesive bonding. XPS illustrates the presence of cupric oxide not only in the 85^{o}C/50%RH and 85^{o}C/85%RH test groups, but also in the 85^{o}C only thermal aging test group. Consequently, identical oxide chemical formations existed at the interface for all environmentally preconditioned test groups. In addition, similar atomic percentages of cupric oxide were obtained when comparing thermal aging at 85^{o}C to the moisture preconditioning environments of 85^{o}C/50%RH and 85^{o}C/85%RH, indicating that the moisture component had a minimal contribution to oxidation growth rates compared to the available oxygen in the air common to all environmental preconditioned environments. Consequently, a similar level of oxidation thickness existed on all environmentally preconditioned test specimens. This is supported by water contact angle measurements, where similar water contact angle measurements were obtained for all environmental preconditioned copper substrates, indicating a similar level of interfacial hydrophobicity for all test groups. Since the water contact angle on copper is significantly affected by oxidation and the oxide layer thickness, the contact angle results

would suggest that a comparable oxidation layer thickness existed in all environmentally preconditioned test groups. Consequently, the effect of the oxide growth on interfacial fracture toughness can be ascertained by comparing the 85°C thermal aging test results to the control test results. The thermal aging at 85°C produced little to no effect on interfacial fracture toughness results, thus oxidation growth displacing the underfill after adhesive bonding had an insignificant effect on the adhesion loss compared to the effect of moisture from moisture preconditioning.

An analytical model was developed based on adsorption theory and using fracture mechanics to predict the loss in interfacial toughness as a function of moisture content. The model was based on the assumptions that transport through the bulk adhesive is the only mechanism by which moisture is delivered to the interface and occurs through the inherent nanopores present in the epoxy network, secondary bonding is the dominant bonding mechanism at the interface, the change in the mechanical properties of both the adhesive and substrate from moisture is small relative to the change in bond area from moisture, the relative change in toughness from moisture is independent of the fracture test method and loading configuration used, and that the interface will become unstable and debond once moisture reaches the interface. The model characterizes the loss in interfacial fracture toughness from moisture in terms of key parameters relevant to moisture identified from the experimental portion of this research, including the interfacial hydrophobicity, active nanopore density, saturation concentration, and the density of water. When compared to experimental data, the model accurately predicted the loss in interfacial fracture toughness as a function of increasing moisture

concentration. Provided adsorption theory dominates the adhesive bonding at the adhesive / substrate interface and the assumptions of the model are satisfied, the model should accurately predict the loss in interfacial fracture toughness for a given moisture concentration.

CHAPTER VII

RECOVERY FROM MOISTURE UPTAKE UPON FULLY DRYING

Exposure to moisture can permanently alter the mechanical characteristics and interfacial adhesion of a bimaterial interface. Absorbed moisture in either the adhesive or substrate can yield both reversible and irreversible components of damage, which can compromise the interfacial adhesion of the bimaterial system even upon fully redrying if a significant component of irreversible damage develops. Consequently, the recovery of the bimaterial system from moisture should be determined to fully characterize the extent and type of damage. Two aspects of recovery are considered. The first is the recovery of the elastic modulus of both the adhesive and substrate from moisture uptake followed by full redrying. The second is the recovery of the bimaterial interface from the addition and removal of moisture directly at the interface itself. The information obtained from the recovery of interfacial adhesion to moisture will provide further insight into moisture damage characteristics and physical mechanisms responsible for damage.

7.1 Introduction

Of particular interest to the long-term reliability of an adhesive bond is ascertaining the permanent damage of the bond from exposure to moisture. It has been shown that moisture will decrease interfacial adhesion; however, very few studies have examined the reversible and irreversible components of the loss in adhesion from moisture and subsequent drying. This has significant practical aspects, as the recoverability of the interface from moisture will identify the severity of the moisture damage. If the loss in adhesion from moisture is largely unrecoverable and irreversible, then the service life of the adhesive joint will be severely, permanently compromised as a result of exposure to moisture.

When evaluating the moisture recovery of an adhesive joint, there are two aspects to consider. The first is the recovery of the materials that constitute to adhesive joint, as absorbed moisture can alter the mechanical performance of those materials and indirectly affect adhesion. Few investigations have evaluated the recovery of adhesives upon drying after moisture absorption. Little information is available regarding the extent of the reversible and irreversible nature of moisture uptake in adhesives. Netravali, *et al*., (1985) have shown for epoxy samples soaked in water at 25^{o}C for 820 hours that much of the loss from moisture results from plasticization and is recoverable upon drying at 30^{o}C for 400 hours; however, samples soaked in water at 70^{o}C for 775 hours were highly irreversible after drying at 70^{o}C for 125 hours. The irreversibility was attributed to water reacting with unreacted epoxide groups. It should be noted that neither groups of

samples were completely dry at the time of testing after exposure to water and subsequent drying. Buehler and Seferis (2000) found epoxy prepegs soaked in water at 71^{o}C for 1200 hours exhibited varying degrees of reversible and irreversible damage to both the flexural modulus and flexural strength upon drying at 50^{o}C for 450 hours. However, more time was needed to fully dry the specimens in this study as well, with 3% weight concentrations of moisture still existing in the specimens at the time of testing after drying. Wright (1981) proposes that the permanent loss of properties that occur due to moisture uptake is most probably due to swelling of the matrix and the production of voids, while Xiao and Shanahan (1997) suggest based on absorption behavior that the irreversible damage component of hydrolysis can play a significant role in the degradation process depending on the duration of exposure. The second aspect to consider when addressing recovery is the recovery of the interface itself, as the direct presence of moisture at the interface can significantly alter adhesion. Butkus (1997) examined the permanent change in Mode I fracture toughness of Aluminum/FM73M/Aluminum and Aluminum/FM73M/Boron-Epoxy joints after 5,000 hours at 71^{o}C and > 90%RH followed by 5,000 hours of desiccation at 22^{o}C/10%RH prior to testing. Both the Al/FM73M/Al joints and the Al/FM73M/Boron-Epoxy joints recovered very little of their fracture toughness on subsequent drying, demonstrating large, permanent losses in toughness after exposure to moisture. Orman and Kerr (1971) have shown that although some of the strength lost in the epoxy-bonded aluminum joints studied was recovered, there was noticeable permanent damage from moisture suggesting an irreversible disruption at the interface as a result of attack by water. Contrary to this

claim, Shaw, *et al*., (1992) found that nearly all of the strength lost after immersing steel/epoxy lap shear joints in distilled water for three weeks was recovered after drying. They attributed the loss in strength after moisture preconditioning to plasticization of the epoxy adhesive, which is generally regarded as a reversible process. Dodiuk, *et al*., (1984) found exposure to moisture of their epoxy/aluminum joints caused a reduction in lap shear strength; however, if the moisture concentration was below 0.3%, the strength was fully recoverable after drying indicating a completely reversible process. The authors gave no explanation to this observed behavior other than to state that moisture concentrations exceeding 0.3% would result in an irreversible process. Undoubtedly the mechanisms responsible for the observed losses in both material behavior and interfacial adhesion from moisture uptake are complex, and the material constitutive damage behavior is not entirely understood.

To further investigate the reversible and irreversible nature of moisture on both material behavior and interfacial adhesion, recovery experiments are performed with moisture preconditioning followed by subsequent drying at 95^{o}C until fully dry. The results will determine the extent of the reversible and irreversible damage from moisture uptake on both the elastic modulus and interfacial fracture toughness, aiding to further characterize the physical mechanisms responsible for the losses in modulus and interfacial fracture toughness addressed in Chapters 5 and 6 respectively.

7.2 Experimental Procedure

7.2.1 Materials

The substrate used in this study was oxygen-free electronic grade copper, alloy 101. The adhesive used in this study was an epoxy based underfill developed for no-flow assembly, designated as UR-B in this research. These are the same materials used to evaluate the effect of moisture on both the elastic modulus and interfacial fracture toughness previously discussed in Chapters 5 and 6 respectively of this research. Since the copper is impermeable to moisture, only the underfill was considered for the effect of moisture uptake on the elastic modulus variation. Underfill/copper interfacial test specimens were used to study the recovery of interfacial fracture toughness from moisture being physically present at the interface and subsequently removed.

7.2.2 Flexural Bend Test

Flexural bend test specimens were tested in a three-point bend test according to ASTM D790 (1999) to determine the recovery of the underfill elastic modulus from moisture uptake. Specimen construction and test procedure is identical to that given in Section 5.2.2, Flexural Bend Test, of Chapter 5, Elastic Modulus Variation due to Moisture Absorption. Five tests were performed for each test group and the results averaged. Error measurements represent the standard deviation in the test results.

7.2.3 Interfacial Fracture Test

Underfill / copper interfacial fracture test specimens were tested in a four-point bend to determine the recovery of interfacial fracture toughness from moisture. Specimen construction and test procedure is identical to that given in Section 6.2.2, Interfacial Fracture Test, of Chapter 6, Effect of Moisture on Interfacial Fracture Toughness. Ten tests were performed for each test group and the results averaged. Error measurements represent the standard deviation in the test results.

7.2.4 Recovery

To evaluate the recoverability of the elastic modulus and interfacial fracture toughness from moisture uptake, recovery test specimens were divided into test groups for moisture preconditioning for 168 hours followed by baking at 95^{o}C until fully dry. The test groups for moisture preconditioning included 85^{o}C/50%RH, 85^{o}C/65%RH, 85^{o}C/85%RH, and 85^{o}C/95%RH, which represent the same conditions and duration used to evaluate the effect of moisture on the elastic modulus of the underfill and underfill/copper interfacial fracture toughness previously discussed in Chapters 5 and 6. After moisture preconditioning, the recovery test specimens were placed in a convection oven and baked at 95^{o}C until fully dry. A fully dried state was established when there was no measurable change in the weight of a specimen for a period of 24 hours. Since there was an insignificant amount of loss from moisture uptake in the underfill elastic modulus for 85^{o}C/50%RH and 85^{o}C/65%RH moisture preconditioning environments, only 85^{o}C/85%RH and 85^{o}C/95%RH environments were evaluated for recoverability of

the elastic modulus. In addition, since 85°C/95%RH moisture preconditioning was not considered for the change in interfacial fracture toughness of the underfill/copper interface from moisture, the recoverability of the fracture toughness from that level of moisture preconditioning was not evaluated. Table 48 shows the test groups used to evaluate recoverability.

Table 48. Recovery experimental test matrix

Test Group	Environment (168 hours of exposure)	Dry Bake	Flexural Bend Test	Interfacial Fracture Test
1	85C / 50%RH	95C	NO	YES
2	85C / 65%RH	95C	NO	YES
3	85C / 85%RH	95C	YES	YES
4	85C / 95%RH	95C	YES	NO

Once fully dry, flexural bend test and interfacial fracture tests were performed to determine the permanent effects from moisture uptake on both the elastic modulus and interfacial fracture toughness respectively. Recovery results can be compared to previously identified values for the elastic modulus and underfill/copper interfacial fracture toughness from both moisture saturated conditions and unaged, control group results to determine the extent of reversible and irreversible damage from moisture.

7.3 Discussion of Results

Two different aspects of recovery from moisture were considered. The first aspect is the recovery of the elastic modulus of the adhesive and substrate after drying from moisture preconditioning. This is important since a change in the elastic modulus in either the substrate or adhesive will affect interfacial fracture toughness results. Since the substrate is metallic and impermeable to moisture, only the change in the underfill elastic modulus was considered. The second aspect is the recovery of the interfacial fracture toughness from the direct presence of moisture being present and subsequently removed from the interface.

Elastic Modulus Recovery

To further characterize the response of the underfill from moisture uptake and identify the mechanisms responsible for the observed losses in the elastic modulus from moisture absorption, test specimens were moisture preconditioned followed by baking at 95^{o}C until fully dry. Since 85^{o}C/85%RH and 85^{o}C/95%RH moisture preconditioning conditions were found to noticeably decrease the elastic modulus of the underfill (shown in Figure 48), only those conditions were evaluated for recovery of the elastic modulus from moisture uptake upon redrying. Tables 49 and 50 give the recovery results for the elastic modulus.

Table 49. Elastic modulus recovery data for underfill test specimens after 85°C/85%RH moisture preconditioning for 168 hours followed by full drying

Flexural Test Specimen	Preconditioning	Csat (wt%)	$E_{recovery}$ (GPa)
46	85C / 85%RH	0.65	2.44
47	85C / 85%RH	0.65	2.58
48	85C / 85%RH	0.65	2.43
49	85C / 85%RH	0.65	2.49
50	85C / 85%RH	0.65	2.38
		AVERAGE:	**2.46**
		STANDARD DEVIATION:	**0.08**

Table 50. Elastic modulus recovery data for underfill test specimens after 85°C/95%RH moisture preconditioning for 168 hours followed by full drying

Flexural Test Specimen	Preconditioning	Csat (wt%)	$E_{recovery}$ (GPa)
51	85C / 95%RH	0.77	2.42
52	85C / 95%RH	0.77	2.33
53	85C / 95%RH	0.77	2.44
54	85C / 95%RH	0.77	2.39
55	85C / 95%RH	0.77	2.44
		AVERAGE:	**2.40**
		STANDARD DEVIATION:	**0.05**

Figure 78 provides a graphical depiction of the recovery results for the underfill elastic modulus.

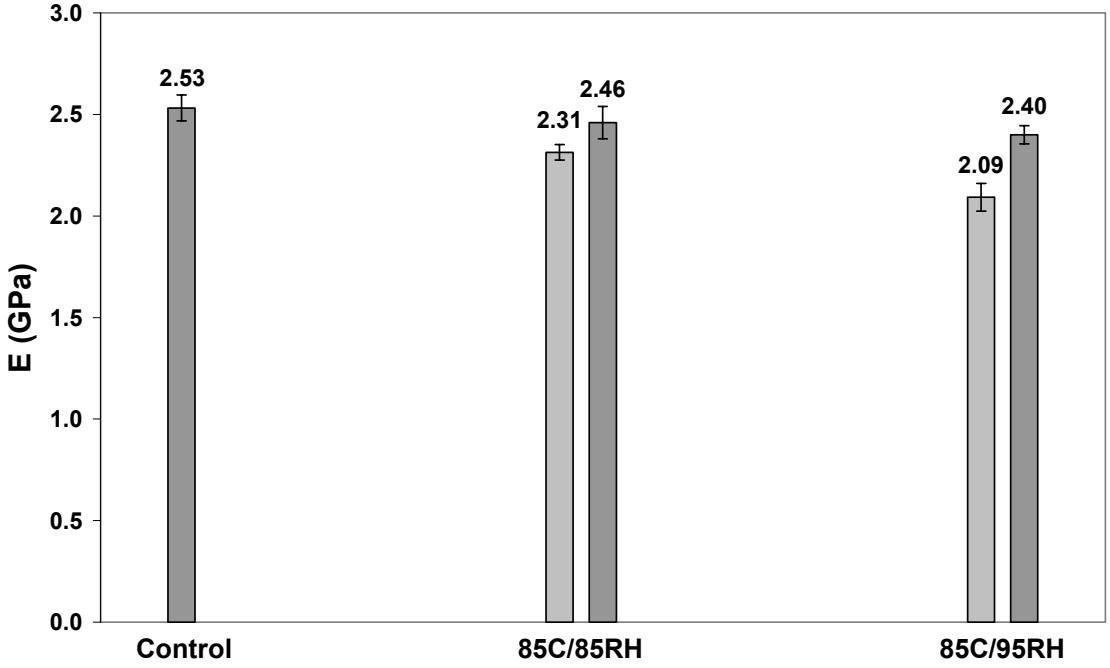

Figure 80. Recovery of underfill elastic modulus on removal of moisture

As shown in Figure 78, a large portion of the observed loss in the elastic modulus from moisture uptake was recoverable upon subsequent drying. Since plasticization is the only primary degradation mechanism attributed to moisture that is regarded as a reversible process, the recovery results show that the majority of the loss in modulus resulted from plasticization of the underfill from moisture uptake. To further evaluate the change in elastic modulus from moisture uptake, the recoverability for the elastic modulus will be defined as follows:

$$Recoverability\,(\%) = \frac{E_{recovery} - E_{sat}}{E_{dry} - E_{sat}} \cdot 100 \qquad (7.1)$$

where $E_{recovery}$ is value of the elastic modulus upon fully drying from the moisture saturated state, E_{sat} is the saturated value of the elastic modulus after moisture absorption, and E_{dry} is the unaged, control value of the elastic modulus. The recoverability of the elastic modulus is given in Table 51.

Table 51. Recoverability of underfill elastic modulus from moisture uptake after subsequent drying

T (°C)	RH (%)	C_{sat} (wt%)	E_{sat} (GPa)	$E_{recovery}$ (GPa)	Recoverability (%)
Control	--	0.00	2.53 ± 0.06	--	--
85	50	0.65	2.49 ± 0.05	--	--
85	65	0.77	2.45 ± 0.04	--	--
85	85	1.02	2.31 ± 0.04	2.46 ± 0.08	68.2
85	95	1.19	2.09 ± 0.07	2.40 ± 0.05	70.5

Although a significant portion of the elastic modulus was recoverable after fully drying, some irreversible, permanent damage did occur. The average recoverable value of the elastic modulus suggests slightly more irreversible damage occurred at higher humidity levels, but it cannot be concluded unequivocally solely based on the modulus results due to the uncertainty associated within the two measurements. However, it can be concluded when considering the results from moisture uptake data. After fully drying, there was a slight net permanent weight increase in the test specimens, with specimens moisture preconditioned at 85°C/85%RH retaining 1.3 ± 0.5% of the total absorbed water while specimens moisture preconditioned at 85°C/95%RH retaining 2.3 ± 0.4% of the

total absorbed water. The permanent weight increase in the test specimens after subsequent fully drying suggests that at least part of the irreversible damage resulted from hydrolysis with a greater extent occurring at higher humidity levels. In addition to hydrolysis, it is possible that moisture induced crazing also contributed to the irreversible damage to the elastic modulus. Overall, the irreversible damage was small with the majority of the loss in the elastic modulus from moisture uptake being fully recoverable after subsequent drying.

Interfacial Fracture Toughness Recovery

Having established the recovery behavior of the underfill elastic modulus from moisture absorption, the recovery of the underfill/copper interface from moisture exposure was evaluated. The underfill/copper interface was found to be very sensitive to moisture, with large decreases in interfacial fracture toughness occurring for moisture preconditioning environments of 85^{o}C/50%RH, 85^{o}C/65%RH, and 85^{o}C/85%RH as shown in Figure 56. To evaluate the recovery of the underfill/copper interface from moisture, test specimens were moisture preconditioned for each condition for 168 hours followed by baking at 95^{o}C until dry. Upon reaching a dry state, they were fracture tested to ascertain the interfacial fracture toughness. It should be noted that test specimens had reached a fully saturated state for each environment at the conclusion of the 168 hours moisture exposure time. Tables 52 - 54 give the recovery results for the interfacial fracture toughness.

Table 52. Interfacial fracture toughness recovery data for underfill/copper test specimens after 85°C/50%RH moisture preconditioning for 168 hours followed by full drying

Underfill Adhesive:
E = 2.51E+9 Pa
v = 0.37
G = 9.16E+8 Pa

Copper Substrate:
E = 1.15E+11 Pa
v = 0.31
G = 4.39E+10 Pa

Interfacial Parameters:
α = 0.955
β = 0.196
$\bar{E}_1$ = 1.27E+11 Pa
$\bar{E}_2$ = 2.91E+9 Pa
Ψ = -37.43°
L = 1.5 mm

Interfacial Test Specimen	Preconditioning	Csat (wt%)	$G_{c,\ recovery}$ (J/m^2)
61	85C / 50%RH	0.65	5.33
62	85C / 50%RH	0.65	5.94
63	85C / 50%RH	0.65	5.96
64	85C / 50%RH	0.65	4.97
65	85C / 50%RH	0.65	5.68
66	85C / 50%RH	0.65	5.07
67	85C / 50%RH	0.65	5.78
68	85C / 50%RH	0.65	4.95
69	85C / 50%RH	0.65	5.67
70	85C / 50%RH	0.65	5.83
		AVERAGE:	**5.52**
		STANDARD DEVIATION:	**0.38**

Table 53. Interfacial fracture toughness recovery data for underfill/copper test specimens after 85°C/65%RH moisture preconditioning for 168 hours followed by full drying

Underfill Adhesive:
E = 2.50E+9 Pa
v = 0.37
G = 9.12E+8 Pa

Copper Substrate:
E = 1.15E+11 Pa
v = 0.31
G = 4.39E+10 Pa

Interfacial Parameters:
α = 0.955
β = 0.196
$\bar{E}_1$ = 1.27E+11 Pa
$\bar{E}_2$ = 2.90E+9 Pa
Ψ = -37.44°
L = 1.5 mm

Interfacial Test Specimen	Preconditioning	Csat (wt%)	$G_{c,\ recovery}$ (J/m^2)
71	85C / 65%RH	0.77	5.00
72	85C / 65%RH	0.77	4.89
73	85C / 65%RH	0.77	5.54
74	85C / 65%RH	0.77	4.29
75	85C / 65%RH	0.77	5.63
76	85C / 65%RH	0.77	4.60
77	85C / 65%RH	0.77	4.27
78	85C / 65%RH	0.77	4.84
79	85C / 65%RH	0.77	4.22
80	85C / 65%RH	0.77	4.78
		AVERAGE:	**4.81**
		STANDARD DEVIATION:	**0.47**

Table 54. Interfacial fracture toughness recovery data for underfill/copper test specimens after 85°C/85%RH moisture preconditioning for 168 hours followed by full drying

Underfill Adhesive:
E = 2.46E+9 Pa
v = 0.37
G = 8.98E+8 Pa

Copper Substrate:
E = 1.15E+11 Pa
v = 0.31
G = 4.39E+10 Pa

Interfacial Parameters:
α = 0.956
β = 0.196
$\bar{E}_1$ = 1.27E+11 Pa
$\bar{E}_2$ = 2.85E+9 Pa
Ψ = -37.48°
L = 1.5 mm

Interfacial Test Specimen	Preconditioning	Csat (wt%)	$G_{c,\ recovery}$ (J/m^2)
81	85C / 85%RH	1.02	4.41
82	85C / 85%RH	1.02	3.62
83	85C / 85%RH	1.02	3.52
84	85C / 85%RH	1.02	3.13
85	85C / 85%RH	1.02	4.10
86	85C / 85%RH	1.02	4.54
87	85C / 85%RH	1.02	4.67
88	85C / 85%RH	1.02	3.40
89	85C / 85%RH	1.02	3.62
90	85C / 85%RH	1.02	3.78
		AVERAGE:	**3.88**
		STANDARD DEVIATION:	**0.50**

The entire range of mode mixity for all interfacial test specimens fell between -37.43^{o} to -37.48^{o}. Since the variation in mode mixity was negligible, the effect of this variation affecting interfacial fracture toughness results between different test groups is insignificant. Consequently, interfacial fracture toughness results for different moisture preconditioned test groups can be compared to one another to ascertain the effect of increasing moisture content on toughness values. Figure 79 provides a graphical depiction of the effect of environmental preconditioning and recovery of the underfill / copper interfacial fracture toughness.

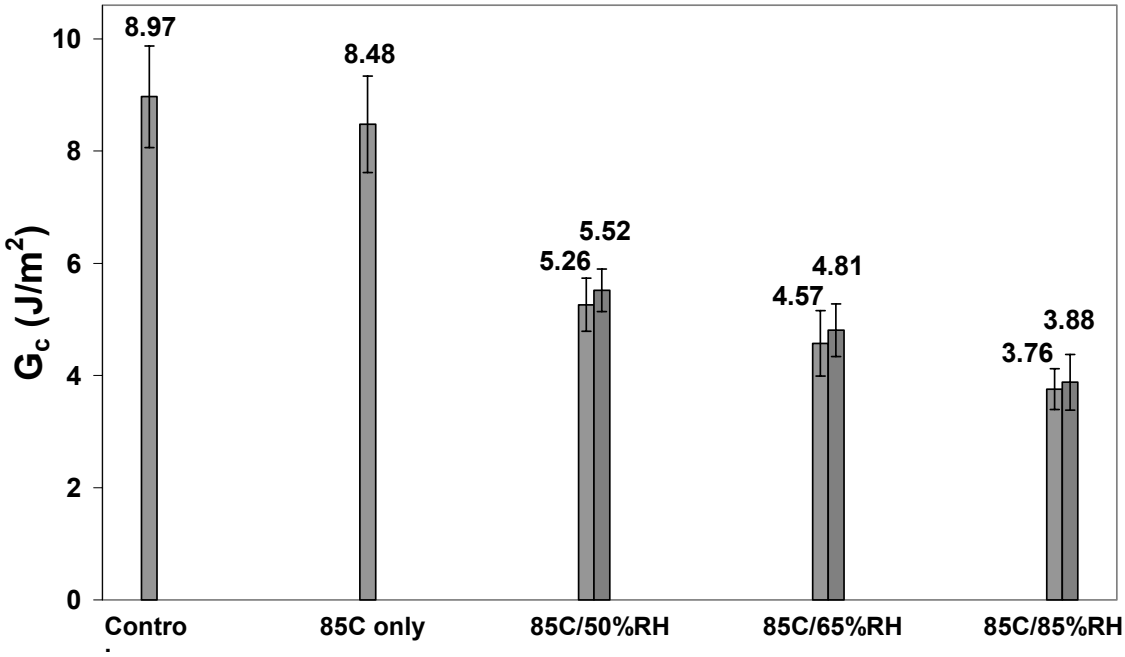

Figure 81. Recovery of underfill/copper interfacial fracture toughness on removal of moisture

As shown in Figure 79, most of the loss in interfacial fracture toughness from moisture was not recovered upon fully drying. Since the small change in the underfill elastic modulus from moisture was recoverable upon fully drying, the permanent reduction in the toughness of the underfill / copper interface is attributed to the direct presence of moisture at the interface debonding the underfill adhesive to the copper substrate. Similar in form to the recoverability of the elastic modulus given by Equation (7.1), the recoverability for the interfacial fracture toughness will be defined as follows:

$$Recoverability\,(\%) = \frac{G_{c,recovery} - G_{c,sat}}{G_{c,dry} - G_{c,sat}} \cdot 100 \qquad (7.2)$$

where $G_{c,recovery}$ is value of the interfacial fracture toughness upon fully drying from the moisture saturated state, $G_{c,sat}$ is the saturated value of the interfacial fracture toughness after moisture absorption, and $G_{c,dry}$ is the unaged, control value of the interfacial fracture toughness. Equation (7.2) only applies when the mode mixity of the interfacial fracture toughness before and after moisture preconditioning remains relatively unchanged, otherwise changes in the toughness due to a contribution from a change in the mode mixity will introduce error in the recoverability results. The recoverability of the underfill/copper interfacial fracture toughness is given in Table 51

Table 55. Recoverability of underfill/copper interfacial fracture toughness from moisture uptake after subsequent drying

T (°C)	RH (%)	C_{sat} (wt%)	$G_{c, sat}$ (J/m^2)	$G_{c, recovery}$ (J/m^2)	Recoverability (%)
Control	--	0.00	8.97 ± 0.91	--	--
85	50	0.65	5.26 ± 0.47	5.52 ± 0.38	7.0
85	65	0.77	4.57 ± 0.58	4.81 ± 0.47	5.5
85	85	1.02	3.76 ± 0.36	3.88 ± 0.50	2.3

As shown by Table 55, very little of the underfill/copper interfacial fracture toughness was recoverable after fully drying, with recoverability values for all moisture preconditioning environments less than 7%. This supports adsorption theory as the primary bonding mechanism for the underfill/copper interface. Through thermodynamic arguments, adsorption theory showed that the underfill/copper interface would debond in the presence of moisture. The slight evidence of small recovery in interfacial fracture toughness could in part be attributed to the contributions of other bonding mechanisms such as mechanical interlocking and diffusion theory; however, it is also plausible that there is no recovery at all relative to the deviation in error for all moisture preconditioned environments when comparing the saturated value for toughness to the recovered value. Since adsorption theory dominates the bonding between the underfill/copper interface and is the basis for the interfacial fracture toughness moisture degradation model detailed in Section 6.3.7, the recovery results support the accuracy of the model in predicting the interfacial fracture toughness for interfaces where adsorption theory is the primary interfacial bonding mechanism.

7.4 Conclusions

The recovery of both the underfill elastic modulus and underfill/copper interfacial fracture toughness from moisture exposure was examined. Test specimens were moisture preconditioned to saturation and subsequently dried to determine the recoverability from moisture of the elastic modulus and interfacial fracture toughness. By comparing the recovery results to previously identified unaged, control results and moisture saturated results, the reversible and irreversible effects from moisture uptake were ascertained.

Flexural bend test specimens were made to determine the mechanisms responsible for the loss in modulus of the underfill from moisture uptake and to evaluate the permanent changes after subsequent drying. Results demonstrate that majority of the loss in modulus from moisture absorption was fully recoverable upon returning to a fully dried state, indicating that plasticization of the underfill from moisture was responsible for most of the observed loss. However, there was a small amount of irreversible damage that did occur. Mass uptake data showed a slight, net permanent increase in weight of the test specimens after moisture preconditioning and fully drying, indicating that hydrolysis contributed to the irreversible damage with a greater extent occurring at higher humidity levels.

Interfacial fracture test specimens were made to evaluate the recovery of the underfill/copper interface from moisture. Results show that the vast majority of loss in toughness from moisture was unrecoverable with large permanent losses in interfacial adhesion occurring. The slight permanent change in the underfill elastic modulus from

irreversible moisture damage insignificantly affected the fracture toughness results; consequently, the loss in interfacial adhesion can be attributed to the presence of moisture directly at the underfill/copper interface. Since interfacial fracture toughness recovery results indicate little to no of the interfacial adhesion was maintained after the removal of moisture from the interface, the bonding at the interface was dominated by adsorption theory, which shows the underfill/copper interface will debond in the presence of moisture. This supports the previously developed interfacial fracture toughness moisture degradation model, which was based on adsorption theory. Consequently, the model should accurately predict the loss in toughness from moisture provided adsorption theory is the dominant bonding mechanism at the interface.

CHAPTER VIII

CONCLUSIONS AND RECOMMENDATIONS

A broad experimental and analytical study was performed to identify the critical factors and physical mechanisms that govern the loss in interfacial adhesion in the presence of moisture. Since the problem of moisture entails a multi-disciplinary study, several aspects were considered. From a global perspective, the primary aspects considered include moisture transport behavior, changes in bulk material properties from moisture absorption, effect of moisture on interfacial adhesion, and recovery from moisture upon fully drying, although several subsections within each major group were addressed due to the complexity of the problem. Based on the results obtained and corresponding analysis, several fundamental conclusions can be made that will help advance current understanding of moisture induced failures. Future work can build from this study to expand the knowledge of moisture degradation mechanisms to yield more robust adhesive structures not only in microelectronic packaging applications, but also in aerospace and structural applications.

8.1 Conclusions

The conclusions presented in this section are of fundamental significance only, with discussion regarding their relevant application and impact to adhesively bonded structures. These conclusions can be divided into three primary sections. The sections include moisture absorption kinetics, elastic modulus variation due to moisture absorption, and the effect of moisture on interfacial fracture toughness, with the latter two sections incorporating aspects of recovery from moisture uptake upon fully drying. Additional details regarding observations and analysis can be obtained by reviewing the conclusions provided at the end of each chapter.

The first consideration is moisture absorption kinetics, as the behavior of transport will govern the amount of moisture that arrives at the interface and corresponding change in interfacial adhesion. Two epoxy-based, no-flow underfills, designated UR-A and UR-B in this research, were examined for moisture transport behavior. Based on the results of the diffusion analysis, it was clear that very different behavior was exhibited by each underfill. Although UR-A absorbed more aggregate moisture than UR-B, the moisture diffused more easily through UR-B than UR-A. This behavior is attributed to the different chemistry in each underfill, where the presence of amine functional groups in UR-A retarded moisture transport, while the absence of amine function groups in UR-B yielded enhanced diffusion rates. A finite element model was developed to analytically and visually depict the moisture transport characteristics of UR-A and UR-B. The model shows that moisture will initially reach the interface for microelectronic assemblies that

use UR-B before comparably sized assemblies utilizing UR-A; however, due to the higher saturation concentration of UR-A, more moisture will arrive at the interface for UR-A assemblies if exposed to the moist environment for longer durations. This presents an interesting scenario for microelectronic applications when considered with interfacial fracture toughness results. Based on interfacial fracture toughness results, it was found that the critical aspect in the loss in interfacial adhesion is not the degradation of the adhesive from moisture uptake, but the amount of moisture that arrives at the interface for the adhesives and substrates evaluated in this study. With that in mind, depending on the service environment and duration of exposure to that environment, one underfill may yield significantly better interfacial adhesion than the other. For instance, if the microelectronic package is exposed to a moist environment for a long duration of time and assuming similar adhesion characteristics for both underfills, the non-amine containing resin UR-B would be a better choice in terms of reliability. This is a result of the lower saturation concentration of UR-B to UR-A; consequently, the total amount of moisture that arrives to the interface is limited by the inherent moisture saturation behavior of the underfill. Conversely, if the microelectronic package is going to be exposed to a moist environment for a short period of time and again assuming similar adhesion characteristics of both underfills, the amine containing resin UR-A would be a better choice for reliability. This is a result of the amine functional groups present in UR-A retarding moisture transport through the resin; consequently, it will take longer for moisture to reach the interface for assemblies using UR-A than comparably sized assemblies encapsulated with UR-B. Naturally both of these scenarios assume that the

only means for moisture transport to the interface is by bulk diffusion through the underfill, and caution should be implemented to insure moisture does not wick at the interface in addition to the bulk diffusion.

The second consideration when evaluating the problem of moisture is the effect of moisture on the bulk properties of the adhesive and substrate. Absorbed moisture can alter the mechanical characteristics of the adhesive and substrate, which can indirectly affect interfacial adhesion. A change in the elastic modulus can alter interfacial fracture toughness results considerably. Since the substrates evaluated in this research where metallic and impermeable to moisture, only the variation in the underfill elastic modulus due to moisture uptake was considered. The elastic modulus was measured for several different moisture preconditioning environments and subsequent saturation concentrations. It is important to note that specimens were fully saturated with moisture at the time of testing, thus a gradient of moisture did not exist within the specimens at the time of testing and the inherent, wet modulus was identified for each condition. In addition, thermal aging test results showed no change in the elastic modulus from the temperature component of the moisture preconditioning environment; consequently, all observed losses can be attributed to the presence of moisture. Results show a gradual decrease in the elastic modulus for concentrations < 1.02 wt% (0.0118 mg H_2O / mm^3) with a more noticeable decrease (17%) occurring at concentrations of 1.19 wt% (0.0138 mg H_2O / mm^3). Since the inherent wet modulus was identified for several different saturation concentrations, results depict the inherent change in elastic modulus of the underfill as a function of increasing moisture concentration, which can be used to model

the transient change in the underfill elastic modulus as moisture is absorbed. To evaluate the recovery of the underfill elastic modulus from moisture uptake, additional test specimens were allowed to reach saturation followed by baking in a convection oven until fully dry. The recovery results indicate that the majority of the loss in underfill elastic modulus was recovered upon fully drying, although some permanent loss did occur. Since plasticization from moisture is the only known reversible mechanism for the change in mechanical characteristics due to moisture uptake, the recovery results demonstrate that plasticization was the dominant mechanism responsible for the loss in the elastic modulus. The slight irreversible effect from moisture uptake can be attributed in part to hydrolysis, which was supported by a slight, net permanent weight gain in the underfill after fully drying. It should be noted that DSC results demonstrated that the underfill was fully cured before moisture preconditioning, so the contribution of incomplete curing in the underfill reacting with moisture is unlikely. Since moisture did not significantly alter the elastic modulus of the underfill and bearing in mind that the majority of change in the elastic modulus was recovered upon drying, the long term reliability of the underfill in microelectronic applications is not a primary concern when considering the effect of moisture. Since plasticization from moisture was found to be the dominant mechanism responsible for the change in the underfill modulus, variations in the underfill chemistry can be addressed to yield products that are intentionally more resistant to plasticization from moisture if known to be exposed to moist environments.

Having established the moisture absorption kinetics and change in properties of the adhesive and substrate from moisture, the final aspect considered is the effect of

moisture on interfacial adhesion. Underfill/copper and undefill/FR-4 board interfacial fracture toughness test specimens were made to evaluate this effect. By implementing several different moisture preconditioning environments and by using the critical load of fracture determined from the test specimens in conjunction with the moisture concentration and elastic modulus variation for each environment, the interfacial fracture toughness was determined as function of increasing moisture concentration. It is important to note that all tests were performed at room temperature and viscoelastic effects were assumed to be negligible. Failures occurred at the underfill/copper interface for the underfill/copper interfacial test specimens and at the solder mask/copper interface for the underfill/FR-4 board test specimens for all environments. Moisture preconditioning results demonstrate that both interfaces were very sensitive to moisture, with significant changes in interfacial toughness for concentrations as lows as 0.65 wt% (0.0089 mg H_2O / mm^3). Since there is both a temperature and moisture component to moisture preconditioning, thermal aging tests were performed to delineate the contributions from both on interfacial fracture results. The thermal aging test results showed no significant change in the toughness from the temperature component of the moisture preconditioning environment; consequently, all observed losses can be attributed to the presence of moisture. In addition, since the moisture did not significantly change the elastic modulus of the underfill adhesive for the moisture conditions evaluated for the interfacial fracture toughness, plasticization of the underfill from moisture contributed little to the change in the interfacial fracture toughness. As a result, the reduction in the toughness is primarily attributed to the weakening of the

interface due to the direct presence of moisture at the interface. This has a very significant implication for practical application, demonstrating that the critical aspect to consider when minimizing the loss in interfacial adhesion from moisture is preventing moisture from physically reaching the interface.

Using adsorption theory, the stability of an adhesive / substrate interface in the presence of moisture can be ascertained from thermodynamic arguments. The work of adhesion was determined to be positive before exposure to moisture and negative after exposure, indicating all adhesion of the epoxy / copper interface is lost if water comes in contact with the interface. This is supported by recovery results, which showed very little if any of the interfacial fracture toughness is recovered upon fully drying. Consequently, the results indicate that the adsorption theory of bonding is the dominant bonding mechanism for the epoxy / metal interfaces studied in this research. Using adsorption theory in conjunction with fracture mechanics, an analytical model was developed that predicts the loss in interfacial fracture toughness as a function of moisture content. The model was based on the assumptions that transport through the bulk adhesive is the only mechanism by which moisture is delivered to the interface and occurs through the inherent nanopores present in the epoxy network, secondary bonding is the dominant bonding mechanism at the interface, the change in the mechanical properties of both the adhesive and substrate from moisture is small relative to the change in bond area from moisture, the relative change in toughness from moisture is independent of the fracture test method and loading configuration used, and that the interface will become unstable and debond once moisture reaches the interface. The model incorporates key parameters

relevant to the problem of moisture in epoxy joints identified in this research, including the interfacial hydrophobicity, active nanopore density, saturation concentration, and the density of water. The model correlated well with experimental results, suggesting that if adsorption theory dominates the adhesive bonding at the adhesive / substrate interface and the assumptions of the model are satisfied, the model should accurately predict the loss in interfacial fracture toughness for a given moisture concentration. The predictive model provides a useful tool for developing new adhesives, innovative surface treatment methods, and effective protection methodologies for enhancing interfacial adhesion.

8.2 Recommendations and Future Work

A multi-disciplinary study was conducted to advance the understanding of the effect of moisture on the interfacial adhesion of microelectronic assemblies. Although materials were used that are common to microelectronic applications, the results of this study extend themselves to any component where maintaining the integrity of the adhesive joint is a critical consideration. Several fundamental mechanisms responsible for the change in adhesion from moisture uptake have been identified from this study; however, future contributions are needed to further advance the understanding of the role of moisture in the reliability of adhesive joints.

Moisture can affect interfacial adhesion through two primary mechanisms. The first mechanism is the direct presence of moisture at the interface altering the interfacial

integrity of the adhesive joint. The second mechanism is the absorbed moisture in either the adhesive and/or substrate altering the mechanical characteristics of those materials, which will indirectly affect the interfacial adhesion when an external load is applied to the structure. The change in the elastic modulus of the epoxy adhesive as a function of moisture content was evaluated in this study, and a trend was established based on several measurements of the inherent, wet modulus for different moisture concentration levels. It would be interesting to evaluate other materials and epoxy systems to observe if the same trend holds, which could lend itself to developing a model accounting for the universal change in the elastic modulus due to moisture uptake. In addition, the variation in other properties due to moisture uptake could be evaluated. One consideration would be to address the change in storage modulus from moisture obtained from dynamic tests. It would also be interesting to document the change in Poisson's ratio due to moisture uptake. In addition to dependence on the elastic modulus, interfacial fracture toughness expressions are dependent on Poisson's ratio. It is important to characterize the change in both when addressing the variation in interfacial fracture toughness due to a particular level of moisture content. Since the elastic modulus variation was small for the moisture preconditioning environments evaluated in the interfacial fracture toughness portion of this study, it was assumed that the variation in Poisson's ratio was negligible; however, it could be significant for other materials and moisture concentration levels.

Another area that could be further developed is addressing the role of interfacial hydrophobicity on interfacial fracture toughness. The analytical model developed in this research defines a parameter, r_{debond}, that characterizes the effect of the interfacial

hydrophobicity of a particular adhesive / substrate interface on interfacial fracture toughness changes due to moisture uptake. A shortcoming of this model is that it requires the measurement of the interfacial fracture toughness at one particular moisture concentration level to determine the r_{debond} parameter for that particular adhesive / substrate interface. Once r_{debond} is obtained, toughness values for any moisture concentration level can be predicted using the analytical model, provided adsorption theory is the dominant bonding mechanism of the interface. It would be interesting to develop an expression that would allow the determination of r_{debond} from more simple tests rather than requiring an interfacial fracture test, which is not a simple test specimen to construct and test. Perhaps an expression could be developed that relates r_{debond} to water contact angle measurements, thus simplifying the data that must be obtained in order to use the model to predict the loss in toughness from moisture.

The analytical model developed in this research could also be extended to account for contributions of other bonding mechanisms in addition to adsorption theory. One of the first mechanisms that could be investigated with tremendous practical application is the effect of mechanical interlocking on interfacial fracture toughness in the presence of moisture. Surface roughening of substrates prior to adhesive bonding has long been used to increase the reliability of adhesive joints, and it would be interesting to evaluate the possible benefit of surface roughening on interfacial adhesion in the presence of moisture. Results could be incorporated to further develop the model in this study to also account for surface roughening effects.

Last, it should be noted that the basis of this work was founded on quasi-static fracture test results. The results have provided groundwork for evaluating the effect of moisture; however, it would be interesting to conduct a study that focuses on the effect of moisture on the fatigue characteristics of adhesive joints. It is well known that fatigue loads much lower than static failure loads yield failures in adhesive joints, and future studies could build from the fundamental results of this study to identify the primary mechanisms responsible for the loss in fatigue life in the presence of moisture. Based on the data generated, a predictive model could be developed that characterizes the effect of moisture on joint reliability for fatigue environments. An additional consideration in addition to fatigue generated from externally applied loads is the issue of environmental fatigue. Fatigue may occur due to repeated absorption and desorption of moisture in an adhesive joint. Recovery results in this study have shown a significant, permanent loss in interfacial fracture toughness upon fully drying after exposure to moisture. It would also be interesting to evaluate the effect of multiple cycles of environmental fatigue on interfacial fracture toughness, with one cycle consisting of saturated conditions followed by fully drying.

REFERENCES

Ardebili, H., Wong, E. H., and Pecht, M., 2003, "Hydroscopic Swelling and Sorption Characteristics of Epoxy Molding Compounds Used in Electronic Packaging," *IEEE Transactions on Components and Packaging Technologies*, Vol. 26, No. 1, pp. 206-214.

Armstrong, K., 1996, "Effect of Absorbed Water in CFRP Composites on Adhesive Bonding," *International Journal of Adhesion and Adhesives*, Vol. 16, pp. 21-28.

ASTM D790, 1999, "Standard Test Methods for Flexural Properties of Unreinforced and Reinforced Plastics and Electrical Insulating Materials," *Annual Book of ASTM Standards*, Vol. 08.01.

Baldwin, D., 2000, *Electronic Assembly Processing Technology*, DBO II Handout, Georgia Institute of Technology, Atlanta, GA.

Bhattacharyya, B., Huffman, W., Jahsman, W., and Natarajan, B., 1988, "Moisture Absorption and Mechanical Performance of Surface Mountable Plastic Packages," *Proceedings of the 38th IEEE Electronic Components and Technology Conference*, pp. 49-58.

Bowditch, M., 1996, "The Durability of Adhesive Joints in the Presence of Water," *International Journal of Adhesion and Adhesives*, Vol. 16, pp. 73-79.

Brewis, D., Comyn, J., Raval, A., and Kinloch, A., 1990, "The Effect of Humidity on the Durability of Aluminum-Epoxide Joints," *International Journal of Adhesion and Adhesives*, Vol. 10, pp. 247-253.

Brown, W., ed., 1999, *Advanced Electronic Packaging with Emphasis on Multichip Modules*, IEEE Press, New York.

Buehler, F., and Seferis, J., 2000, "Effect of Reinforcement and Solvent Content on Moisture Absorption in Epoxy Composite Materials," *Composites: Part A: Applied Science and Manufacturing*, Vol. 31, pp. 741-748.

Butkus, L., 1997, "Environmental Durability of Adhesively Bonded Joints," Doctoral Thesis, Georgia Institute of Technology, Woodruff School of Mechanical Engineering, Atlanta, GA.

Cengel, Y., and Boles, M., 1994, *Thermodynamics: An Engineering Approach*, McGraw-Hill, Inc., New York.

Charalambides, P., *et al.*, 1989, "A Test Specimen for Determining the Fracture Resistance of Bimaterial Interfaces," *Journal of Applied Mechanics,* Vol. 56, pp. 77-82.

Charalambides, M., Kinloch, A.J., Wang, Y., and Williams, J.G., 1992, "On the Analysis of Mixed-Mode Fracture," *International Journal of Fracture*, Vol. 54, pp. 269-291.

Cho, K, and Cho, E., 2000, "Effect of the Microstructure of Copper Oxide on the Adhesion Behavior or Epoxy/Copper Leadframe Joints," *Journal of Adhesion Science and Technology*, Vol. 14, No. 11, pp. 1333-1353.

Chong, C., Leslie, A., Beng, L., and Lee, C., 1995, "Investigation on the Effect of Copper Leadframe Oxidation on Package Delamination," *Proceedings of the 45th Electronic Components and Technology Conference*, pp. 463 – 469.

Chung, P., Yuen, M., Chan, P., Ho, N., and Lam, D., 2002, "Effect of Copper Oxide on the Adhesion Behavior of Epoxy Molding Compound-Copper Interface," *Proceedings of the 52nd Electronic Components and Technology Conference*, pp. 1665-1670.

Comyn, J., Groves, C., and Saville, R., 1994, "Durability in High Humidity of Glass-to-Lead Alloy Joints Bonded with and Epoxide Adhesive," *International Journal of Adhesion and Adhesives*, Vol. 14, pp. 15-20.

Cotter, J., 1977, in *Developments in Adhesives* (Ed. W.C. Wake), Vol. 1, Applied Science Publishers, London.

Crank, J., 1956, *The Mathematics of Diffusion*, Clarendon Press, Oxford.

Crank, J., and Park, G., Eds., 1968, *Diffusion in Polymers*, Academic Press, London.

Crocombe, A., 1997, "Durability Modeling Concepts and Tools for the Cohesive Environmental Degradation of Bonded Structures," *International Journal of Adhesion and Adhesives*, Vol. 17, pp. 229-238.

Cui, C., Tay, H., Chai, T., Gopalakrishan, R., and Lim, T., 1998, "Surface Treatment of Copper for the Adhesion Improvement to Epoxy Mold Compounds," *Proceedings of the 48th IEEE Electronic Components and Technology Conference*, pp. 1162-1166.

Dai, X., Brillhart, M., and Ho, P., 2000, "Adhesion Measurement for Electronic Packaging Applications Using Double Cantilever Beam Method," *IEEE Transactions on Components and Packaging Technology*, Vol. 23, pp. 101-116.

Dai, X., Brillhart, M., Roesch, M., and Ho, P., 2000, "Adhesion and Toughening Mechanisms at Underfill Interfaces for Flip-Chip-on-Organic-Substrate Packaging," *IEEE Trans. Of Components and Packaging Technology*, Vol. 23, No. 1, pp. 117-127.

DeNeve, B, and Shanahan, M., 1992, "Effects of Humidity on an Epoxy Adhesive," *International Journal of Adhesion and Adhesives*, Vol. 12, pp. 191-196.

Dodiuk, H., Drori, L., and Miller, J., 1984, "The Effect of Moisture in Epoxy Film Adhesives on Their Performance: I. Lap Shear Strength," *Journal of Adhesion*, Vol. 17, pp. 33-44.

Drain, K., Guthrie, J., Leung, C., Martin, F., and Otterburn, M., 1984, "The Effect of Moisture on the Strength of Steel-Steel Cyanoacrylate Adhesive Bonds," *Journal of Adhesion*, Vol. 17, pp. 71-82.

Dundurs, J., 1969, "Edge-bonded Dissimilar Orthogonal Elastic Wedges," *Journal of Applied Mechanics*, Vol. 36, pp. 650-652.

Fan, L, Tison, C., and Wong, C., 2002, "Study on Underfill/Solder Adhesion in Flip-Chip Encapsulation," *IEEE Trans. On Advanced Packaging*, Vol. 25, No. 4, pp. 473-480.

Ferguson, T., and Qu, J., 2003, "Moisture Absorption Analysis of Interfacial Fracture Test Specimens Composed of No-Flow Underfill Materials," *ASME Journal of Electronic Packaging*, Vol. 125, pp. 24-30.

Ferguson, T., and Qu, J., 2002, "Effect of Moisture on the Interfacial Adhesion of the Underfill/Soldermask Interface," *Journal of Electronic Packaging*, Vol. 124, pp. 106-110.

Ferguson, T., and Qu, J., 2001, "Moisture Absorption in No-Flow Underfills and its Effect on Interfacial Adhesion to Solder Mask Coated FR-4 Printed Wiring Board," *International Symposium and Exhibition on Advanced Packaging Materials, Processes, Properties, and Interfaces*, pp. 327-332.

Gledhill, R., Kinloch, A., and Shaw, J., 1980, "A Model for Predicting Joint Durability," *Journal of Ahdesion*, Vol. 11, pp. 3-15.

Gledhill, R., and Kinloch A., 1974, "Environmental Failure of Structural Adhesive Joints," *Journal of Adhesion*, Vol. 6, pp. 315-330.

Harper, B., and Kenner, V., 1997, "Effects of Temperature and Moisture Upon the Mechanical Behavior of an Epoxy Molding Compound," *ASME Advances in Electronic Packaging*, Vol. 1, pp. 1207-1212.

Hong, K., Imadojemu, H., and Webb, R., 1994, "Effects of Oxidation and Surface Roughness on Contact Angle," *Experimental Thermal and Fluid Science*, Vol. 8, pp. 279-285.

Hutchinson, J., and Suo, Z., 1992, "Mixed Mode Cracking in Layered Materials," *Advances in Applied Mechanics*, Vol. 29, Academic Press, New York.

Johnson, W. S., and Butkus, L., 1998, Considering Environmental Conditions in the Design of Bonded Structures: A Fracture Mechanics Approach," *Fatigue and Fracture of Engineering Materials and Structures*, Vol. 21, pp. 465-478.

Jurf, R., and Vinson, J., 1985, "Effect of Moisture on the Static and Viscoelastic Shear Properties of Epoxy Adhesives," *Journal of Materials Science*, Vol. 20, pp. 2979-2989.

Kim, S., 1991, "The Role of Plastic Package Adhesion in IC Performance," Proceedings of the 41st Electronic Components and Technology Conference, pp. 750 – 758.

Kim, J.K., Lebbai, M., Liu, J., Kim, J.H., and Yuen, M., 2000, "Interface Adhesion Between Copper Lead Frame and Epoxy Molding Compound: Effects of Surface Finish, Oxidation, and Dimples," *Proceedings of the 50th Electronic Components and Technology Conference*, pp. 601-608.

Kinloch, A. J., 1987, *Adhesion and Adhesives Science and Technology*, Chapman and Hall, London.

Kinloch, A., 1979, "Interfacial Fracture Mechanical Aspects of Adhesive Bonded Joints---A Review," *Journal of Adhesion*, Vol. 10, pp. 193-219.

Kook, S., Snodgrass, J., Kirtikar, A., Dauskardt, R., 1998, "Adhesion and Reliability of Polymer/Inorganic Interfaces," *Journal of Electronic Packaging*, Vol. 120, pp. 328-335.

Kuhl, A., 1998, "A Technique to Measure Interfacial Fracture Toughness," Masters Thesis, Georgia Institute of Technology, Woodruff School of Mechanical Engineering, Atlanta, GA.

Lee, L., 1979, *Polymer Science and Technology*, Plenum Press, New York.

Lee, H., and Qu, J., 2003, "Microstructure, Adhesion Strength and Failure Path at a Polymer/Roughened Metal Interface," *Journal of Adhesion and Science Technology*, Vol. 17, No. 2, pp. 195-215.

Lu, M., Shim, M., and Kim, S., 2001, "Effects of Moisture on Properties of Epoxy Molding Compounds," *Journal of Applied Polymer Science*, Vol. 81, pp. 2253-2259.

Lu, X., Xu, G., Hofstra, P., and Bajcar, R., 1998, "Moisture – Absorption, Dielectric Relaxation, and Thermal Conductivity Studies of Polymer Composites," *Journal of Polymer Science: Part B: Polymer Physics*, Vol. 36, pp. 2259-2265.

Lubke, K., 1999, "Investigation of Cold Temperature and Environmental Effects on Adhesively Bonded Joints," Master's Thesis, Georgia Institute of Technology, School of Materials Science and Engineering, Atlanta, GA.

Lubke, K., Butkus, L., and Johnson, W. S., 2001, "Effect of Environment on Fracture Toughness and Debond Growth of Aluminum/FM73/Boron-Epoxy Adhesively Bonded Joints," *Journal of Composites Technology and Research*, Vol. 23, pp. 42-49.

Luo, S., 2003, "Study on Adhesion of Underfill Materials for Flip Chip Packaging," Doctoral Thesis, Georgia Institute of Technology, School of Textile and Fibers Engineering, Atlanta, GA.

Luo, S., and Wong, C. P., 2001, "Influence of Temperature and Humidity on Adhesion of Underfills for Flip Chip Packaging," *Proceedings. of the 51st Electronic Components and Technology Conference*, pp. 155-162.

Malyshev, B., and Salganik, R., 1965, "The Strength of Adhesive Joints Using the Theory of Cracks," *International Journal of Fracture Mechanics*, Vol. 1, pp. 114-128.

McMaster, M., and Soane, D., 1989, "Water Sorption in Epoxy Thin Films," *IEEE Transactions on Components, Hybrids, and Manufacturing Technology*, Vol. 12, pp. 373-386.

Mino, T., Sawada, K., Kurosu, A., Otsuka, M., Kawamura, N., and Yoo, H., 1998, "Development of Moisture-proof Thin and Large QFP with Copper Lead Frame," *Proceedings of the 48th Electeonic Components and Technology Conference*, pp. 1125-1131.

Morgan, R., O'Neal, J., and Fanter, D., 1980, "The Effect of Moisture on the Physical and Mechanical Integrity of Epoxies," *Journal of Materials Science*, Vol. 15, pp. 751-764.

Morgan, R., O'Neal, J., and Miller, D., 1979, "The Structure, Modes of Deformation and Failure, and Mechanical Properties of Diaminodiphenyl Sulphone-Cured Tetragylcidyl 4,4' Diaminodiphenyl Methane Epoxy" *Journal of Materials Science*, Vol. 14, pp. 109-124

Netravali, A., Fornes, R., Gilbert, R. and Memory, J., 1986, "Thermogravimetric Analysis of Water-Epoxy Interaction," *Journal of Applied Polymer Science*, Vol. 31, pp.1531-1535.

O'Dowd, N.P., Shih, C.F., and Stout, M.G., 1992, "Test Geometries for Measuring Interfacial Fracture Toughness," *International Journal of Solids and Structures*, Vol. 29, pp. 571-589.

Orman, S., and Kerr, C., 1971, in *Aspects of Adhesion* (Ed. D.J. Alner), University of London Press, London.

Pang, H.L.J., and Seetoh, C.W., 1997, "A Compact Mixed Mode (CMM) Fracture Specimen for Adhesive Bonded Joints," *Engineering Fracture Mechanics*, Vol. 57, pp. 57-65.

Pasztor, A., 1997, in *Handbook of Instrumental Techniques for Analytical Chemistry*, Ed. F. Settle, Chapter 50, Prentice Hall, New Jersey.

Prime, B., 1997, in *Thermal Characterization of Polymeric Materials*, Ed. E. Turi, Vol. 2, Chapter 10, San Diego, Academic Press, San Diego.

Ramani, K., Verhoff, J., Kumar, G., Blank, N., and Rosenberg S., 2000, "Environmental Durability of Moisture-Cured Urethane Adhesive Joints," *International Journal of Adhesion and Adhesives*, Vol. 20, pp. 377-385.

Rice, J.R., 1988, "Elastic Fracture Mechanics Concepts for Interfacial Cracks," *Journal of Applied Mechanics*, Vol. 55, pp. 98-103.

Ritter, J., and Conley, K., 1992, "Moisture Assisted Crack Propagation at Polymer/Glass Interfaces," *International Journal of Adhesion and Adhesives*, Vol. 12, pp. 245-250.

Rosen, S., 1993, *Fundamental Principles of Polymeric Materials*, John Wiley and Sons, New York.

Sharon, G., Dodiuk, H., and Kenig, S., 1989, "Hygrothermal Properties of Epoxy Film Adhesives," *Journal of Adhesion*, Vol. 30, pp. 87-104.

Shaw, G., Rogers, C., and Payer, J., 1992, "The Effect of Immersion on the Breaking Force and Failure Locus in an Epoxy/Mild Steel System," *Journal of Adhesion*, Vol. 38, pp. 255-268.

Shen, C.H., and Springer, G. S., 1976, "Moisture Absorption and Desorption of Composite Materials," *Journal of Composite Materials*, Vol. 10, pp. 2-20.

Shi, S., 2000, "Study on No-Flow Underfill Materials for Low-Cost Flip-Chip Applications," Doctoral Thesis, Georgia Institute of Technology, School of Materials Science and Engineering, Atlanta, GA.

Shi, S., and Wong, C. P., 1999, "Recent Advances in the Development of No-Flow Underfill Encapsulants – A Practical Approach Towards the Actual Manufacturing Application," *Proceedings of the 49th IEEE Electronic Components and Technology Conference*, pp. 770-776.

Shi, S., and Wong, C. P., 1998, "Study of the Fluxing Agent Effects on the Properties of No-Flow Underfill Materials for Flip-Chip Applications," *Proceedings of the 48th Electronic Components and Technology Conference*, pp. 117-124.

Shih, C. F., 1991, "Cracks on Bimaterial Interfaces: Elasticity and Plasticity Aspects," *Materials Science and Engineering*, Vol. A143, pp. 77-90.

Soles, C., Chang, F., Gidley, D., and Yee, A., 2000, "Contributions of the Nanovoid Structure to the Kinetics of Moisture Transport in Epoxy Resins," *Journal of Polymer Science: Part B: Polymer Physics*, Vol. 38, pp. 776-791.

Soles, C., and Yee, A., 2000, "A Discussion of the Molecular Mechanisms of Moisture Transport in Epoxy Resins," *Journal of Polymer Science: Part B: Polymer Physics*, Vol. 38, pp. 792-802.

Soles, C., Chang, F., Bolan, B., Hristov, H., Gidley, D., and Yee, A., 1998, "Contributions of the Nanovoid Structure to the Moisture Absorption Properties of Epoxy Resins," *Journal of Polymer Science: Part B: Polymer Physics*, Vol. 36, pp. 3035-3048.

Su, N., Mackie, R., and Harvey, W., 1992, "The Effects of Aging and Environment on the Fatigue Life of Adhesive Joints," *International Journal of Adhesion and Adhesives*, Vol. 9, pp. 85-91.

Sundararaman, V., and Davidson, B.D., 1995, "New Test Methods for Determining Fracture Toughness as a Function of Mode Mix for Bimaterial Interfaces," *Application of Fracture Mechanics in Electronic Packaging and Materials*, EEP-Vol.11/MD-Vol.64, pp. 141-154.

Suo, Z., and Hutchinson, J.W., 1989, "On Sandwich Test Specimens for Measuring Interface Crack Toughness," *Materials Science and Engineering*, Vol. A107, Pp. 135-143.

Suryanarayana, D., Hsiao, R., Gall, T., and McCreary, J., 1991, "Enhancement of Flip-Chip Fatigue Life by Encapsulation," *IEEE Transactions on Components, Hybrids, and Manufacturing Technology*, Vol.14, No. 1, pp. 218-223.

Thurston, M., and Zehnder, A., 1993, "Experimental Determination of Silica/Copper Interfacial Toughness," *Acta Metallurgica et Materialia*, Vol. 41, pp. 2985-2992.

Tummala, R., ed., 2001, *Fundamentals of Microsystems Packaging*, McGraw Hill, New York.

Tummala, R., Rymaszewski, E., and Klopfenstein, A., 1997, *Microelectronics Packaging Handbook*, Kluwer Academic Publishers, Boston.

Uschitsky, M., and Suhir, E., 2001, "Moisture Diffusion in Epoxy Molding Compounds Filled with Particles," *Journal of Electronic Packaging*, Vol. 123, pp. 47-51.

Uschitsky, M., and Suhir, E., 1997, "Moisture Diffusion in Epoxy Molding Compounds Filled with Silica Particles," *ASME Structural Analysis in Microelectronics and Fiber Optics*, Vol. 21, pp. 141-170.

Vanlandingham, M., Eduljee, R., and Gillespie, J., 1999, "Moisture Diffusion in Epoxy Systems," *Journal of Applied Polymer Science*, Vol. 71, pp. 787-798.

Vincent, M., Meyers, L, and Wong, C. P., 1998, "Enhancement of Underfill Performance for Flip-Chip Applications by Use of Silane Additives," *Proceedings of the 48th IEEE Electronic Components and Technology Conference*, pp. 125-131.

Vroonhoven, J., 1993, "Effects of Adhesion and Delamination on Stress Singularities in Plastic-Packaged Integrated Circuits," *Journal of Electronic Packaging*, Vol. 115, pp. 28-33.

Wahab, M., Crocombe, A., Beevers, A., and Ebtehaj, K., 2002, "Coupled Stress-Diffusion Analysis for Durability Study in Adhesively Bonded Joints," *International Journal of Adhesion and Adhesives*, Vol. 22, pp. 61-73.

Wong, C. P., 2000, *Purpose of IC Encapsulation*, DBO II Handout, Georgia Institute of Technology, Atlanta, GA.

Wong, E., Chan, K., Lim, T., and Lam, T., 1999, "Non-Fickian Moisture Properties Characterization and Diffusion Modeling for Electronic Packages," *Proceedings of the 49th IEEE Electronic Components and Technology Conference*, pp. 302- 306.

Wong, T., and Broutman, L, 1985, "Moisture Diffusion in Epoxy Resins Part I. Non-Fickian Sorption Processes," *Polymer Engineering and Science*, Vol. 25, pp. 521-528.

Wong, T., and Broutman, L, 1985, "Water in Epoxy Resins Part II. Diffusion Mechanism," *Polymer Engineering and Science*, Vol. 25, pp. 529-534.

Wylde, J., and Spelt, J., 1998, "Measurement of Adhesive Joint Fracture Properties as a Function of Environmental Degradation," *International Journal of Adhesion and Adhesives*, Vol. 18, pp. 237-246.

Xiao, F., Hui, C. Y., and Kramer, J., 1993, "Analysis of a Mixed Mode Fracture Specimen: The Asymmetric Double Cantilever Beam," *Journal of Materials Science*, Vol. 28, pp. 5620-5629.

Xiao, G. Z., and Shanahan, M., 1997, "Water Absorption and Desorption in an Epoxy Resin with Degradation," *Journal of Polymer Science: Part B: Polymer Physics*, Vol. 35, pp. 2659-2670.

Yan, X., and Agarwal, R., 1998, "Two Test Specimens for Determining the Interfacial Fracture Toughness in Flip-Chip Assemblies," *Journal of Electronic Packaging*, Vol. 120, pp. 150-155.

Yao, Q., 2000, "Modeling and Characterization of Interfacial Adhesion and Fracture," Doctoral Thesis, Georgia Institute of Technology, Woodruff School of Mechanical Engineering, Atlanta, GA.

Yeung, D., Yuen, M., Lam, D., and Chan, P., 2000, "Measurement of Interfacial Fracture Toughness for Microelectronic Packages," *Journal of Electronics Manufacturing*, Vol. 10, pp. 139-145.

Yi, S., Yue, C., Hsieh, J., Fong, L., and Lahiri, S., 1999, "Effects of Oxidation and Plasma Cleaning on the Adhesion Strength of Molding Compounds to Copper Leadframes," *Journal of Adhesion Science and Technology*, Vol. 13, pp. 789-804.

Yoshioka, O., Okabe, N., Nagayama, S., Yamagishi, R., and Murakami, G., 1989, "Improvement of Moisture Resistance in Plastic Encapsulants MOS-IC by Surface Finishing Copper Leadframe," *Proceedings of the 39th Electronic Components and Technology Conference*, pp. 464-471.

Zanni-Deffarges, M., and Shanahan, M., 1995, "Diffusion of Water into an Epoxy Adhesive: Comparison Between Bulk Behaviour and Adhesive Joints," *International Journal of Adhesion and Adhesives*, Vol. 15, pp. 137-142.

Zanni-Deffarges, M., and Shanahan, M., 1994, "Bulk and Interphase Effects in Aged Structural Joints," *Journal of Adhesion*, Vol. 45, pp. 245-257.

VITA

The author was born on November 12, 1975, and spent the first fifteen years of his life in Tuscaloosa, Alabama. In June of 1991, the author moved to Russellville, AR, where he attended Russellville High School, graduating in May of 1994. The following fall, he enrolled at the University of Arkansas to pursue undergraduate studies in Mechanical Engineering. While at the University of Arkansas, he participated in undergraduate research with Mr. Joel Funkhouser and worked under the direction of Dr. Robert Reynolds. The research addressed the relaxation of wrinkles in polymer films. In December of 1998, he graduated with a Bachelor of Science in Mechanical Engineering and was named Senior Scholar of the College of Engineering, speaking at his graduation commencement ceremonies. In August of 1999, the author began graduate studies at the Georgia Institute of Technology in Mechanical Engineering. Under the direction of Dr. Jianmin Qu, the author investigated the effect of moisture on interfacial adhesion in electronic packaging assemblies. In the spring of 2000, the author received a National Science Foundation Graduate Research Fellowship, and started his tenure the following fall. In December of 2000, he graduated with a Master of Science in Mechanical Engineering and continued his study at the Georgia Institute of Technology for a Ph.D. in Mechanical Engineering. During the course of his Ph.D. study, the author has published three journal articles with two additional journal articles currently under

review. He has published six papers in conference proceedings and received the Best Paper of Session award at the 2001 International Symposium and Exhibition on Advanced Packaging Materials: Processes, Properties, and Interfaces. He is a member of the American Society of Mechanical Engineers, American Society of Heating, Refrigeration, and Air Conditioning Engineers, Tau Beta Pi Engineering Honor Society, Pi Tau Sigma Mechanical Engineering Honor Society, and the Surface Mount Technology Association. The author is married to the former Christina Dawn Littlefield of Russellville, AR.